Staphylococcal infections

Can antibodies help?

Lisanne de Vor

Staphylococcal infections

Can antibodies help?

Lisanne de Vor

Staphylococcal infections – can antibodies help?
PhD thesis, Utrecht University, the Netherlands

ISBN: 978-94-6469-018-7
doi: https://doi.org/10.33540/1361

Author: Lisanne de Vor
Cover design: Lisanne de Vor
Layout: Eefke Schreur-Meilink || ProefschriftMaken.nl
Printing: ProefschriftMaken.nl

Printing of this thesis was kindly financially supported by Genmab; MILabs; Infection & Immunity Utrecht; the Dutch society for Medical Microbiology (NVMM) and the Royal Netherlands Society for Microbiology (KNVM); and the University Medical Center Utrecht, the Netherlands.

Staphylococcal infections

Can antibodies help?

Infecties door stafylokokken

Kunnen antistoffen helpen?

(met een samenvatting in het Nederlands)

Proefschrift

ter verkrijging van de graad van doctor aan de
Universiteit Utrecht op gezag van de
rector magnificus, prof.dr. H.R.B.M. Kummeling,
ingevolge het besluit van het college voor promoties
in het openbaar te verdedigen op

vrijdag 4 november 2022 des ochtends te 10.15 uur

door

Lisanne de Vor

geboren op 30 maart 1993
te Nieuwegein

Promotoren

Prof. dr. S.H.M. Rooijakkers

Prof. dr. H.H. Weinans

Copromotor

Dr. C.P.M. van Kessel

Beoordelingscommissie

Prof. dr. L. Koenderman (voorzitter)

Prof. dr. A. Horswill

Prof. dr. J.A.J.W. Kluijtmans

Prof. dr. C.A.C.M. van Els

Prof. dr. S.J.B. Nijs

Paranimfen

Dr. Dennis J. Doorduijn

Remy M. Muts

Misschien moeten we de vragen in een andere richting stellen

No-land expositie, kunsthal NDSM-werf, Amsterdam

Table of contents

CHAPTER 1

General introduction

Antibody-based therapy for staphylococcal infections

Lisanne de Vor

Department of Medical Microbiology, University Medical Center Utrecht, Utrecht, The Netherlands

Adapted from:
FEBS Lett. 2020; **594***(16): 2556- 2569. doi: 10.1002/1873-3468.13767*

Antibody-based therapy for staphylococcal infections

Staphylococci (in particular S. aureus and S. epidermidis) are human pathogens that can cause a wide range of infections, including skin infections, sepsis, and implant related infections. Due to the emergence of multidrug resistant strains, effective antibiotic treatment of staphylococcal infections becomes increasingly complicated. Treatment is also complicated because of staphylococcus' ability to form biofilm on medical implants. In the biofilm environment, bacteria are protected from antimicrobial therapy and the immune system. It has been difficult to find new antibiotics that act on multi resistant strains and biofilm, and there is a clear need for the development of alternative therapies. Monoclonal antibodies (mAbs) are a promising alternative because they are specific, safe, and easy to engineer. In this thesis, we explored the use of mAbs for staphylococcal infections. In particular, we focused on the capacity of antibodies to boost the host immune system.

Staphylococcal infections are difficult to treat

Staphylococci, most importantly *Staphylococcus (S.) aureus* and *S. epidermidis*, are Gram-positive bacteria that frequently cause nosocomial infections. They can cause a broad range of infections, ranging from acute diseases, such as skin abscesses and sepsis, to chronic infections such as implant related infections [1–3]. The coagulase positive *S. aureus* asymptomatically colonizes approximately 80% of the human population [4,5]. The anterior nares are the most frequent site of colonization [4]. In contrast to *S. aureus, S. epidermidis* is found on other body parts and is seen as a common human skin commensal, but once the host epithelial barrier is compromised, *S. epidermidis* can cause serious infections [6]. Although less virulent than *S. aureus,* the coagulase negative *S. epidermidis* is also an important human pathogen. Especially (pre-term) neonates and elderly that have undergone surgery (e.g. joint replacement) are vulnerable to the development of *S. epidermidis* induced sepsis [7,8]. Together, *S. aureus* and *S. epidermidis* account for the majority of hospital acquired sepsis and foreign body-related infections [9,10] [11].

The treatment of staphylococcal infections is complicated due to the steep rise of antibiotic resistant strains such as MRSE [12–18] (methicillin-resistant *S. epidermidis*), MRSA [19] (methicillin resistant *S. aureus*) and VRSA [19] (vancomycin-resistant *S. aureus*). Only a few last resort antibiotics are effective against these strains. Next to antibiotic resistance, another problem with the treatment of staphylococcal infections is the bacterial ability to

form biofilms on implanted devices (e.g. heart valves, catheters, prosthetic joints) and host tissues (e.g. chronic wounds, endocarditis, osteomyelitis) [20]. The increasing use of medical implants in the past 50 years has made implant related infections become more prevalent [21]. Today, 25% of health care associated infections are implant related and involve biofilm formation [22]. Biofilms are bacterial communities adhering to a biotic or abiotic surface with a self-made extracellular polymeric substance (EPS) that surrounds resident bacteria (**Figure 1)**. Biofilm infections are difficult to treat because bacteria in a biofilm are unresponsive to antimicrobial therapy and they are protected against the immune system [20]. Furthermore, they often occur in places in the body that are not easily accessible for treatment. Consequently, medical treatments consist of long-term antibiotics or complete removal of the infected implant. The most serious complication of biofilm associated infection is dispersal of biofilm embedded bacteria, which can develop into sepsis. While *S. epidermidis* lacks most virulence factors that *S. aureus* expresses, both are found almost equally frequent in implant associated infections – indicating that biofilm formation is also a very important evasion mechanism [23,24].

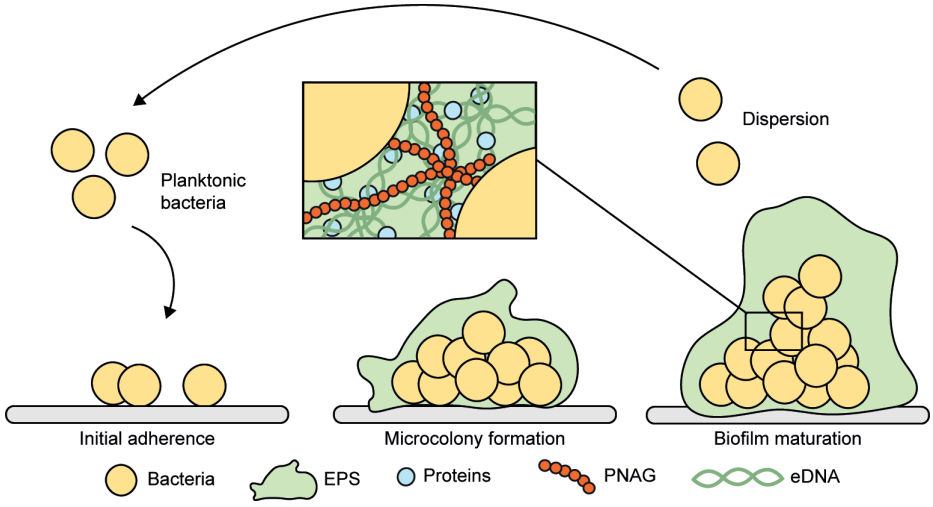

Figure 1. Model of the biofilm life cycle. A biofilm starts growing from planktonic bacteria that adhere to a surface. After adhering the bacteria start to divide and begin the production of an Extracellular Polymeric Substance (EPS) that helps them stick together, which leads to the formation of a microcolony. The EPS consists of polysaccharides, eDNA and proteins. As cell division and EPS production continues, the biofilm matures. From a mature biofilm, bacteria can be released via a process called dispersion. When they disseminate to other locations, they can start a new infection.

Because of increased antibiotic resistance and biofilms being tolerant to antibiotics, there is a clear need for the development of alternative therapies. Antibody-based biologicals could provide an alternative approach to improve treatment of staphylococcal infections. Monoclonal antibodies (mAbs) are fine tools that on one hand have variable domains that can be changed to bind an almost infinite variety of molecules. On

the other hand, the constant Fc region can trigger several potent arms of the immune system. Recent advances in human recombinant antibody production made it possible to easily engineer therapeutic antibodies that can be administered in a safe and non-immunogenic way [25]. Of particular interest for the treatment of staphylococcal infections are immune enhancing mAbs that boost the host immune system to clear bacteria. In the sections below, we will discuss the innate immune response against staphylococci and explain how antibodies play a central role in this process. Furthermore, we will discuss opportunities to use mAbs for the treatment of biofilm related infections.

The innate immune response against staphylococci

Neutrophils

Neutrophils are key players in the host defense against staphylococci. They are abundantly present in the human blood and make up 60% of the total leukocyte population in the blood. They are loaded with an arsenal of broadly effective antimicrobials, safely stored in granules which are only released upon activation. The importance of neutrophil mediated killing in the immune reaction against staphylococci is underlined by the fact that staphylococci cause recurrent infections in patients that suffer from neutrophil deficiencies. Neutrophils circulate in the bloodstream and are recruited to the tissue by chemo attractants that are locally produced following infection by the bacterium, the surrounding tissue, immune cells, and by activation of the complement system [26, 27, 28]. After arrival at the infection, neutrophils can kill bacteria by phagocytosis, degranulation of antimicrobial substances into the environment or by neutrophil extracellular trap (NET) formation **(Figure 2)** [29]. The most effective way for neutrophils to eliminate staphylococci is intracellular killing in the phagolysosome after uptake. After phagocytosis, bacteria are subjected to high levels of reactive oxygen species (ROS) and degranulation of antimicrobial products into the phagosome [28]. Antimicrobial products effective against staphylococci present in the granules include lactoferrin, lysozyme, antimicrobial peptides (AMPs) such as LL-37 and neutrophil serine proteases [28,30]. In the extremely small volume of the phagosome, a very high local concentration of antimicrobial products and ROS can easily be reached, sufficient to create an environment that is destructive to staphylococci [28,31]. For efficient phagocytosis, bacteria need to be opsonized with immunoglobulins (Igs) and/or complement proteins. Neutrophils can recognize Igs and C3-derived products deposited on the bacterial surface via Fc receptors (FcRs) and complement receptors (CRs), expressed on the membrane. IgG antibody opsonization by itself induces phagocytosis of staphylococci by neutrophils via interaction with Fcγ receptors. However, in presence of complement opsonization and subsequent engagement of complement receptors (CRs), this is strongly enhanced [32,33].

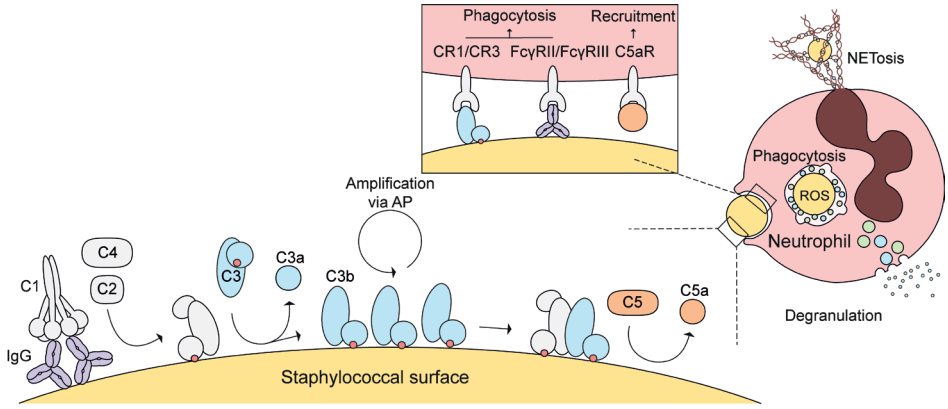

Figure 2. The innate immune response against staphylococci. Recognition of staphylococci via the classical pathway occurs via IgG binding to the bacterial surface. Binding of C1 triggers the formation of C3 convertases that cleave C3 into C3a and C3b. The AP amplification loop leads to high densities of C3b on the surface. At high C3b densities, the C3 convertases switch substrate to C5. C5a recruits and primes neutrophils for phagocytosis, NET formation or degranulation. Interaction of CR1/CR3 with C3b and FcγRII/ FcγRIII with IgG leads to efficient phagocytosis. After phagocytosis, staphylococci are killed by high concentrations of AMPs and ROS. Abbreviations: IgG – immunoglobulin G; AP – alternative pathway; CR – complement receptor; FcγR – Fc gamma receptor; C5aR – C5a receptor; ROS - reactive oxygen species; AMPs – antimicrobial peptides; NET - neutrophil extracellular trap.

Antibodies

Immunoglobulins or antibodies play a central role in the immune response against bacteria. They consist of two functional domains: the fragment antigen binding (Fab) region confers antigen specificity, while the crystallizable fragment (Fc) region drives interaction with other components of the immune system [34]. The importance of antibodies in fighting bacterial infections is highlighted by the fact that antibody deficiencies are associated with recurrent bacterial infections [35,36]. Antibodies provide protection via multiple mechanisms: they can neutralize pathogens after binding to virulence factors, they can induce complement activation via the interaction with C1 and they can induce different immune functions via the interaction with Fc receptors.

Immunoglobulins are produced by B cells in five different isotypes classified as IgM, IgD, IgG, IgA and IgE. The isotypes have identical Fab domains but structurally differ in their heavy chains and effector functions. IgG is the most abundant isotype in human serum (75%) [37] and is the classic choice for therapeutic antibodies. IgG molecules are further divided in four subclasses: IgG1, IgG2, IgG3 and IgG4, named in order of decreasing abundance in serum. All four subclasses have a typical Y-shaped structure that consists of two identical heavy chains ((each ±50 kDa (IgG1, IgG2, IgG4) or ±70 kDa (IgG3)) and two identical light chains (each ± 26 kDa) **Figure 3**. The heavy chain consists of a variable domain (VH) and three constant domains (CH1,CH2,CH3). Between the CH1 and CH2 region there is a hinge region. The two heavy chains are connected by disulfide

bonds in the hinge region and non-covalent interactions between the ch3 domains [38]. The light chain consists only of a variable domain (VL) and a constant domain (CL). The VL, CL, VH and CH1 regions together is also referred to as the antibody's fragment antigen binding (Fab) arm, whereas the CH2 and CH3 domains make up the antibody's Fc tail [39].

The four subclasses are highly conserved in structure and show more than 90% homology in their amino acid sequence. However, they slightly differ in their Fc region, the region that interacts with the immune system, and because of these differences (summarized in **Figure 3**), they activate the immune system differently. The subclasses differ particularly in the length of the hinge region, which has consequences for the flexibility of the fab arms with respect to the fc tail. This in turn influences the antibodies antigen binding capacity and their capacity to oligomerize [38]. The intramolecular flexibility of the subclasses is highest for IgG3, followed by IgG1, IgG4 and IgG2 [40]. Next to the hinge region, the subclasses differ in the CH2 domain, where Fc receptors and complement protein C1q bind with overlapping binding sites, as highlighted in **Figure 3**. Because of these differences, the IgG subclasses have different affinities for C1q and Fc receptors.

Regarding C1q binding, it has become clear in the past years that target bound IgG molecules should organize in multimeric structures such as hexamers [41,42] which is driven by non-covalent interactions between Fc regions of neighboring IgG molecules. Thus, C1q binds IgG molecules with a 1:6 stoichiometry. The long and flexible hinge of IgG3 likely improves its ability to cluster into hexamer structures [38,40]. IgG3 is therefore the subclass that shows the strongest interaction with C1q, followed by IgG1. IgG2, due

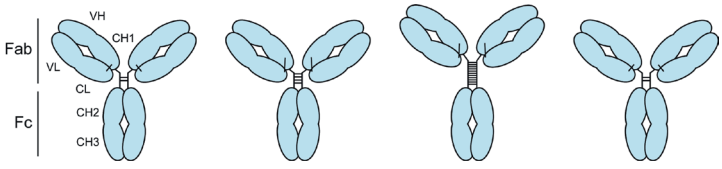

	IgG1	IgG2	IgG3	IgG4
Adult serum level (g/L)	6.98	3.8	0.51	0.56
Relative abundance (%)	60	32	4	4
Intramolecular flexibility	++	-	+++	+
Half-life (days)	21	21	7/21#	21
C1q binding	++	+	+++	-
FcγR binding	+++	-	+++	+

Dependent on the allotype

Figure 3. General characteristic of human IgG subclasses.

to its low flexibility and missing C1q binding residues, binds C1q inefficiently [43]. IgG4 does not bind C1q at all [44].

IgG molecules can induce several different immune functions, including phagocytosis, via the interaction with Fc gamma receptors (FcγRs). Immune cells can express six classes of Fc receptors that interact with IgG molecules in a 1:1 stoichiometry: FcγRI (CD64), FcγRIIA (CD32A), FcγRIIB (CD32B – the only inhibitory FcγR), FcγRIIIA (CD16A) and FcγRIIIB (CD16B) [39]. All receptors are low-affinity and bind to aggregated IgG molecules, except for FcγRI which is a high-affinity receptor and can bind to monomeric IgG molecules. Neutrophils express high levels of FcγRIIA and FcγRIIIB, while other FcγRs are found at low levels [45,46]. After activation, FcγR expression of FcγRI can increase up to 10-fold [47,48]. Because FcγRs all bind to the lower hinge region and the adjacent surface of the CH2 domain [49], as indicated in **Figure 3**, the IgG subclasses differ in their interaction with FcγRs. IgG3 and IgG1 strongly interact with all FcγRs, while IgG2 only binds to FcγRII and IgG4 only (weakly) binds to FcγRII and FcγRIII [37,46,50].

The complement system

The complement system is a group of more than 30 proteins circulating in the human plasma that can rapidly detect and eliminate pathogens. Complement provides protection against bacterial infections by 1) labeling bacteria for phagocytosis by immune cells, 2) the production of chemo attractants (C3a and C5a) that recruit phagocytes to the site of infection and 3) the formation of the membrane attack complex in the bacterial membrane, which results in direct lysis of cells. In staphylococcal infections, the primary role of the complement system is enhancement of uptake by phagocytic immune cells via opsonization with C3-derived products and the attraction and activation of leukocytes through the release of anaphylatoxins C3a and C5a. Indeed, complement C3 deficiencies are associated with staphylococcal infections [51–53] Furthermore, mice deficient in complement C5 are unable to clear *S. aureus* bloodstream infections [54].

There are three pathways to activate the complement system: the classical pathway, the lectin pathway and the alternative pathway. Although complement is always present in the body, the molecular mechanisms driving the complement reaction at the bacterial surface is constantly changing within an individual. For instance, if a person has not been exposed to the bacterium before, complement is only activated by basic recognition pathways in which innate molecules (lectins and IgM by naïve B cells) recognize conserved bacterial surface structures. The lectin pathway involves binding of mannose binding lectins (MBL) or ficolin and association of MBL-associated serine protease (MASP) complexes. MBLs bind WTA and peptidoglycan [55,56], while ficolins bind LTA [57]. The alternative pathway lacks a specific recognition molecule and involves spontane-

ous breakdown of C3 which only occurs at surfaces that do not contain complement inhibitors, such as bacterial surfaces. The alternative pathway also functions as an amplification loop after C3b deposition on the bacterial surface via the lectin or classical pathways. When an individual develops specific antibodies against bacterial surface structures, these antibodies will induce the more specific classical complement pathway **(Figure 2)**. The classical pathway is activated upon binding of the large C1 complex to IgG clusters or IgM on the bacterial surface. The C1 complex consists of an antibody recognition component (C1q) which binds to the lower hinge region and CH2 region of the antibody's Fc tail (as indicated in **Figure 3**), and a heterotetramer of two different serine proteases ($C1r_2$ $C1s_2$). After C1q binding, C1r and C1s become enzymatically active and C1s cleaves complement components C4 and C2, leading to the formation of the C3 convertase C4b2b.

The three pathways converge after the assembly of a C3 convertase on the staphylococcal surface. C3 convertases cleave C3 into C3a and C3b. C3a is released in the environment and C3b becomes covalently linked to the staphylococcal surface and acts as an opsonin. Although all three pathways contribute to C3b deposition on staphylococcal surfaces, many studies indicate that the classical pathway is most important and required for optimal complement opsonization [58–60]. C3b can be processed to iC3b, which also acts as an opsonin but is not able to form alternative pathway C3 convertases and C5 convertases. Remaining C3b on the bacterial surface can form alternative pathway C3 convertases and thereby amplify the opsonization process. Later, high C3b densities on the surface lead to the change of C3 convertases into C5 convertases that cleave C5 into C5a and C5b [61]. C5a is a potent chemoattractant for phagocytes such as neutrophils [61]. Deposition of C5b on the bacterial surface leads to the formation of a lethal pore, the membrane attack complex, which kills Gram-negative bacteria within minutes. In contrast, Gram-positive bacteria such as staphylococci are resistant to direct killing by the membrane attack complex due to their thick peptidoglycan layer [62], thus elimination of these bacteria relies on phagocytosis by neutrophils.

Efforts in the development of antibody-based therapies against staphylococcal infections.

Scientific progress in the last years has now made it possible to produce and engineer human mAbs in an efficient way, yielding non-immunogenic drugs that can be safely administered to human patients. Since 2021, over 100 mAbs are approved by the FDA [63] of which the majority is used for the treatment of cancer. Of the mAbs approved in

2022, only a handful (8%) have infectious indications. They are directed against viruses or bacterial toxins and all function via neutralization mechanisms [64].

During staphylococcal infections there is a continuous battle between staphylococci and innate immune system. As discussed above, antibodies play a powerful role in this fight. Given the importance of phagocytosis in the fight against staphylococci and the central role antibodies play in this process, there is great interest in the development of therapeutic antibodies that boost the host immune system and tip the balance towards the host. In this regard, much attention has been placed on the development of antibody-based therapies for planktonic staphylococci. However, as described above, a significant part of staphylococcal infections involves biofilm formation. It is unclear how well neutrophils, the complement system and antibodies can respond to bacteria in a biofilm, and most likely these types of infections require a different approach. For example, current research focuses on the use of biofilm degrading enzymes such as Dispersin B [65], DNases or proteinases to release bacteria from the biofilm and expose them to antibiotics and the immune system [66,67].

Aim of this thesis

In this thesis, we explore the use of mAbs against *S. aureus* and *S. epidermidis* in single cell and biofilm form. More specifically, we try to identify antibodies and antigens that potently drive immune activation. Next, we explore whether a recently proposed Fc engineering strategy to enhance complement activation on tumor cells can be used for multiple different anti-staphylococcal antibodies. Moreover, we aim to get more insight in the phagocytic receptors that are engaged after opsonization of staphylococci with IgG molecules and complement factors. Next to understanding the effect of IgG and complement on planktonic bacteria, we aim to identify mAbs that recognize bacteria in a biofilm. The work in this thesis may help to gain insight for the development of successful anti-staphylococcal therapies.

References

1. Lowy, F. D. *Staphylococcus aureus* Infections. *N. Engl. J. Med.* **339**, 520–532 (1998).
2. Otto, M. *Staphylococcus epidermidis* - The 'accidental' pathogen. *Nat. Rev. Microbiol.* **7**, 555–567 (2009).
3. Lister, J. L. & Horswill, A. R. *Staphylococcus aureus* biofilms: recent developments in biofilm dispersal. *Front. Cell. Infect. Microbiol.* **4**, (2014).
4. Williams, R. E. O. Healthy carriage of *staphylococcus aureus* : its prevalence and importance. *Bacteriol. Rev.* **27**, 56–71 (1963).
5. Kluytmans, J., van Belkum, A. & Verbrugh, H. Nasal carriage of *Staphylococcus aureus*: epidemiology, underlying mechanisms, and associated risks. *Clin. Microbiol. Rev.* **10**, 505–520 (1997).
6. Kloos, W. E. & Musselwhite, M. S. Distribution and Persistence of Staphylococcus and Micrococcus Species and Other Aerobic Bacteria on Human Skin. *Appl. Microbiol.* **30**, 381–395 (1975).
7. Dong, Y., Speer, C. P. & Glaser, K. Beyond sepsis: *Staphylococcus epidermidis* is an underestimated but significant contributor to neonatal morbidity. *Virulence* **9**, 621–633 (2018).
8. Watson, R. S. *et al.* The Epidemiology of Severe Sepsis in Children in the United States. *Am. J. Respir. Crit. Care Med.* **167**, 695–701 (2003).
9. Becker, K., Heilmann, C. & Peters, G. Coagulase-negative staphylococci. *Clin. Microbiol. Rev.* **27**, 870–926 (2014).
10. DiGiovine, B., Chenoweth, C., Watts, C. & Higgins, M. The attributable mortality and costs of primary nosocomial bloodstream infections in the intensive care unit. *Am. J. Respir. Crit. Care Med.* **160**, 976–981 (1999).
11. Boucher, H. W. & Corey, G. R. Epidemiology of methicillin-resistant *Staphylococcus aureus*. *Clin. Infect. Dis.* **46**, (2008).
12. Krediet, T. G. *et al.* Molecular Epidemiology of Coagulase-Negative Staphylococci Causing Sepsis in a Neonatal Intensive Care Unit over an 11-Year Period. *J. Clin. Microbiol.* **42**, 992–995 (2004).
13. Huang, C. R. *et al.* Coagulase-negative staphylococcal meningitis in adults: Clinical characteristics and therapeutic outcomes. *Infection* **33**, 56–60 (2005).
14. Chabi, R. & Momtaz, H. Virulence factors and antibiotic resistance properties of the *Staphylococcus epidermidis* strains isolated from hospital infections in Ahvaz, Iran. *Trop. Med. Health* **47**, 1–9 (2019).
15. Hamad, T., Hellmark, B., Nilsdotter-Augustinsson, Å. & Söderquist, B. Antibiotic susceptibility among *Staphylococcus epidermidis* isolated from prosthetic joint infections, with focus on doxycycline. *APMIS* **123**, 1055–1060 (2015).
16. Monsen, T., Karlsson, C. & Wiström, J. Spread of Clones of Multidrug-Resistant, Coagulase-Negative Staphylococci Within a University Hospital. *Infect. Control Hosp. Epidemiol.* **26**, 76–80 (2005).
17. Widerström, M., McCullough, C. A., Coombs, G. W., Monsen, T. & Christiansen, K. J. A multidrug-resistant *Staphylococcus epidermidis* clone (ST2) is an ongoing cause of hospital-acquired infection in a Western Australian Hospital. *J. Clin. Microbiol.* **50**, 2147–2151 (2012).

18. Zalewska, A. *et al.* Epidemiological Analysis of Antimicrobial Resistance in *Staphylococcus epidermidis* in Scotland, 2014-2018. *Microbial Drug Resistance* vol. 27 485–491 at https://doi.org/10.1089/mdr.2019.0502 (2021).
19. Tacconelli, E. *et al.* Discovery, research, and development of new antibiotics: the WHO priority list of antibiotic-resistant bacteria and tuberculosis. *Lancet Infect. Dis.* **18**, 318–327 (2018).
20. Otto, M. Staphylococcal Biofilms. *Microbiol. Spectr.* **6**, (2018).
21. Arciola, C. R., Campoccia, D. & Montanaro, L. Implant infections: Adhesion, biofilm formation and immune evasion. *Nat. Rev. Microbiol.* **16**, 397–409 (2018).
22. Magill, S. S. *et al.* Multistate point-prevalence survey of health care-associated infections. *N. Engl. J. Med.* **370**, 1198–1208 (2014).
23. Aggarwal, V. K. *et al.* Organism profile in periprosthetic joint infection: pathogens differ at two arthroplasty infection referral centers in Europe and in the United States. *J. Knee Surg.* **27**, 399–406 (2014).
24. Le, K. Y., Park, M. D. & Otto, M. Immune evasion mechanisms of *Staphylococcus epidermidis* biofilm infection. *Front. Microbiol.* **9**, 1–8 (2018).
25. Irani, V. *et al.* Molecular properties of human IgG subclasses and their implications for designing therapeutic monoclonal antibodies against infectious diseases. *Mol. Immunol.* **67**, 171–182 (2015).
26. Schiffmann, E., Corcoran, B. A. & Wahl, S. M. N formylmethionyl peptides as chemoattractants for leucocytes. *Proc. Natl. Acad. Sci. U. S. A.* **72**, 1059–1062 (1975).
27. Tecchio, C. & Cassatella, M. A. Neutrophil-derived chemokines on the road to immunity. *Semin. Immunol.* **28**, 119–128 (2016).
28. Rigby, K. M. & DeLeo, F. R. Neutrophils in innate host defense against *Staphylococcus aureus* infections. *Semin. Immunopathol.* **34**, 237–259 (2012).
29. Amulic, B., Cazalet, C., Hayes, G. L., Metzler, K. D. & Zychlinsky, A. Neutrophil Function: From Mechanisms to Disease. *Annu. Rev. Immunol.* **30**, 459–489 (2012).
30. de Jong, N. W. M., van Kessel, K. P. M. & van Strijp, J. A. G. Immune Evasion by *Staphylococcus aureus*. *Microbiol. Spectr.* **7**, 1–27 (2019).
31. Segal, A. W. How neutrophils kill microbes. *Annu. Rev. Immunol.* **23**, 197–223 (2005).
32. Rooijakkers, S. H. M. M. *et al.* Immune evasion by a staphylococcal complement inhibitor that acts on C3 convertases. *Nat. Immunol.* **6**, 920–927 (2005).
33. Laarman, A. J. *et al. Staphylococcus aureus* Metalloprotease Aureolysin Cleaves Complement C3 To Mediate Immune Evasion . *J. Immunol.* **186**, 6445–6453 (2011).
34. Lu, L. L., Suscovich, T. J., Fortune, S. M. & Alter, G. Beyond binding: Antibody effector functions in infectious diseases. *Nat. Rev. Immunol.* **18**, 46–61 (2018).
35. JEFFERIS, R. & KUMARARATNE, D. S. Selective IgG subclass deficiency: quantification and clinical relevance. *Clin. Exp. Immunol.* **81**, 357–367 (2008).
36. Kuijpers, T. W., Weening, R. S. & Out, T. A. IgG subclass deficiencies and recurrent pyogenic infections, unresponsiveness against bacterial polysaccharide antigens. *Allergologia et immunopathologia* vol. 20 28–34 at (1992).
37. Schroeder, H. W. & Cavacini, L. Structure and function of immunoglobulins. *J. Allergy Clin. Immunol.* **125**, (2010).
38. Vidarsson, G., Dekkers, G. & Rispens, T. IgG Subclasses and Allotypes: From Structure to Effector Functions. *Front. Immunol.* **5**, 520 (2014).

39. Brezski, R. J. & Georgiou, G. Immunoglobulin isotype knowledge and application to Fc engineering. *Current Opinion in Immunology* vol. 40 at https://doi.org/10.1016/j.coi.2016.03.002 (2016).
40. Roux, K. H., Strelets, L. & Michaelsen, T. E. Flexibility of human IgG subclasses. *J. Immunol.* **159**, (1997).
41. Diebolder, C. A. *et al.* Complement Is Activated by IgG Hexamers Assembled at the Cell Surface. *Science (80-.).* **343**, 1260–1263 (2014).
42. Strasser, J. *et al.* Unraveling the Macromolecular Pathways of IgG Oligomerization and Complement Activation on Antigenic Surfaces. *Nano Lett.* **19**, 4787–4796 (2019).
43. Ferrante, A., Beard, L. J. & Feldman, R. G. IgG subclass distribution of antibodies to bacterial and viral antigens. *Pediatr. Infect. Dis. J.* **9**, S16-24 (1990).
44. Tao, M. H., Canfield, S. M. & Morrison, S. L. The differential ability of human IgG1 and IgG4 to activate complement is determined by the COOH-terminal sequence of the CH2 domain. *J. Exp. Med.* **173**, 1025–8 (1991).
45. Kerntke, C., Nimmerjahn, F. & Biburger, M. There Is (Scientific) Strength in Numbers: A Comprehensive Quantitation of Fc Gamma Receptor Numbers on Human and Murine Peripheral Blood Leukocytes. *Front. Immunol.* **11**, 118 (2020).
46. Bruhns, P. *et al.* Specificity and affinity of human Fcγ receptors and their polymorphic variants for human IgG subclasses. *Blood* **113**, 3716–3725 (2009).
47. Wallace, P. K., Howell, A. L. & Fanger, M. W. Role of Fcγ receptors in cancer and infectious disease. *Journal of Leukocyte Biology* vol. 55 at https://doi.org/10.1002/jlb.55.6.816 (1994).
48. Repp, R. *et al.* Neutrophils express the high affinity receptor for IgG (Fc gamma RI, CD64) after in vivo application of recombinant human granulocyte colony-stimulating factor. *Blood* **78**, 885–9 (1991).
49. Caaveiro, J. M. M., Kiyoshi, M. & Tsumoto, K. Structural analysis of Fc/FcγR complexes: A blueprint for antibody design. *Immunol. Rev.* **268**, 201–221 (2015).
50. Parren, P. W. *et al.* On the interaction of IgG subclasses with the low affinity Fc gamma RIIa (CD32) on human monocytes, neutrophils, and platelets. Analysis of a functional polymorphism to human IgG2. *J. Clin. Invest.* **90**, 1537–46 (1992).
51. Homann, C. *et al.* Acquired C3 deficiency in patients with alcoholic cirrhosis predisposes to infection and increased mortality. *Gut* **40**, 544–549 (1997).
52. Winkelstein, J. A. *et al.* Chronic granulomatous disease: Report on a national registry of 368 patients. *Medicine (Baltimore).* **79**, 155–169 (2000).
53. S. Reis, E., Falcão, D. A. & Isaac, L. Clinical aspects and molecular basis of primary deficiencies of complement component C3 and its regulatory proteins factor I and factor H. *Scand. J. Immunol.* **63**, 155–168 (2006).
54. Von Köckritz-Blickwede, M., Konrad, S., Foster, S., Gessner, J. E. & Medina, E. Protective role of complement C5a in an experimental model of *staphylococcus aureus* bacteremia. *J. Innate Immun.* **2**, 87–92 (2009).
55. Park, K. H. *et al.* Human serum mannose-binding lectin senses wall teichoic acid glycopolymer of *Staphylococcus aureus*, which is restricted in infancy. *J. Biol. Chem.* **285**, 27167–27175 (2010).
56. Nadesalingam, J., Dodds, A. W., Reid, K. B. M. & Palaniyar, N. Mannose-Binding Lectin Recognizes Peptidoglycan via the N -Acetyl Glucosamine Moiety, and Inhibits Ligand-Induced Proinflammatory Effect and Promotes Chemokine Production by Macrophages . *J. Immunol.* **175**, 1785–1794 (2005).

57. Lynch, N. J. *et al.* L-Ficolin Specifically Binds to Lipoteichoic Acid, a Cell Wall Constituent of Gram-Positive Bacteria, and Activates the Lectin Pathway of Complement. *J. Immunol.* **172**, 1198–1202 (2004).
58. Brouwer, N. *et al.* Mannose-Binding Lectin (MBL) Facilitates Opsonophagocytosis of Yeasts but Not of Bacteria despite MBL Binding. *J. Immunol.* **180**, 4124–4132 (2008).
59. Cunnion, K. M., Zhang, H. M. & Frank, M. M. Availability of complement bound to *Staphylococcus aureus* to interact with membrane complement receptors influences efficiency of phagocytosis. *Infect. Immun.* **71**, 656–662 (2003).
60. Jung, D.-J. *et al.* Specific Serum Ig Recognizing Staphylococcal Wall Teichoic Acid Induces Complement-Mediated Opsonophagocytosis against *Staphylococcus aureus* . *J. Immunol.* **189**, 4951–4959 (2012).
61. Ricklin, D., Reis, E. S., Mastellos, D. C., Gros, P. & Lambris, J. D. Complement component C3 – The “Swiss Army Knife” of innate immunity and host defense. *Immunol. Rev.* **274**, 33–58 (2016).
62. Berends, E. T. M. *et al.* Distinct localization of the complement C5b-9 complex on Gram-positive bacteria. *Cell. Microbiol.* **15**, 1955–1968 (2013).
63. Mullard, A. FDA approves 100th monoclonal antibody product. *Nat. Rev. Drug Discov.* **20**, 491–495 (2021).
64. Whaley, K. J. & Zeitlin, L. Emerging antibody-based products for infectious diseases: Planning for metric ton manufacturing. *Hum. Vaccin. Immunother.* **18**, (2022).
65. Kaplan, J. B. *et al.* Detachment of Actinobacillus actinomycetemcomitans Biofilm Cells by an Endogenous β-Hexosaminidase Activity. *J. Bacteriol.* **185**, 4693 LP – 4698 (2003).
66. Lauderdale, K. J., Malone, C. L., Boles, B. R., Morcuende, J. & Horswill, A. R. Biofilm dispersal of community-associated methicillin-resistant *Staphylococcus aureus* on orthopedic implant material. *J. Orthop. Res.* **28**, 55–61 (2010).
67. Kaplan, J. B. *et al.* Recombinant human DNase i decreases biofilm and increases antimicrobial susceptibility in staphylococci. *J. Antibiot. (Tokyo).* **65**, 73–77 (2012).

CHAPTER 2

Human monoclonal antibodies against *Staphylococcus aureus* surface antigens recognize *in vitro* and *in vivo* biofilm

Lisanne de Vor[1*], Bruce van Dijk[2*], Kok P.M. van Kessel[1], Jeffrey S. Kavanaugh[7], Carla J.C. de Haas[1], Piet C. Aerts[1], Marco C. Viveen[1], Edwin C.H. Boel[1], Ad C. Fluit [1], Jakub M. Kwiecinski[7], Gerard C. Krijger[4], Ruud M. Ramakers[6,9,10], Freek J. Beekman[6,9,10], Ekaterina Dadachova[3], Marnix G.E.H. Lam[4], H. Charles Vogely[2], Bart C.H. van der Wal[2], Jos A.G. van Strijp[1], Alexander R. Horswill[7,8], Harrie Weinans[2,5], Suzan H.M. Rooijakkers[1]

1. Department of Medical Microbiology, University Medical Center Utrecht, Utrecht, The Netherlands
2. Department of Orthopedics, University Medical Center Utrecht, Utrecht, The Netherlands
3. College of Pharmacy and Nutrition, University of Saskatchewan, Saskatoon, Canada
4. Department of Radiology and Nuclear Medicine, University Medical Center Utrecht, Utrecht, The Netherlands
5. Department of Biomechanical engineering, TU Delft, Delft, The Netherlands
6. MILabs B.V., Utrecht, The Netherlands
7. Department of Immunology and Microbiology, University of Colorado School of Medicine, Aurora, Colorado, USA
8. Department of Veterans Affairs, Eastern Colorado Health Care System, Denver, USA.
9. Department of Translational Neuroscience, Brain Center Rudolf Magnus, University Medical Center Utrecht, The Netherlands
10. Department of Radiation Science and Technology, Delft University of Technology, Delft, The Netherlands

[*] *These authors contributed equally to this work as first authors.*

Published in eLife, 2021 Jan 11: e67301; doi: 10.7554/eLife.67301

Abstract

Implant-associated *Staphylococcus aureus* infections are difficult to treat because of biofilm formation. Bacteria in a biofilm are often insensitive to antibiotics and host immunity. Monoclonal antibodies (mAbs) could provide an alternative approach to improve the diagnosis and potential treatment of biofilm-related infections. Here, we show that mAbs targeting common surface components of *S. aureus* can recognize clinically relevant biofilm types. The mAbs were also shown to bind a collection of clinical isolates derived from different biofilm-associated infections (endocarditis, prosthetic joint, catheter). We identify two groups of antibodies: one group that uniquely binds *S. aureus* in biofilm state and one that recognizes *S. aureus* in both biofilm and planktonic state. Furthermore, we show that a mAb recognizing wall teichoic acid (clone 4497) specifically localizes to a subcutaneously implanted pre-colonized catheter in mice. In conclusion, we demonstrate the capacity of several human mAbs to detect *S. aureus* biofilms in vitro and in vivo.

Introduction

Implant-related infections are difficult to treat because of the ability of many bacterial species to form biofilm [1]. Biofilms are bacterial communities that adhere to abiotic surfaces (such as medical implants) using a self-made extracellular polymeric substance (EPS), consisting of proteins, polysaccharides, and extracellular DNA [2,3]. Bacteria in a biofilm are physically different from planktonic (free floating) bacteria and often more tolerant to antibiotics [4]. For instance, the EPS forms an important penetration barrier for many antimicrobial agents [2,5]. In addition, most antibiotics cannot kill bacteria in a biofilm because they are in a metabolically inactive state [6] and thus resistant to the antibiotics that act on active cellular processes (such as transcription/translation or cell wall formation [7]. Another complication is that biofilm infections often occur in areas of the body that are not easily accessible for treatment without invasive surgical procedures. Consequently, treatment consists of long-term antibiotic regimens or replacement of the infected implant. Specific and noninvasive laboratory tests for early detection are not yet available and the diagnosis is often made only at advanced stages. This failure to detect biofilms adds further complications to effective diagnosis and treatment of these infections.

The human pathogen *Staphylococcus aureus* is the leading cause of healthcare-associated infections [8,9]. Today, 25% of healthcare-associated infections are related to medical implants such as heart valves, intravenous catheters, and prosthetic joints [10]. *S. aureus* causes one-third of all implant-related infections in Europe and the United States [11,12] and is known for its ability to form biofilm [1]. Due to the absence of a vaccine and the emergence of methicillin-resistant *S. aureus* (MRSA), there is a clear need for diagnostic tools and alternative therapies for *S. aureus* biofilm infections.

Antibody-based biologicals could provide an alternative approach to improve the diagnosis and/or treatment of *S. aureus* biofilm-related infections. Monoclonal antibodies (mAb) may be exploited as vehicles to specifically bring anti-biofilm agents (such as radionuclides, enzymes, or photosensitizers) to the site of infection [13–20]. Furthermore, radioactively labeled mAbs could be used for early diagnosis of biofilm-related infections. At present, only one mAb recognizing *S. aureus* biofilm has been identified. This F598 antibody recognizes poly-*N*-acetyl glucosamine (PNAG) [21,22] (also known as polysaccharide intercellular adhesion [PIA] [23,24], a highly positively charged polysaccharide that was first recognized as a major EPS component of *S. aureus* biofilm. However, PNAG is not the only component of *S. aureus* biofilms. Recently, it has become clear that *S. aureus* may also use cell wall anchored proteins and eDNA to facilitate initial attachment and intercellular adhesion [25–28]. In fact, deletion of the *icaADBC* locus (encoding PNAG) does not impair biofilm formation in multiple *S. aureus* strains [4,28,29]. These biofilms,

referred to as PNAG-negative, are phenotypically different from PNAG-positive biofilm [30–35]. Because both types of biofilm occur in the clinic, we here focus on identifying mAbs that recognize PNAG-positive and PNAG-negative biofilm. In this study, we show that previously identified mAbs against staphylococcal surface structures can recognize both PNAG-negative and PNAG-positive *S. aureus* biofilms. Importantly, we show that some of these mAbs recognize *S. aureus* in both biofilm and planktonic state, which is crucial because release and dissemination of planktonic cells from biofilm-infected implants lead to life-threatening complications [36]. Finally, using SPECT/CT imaging, we show that radiolabeled mAbs have the potential to detect biofilm in vivo.

Results

Production of mAbs and validation of *S. aureus* biofilms

In order to study the reactivity of mAbs with *S. aureus* biofilms, we selected mAbs that were previously found to recognize surface components of planktonic *S. aureus* cells [14,37]. Specifically, we generated two antibodies recognizing cell wall teichoic acids (WTA) (4461-IgG and 4497-IgG) [38,39], one antibody against surface proteins of the SDR family (rF1-IgG) [40], one antibody against clumping factor A (ClfA) (T1-2-IgG), and one antibody of which the exact target is yet unknown (CR5132-IgG) (**Figure 1A**). As a positive control, we generated F598-IgG against PNAG [21]. As negative controls, we produced one antibody recognizing the hapten dinitrophenol (DNP) (G2a-2-IgG) [41] and one recognizing HIV protein gp120 (b12-IgG) [42,43]. The variable heavy and light chain sequences of all antibodies were obtained from different scientific and patent publications [44] (**Supplementary file 1**) and cloned into expression vectors to produce full-length human IgG1 (kappa) antibodies in EXPI293F cells.

Since we were interested in the reactivity of these mAbs with both PNAG-positive and PNAG-negative biofilms, we selected two *S. aureus* to serve as models for these different biofilm phenotypes. We used Wood46 as a model strain for PNAG-positive biofilm because strain Wood46 is known to produce PNAG [45] and known for its low surface expression of IgG binding staphylococcal protein A (SpA). This is an advantage in antibody binding assays because nonspecific binding of the IgG1 Fc domain to SpA complicates the detection of antibodies [46,47]. As a model strain for PNAG-negative biofilms, we used LAC [48–50], a member of the USA300 lineage that has emerged as the common cause of healthcare-associated MRSA infections, including implant infections [51–54]. Previous studies have demonstrated that LAC is capable of forming robust biofilm with no detectable PNAG [15,28,30,55,56]. Here, we used LAC∆*spa*∆*sbi*, a mutant that lacks both SpA and a second immunoglobulin-binding protein (Sbi). To confirm the EPS

composition of Wood46 and LAC∆*spa*∆*sbi* biofilm, we treated biofilms with different EPS-degrading enzymes that degrade either PNAG (dispersin B [DspB]) or extracellular DNA (DNase I). As expected, LAC∆*spa*∆*sbi* biofilm (**Figure S1A)** was sensitive to DNase I but not DspB while Wood46 biofilm (**Figure S1B**) was sensitive to DspB but not DNase I. The fact that Wood46 was insensitive to DNAse can be explained by shielding or DNA network stabilization by PNAG [30]. At ultrastructural level, scanning electron microscopy (SEM) also verified the formation of phenotypically different biofilm by both strains (**Figure S1C,D**). Additionally, we verified that F598-IgG1, the only mAb in our panel that has been reported to bind biofilm [21], indeed recognizes PNAG-positive biofilm of Wood46 (**Figure 1B**) but not PNAG-negative biofilm of LAC∆*spa*∆*sbi* (**Figure 1C**).

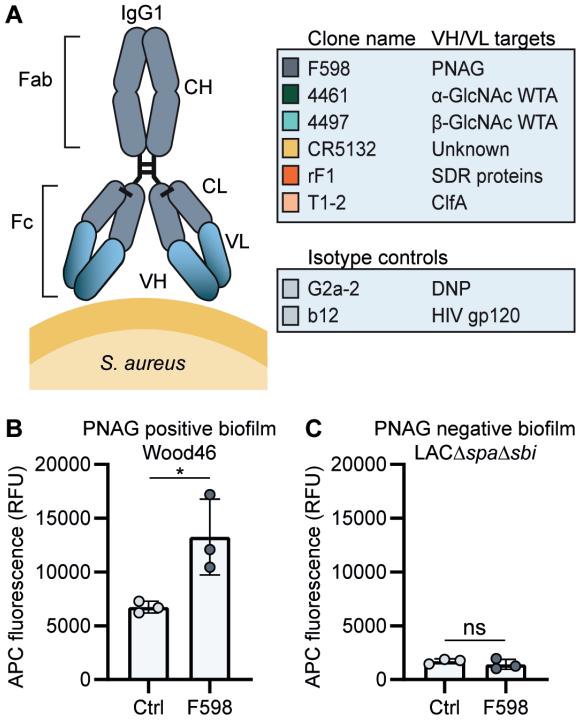

Figure 1. Production of monoclonal antibodies (mAbs) and validation of biofilm. (**A**) Human IgG1 antibodies are large (150 kDa) proteins, consisting of two functional domains. The fragment antigen binding (Fab) region confers antigen specificity, while the crystallizable fragment (Fc) region drives interactions with the immune system. Each IgG1 is composed of two identical heavy chains and two identical light chains, which all consist of a constant (CH, CL) and a variable (VH, VL) domain. A panel of six human IgG1 mAbs that recognize polysaccharide and protein components on the cell surface of and two nonspecific isotype controls was produced. Variable heavy (VH) and light (VL) chain sequences obtained from different scientific and patent publications were cloned in homemade expression vectors containing human heavy chain (HC) and light chain (LC) constant regions, respectively. (**B, C**) Biofilms of Wood46 (**B**) and LAC∆∆ (**C**) were grown for 24 hr and incubated with 66 nM F598-IgG1 or ctrl-IgG1 (G2a-2). mAb binding was detected using APC-labeled anti-human IgG antibodies and a plate reader and plotted as fluorescence intensity per well. Data represent mean + SD of three independent experiments. A ratio paired t-test was performed to test for differences in antibody binding versus control and displayed only when significant as *p≤0.05, **p≤0.01, ***p≤0.001, or ****p≤0.0001.

4461-IgG1 and 4497-IgG1 against WTA recognize PNAG-positive and PNAG-negative *S. aureus* biofilm.

Next, we tested the binding of other mAbs to *S. aureus* biofilms, starting with two well-defined antibodies recognizing WTA, the most abundant glycopolymer on the surface of *S. aureus* [57]. mAbs 4461 and 4497 recognize different forms of WTA: while 4461 binds WTA with α-linked GlcNAc, 4497 recognizes β-linked GlcNAc [38,39]. The extent to which WTA is modified with GlcNAc depends both on the presence of genes encoding enzymes responsible for α- or β-glycosylation [58] and the expression of these genes based on environmental conditions [59]. First, we studied binding of 4461-IgG1 and 4497-IgG1 to exponential planktonic cultures of Wood46 and LAC∆*spa*∆*sbi* (**Figure 2A**). In line with the fact that Wood46 is negative for the enzyme responsible for α-GlcNAc glycosylation of WTA (TarM; [59]), we observed no binding of 4461-IgG1 to planktonic Wood46. In contrast, 4461-IgG1 bound strongly to planktonic LAC∆*spa*∆*sbi*. For 4497-IgG, we observed that 4497-IgG1 bound strongly to planktonic Wood46 cells but very weakly to planktonic LAC∆*spa*∆*sbi* (**Figure 2A**).

Upon studying binding of WTA-specific antibodies to biofilms, we observed that 4497-IgG1 strongly bound to PNAG-positive biofilm formed by Wood46 (**Figure 2B**). While F598-IgG1 exclusively binds PNAG-positive biofilms but not planktonic *S. aureus* (**Figure S2**), 4497-IgG1 can bind *S. aureus* Wood46 in both planktonic and biofilm states (Figure 2A and B). This is important because in the biofilm life cycle planktonic cells can be released from a biofilm and disseminate to other locations in the body [36]. Apart from recognizing PNAG-positive biofilms, 4497-IgG1 also bound the PNAG-negative biofilm formed by LAC∆*spa*∆*sbi* (**Figure 2B**). This is remarkable because 4497-IgG1 did not potently bind planktonic LAC∆*spa*∆*sbi* (**Figure 2A**). Finally, we observe that also 4461-IgG1 effectively recognizes PNAG-negative biofilms. In all, these data identify mAbs against WTA as potent binders of PNAG-positive (4497) and PNAG-negative (4461 and 4497) biofilms.

Because we observed background binding of control IgG1 to Wood46 biofilm compared to planktonic Wood46 (**Figure S2**), we wondered whether this could be explained by secreted SpA being incorporated in the biofilm matrix as Wood46 is unable to link secreted SpA to the surface due to a sortase defect [60]. To test this hypothesis, we performed a binding assay on planktonic versus biofilm Wood46 using nonspecific IgG1, nonspecific IgG3 (which is unable to bind to SpA via the Fc domain [61], and anti-SpA-IgG3 (binding SpA via the Fab-domain but not the Fc domain). Here, we observed high binding of anti-SpA-IgG3 to Wood46 biofilm (**Figure S3A**) but not planktonic (**Figure S3B**) bacteria. Thus, SpA is incorporated in Wood46 biofilm but is washed away in the planktonic binding assay.

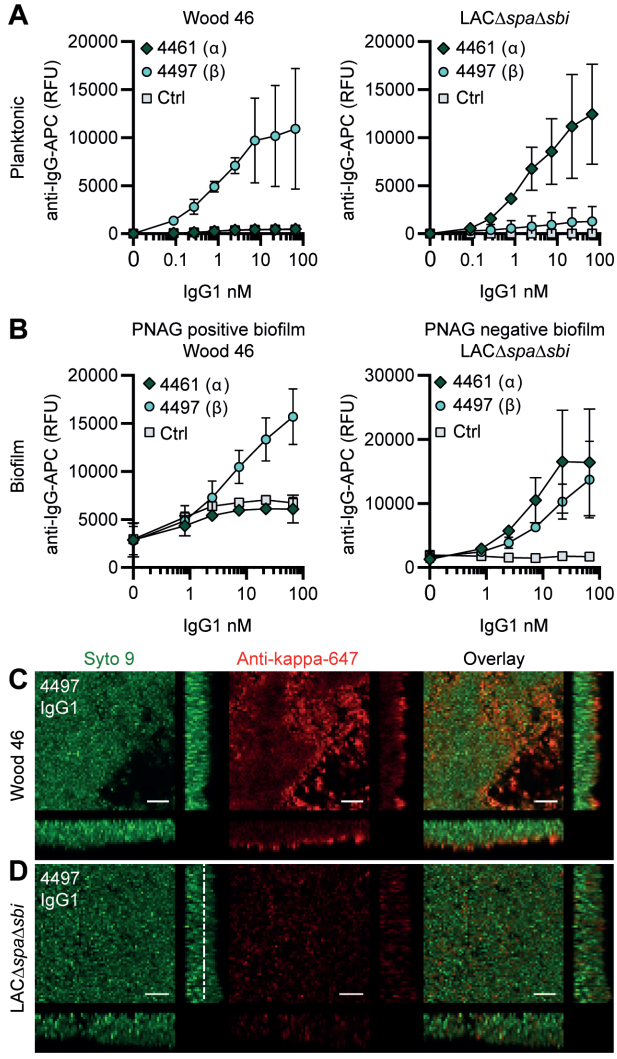

Figure 2. IgG1 monoclonal antibodies (mAbs) against wall teichoic acid (WTA) bind *S. aureus* in planktonic and biofilm mode. (**A**) Planktonic bacteria of Wood46 (left) and LAC (right) were grown to exponential phase and incubated with a concentration range of 4461-IgG1 or 4497-IgG1. mAb binding was detected using APC-labeled anti-human IgG antibodies and flow cytometry and plotted as geoMFI of the bacterial population. (**B**) Biofilms of Wood46 (left) and LAC (right) were grown for 24 hr and incubated with a concentration range of 4461-IgG1 or 4497-IgG1. mAb binding was detected using APC-labeled anti-human IgG antibodies and a plate reader and plotted as fluorescence intensity per well. Data represent mean + SD of three independent experiments. (**C, D**) Biofilm was grown for 24 hr and incubated with 66 nM IgG1 mAb. Bacteria were visualized by Syto9 (green), and mAb binding was detected by staining with Alexa Fluor 647-conjugated goat-anti-human-kappa $F(ab')_2$ antibody (red). Orthogonal views are representative for a total of three Z-stacks per condition and at least two independent experiments. Scale bars: 10 µm.

Using confocal microscopy as an independent method, we confirmed binding of anti-WTA mAbs to in vitro biofilm. Biofilm was cultured in chambered microscopy slides and incubated with IgG1 mAbs or isotype controls (**Figure S4, S5**). Bound mAbs were detected by using AF647-labeled anti-human-kappa-antibodies; bacteria were visualized using DNA dye Syto9. A total of three Z-stacks were acquired at random locations in each chamber of the slide. Z-stacks were visualized as orthogonal views. Using this technique, we visualized binding of 4497-IgG1 to PNAG-positive (**Figure 2C**) and PNAG negative biofilm (**Figure 2D**) and binding of 4461-IgG1 to PNAG-negative biofilm (**Figure S4**). Importantly, isotype controls showed no binding (**Figure S4, S5**). In conclusion, we show that mAbs recognizing polysaccharides WTA α-GlcNAc and WTA β-GlcNAc are able to bind their targets when bacteria are growing in biofilm mode.

CR5132-IgG1 discriminates between planktonic bacteria and biofilm

mAb CR5132 was discovered through phage display libraries from human memory B cells (US 2012/0141493 A1) and was selected for binding to staphylococcal colonies scraped from plates. Since such colonies more closely resemble a surface attached biofilm than free-floating cells [62], we were curious whether this mAb could recognize biofilm. Intriguingly, CR5132-IgG1 showed almost no detectable binding to exponential planktonic LAC∆*spa*∆*sbi* or Wood46 (**Figure 3A**), but it bound strongly to both PNAG-negative and PNAG-positive biofilms formed by these strains (**Figure 3B**). Confocal microscopy confirmed CR5132-IgG1 binding to PNAG-positive (**Figure 3C**) and PNAG-negative biofilms (**Figure 3D**). The ability of CR5132-IgG1 to target both types of *S. aureus* biofilms and to discriminate between planktonic bacteria and biofilm makes CR5132 a unique and interesting mAb. Because of the interesting binding phenotype of CR5132-IgG1, we performed experiments to identify its target. LTA was originally identified as one of the targets of CR5132 (US 2012/0141493 A1), but the quality of commercial LTA preparations varies greatly and often contains other components [63,64]. Therefore, we first tested CR5132-IgG1 binding to *S. aureus* purified cell wall components LTA and peptidoglycan coated on ELISA plates. As a positive control, we used the established A120-IgG1, which is known to bind to LTA (EP2027155A2). Interestingly, we could not detect CR5132-IgG1 binding to LTA **(Figure S6A**) or peptidoglycan (**Figure S6B**), while A120-IgG1 showed detectable binding to LTA. Next, we tested CR5132-IgG1 binding to pure α-GlcNAc or β-GlcNAc WTA structures. To do this, we used magnetic beads that were artificially coated with the WTA backbone and then glycosylated by recombinant TarM, TarS, or TarP, resulting in pure β 1,4-GlcNAc, β 1,3- GlcNAc, or α 1,4-GlcNAc WTA structures in their natural conformation on a surface [65]. This way, we identified WTA β-GlcNAc instead of LTA as one of the targets of CR5132 (**Figure S6C**).

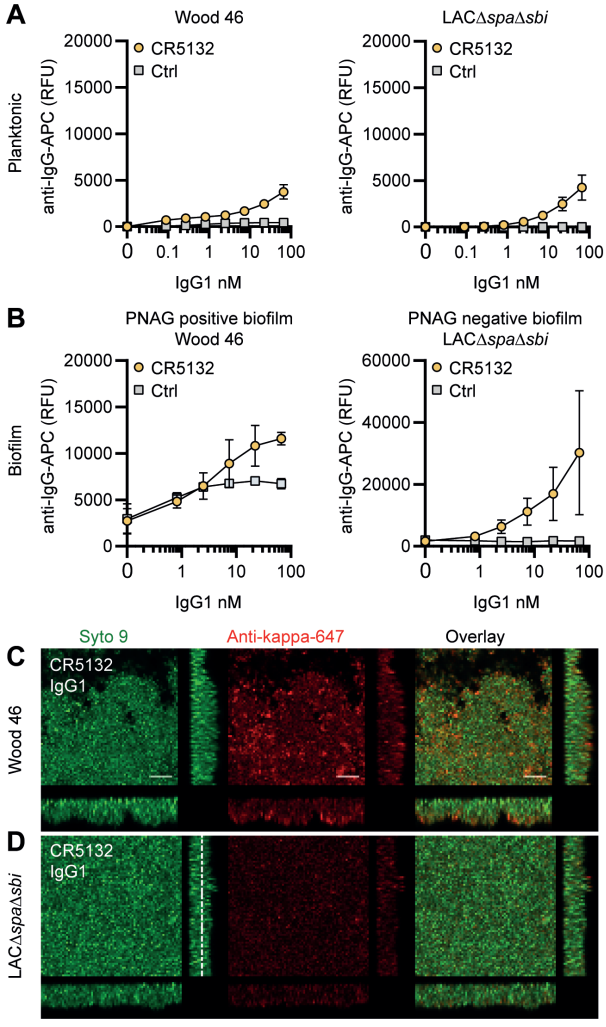

Figure 3. CR5132-IgG1 discriminates between planktonic bacteria and biofilm. (**A**) Planktonic bacteria of Wood46 (left) and LAC (right) were grown to exponential phase and incubated with a concentration range of CR5132-IgG1. Monoclonal antibody (mAb) binding was detected using APC-labeled anti-human IgG antibodies and flow cytometry and plotted as geoMFI of the bacterial population. (**B**) Biofilms of Wood46 (left) and LAC (right) were grown for 24 hr and incubated with a concentration range of CR5132-IgG1. mAb binding was detected using APC-labeled anti-human IgG antibodies and a plate reader and plotted as fluorescence intensity per well. Data represent mean + SD of at least three independent experiments. (**C, D**) Biofilm was grown for 24hr and incubated with 66 nM IgG1 mAb. Bacteria were visualized by Syto9 (green), and mAb binding was detected by staining with Alexa Fluor 647-conjugated goat-anti-human-kappa F(ab′)$_2$ antibody (red). Orthogonal views are representative for a total of three Z-stacks per condition and at least two independent experiments. Scale bars: 10 µm.

RF1-IgG1 against the SDR protein family binds *S. aureus* in planktonic and biofilm form

Finally, we tested whether mAbs recognizing proteins on the staphylococcal cell surface are able to bind *S. aureus* biofilm. mAb rF1 recognizes the SDR family of proteins, which is characterized by a large stretch of serine-aspartate dipeptide repeats (SDR) and includes *S. aureus* ClfA, clumping factor B (ClfB), and SDR proteins C, D, and E and three additional SDR proteins from *Staphylococcus epidermidis* [66]. mab rF1 recognizes glycosylated SDR repeats that are present in all members of this protein family. Additionally, the well-described mAb T1-2 recognizes SDR family member ClfA [67,68]. We confirmed effective binding of rF1-IgG1 to exponential planktonic cultures of Wood46 and LAC∆*spa*∆*sbi* (**Figure 4A**). In addition, both PNAG-positive and PNAG-negative biofilms formed by these strains were bound by rF1-IgG1 (**Figure 4B**). T1-2-IgG1 binding to planktonic bacteria was only detectable in stationary LAC∆*spa*∆*sbi* cultures (**Figure S7**) and not in exponential cultures (**Figure 4A**) because ClfA is known to be

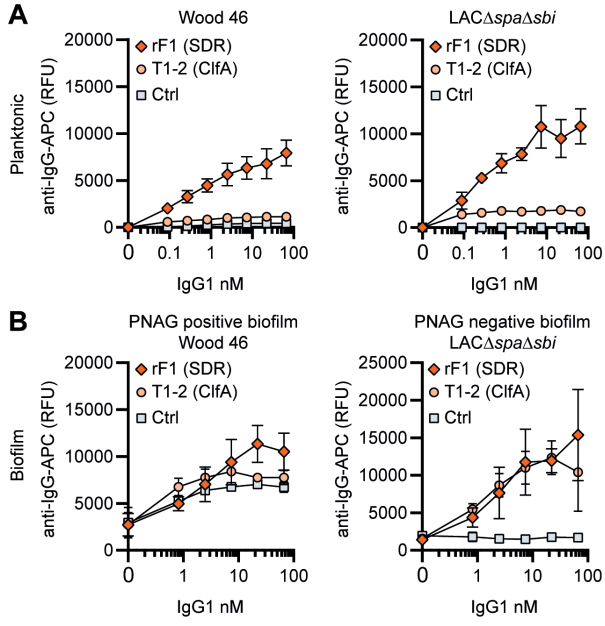

Figure 4. IgG1 monoclonal antibodies (mAbs) against protein components bind planktonic bacteria as well as biofilm. (**A**) Planktonic bacteria of Wood46 (left) and LAC (right) were grown to exponential phase and incubated with a concentration range of rF1-IgG1 or T1-2-IgG1. mAb binding was detected using APC-labeled anti-human IgG antibodies and flow cytometry and plotted as geoMFI of the bacterial population. (**B**) Biofilms of Wood46 (left) and LAC (right) were grown for 24 hr and incubated with a concentration range of rF1-IgG1 or T1-2-IgG1. mAb binding was detected using APC-labeled anti-human IgG antibodies and a plate reader and plotted as fluorescence intensity per well. Data represent mean + SD of three independent experiments.

expressed in the stationary phase [69]. Furthermore, effective binding of T1-2-IgG1 to LAC∆*spa*∆*sbi* PNAG-negative biofilm was detected (**Figure 4B**). In contrast, we could not detect T1-2-IgG1 binding to Wood46 PNAG-positive biofilm (**Figure 4B**). This difference in binding might be explained by a greater abundance of ClfA in PNAG-negative biofilm than PNAG-positive biofilm or PNAG shielding ClfA from T1-2-IgG1 binding. In conclusion, we show that rF1-IgG1 and T1-2-IgG1 bind surface proteins on planktonic bacteria as well as biofilm formed by these bacteria. This means that besides *S. aureus* surface polysaccharides, surface proteins in a biofilm can also be recognized by mAbs.

Comparative binding of mAbs to *S. aureus* biofilm

A direct comparison of all biofilm-binding mAbs revealed 4497-IgG1 as the best binder to PNAG-positive biofilm (**Figure 5A**) and CR5132 as the best binder to PNAG-negative biofilm (**Figure 5B).** Furthermore, all mAbs that bind to exponential planktonic bacteria (**Figure S8**) were able to bind biofilm (**Figure 5**) formed by that strain. Additionally, some mAbs, that is, F598-IgG1 (anti-PNAG) and CR5132-IgG1 (anti-β-GlcNAc WTA), showed enhanced binding to biofilm compared to planktonic bacteria. Thus, we can identify two classes of mAbs: one class recognizing both planktonic bacteria and biofilm, and one class recognizing biofilm only (**Table 1**). Importantly, the mean AF647 fluorescence levels of Z-stacks acquired with the microscope (**Figure S9**) corresponded to our plate reader data (**Figure 5**). As most humans possess antibodies against *S. aureus*, we wondered whether preexisting antibodies might compete with the IgG1 mAbs for binding to epitopes. To test this possibility, biofilm cultures were incubated with AF647-labeled mAbs in the presence of excess IgG (mAb:IgG ratio 1:25) isolated from

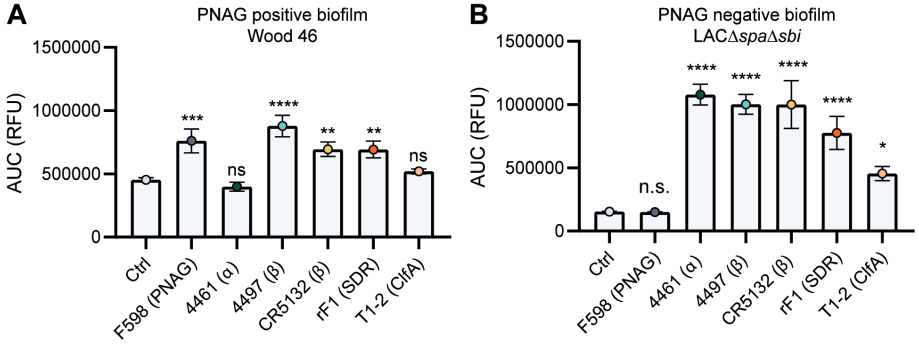

Figure 5. Comparative binding of IgG1 monoclonal antibodies (mAbs) to *S. aureus* biofilm. Biofilms of Wood46 (**A**) and LAC∆*spa*∆*sbi* (**B**) were grown for 24 hr and incubated with a concentration range of IgG1 mAbs. mAb binding was detected using APC-labeled anti-human IgG antibodies and a plate reader. Data are expressed as area under the curve (AUC) of the binding curve (mean + SD) of three independent experiments. One-way ANOVA followed by Dunnett test was performed to test for differences in antibody binding versus control and displayed only when significant as *p≤0.05, **p≤0.01, ***p≤0.001, or ****p≤0.0001.

pooled human serum. This ratio was based on ongoing clinical trials for mAb therapy for *S. aureus* infections (**NCT02296320**), where 2 g and 5 g is administered to patients, reaching a 1:25 mAb:natural IgG ratio in the human circulation. Despite the excess IgG, the AF647-labeled mAbs retained, on average, approximately 60% of the fluorescence they had in the absence of IgG (**Figure S10**). This indicates that the mAbs are able to recognize *S. aureus* biofilm in the presence of preexisting antibodies.

The majority of mAbs recognize PNAG-positive and PNAG-negative biofilm formed by clinical isolates from biofilm-associated infections

Because clinical *S. aureus* isolates express SpA, we wanted to test mAb binding in the presence of this surface protein. To rule out nonspecific binding, we produced all mAbs in the IgG3 subclass, which is unable to bind SpA via the Fc domain [61]. Then, we compared our data acquired with LAC∆*spa*∆*sbi* to the LAC WT strain. Binding of IgG3 mAbs to LAC WT in planktonic (**Figure S11A**) and biofilm (**Figure S11B**) was comparable to binding of IgG1 mAbs to planktonic (**Figure S8**) and biofilm (**Figure 5B**) LAC∆*spa*∆*sbi*. Interestingly, we observed binding of 4497-IgG3 to LAC WT (**Figure S11**), suggesting that knocking out *spa* and *sbi* altered the WTA glycosylation pattern.

Next, we wanted to test if our data acquired on two model bacterial strains translated to clinical isolates from patients with biofilm-related infections. In literature, no correlation between *S. aureus* biofilm phenotypes (PNAG-positive and PNAG-negative) and the source of clinical biofilm infections has been described. Therefore, we collected a variety of *S. aureus* isolates from endocarditis (n = 4), prosthetic joint infections (PJIs) (n = 16), and catheter tip infections (n = 25). First, we determined whether these clinical isolates produced PNAG-positive or PNAG-negative biofilm by using a crystal violet assay and staining with F598-IgG3 (unable to bind SpA). We could detect significant F598-IgG3 binding to 1/4 endocarditis isolates, 5/25 catheter tip isolates, and 6/16 PJI isolates (**Figure 6A**). This indicates that production of PNAG is not a hallmark of one specific source of biofilm-related infections and that approximately one-third of isolates form PNAG-positive biofilm in vitro. This observation also underlines the importance of identifying mAbs that recognize both types of biofilm. As expected, there was a high variation in the amount of biofilm formation and the amount of PNAG produced (**Figure 6B**). These data show that our model bacterial strains Wood46 and LAC∆*spa*∆*sbi* represent the different types of biofilm that is formed by clinical isolates. Next, we tested binding of the other anti-*S. aureus* IgG3 mAbs to six PNAG-positive clinical isolates and six PNAG-negative clinical isolates that were good biofilm formers (**Figure 6C**). Most importantly, we found that 4/6 mAbs (4497, CR5132, rF1, T1-2) recognize PNAG-positive and PNAG-negative biofilm formed by all clinical isolates. Furthermore, we found that mAb 4461 (against α-GlcNAc WTA) recognizes 4 out of total 12 clinical

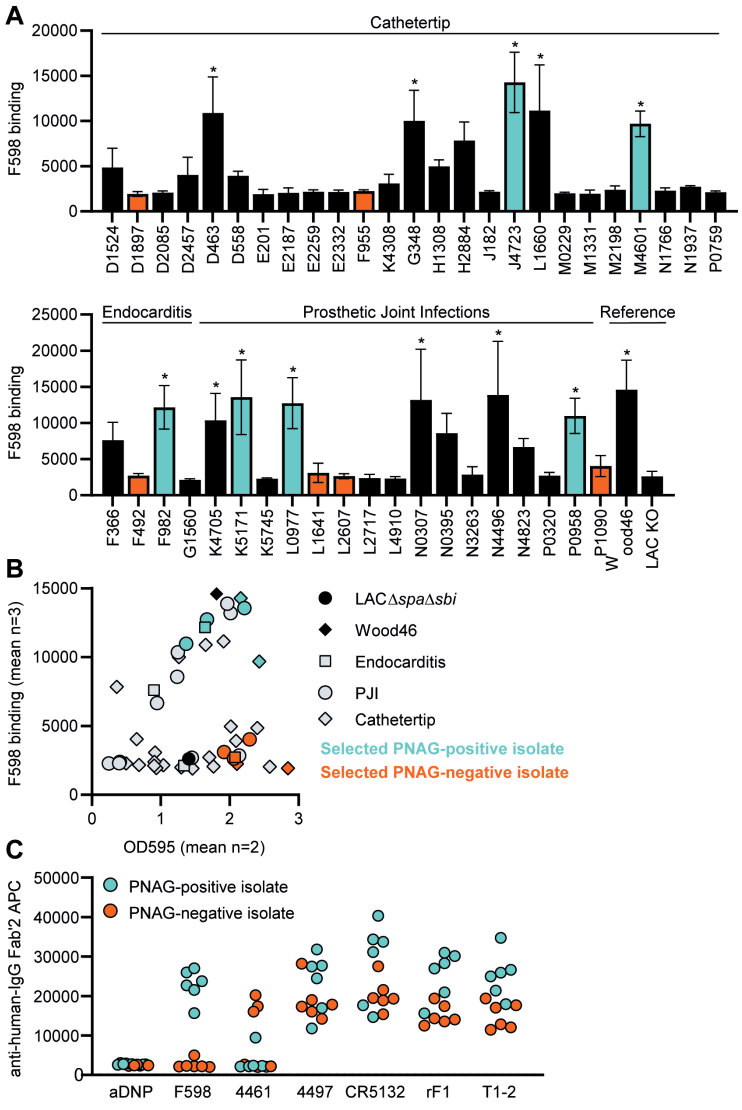

Figure 6. Binding of monoclonal antibodies (mAbs) to *S. aureus* clinical isolate biofilm. (**A**) Biofilm of clinical isolates derived from catheter tip, endocarditis, and prosthetic joint infections (PJIs) was grown for 24 hr and incubated with 33 nM F598-IgG3. mAb binding was detected using APC-labeled anti-human IgG antibodies and a plate reader. (**B**) Scatter plot of F598-IgG3 binding to isolates and biofilm adherent biomass measured by crystal violet staining after mAb binding assay. Isolates selected for (**C**) are indicated. (**C**) Biofilms of clinical isolates was grown for 24 hr and incubated with 33 nM IgG3 mAbs. mAb binding was detected using APC-labeled anti-human IgG antibodies and a plate reader. Data (**A**) represent mean + SD of three independent experiments. One-way ANOVA followed by Dunnett test was performed to test for differences in antibody binding versus LAC KO and displayed only when significant as *. Data (**B**) represent mean two independent experiments.

isolates, in line with literature describing 35.7% of clinical isolates being TarM positive [70].

Indium-111 labeled 4497-IgG1 localizes to subcutaneously implanted pre-colonized catheter in mice

Lastly, we studied whether mAbs against *S. aureus* biofilm could be used to localize in vivo to a subcutaneous implant pre-colonized with biofilm. Mice received a 5 mm catheter that was pre-colonized with *S. aureus* biofilm in one flank. As an internal control, a sterile catheter was inserted into the other flank. Pre-colonized catheters were generated by incubating catheters with *S. aureus* USA300 LAC (AH4802 [71]) for 48 hr. Bacterial loads on the catheters before implantation were approximately 4.5 × 10^7 CFU (**Figure S12).** We selected 4497-IgG1 (against β-GlcNAc WTA) because it potently binds to LAC biofilm in vitro (**Figure 5**). To detect antibody localization in the mouse body, we radiolabeled 4497-IgG1 with indium-111 (^{111}In). Two days after implantation of the catheters, mice were injected intravenously with ^{111}In-labeled 4497-IgG1 and distribution of the radiolabel was visualized with total-body SPECT-CT scans at 24, 72, and 120 hr after injection. Maximum intensity projections of SPECT/CT scans showed typical distribution patterns for IgG distribution in mice [72,73]. At 24 hr, activity was detected in blood-rich organs such as heart, lungs, and liver (**Figure 7A**, **S13**). In line with literature describing 2–3 days half-life of human IgG1 in mice [72], antibodies were cleared from the circulation and blood-rich organs over time, while the specific activity of radiolabeled 4497-IgG1 around pre-colonized implants remained. Remaining activity that was detected at incision sites of the pre-colonized catheters was likely explained by nonspecific accumulation of antibodies at inflammatory sites.

To quantify the amount of antibody accumulating at pre-colonized and sterile implants, a volume of interest was drawn manually around the implants visible on SPECT-CT. The activity measured in the volume of interest was quantified as a percentage of the total body activity (**Figure 7B**). At all time points, 4497-IgG1 accumulated selectively at the pre-colonized catheter with a mean of 7.7% (24 hr), 8.1% (72 hr), and 6.4% (120 hr) of the total body activity in the region of interest around the pre-colonized implant compared to 1.1% (24 hr), 0.7% (72 hr), and 0.2% (120 hr) around the sterile implant. At each time point, we could detect a significant difference in 4497-IgG1 localization to pre-colonized implants compared to sterile implants. The same results were found in a similar pilot experiment with one mouse and less mAbs administered (**Figure S15**). At the end point (120 hr), thus 5 days after implantation of the catheter, CFU counts on implants (n = 3) were determined and a mean of ~1.1 × 10^6 CFU were recovered from pre-colonized implants, whereas no bacteria were recovered from sterile controls (**Figure S12**). Interestingly, when a higher bacterial burden was recovered from a pre-

colonized implant (n = 3) at the end point (**Figure S12**, each shape is one mouse), a higher 4497-IgG1 activity was measured at the implant (**Figure 7B**, 120 hr, see corresponding shapes), suggesting that a larger infection recruits more specific antibodies.

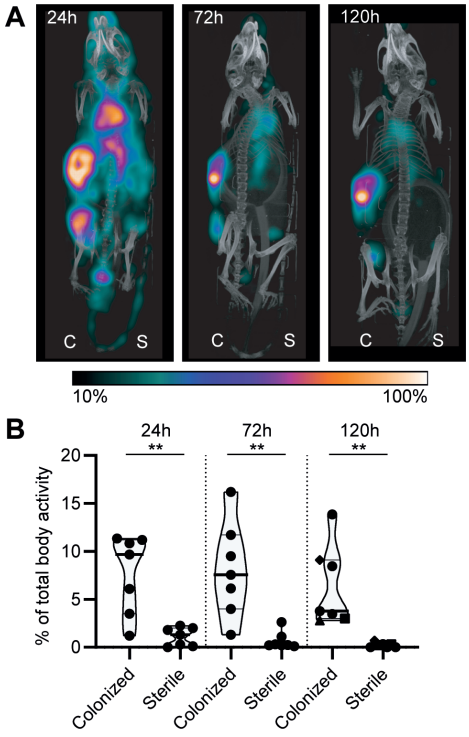

Figure 7. Localization of [^{111}In]In-4497-IgG1 to a subcutaneous implant pre-colonized with biofilm. Two days after implantation, mice were injected with 7.5 MBq [^{111}In]In-4497-IgG1 (n = 7) and imaged at 24 hr, 72 hr, and 120 hr after injection. (**A**) Maximum intensity projection (corrected for decay) of a mouse subcutaneously bearing pre-colonized (C; left flank) and sterile (S; right flank) catheter. Additional scans can be seen in the supplementary information (**Figure S13**). (**B**) The activity detected in regions of interests was expressed as a percentage of total body activity. Each data point represents one mouse. A two-tailed paired t-test was performed to test for differences in activity in sterile versus colonized implants displayed as *p≤0.05, **p≤0.01, ***p≤0.001, or ****p≤0.0001.

We used an SpA-expressing LAC USA300 strain in vivo because *S. aureus* clinical isolates express SpA. To control for nonspecific binding of mAbs via the IgG1 Fc tail, we used nonspecific ^{111}In-labeled palivizumab (an antiviral IgG1) in a different set of mice. In two out of four mice, we saw increased ^{111}In activity at the colonized implant compared to the sterile implant. ^{111}In-labeled palivizumab was detected at pre-colonized catheters with a mean of 5.0% (24 hr), 5.2% (72 hr), and 2.9% (120 hr) of the total body radiolabel activity and at sterile catheters with 1.4% (24 hr), 0.4% (72 hr), and 0.2% (120 hr) (**Figure S14**). Because the mean ^{111}In-labeled 4497-IgG1 localization

to colonized implants was higher than the mean ^{111}In-labeled palivizumab localization at each time point (6.4% vs. 2.9% at 120 hr), localization of ^{111}In-labeled 4497-IgG1 is likely a combination of specific and nonspecific binding at the colonized implant.

Discussion

Identification of mAbs against *S. aureus* biofilms is a crucial starting point for the diagnosis of implant- or catheter-related infections. In this study, we show that previously identified mAbs against *S. aureus* surface structures have the capacity to bind *S. aureus* biofilm. At the start of this study, the only mAb known to react with *S. aureus* biofilm was the F598 antibody recognizing PNAG. F598 was selected to bind to planktonic *S. aureus* MN8m, which is a spontaneous PIA/PNAG-overproducing mutant of strain Mn8 [74]. Because numerous studies have shown that *S. aureus* is capable of forming different biofilm matrices (PNAG-positive and PNAG-negative) [4,28,29], we here focused on identifying antibodies recognizing different biofilm forms. Our study identified several mAbs (**Figures 5** and **6**) capable of binding both types of biofilm (4497-, CR5132-, and rF1-IgG1). This indicates that mAbs directed against WTA or the SDR protein family may be interesting candidates for targeting *S. aureus* biofilm infections. WTA comprises ~30% of the *S. aureus* bacterial surface, and therefore, it is an attractive mAb target [57]. However, WTA glycosylation can be strain specific and *S. aureus* can adapt WTA glycosylation upon environmental cues [59]. Indeed, we found that 4461-IgG1 (anti-α-GlcNAc WTA) and 4497-IgG1 (anti-β-GlcNAc WTA) recognized different *S. aureus* strains and their biofilm. Thus, mAbs targeting WTA may best be composed of a mix of mAbs recognizing both α- and β-glycosylated WTA.

Our study also shows that it is possible for antibodies to recognize both *S. aureus* biofilm and planktonic bacteria. This is crucial because during biofilm infection individual bacteria can disperse from the biofilm by secretion of various enzymes and surfactants to degrade the EPS [36]. These dispersed bacteria can then disseminate and colonize new body sites or develop into sepsis, which is the most serious complication of biofilm-associated infections. With antibodies recognizing both biofilms and planktonic bacteria (like mAbs recognizing WTA [4461, 4497]) and SDR protein family (rF1), it should be possible to target *S. aureus* bacteria in vivo throughout the entire infection cycle (**Table 1**). We also observed that some mAbs (F598 and CR5132) bind better to biofilm than the planktonic form of *S. aureus*. Such antibodies might be useful for the development of assays to discriminate between biofilm and planktonic cultures. Importantly, none of the mAbs in our panel bound planktonic *S. aureus* but not biofilm produced by the same strain. As our data suggest that the ability to form PNAG dependent biofilm is not a hall-

mark of certain infections, we think it is important to identify antibodies that recognize both phenotypes. Here, we show that 4497, CR5132, rF1, and T1-2 recognize a large set of clinical isolates derived from biofilm-related infections, being PNAG-dependent and -independent. Potentially, these results can be extended to other bacterial species such as *S. epidermidis*, which is the other main cause of implant-associated infections. Three mAbs in the panel (rF1[40], F598[74], CR5132 [US 2012/0141493 A1]) have been described to bind *S. epidermidis* in its planktonic state.

Table 1. MAb binding to biofilm and planktonic bacteria. Significant binding ($p < 0.05$) of IgG1 mAbs compared to control IgG1 s indicated with "+", weak binding ($p > 0.05$ - $p < 0.99$) is indicated with "+/-" and no significant binding ($p > 0.99$) is indicated with "–".

Clone	Target	Biofilm		Planktonic	
		PNAG (+)	PNAG (-)	Wood46	LAC ∆*spa*∆*sbi*
F598	PNAG	+	-	+/-	-
4461	WTA(α)	+/-	+	-	+
4497	WTA(β)	+	+	+	+/-
CR5132	WTA(β)	+	+	+/-	+
rF1	SDR proteins	+	+	+	+
T1-2	ClfA	+/-	+	+/-	+/-

Altogether, our in vitro data suggested that mAbs against *S. aureus* surface antigens may be suited to detect biofilms in vivo. As a proof of principle, we tested ^{111}In-labeled 4497-IgG1 localization to a subcutaneously implanted pre-colonized catheter in mice and found increased radiolabel around the colonized implant compared to the sterile implant within 24 hr after mAb injection**,** suggesting rapid localization of 4497-IgG1 to biofilm in vivo. The nonspecific localization of control-IgG1 to pre-colonized catheters at lower levels than specific IgG1 suggests that localization is a combination-specific binding to target antigens and nonspecific binding to SpA expressed by *S. aureus*. Of note, we used a pre-colonized implant model and not an infection model where biofilm is developed in vivo. In the latter model, host factors such as fibrinogen will be incorporated in the in vivo biofilm EPS [75–78], which is why clinical biofilm is described as very heterogenic. Therefore, it is important to further test mAb binding in different in vivo models such as PJIs and osteomyelitis models.

We consider these results as a good starting point to further evaluate the diagnostic and therapeutic purposes of these mAbs. For advanced diagnostic purposes, specific mAbs could also be coupled to gamma- or positron-emitting radionuclides and then be used to detect the presence of *S. aureus* in a biofilm in a patient or during revision surgery. Alternatively, mAbs could be used in vitro to detect the presence of biofilm on explanted implants. For therapeutic purposes, mAbs that bind to biofilm could function as a delivery

vehicle to specifically direct biofilm degrading enzymes, antibiotics, photosensitizers, or alpha-/beta-emitting radionuclides to the site of infection. Alternatively, biofilm-binding mAbs could be tested for their ability to induce the activation of the immune system via the Fc domain [5]. In all cases, the identification of mAbs recognizing *S. aureus* biofilm will have vast utility in the development of diagnostic and therapeutic tools for patients undergoing medical procedures.

Methods

Expression and isolation of human mAbs

For human mAb expression, variable heavy (VH) and light (VL) chain sequences were cloned in homemade pcDNA3.4 expression vectors containing human heavy chain (HC) and light chain (LC) constant regions, respectively. To generate these homemade HC and LC constant region expression vectors, HC and LC constant regions from pFUSE-CHIg-hG1, pFUSE-CHIg-hG3, and pFUSE-CLIg-hk (Invivogen) were amplified by PCR and cloned separately into pcDNA3.4 (Thermo Fisher Scientific). All sequences used are shown in **Supplementary file 1**. VH and VL sequences were derived from antibodies previously described in scientific publications and patents listed in **Supplementary file 1**. Originally, all antibodies have been described as fully human, except for A120 was raised in mice by immunization with *S. aureus* LTA (EP2027155A2) and T1-2, which was raised in mice by immunization with ClfA [79] and later humanized to T1-2 [68]. CR5132 was discovered using ScFv phage libraries (US 2012/0141493 A1), and F598[74], 4461, 4497[38], and rF1[40] were cloned from human B cells derived from *S. aureus*-infected patients. For each VH and VL, human codon-optimized genes with an upstream KOZAK sequence and a HAVT20 signal peptide (MACPGFLWALVISTCLEFSMA) were ordered as gBlocks (Integrated DNA Technologies) and cloned into pcDNA3.4 HC and LC constant region expression vectors using Gibson assembly (BIOKÉ). TOP10F' *Escherichia coli* were used for propagation of the generated plasmids. After sequence verification, plasmids were isolated using NucleoBond Xtra Midi plasmid DNA purification (MACHEREY-NAGEL). For recombinant antibody expression, 2×10^6 cells/ml EXPI293F cells (Life Technologies) were transfected with 1 µg DNA/ml cells in a 3:2 (LC:HC) ratio and transfected using polyethylenimine HCl MAX (Polysciences). EXPI293F cells were routinely screened negative for mycoplasma contamination. After 4–5 days of expression, IgG1 antibodies were isolated from cell supernatant using a HiTrap protein A column (GE Healthcare) and IgG3 antibodies were isolated with a HiTrap Protein G High Performance column (GE Healthcare) using the Äkta Pure protein chromatography system (GE Healthcare). Antibody fractions were dialyzed overnight in PBS and filter-sterilized though 0.22 µm Spin-X filters. Antibodies were analyzed by size-exclusion chromatog-

raphy (GE Healthcare) and separated for monomeric fraction in case aggregation levels were >5%. Antibody concentration was determined by measurement of the absorbance at 280 nm and stored at –20°C.

Bacterial strains and growth conditions

S. aureus strains Wood46 (ATCC 10832) [46,47,60], USA300 LAC (AH1263) [29], and USA300 LAC Δ*spa, sbi*::Tn (AH4116) were used in this study. Strain USA300 LAC Δ*spa, sbi*::Tn (AH4116) was constructed by transducing *sbi*::Tn from Nebraska Transposon Library [80] into USA300 LAC Δ*spa* (AH3052) [81] with phage 11. Strains were grown overnight on sheep blood agar (SBA) at 37°C and were cultured overnight in Tryptic Soy Broth (TSB) before each experiment. For exponential phase planktonic cultures, overnight cultures were sub cultured in fresh TSB for 2 hr. For stationary phase planktonic cultures, overnight cultures in TSB were used.

Biofilm culture

For PNAG-negative biofilm, overnight cultures of LAC or LAC Δ*spa sbi*::Tn were diluted to an OD_{600} of 1 and then diluted 1:1000 in fresh TSB containing 0.5% (wt/vol) glucose and 3% (wt/vol) NaCl. 200 µL was transferred to wells in a flat-bottom 96-well plate (Corning Costar 3598, Tissue Culture treated) and incubated statically for 24 hr at 37°C. To facilitate attachment of PNAG-negative bacteria to the wells, plates were coated overnight at 4°C before inoculation. For experiments with EPS degrading enzymes, plates were coated with 20% human plasma (Sigma) in carbonate–bicarbonate buffer. For IgG1 binding assays, plates were coated with 20 µg/mL human fibronectin (Sigma) in 0.1 M carbonate–bicarbonate buffer (pH 9.6). PNAG-positive Wood46 biofilms were grown similarly, except that no coating was used and growth medium was TSB supplemented with 0.5% (wt/vol) glucose.

Crystal violet assay

To determine the sensitivity of biofilms to DNase I, 1 mg/mL bovine DNase I (Roche) was added at the same time as inoculation and incubated during biofilm formation for 24 hr. To determine biofilm sensitivity to DspB, 30 nM DspB (MTA-Kane Biotech Inc) was added to 24 hr biofilm and incubated statically for 2 hr at 37°C. Biofilm adherence after treatment with DNase I or DspB compared to untreated controls was analyzed as follows. Wells were washed once with PBS, and adherent cells were fixed by drying plates at 60°C for 1 hr. Adherent material was stained with 0.1% crystal violet for 5 min, and excess stain was removed by washing with distilled water. Remaining dye was solubilized in 33% acetic acid, and biofilm formation was quantified by measuring the absorbance at 595 nm using a CLARIOstar plate reader (BMG LABTECH).

Scanning electron microscopy

Biofilms were grown as described above but on 12 mm round poly-L-lysin-coated glass coverslip (Corning). Coverslips were washed 1× with PBS and fixed for 24 hr at room temperature with 2% (v/v) formaldehyde, 0.5% (v/v) glutaraldehyde, and 0.15% (w/v) Ruthenium Red in 0.1 M phosphate buffer (pH 7.4). Coverslips were then rinsed two times with phosphate buffer and post-fixed for 2 hr at 4°C with 1% osmium tetroxide and 1.5% (w/v), potassium ferricyanide (K3[Fe(CN)6]) in 0.065 M phosphate buffer (pH 7.4). Coverslips were rinsed once in distilled water followed by a stepwise dehydration with ethanol (i.e., 50%, 70%, 80%, 95%, 2 × 100%). Samples were then treated stepwise with hexamethyldisilizane (i.e., 50% HMDS/ethanol, 2 × 100% HMDS) and air-dried overnight. The next day samples were mounted on 12 mm aluminum stubs for SEM using carbon adhesive discs (Agar Scientific), and additional conductive carbon tape (Agar Scientific) was placed over part of the sample to establish a conductive path to reduce charging effects. To further improve conductivity, the surface of the samples was coated with a 6 nm layer of Au using a Quorum Q150R S sputter coater. Samples were imaged with a Scios FIB-SEM (Thermo Scientific) under high-vacuum conditions at an acceleration voltage of 20 kV and a current of 0.40 nA.

Antibody binding to planktonic cultures

To determine mAb binding capacity, planktonic bacterial cultures were suspended and washed in PBS containing 0.1% BSA (Serva) and mixed with a concentration range of IgG1-mAbs in a round-bottom 96-well plate in PBS-BSA. Each well contained 2.5 × 10^6 bacteria in a total volume of 55 µL. Samples were incubated for 30 min at 4°C, shaking (~700 rpm), and washed once with PBS-BSA. Samples were further incubated for another 30 min at 4°C, shaking (~700 rpm), with APC-conjugated polyclonal goat-anti-human IgG $F(ab')_2$ antibody (Jackson ImmunoResearch, 1:500). After washing, samples were fixed for 30 min with cold 1% paraformaldehyde. APC fluorescence per bacterium was measured on a flow cytometer (FACSVerse, BD). Control bacteria were used to set proper FSC and SSC gate definitions to exclude debris and aggregated bacteria. Data were analyzed with FlowJo (version 10).

Antibody binding to biofilm cultures

To determine mAb binding capacity to biofilm, wells containing 24 hr biofilm were blocked for 30 min with 4% BSA in PBS. After washing with PBS, wells were incubated with a concentration range of IgG1-mAbs, or Fab fragments when indicated, in PBS-BSA (1%) for 1 hr at 4°C, statically. After washing two times with PBS, samples were further statically incubated for 1 hr at 4°C with APC-conjugated polyclonal goat-anti-human IgG $F(ab')_2$ antibody (Jackson ImmunoResearch, 1:500). Fab fragments were detected with Alexa Fluor 647-conjugated goat-anti-human-kappa $F(ab')_2$ antibody (Southern Biotech,

1:500). After washing, fluorescence per well was measured using a CLARIOstar plate reader (BMG LABTECH).

Peptidoglycan and LTA ELISA

Peptidoglycan from Wood46 was isolated as described in [82], and purified LTA was a kind gift from Sonja von Aulock and Siegfried Morath (University of Konstanz). We coated Maxisorb plates (Nunc) overnight at 4°C with 1 µg/mL peptidoglycan or LTA. The plates were washed three times with PBS 0.05% Tween, blocked with PBS 4% BSA, and incubated 1 hr with a concentration range of CR5132-IgG1, A120-IgG1 (directed against LTA), or control IgG1. The plates were washed and incubated 1 hr with 1:6000 goat-fab'2-anti-human-kappa-HRP (Southern Biotech). Finally, the plates were washed and developed using 3,3′,5,5′-tetramethylbenzidine (Thermo Fisher). The reaction was stopped by addition of 1 N H_2SO_4. Absorption at 450 nm was measured using a CLARI-Ostar plate reader (BMG LABTECH).

IgG1 binding to WTA glycosylated beads

Synthetic WTA (a kind gift of Jeroen Codee, Leiden University) was immobilized on magnetic beads as in van Dalen et al. [65]. Shortly, biotinylated RboP hexamers were enzymatically glycosylated by recombinant TarM, TarS, or TarP with UDP-GlcNAc (Merck) as substrate. After 2 hr incubation at room temperature, 5×10^7 pre-washed Dynabeads M280 Streptavidin (Thermo Fisher) were added and incubated for 15 min at room temperature. The coated beads were washed three times in PBS using a plate magnet, resuspended in PBS 0.1% BSA, and stored at 4°C. To determine CR5132 binding capacity, beads were suspended and washed in PBS/0.05% Tween/0.1% BSA and mixed with a concentration range of CR5132-IgG1 or control IgG1 in a round-bottom 96-well plate in PBS/Tween/BSA. Each well contained 10^5 beads. Samples were incubated for 30 min at 4°C, shaking (~700 rpm), and washed once with PBS/Tween/BSA. Samples were further incubated for another 30 min at 4°C, shaking (~700 rpm), with APC-conjugated polyclonal goat-anti-human IgG $F(ab')_2$ antibody (Jackson ImmunoResearch, 1:500). After washing, APC fluorescence per bead was measured on a flow cytometer (FACSVerse, BD).

Antibody binding in the presence of human pooled IgG

MAb binding in the presence of human pooled IgG was assessed with mAbs that were directly fluorescently labeled. Briefly, mAbs were labeled with AF647 NHS ester (Thermo Fisher Scientific) by following the manufacturer's protocol. Labeled mAbs were buffer exchanged into PBS using desalting Zeba columns (Thermo Fisher Scientific), checked for degree of labeling (ranging from 2.9 to 4.5), and stored at 4°C. To isolate human pooled IgG, blood was drawn from 22 healthy volunteers and allowed to clot for

15 min at room temperature. After centrifugation for 10 min at 3220 × *g* at 4°C, serum was collected, pooled, and subsequently stored at –80°C. IgG was isolated from pooled serum as described above. Biofilm cultures were prepared, washed, and incubated as described above. Samples were incubated with 10 µg/mL AF647-conjugated IgG1 mAbs in buffer or buffer containing 250 µg/mL pooled IgG. AF647 fluorescence per well was measured using a CLARIOstar plate reader (BMG LABTECH).

Confocal microscopy of static biofilm

Wood46 and LAC Δ*spa sbi::*Tn biofilm were grown in glass-bottom cellVIEW slides (Greiner Bio-One [543079]) similarly as described above. cellVIEW slides were placed in a humid chamber during incubation to prevent evaporation of growth medium. After 24 hr, wells were gently washed with PBS and fixed for 30 min with cold 1% paraformaldehyde, followed by blocking with 4% BSA in PBS. After washing with PBS, wells were incubated with 66 nM IgG1-mAbs in PBS-BSA (1%) for 1 hr at 4°C, statically. After washing two times with PBS, samples were further statically incubated for 1 hr at 4°C with Alexa Fluor 647-conjugated goat-anti-human-kappa $F(ab')_2$ antibody (Southern Biotech, 1:300) and 6 µM Syto9 (Live/Dead BacLight Bacterial Viability Kit; Invitrogen). Z-stacks at three random locations per sample were collected at 0.42 µm intervals using a Leica SP5 confocal microscope with a HCX PL APO CS 63×/1.40–0.60 OIL objective (Leica Microsystems). Syto9 fluorescence was detected by excitation at 488 nm, and emission was collected between 495 nm and 570 nm. Alexa Fluor 647 fluorescence was detected by excitation at 633 nm, and emission was collected between 645 and 720 nm. Image acquisition and processing was performed using Leica LAS AF imaging software (Leica Microsystems).

Subcutaneous implantation of pre-colonized catheters in mice

To determine in vivo mAb localization to implant-associated biofilm, we subcutaneously implanted pre-colonized catheters in mice, as described in Kadurugamuwa et al. [83]. Balb/cAnNCrl male mice weighing >20 g obtained from Charles River Laboratories were housed in our Laboratory Animal Facility. 1 hr before surgery, all mice were given 5 mg/kg carprofen. Anesthesia was induced with 5% isoflurane and maintained with 2% isoflurane. Their backs were shaved and the skin was disinfected with 70% ethanol. A 5 mm skin incision was made using scissors after which a 14 gauge piercing needle was carefully inserted subcutaneously at a distance of approximately 1–2 cm. A 5 mm segment of a 7 French polyurethane catheter (Access Technologies) was inserted into the piercing needle and correctly positioned using a k-wire. The incision was closed using one or two sutures, and the skin was disinfected with 70% ethanol. Mice received one s.c. catheter in each flank. One catheter served as a sterile control, whereas the other was pre-colonized for 48 hr with an inoculum of ~10^7 CFU *S. aureus* LAC AH4802.

Strain AH4802 is identical to AH4807 as reported in Miller et al. [71]. The implantation of sterile and pre-colonized catheters in the left or the right flank was randomized. Before inoculation, the implants were sterilized with 70% ethanol and air dried. The inoculated implants were incubated at 37°C for 48 hr under agitation (200–300 RPM). New growth medium was added at 24 hr to maintain optimal growing conditions. Implants were washed three times with PBS to remove nonadherent bacteria and stored in PBS until implantation or used for determination of viable CFU counts. To this end, implants were placed in PBS and sonicated for 10 min in a Branson M2800E Ultrasonic Waterbath (Branson Ultrasonic Corporation). After sonication, total viable bacterial counts per implant were determined by serial dilution and plating.

Radionuclides and radiolabeling of antibodies

4497-IgG1 (anti-β-GlcNAc WTA) and control IgG1 antibody palivizumab (MedImmune) were labeled with indium-111 (^{111}In) using the bifunctional chelator CHXA″ as described previously by Allen et al. [72]. In short, antibodies were buffer exchanged into conjugation buffer and incubated at 37°C for 1.5 hr with a fivefold molar excess of bifunctional CHXA″ (Macrocyclics, prepared less than 24 hr before use). The mAb-CHXA″ conjugate was then exchanged into 0.15 M ammonium acetate buffer to remove unbound CHXA″ and subsequently incubated with approximately 150 kBq ^{111}In (purchased as [^{111}In]$InCl_3$ from Curium Pharma) per µg mAb. The reaction mixture was incubated for 60 min at 37°C after which free $^{111}In^{3+}$ was quenched by the addition of 0.05 M EDTA. Quality control was done by instant thin layer chromatography (iTLC) and confirmed radiolabeling at least 95% radiochemical purity of the antibodies.

USPECT-CT and CFU count

G*power 3.1.9.2 software was used to estimate group sizes for mouse experiments, aiming for a power of 0.95. A minimum of four mice per group was calculated based on the expected difference between 4497-IgG1 localization to sterile implants versus pre-colonized implants and experimental variation obtained in a pilot study. In the event that mAbs were incorrectly injected into the tail vain, mice were excluded from the analyses. Incorrect injection was determined by visual inspection during injection and with SPECT/CT scan, showing radioactivity in the tail tissue instead of the bloodstream.

Two days after subcutaneous implantation of catheters, 50 µg radiolabeled antibody (7.5 MBq) was injected into the tail vein. Four mice were injected with [^{111}In]In-4497-IgG1 and four mice were injected with [^{111}In]In-palivizumab. At 24, 72, and 120 hr post injection, multimodality SPECT/CT imaging of mice was performed with a VECTor^6 CT scanner (MILabs, The Netherlands) using a MILabs HE-UHR-M mouse collimator with 162 pinholes (diameter, 0.75 mm) [84]. At 24 hr, a 30 min total-body SPECT-CT scan

was conducted under anesthesia. Scanning duration at 72 and 120 hr was corrected for the decay of ^{111}In. Immediately after the last scan, mice were sacrificed by cervical dislocation while under anesthetics. The carcasses were stored at –20°C until radiation exposure levels were safe for further processing. Implants were aseptically removed, placed in PBS, and sonicated for 10 min in a Branson M2800E Ultrasonic Waterbath (Branson Ultrasonic Corporation). After sonication, total viable bacterial counts per implant were determined by serial dilution and plating.

Image visualization and SPECT/CT data analyses

The analyzing investigator was blinded for the injection of [^{111}In]–4497-IgG1 or [^{111}In]-palivizumab. Image processing and volume of interest analysis of the total-body SPECT scans were done using PMOD software (PMOD Technologies). SPECT image reconstruction was performed using Similarity Regulated OSEM [85], using 6 iterations and 128 subsets, and the total-body SPECT volumes were smoothed using a 3D Gaussian filter of 1.5 mm. To quantify the accumulation of ^{111}In around the catheters, regions of interest (ROIs) were delineated on SPECT/CT fusion scans as in Branderhorst et al. [86]. 2D ROIs were manually drawn around the catheters and the full body on consecutive transversal slices that were reconstructed into a 3D volume of interest. Delineating the ROIs was done using an iso-contouring method with a threshold of 0.11. For each ROI, the reconstructed voxel intensity sums (total counts) were related to calibrator dose measurements (kBq). Accumulation of ^{111}In was defined as a percentage of total body activity, calculated as (total activity in the implant ROI/total activity in the body ROI) * 100. Reconstructed 3D body scans were visualized as maximum intensity projections, and the SPECT scale was adjusted by cutting 10% of the lower signal intensity to make the high-intensity regions readily visible.

Statistical testing

Statistical analyses were performed in GraphPad Prism 8. The tests and n-values used to calculate p-values are indicated in the figure legends. Unless stated otherwise, graphs comprised at least three biological replicates (independent experiments). When indicated, experiments were performed with technical replicates (duplicate/triplicate).

Acknowledgements

The authors greatly thank Reindert Nijland (Department of Animal Sciences, Wageningen University and Research, Wageningen, The Netherlands) and Fernanda Paganelli (Department of Medical Microbiology, UMC Utrecht) for assistance with biofilm work; Miquel Ekkelenkamp and Sebastian van Marm (Department of Medical Microbiology,

UMC Utrecht) for providing *S. aureus* clinical isolates; Astrid Hendriks (Department of Medical Microbiology, UMC Utrecht), Nina van Sorge (Department of Medical Microbiology and Infection Prevention, Amsterdam UMC, The Netherlands), and Jeroen Codee (Leiden Institute of Chemistry, Leiden University, The Netherlands) for providing WTA glycosylated beads; Frank Beurskens (Genmab BV, Utrecht, The Netherlands) for help with selection of mAbs; Sonja von Aulock and Siegfried Morath (Department of Biochemical Pharmacology, University of Konstanz, Konstanz, Germany) for providing LTA preparates. LdV and BvD were supported by a grant from Health~Holland (LSHM17026 to JvS and HW). FJB and RMR were supported by the research grant QUARAT: Quantitative Universal Radiotracer Tomography (TTW16885, Dutch Research Council (NWO)). ARH was supported by a merit award (BX002711) from the U.S. Department of Veteran Affairs and grant AI083211 from the National Institutes of Health.

References

1. Arciola, C. R., Campoccia, D. & Montanaro, L. Implant infections: Adhesion, biofilm formation and immune evasion. *Nat. Rev. Microbiol.* **16**, 397–409 (2018).
2. Otto, M. Staphylococcal Biofilms. *Microbiol. Spectr.* **6**, (2018).
3. Schilcher, K. & Horswill, A. R. Staphylococcal Biofilm Development: Structure, Regulation, and Treatment Strategies. *Microbiol. Mol. Biol. Rev.* **84**, (2020).
4. Beenken, K. E. *et al.* Global Gene Expression in *Staphylococcus aureus* Biofilms. *Society* **186**, 4665–4684 (2004).
5. de Vor, L., Rooijakkers, S. H. M. & van Strijp, J. A. G. Staphylococci evade the innate immune response by disarming neutrophils and forming biofilms. *FEBS Lett.* **594**, 2556–2569 (2020).
6. Resch, A., Rosenstein, R., Nerz, C. & Götz, F. Differential gene expression profiling of *Staphylococcus aureus* cultivated under biofilm and planktonic conditions. *Appl. Environ. Microbiol.* **71**, 2663–2676 (2005).
7. Mah, T. F. C. & O'Toole, G. A. Mechanisms of biofilm resistance to antimicrobial agents. *Trends in Microbiology* vol. 9 34–39 at https://doi.org/10.1016/S0966-842X(00)01913-2 (2001).
8. Lowy, F. D. *Staphylococcus aureus* Infections. *N. Engl. J. Med.* **339**, 520–532 (1998).
9. Tong, S. Y. C., Davis, J. S., Eichenberger, E., Holland, T. L. & Fowler, V. G. *Staphylococcus aureus* infections: Epidemiology, pathophysiology, clinical manifestations, and management. *Clin. Microbiol. Rev.* **28**, 603–661 (2015).
10. Magill, S. S. *et al.* Multistate point-prevalence survey of health care-associated infections. *N. Engl. J. Med.* **370**, 1198–1208 (2014).
11. Aggarwal, V. K. *et al.* Organism profile in periprosthetic joint infection: pathogens differ at two arthroplasty infection referral centers in Europe and in the United States. *J. Knee Surg.* **27**, 399–406 (2014).
12. Arciola, C. R., An, Y. H., Campoccia, D., Donati, M. E. & Montanaro, L. Etiology of implant orthopedic infections: A survey on 1027 clinical isolates. *Int. J. Artif. Organs* **28**, 1091–1100 (2005).
13. Tursi, S. A. *et al.* Salmonella Typhimurium biofilm disruption by a human antibody that binds a pan-amyloid epitope on curli. *Nat. Commun.* **11**, 1–13 (2020).
14. Raafat, D., Otto, M., Reppschläger, K., Iqbal, J. & Holtfreter, S. Fighting *Staphylococcus aureus* Biofilms with Monoclonal Antibodies. *Trends Microbiol.* **27**, 303–322 (2019).
15. Lauderdale, K. J., Malone, C. L., Boles, B. R., Morcuende, J. & Horswill, A. R. Biofilm dispersal of community-associated methicillin-resistant *Staphylococcus aureus* on orthopedic implant material. *J. Orthop. Res.* **28**, 55–61 (2010).
16. Kaplan, J. B. *et al.* Recombinant human DNase i decreases biofilm and increases antimicrobial susceptibility in staphylococci. *J. Antibiot. (Tokyo).* **65**, 73–77 (2012).
17. Goodman, S. D. *et al.* Biofilms can be dispersed by focusing the immune system on a common family of bacterial nucleoid-associated proteins. *Mucosal Immunol.* **4**, 625–637 (2011).
18. Brockson, M. E. *et al.* Evaluation of the kinetics and mechanism of action of anti-integration host factor-mediated disruption of bacterial biofilms. *Mol. Microbiol.* **93**, 1246–1258 (2014).

19. Estellés, A. *et al.* A high-affinity native human antibody disrupts biofilm from *Staphylococcus aureus* bacteria and potentiates antibiotic efficacy in a mouse implant infection model. *Antimicrob. Agents Chemother.* **60**, 2292–2301 (2016).
20. van Dijk, B. *et al.* Radioimmunotherapy of methicillin-resistant *Staphylococcus aureus* in planktonic state and biofilms. *PLoS One* **15**, e0233086 (2020).
21. Soliman, C. *et al.* Structural basis for antibody targeting of the broadly expressed microbial polysaccharide poly-N-acetylglucosamine. *J. Biol. Chem.* **293**, 5079–5089 (2018).
22. Soliman, C., Pier, G. B. & Ramsland, P. A. Antibody recognition of bacterial surfaces and extracellular polysaccharides. *Curr. Opin. Struct. Biol.* **62**, 48–55 (2020).
23. Maira-Litrán, T. *et al.* Immunochemical Properties of the Staphylococcal poly-N-acetylglucosamine Surface Polysaccharide. *Infect. Immun.* **70**, 4433–4440 (2002).
24. Mack, D. *et al.* The intercellular adhesin involved in biofilm accumulation of *Staphylococcus epidermidis* is a linear β-1,6-linked glucosaminoglycan: Purification and structural analysis. *J. Bacteriol.* **178**, 175–183 (1996).
25. Cucarella, C. *et al.* Bap, a *Staphylococcus aureus* surface protein involved in biofilm formation. *J. Bacteriol.* **183**, 2888–2896 (2001).
26. Corrigan, R. M., Rigby, D., Handley, P. & Foster, T. J. The role of *Staphylococcus aureus* surface protein SasG in adherence and biofilm formation. *Microbiology* **153**, 2435–2446 (2007).
27. O'Neill, E. *et al.* A novel *Staphylococcus aureus* biofilm phenotype mediated by the fibronectin-binding proteins, FnBPA and FnBPB. *J. Bacteriol.* **190**, 3835–3850 (2008).
28. D.E., M. *et al.* Temporal and Stochastic Control of *Staphylococcus aureus* Biofilm Development. *MBio* **5**, 1–12 (2014).
29. Boles, B. R., Thoendel, M., Roth, A. J. & Horswill, A. R. Identification of Genes Involved in Polysaccharide-Independent *Staphylococcus aureus* Biofilm Formation. *PLoS One* **5**, e10146 (2010).
30. Mlynek, K. D. *et al.* Genetic and biochemical analysis of cody-mediated cell aggregation in *staphylococcus aureus* reveals an interaction between extracellular DNA and polysaccharide in the extracellular matrix. *J. Bacteriol.* **202**, 1–21 (2020).
31. Rohde, H. *et al.* Polysaccharide intercellular adhesin or protein factors in biofilm accumulation of *Staphylococcus epidermidis* and *Staphylococcus aureus* isolated from prosthetic hip and knee joint infections. *Biomaterials* **28**, 1711–1720 (2007).
32. O'Neill, E. *et al.* Association between methicillin susceptibility and biofilm regulation in *Staphylococcus aureus* isolates from device-related infections. *J. Clin. Microbiol.* **45**, 1379–1388 (2007).
33. Sugimoto, S. *et al.* Broad impact of extracellular DNA on biofilm formation by clinically isolated Methicillin-resistant and -sensitive strains of *Staphylococcus aureus*. *Sci. Rep.* **8**, 2254 (2018).
34. McCarthy, H. *et al.* Methicillin resistance and the biofilm phenotype in *staphylococcus aureus*. *Front. Cell. Infect. Microbiol.* **5**, 1–9 (2015).
35. Fitzpatrick, F., Humphreys, H. & O'Gara, J. P. Evidence for icaADBC-independent biofilm development mechanism in methicillin-resistant *Staphylococcus aureus* clinical isolates. *J. Clin. Microbiol.* **43**, 1973–1976 (2005).
36. Lister, J. L. & Horswill, A. R. *Staphylococcus aureus* biofilms: recent developments in biofilm dispersal. *Front. Cell. Infect. Microbiol.* **4**, (2014).

37. Sause, W. E., Buckley, P. T., Strohl, W. R., Lynch, A. S. & Torres, V. J. Antibody-Based Biologics and Their Promise to Combat *Staphylococcus aureus* Infections. *Trends Pharmacol. Sci.* **37**, 231–241 (2016).
38. Lehar, S. M. *et al.* Novel antibody-antibiotic conjugate eliminates intracellular *S. aureus*. *Nature* **527**, 323–328 (2015).
39. Fong, R. *et al.* Structural investigation of human *S. aureus*-targeting antibodies that bind wall teichoic acid. *MAbs* **10**, 979–991 (2018).
40. Hazenbos, W. L. W. *et al.* Novel Staphylococcal Glycosyltransferases SdgA and SdgB Mediate Immunogenicity and Protection of Virulence-Associated Cell Wall Proteins. *PLoS Pathog.* **9**, e1003653 (2013).
41. Gonzalez, M. L., Frank, M. B., Ramsland, P. A., Hanas, J. S. & Waxman, F. J. Structural analysis of IgG2A monoclonal antibodies in relation to complement deposition and renal immune complex deposition. *Mol. Immunol.* **40**, 307–317 (2003).
42. Barbas, C. F. *et al.* Molecular profile of an antibody response to HIV-1 as probed by combinatorial libraries. *J. Mol. Biol.* **230**, 812–823 (1993).
43. Saphire, E. O. *et al.* Crystal structure of a neutralizing human IgG against HIV-1: A template for vaccine design. *Science (80-.).* **293**, 1155–1159 (2001).
44. Kabat, E. A., Wu, T. T., Perry, H. M., Gottesman, K. S. & Foeller, C. *Sequences of proteins of immunological interest*. *Analytical Biochemistry* vol. 138 (1984).
45. Cramton, S. E., Ulrich, M., Götz, F. & Döring, G. Anaerobic Conditions Induce Expression of Polysaccharide Intercellular Adhesin in *Staphylococcus aureus* and *Staphylococcus epidermidis*. *Infect. Immun.* **69**, 4079–4085 (2001).
46. Amend, A., Chhatwal, G. S., Schaeg, W. & Blobel, H. Characterization of immunoglobulin G binding to *Staphylococcus aureus* strain Wood 46. *Zentralblatt fur Bakteriol. Mikrobiol. und Hyg. - Abt. 1 Orig. A* **258**, 472–479 (1984).
47. Balachandran, M., Riley, M. C., Bemis, D. A. & Kania, S. A. Complete Genome Sequence of *Staphylococcus aureus* Strain Wood 46. *Genome Announc.* **5**, (2017).
48. Kennedy, A. D. *et al.* Epidemic community-associated methicillin-resistant *Staphylococcus aureus*: Recent clonal expansion and diversification. *Proc. Natl. Acad. Sci. U. S. A.* **105**, 1327–1332 (2008).
49. Voyich, J. M. *et al.* Insights into Mechanisms Used by *Staphylococcus aureus* to Avoid Destruction by Human Neutrophils . *J. Immunol.* **175**, 3907–3919 (2005).
50. Montgomery, C. P. *et al.* Comparison of Virulence in Community-Associated Methicillin-Resistant *Staphylococcus aureus* Pulsotypes USA300 and USA400 in a Rat Model of Pneumonia . *J. Infect. Dis.* **198**, 561–570 (2008).
51. Seybold, U. *et al.* Emergence of Community-Associated Methicillin-Resistant *Staphylococcus aureus* USA300 Genotype as a Major Cause of Health Care--Associated Blood Stream Infections. *Clin. Infect. Dis.* **42**, 647–656 (2006).
52. Carrel, M., Perencevich, E. N. & David, M. Z. USA300 methicillin-resistant *Staphylococcus aureus*, United States, 2000–2013. *Emerg. Infect. Dis.* **21**, 1973–1980 (2015).
53. See, I. *et al.* Trends in Incidence of Methicillin-resistant *Staphylococcus aureus* Bloodstream Infections Differ by Strain Type and Healthcare Exposure, United States, 2005-2013. *Clin. Infect. Dis.* **70**, 19–25 (2020).
54. Haque, N. Z. *et al.* Infective endocarditis caused by USA300 methicillin-resistant *Staphylococcus aureus* (MRSA). *Int. J. Antimicrob. Agents* **30**, 72–77 (2007).

55. Lauderdale, K. J., Boles, B. R., Cheung, A. L. & Horswill, A. R. Interconnections between sigma b, agr, and proteolytic activity in *staphylococcus aureus* biofilm maturation . *Infect. Immun.* **77**, 1623–1635 (2009).
56. Atwood, D. N. *et al.* Comparative impact of diverse regulatory loci on *Staphylococcus aureus* biofilm formation. *Microbiologyopen* **4**, 436–451 (2015).
57. Brown, S., Santa Maria, J. P. & Walker, S. Wall Teichoic Acids of Gram-Positive Bacteria. *Annu. Rev. Microbiol.* **67**, 313–336 (2013).
58. Li, X. *et al.* An accessory wall teichoic acid glycosyltransferase protects *Staphylococcus aureus* from the lytic activity of Podoviridae. *Sci. Rep.* **5**, 17219 (2015).
59. Mistretta, N. *et al.* Glycosylation of *Staphylococcus aureus* cell wall teichoic acid is influenced by environmental conditions. *Sci. Rep.* **9**, 1–11 (2019).
60. Balachandran, M., Giannone, R. J., Bemis, D. A. & Kania, S. A. Molecular basis of surface anchored protein A deficiency in the *Staphylococcus aureus* strain Wood 46. *PLoS One* **12**, e0183913 (2017).
61. Jendeberg, L. *et al.* Engineering of Fc1 and Fc3 from human immunoglobulin G to analyse subclass specificity for staphylococcal protein A. *J. Immunol. Methods* **201**, 25–34 (1997).
62. Serra, D. O., Klauck, G. & Hengge, R. Vertical stratification of matrix production is essential for physical integrity and architecture of macrocolony biofilms of Escherichia coli. *Environ. Microbiol.* **17**, 5073–88 (2015).
63. Morath, S., Geyer, A., Spreitzer, I., Hermann, C. & Hartung, T. Structural decomposition and heterogeneity of commercial lipoteichoic acid preparations. *Infect. Immun.* **70**, 938–944 (2002).
64. Morath, S., von Aulock, S. & Hartung, T. Structure/function relationships of lipoteichoic acids. *J. Endotoxin Res.* **11**, 348–356 (2005).
65. van Dalen, R. *et al.* Do not discard *Staphylococcus aureus* WTA as a vaccine antigen. *Nature* **572**, E1–E2 (2019).
66. Josefsson, E. *et al.* Three new members of the serine-aspartate repeat protein multigene family of *Staphylococcus aureus*. *Microbiology* **144**, 3387–3395 (1998).
67. Ganesh, V. K. *et al.* Lessons from the Crystal Structure of the *S. aureus* Surface Protein Clumping Factor A in Complex With Tefibazumab, an Inhibiting Monoclonal Antibody. *EBioMedicine* **13**, 328–338 (2016).
68. Domanski, P. J. *et al.* Characterization of a humanized monoclonal antibody recognizing clumping factor A expressed by *Staphylococcus aureus*. *Infect. Immun.* **73**, 5229–5232 (2005).
69. Wolz, C., Goerke, C., Landmann, R., Zimmerli, W. & Fluckiger, U. Transcription of clumping factor A in attached and unattached *Staphylococcus aureus* in vitro and during device-related infection. *Infect. Immun.* **70**, 2758–2762 (2002).
70. Winstel, V. *et al.* Wall Teichoic Acid Glycosylation Governs *Staphylococcus aureus* Nasal Colonization. *MBio* **6**, (2015).
71. Miller, R. J. *et al.* Development of a *Staphylococcus aureus* reporter strain with click beetle red luciferase for enhanced in vivo imaging of experimental bacteremia and mixed infections. *Sci. Rep.* **9**, (2019).
72. Allen, K., Jiao, R., Malo, M., Frank, C. & Dadachova, E. Biodistribution of a Radiolabeled Antibody in Mice as an Approach to Evaluating Antibody Pharmacokinetics. *Pharmaceutics* **10**, 262 (2018).

73. Yip, V. *et al.* Quantitative cumulative biodistribution of antibodies in mice: Effect of modulating binding affinity to the neonatal Fc receptor. *MAbs* **6**, 689–696 (2014).
74. Kelly-Quintos, C., Cavacini, L. A., Posner, M. R., Goldmann, D. & Pier, G. B. Characterization of the opsonic and protective activity against *Staphylococcus aureus* of fully human monoclonal antibodies specific for the bacterial surface polysaccharide poly-N-acetylglucosamine. *Infect. Immun.* **74**, 2742–2750 (2006).
75. Zapotoczna, M., McCarthy, H., Rudkin, J. K., O'Gara, J. P. & O'Neill, E. An Essential Role for Coagulase in *Staphylococcus aureus* Biofilm Development Reveals New Therapeutic Possibilities for Device-Related Infections. *J. Infect. Dis.* **212**, 1883–1893 (2015).
76. Kwiecinski, J., Kahlmeter, G. & Jin, T. Biofilm formation by *Staphylococcus aureus* isolates from skin and soft tissue infections. *Curr. Microbiol.* **70**, 698–703 (2015).
77. Kwiecinski, J. *et al.* Staphylokinase Control of *Staphylococcus aureus* Biofilm Formation and Detachment Through Host Plasminogen Activation. *J. Infect. Dis.* **213**, 139–48 (2016).
78. Nishitani, K. *et al.* Quantifying the natural history of biofilm formation in vivo during the establishment of chronic implant-associated *Staphylococcus aureus* osteomyelitis in mice to identify critical pathogen and host factors. *J. Orthop. Res.* **33**, 1311–1319 (2015).
79. Hall, A. E. *et al.* Characterization of a Protective Monoclonal Antibody Recognizing *Staphylococcus aureus* MSCRAMM Protein Clumping Factor A. *Infect. Immun.* **71**, 6864–6870 (2003).
80. Fey, P. D. *et al.* A Genetic Resource for Rapid and Comprehensive Phenotype Screening of Nonessential *Staphylococcus aureus* Genes. *MBio* **4**, (2013).
81. Ibberson, C. B. *et al. Staphylococcus aureus* hyaluronidase is a CodY-regulated virulence factor. *Infect. Immun.* **82**, 4253–4264 (2014).
82. Timmerman, C. P. *et al.* Induction of release of tumor necrosis factor from human monocytes by staphylococci and staphylococcal peptidoglycans. *Infect. Immun.* **61**, 4167–4172 (1993).
83. Kadurugamuwa, J. L. *et al.* Direct continuous method for monitoring biofilm infection in a mouse model. *Infect. Immun.* **71**, 882–90 (2003).
84. Goorden, M. C. *et al.* VECTor: A preclinical imaging system for simultaneous submillimeter SPECT and PET. *J. Nucl. Med.* **54**, 306–312 (2013).
85. Vaissier, P. E. B., Beekman, F. J. & Goorden, M. C. Similarity-regulation of OS-EM for accelerated SPECT reconstruction. *Phys. Med. Biol.* **61**, 4300–4315 (2016).
86. Branderhorst, W. *et al.* Three-Dimensional Histologic Validation of High-Resolution SPECT of Antibody Distributions Within Xenografts. *J. Nucl. Med.* **55**, 830–837 (2014).

Supplementary information

Supplementary figures

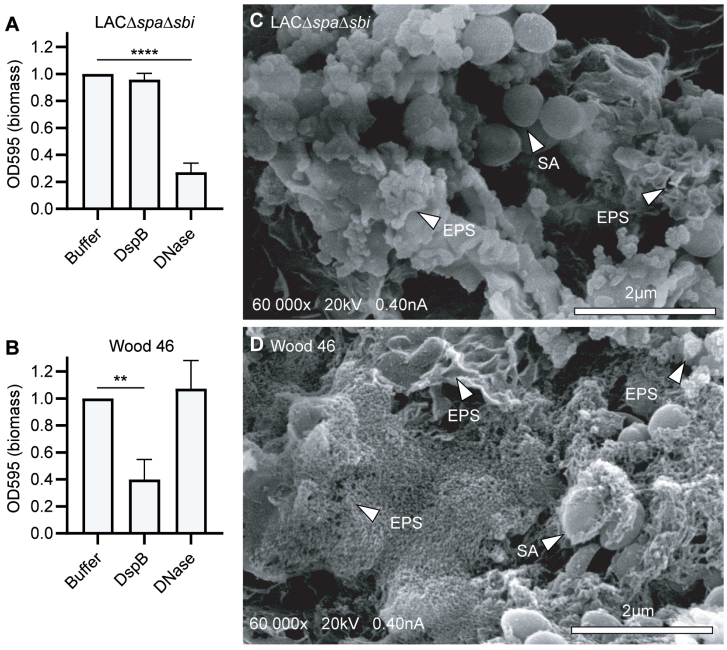

Figure S1. *S. aureus* strains LAC and Wood46 form different types of biofilm. (**A, C**) Biofilm of strain LAC (**A**) and Wood46 (**C**) was grown for 24 hr with buffer or DNase (1 mg/mL). DspB (30 nM) was added after 24 hr of biofilm formation. Adherent biofilm biomass was measured by crystal violet staining. Data represent mean + SD of three independent experiments. Triplicates were averaged and expressed as relative biomass by dividing the OD595 of treated samples by the OD595 of control samples. One-way ANOVA followed by Dunnett test was performed to test for differences in biofilm biomass and displayed only when significant as *p≤0.05, **p≤0.01, ***p≤0.001, or ****p≤0.0001. (**B, D**) Representative scanning electron microscopy (SEM) images of LAC (**B**) and Wood46 (**D**) biofilms established on glass coverslips following 24 hr incubation at 37°C. SA, ; EPS, extracellular polymeric substance structure.

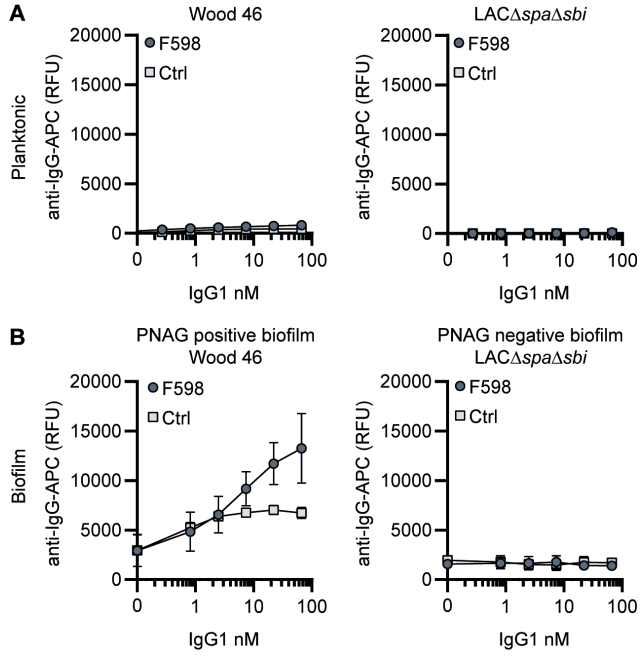

Figure S2. F598-IgG1 binds poly-N-acetyl glucosamine (PNAG)-dependent biofilms specifically. (**A**) Planktonic bacteria of LAC (left) and Wood46 (right) were grown to exponential phase and incubated with a concentration range of F598-IgG1. MAb binding was detected using APC-labeled anti-human IgG antibodies and flow cytometry and plotted as geoMFI of the bacterial population. (**B**) Biofilm of Wood46 and LAC were grown for 24 h and incubated with a concentration range of F598-IgG1. MAb binding was detected using APC-labeled anti-human IgG antibodies and a plate reader and plotted as fluorescence intensity per well. Data represent mean + SD of three independent experiments.

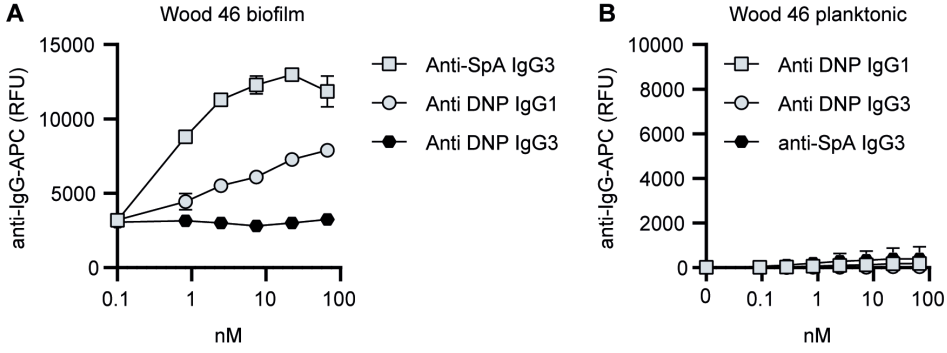

Figure S3. Background control monoclonal antibody (mAb) binding to Wood46 biofilm due to incorporation of secreted SpA in biofilm. (**A**) Wood46 biofilm was grown for 24 h and incubated with control IgG1, IgG3 and anti-SpA IgG3. Mab binding was detected using anti-human-kappa-AF647 antibodies and a plate reader. (**B**) Planktonic exponential Wood46 bacteria were incubated with control IgG1, IgG3 and anti-SpA IgG3. Mab binding was detected using anti-human-kappa-AF647 antibodies and flow cytometry. Data represent mean + SD of three independent experiments.

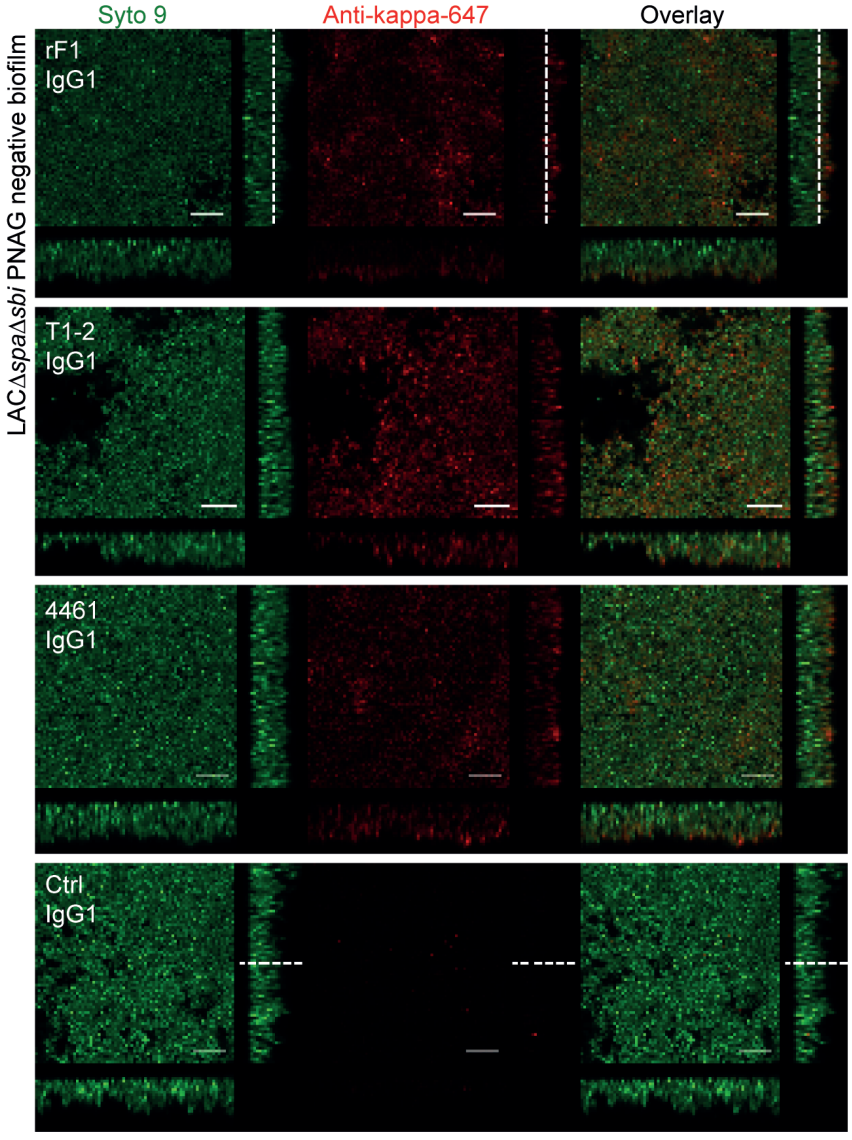

Figure S4. Orthogonal views of poly-N-acetyl glucosamine (PNAG)-negative biofilm incubated with IgG1 monoclonal antibodies (mAbs). Biofilm was grown for 24 h and incubated with 66 nM IgG1 mAbs or isotype controls. Bacteria were visualized by Syto 9 (green) and mAb binding was detected by staining with Alexa Fluor 647 conjugated goat-anti-human-kappa F(ab')2 antibody (red). Syto 9 and AF647 were imaged using 488 and 633 nm lasers. Images are representative for a total of three Z-stacks per condition and two independent experiments. Scale bars: 10 µm.

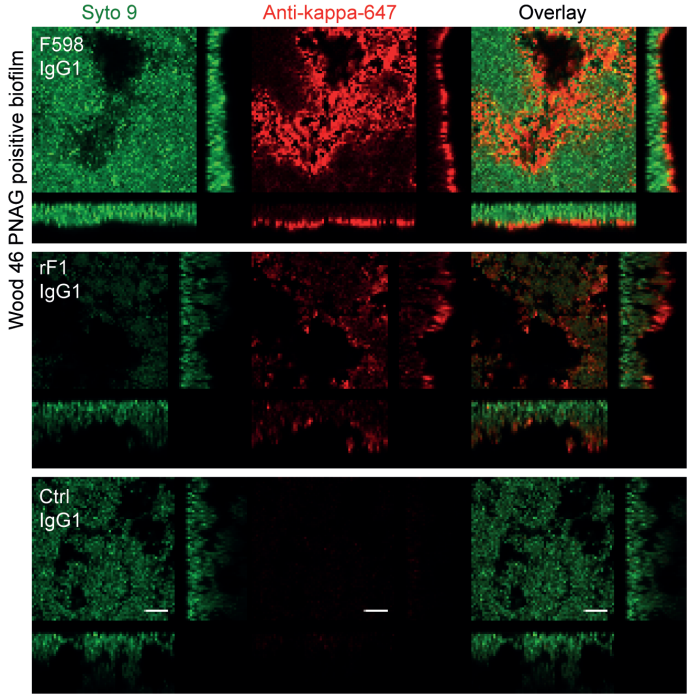

Figure S5. Orthogonal views of poly-N-acetyl glucosamine (PNAG)-positive biofilm incubated with IgG1 monoclonal antibodies (mAbs). Biofilm was grown for 24 h and incubated with 66 nM IgG1 mAbs or isotype controls. Bacteria were visualized by Syto 9 (green) and mAb binding was detected by staining with Alexa Fluor 647 conjugated goat-anti-human-kappa F(ab')2 antibody (red). Syto 9 and AF647 were imaged using 488 and 633 nm lasers. Images are representative for a total of three Z-stacks per condition and two independent experiments. Scale bars: 10 µm.

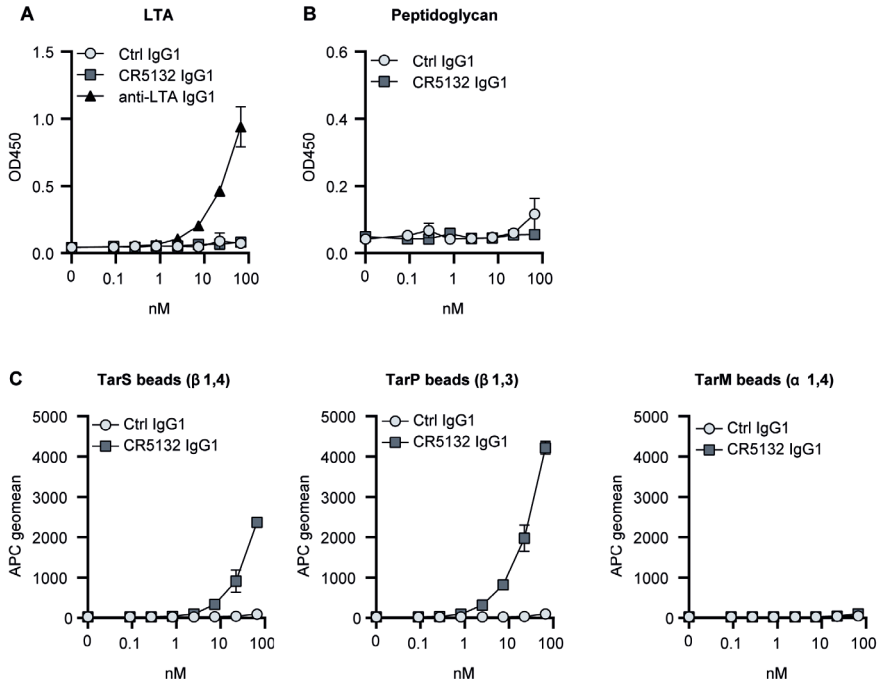

Figure S6. Target identification of CR5132. (**A, B**) ELISA plates were coated with purified peptidoglycan (**A**) and LTA (**B**). Plates were incubated with a concentration range of monoclonal antibodies (mAbs), and mAb binding was detected using anti-human kappa-HRP antibodies. (**C**) Wall teichoic acid (WTA)-coated beads were incubated with a concentration range of mAbs. mAb binding was detected using APC-labeled anti-human IgG antibodies and flow cytometry and plotted as geoMFI + SD of duplicates in one independent experiment (**B, C**).

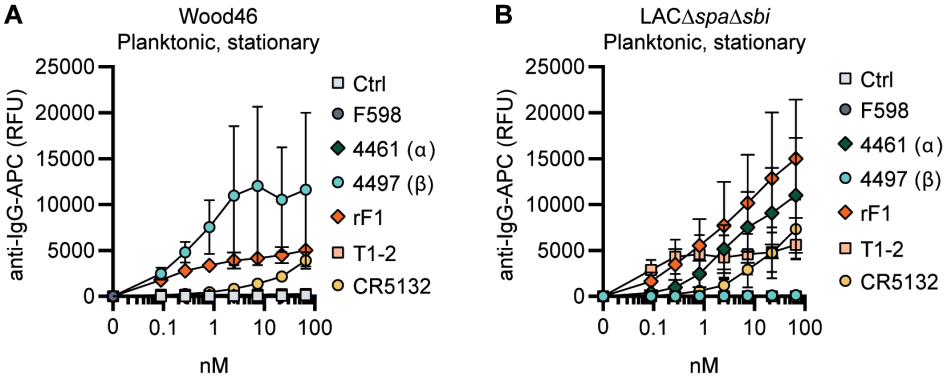

Figure S7. Binding of the monoclonal antibody (mAb) panel to stationary phase planktonic cultures.Planktonic bacteria of Wood46 (**A**) LAC (**B**) were grown to stationary phase and incubated with a concentration range of mAbs. mAb binding was detected using APC-labeled anti-human IgG antibodies and flow cytometry and plotted as geoMFI of the bacterial population. Data represent mean + SD of three independent experiments.

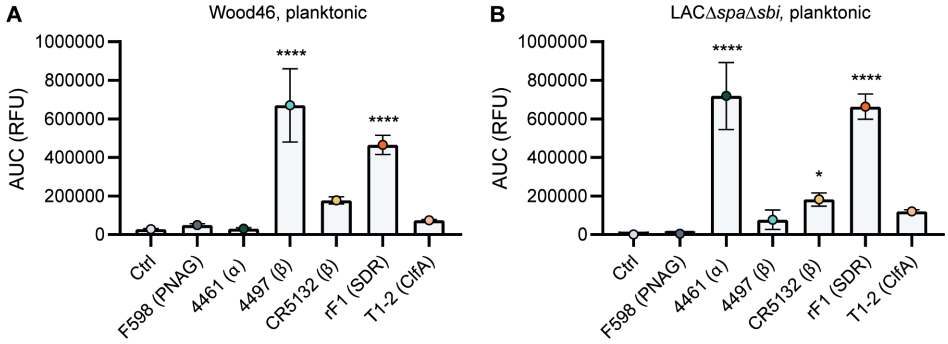

Figure S8. Comparative binding of IgG1 monoclonal antibodies (mAbs) to planktonic bacteria. Planktonic bacteria of Wood46 (**A**) and LAC (**B**) were grown to exponential phase and incubated with a concentration range of IgG1 mAbs. mAb binding was detected using APC-labeled anti-human IgG antibodies and flow cytometry. Data are expressed as area under the curve (AUC) of the binding curve (mean + SD) of three independent experiments. One-way ANOVA followed by Dunnett test was performed to test for differences in antibody binding versus control and displayed only when significant as *p≤0.05, **p≤0.01, ***p≤0.001, or ****p≤0.0001.

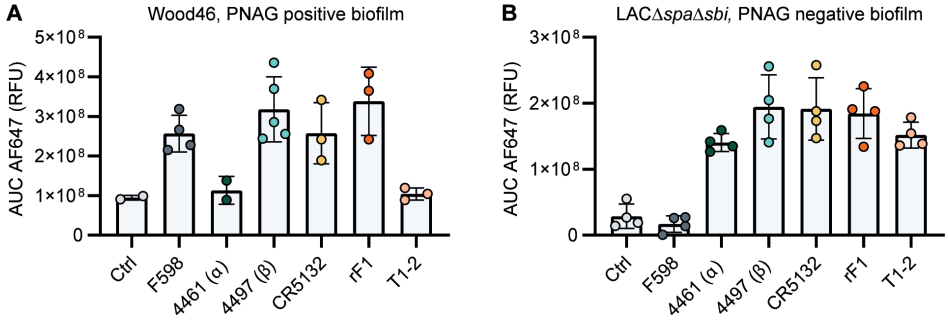

Figure S9. Mean total fluorescence per Z-stack corresponds to plate reader data. The total AF647 signal of obtained Z-stack profiles of biofilms Wood46 (**A**) and LAC (**B**) was calculated using Leica LAS AF imaging software. Data are representative for two independent experiments.

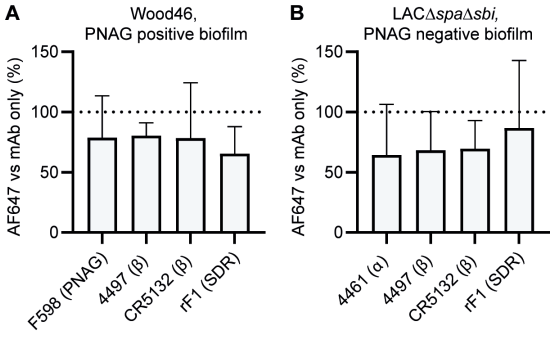

Figure S10. Binding in the presence of pooled serum IgG. Biofilm cultures of Wood46 (**A**) and LAC (**B**) were incubated with 10 µg/mL AF647-conjugated IgG1 monoclonal antibodies (mAbs) in buffer or buffer containing 250 µg/mL pooled IgG. Data are expressed as % relative to mAb binding in buffer of three independent experiments performed in duplicate.

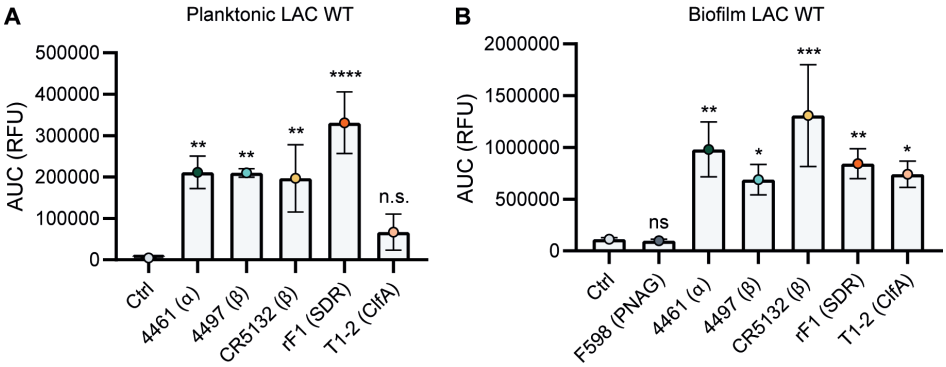

Figure S11. Binding of IgG3 monoclonal antibodies (mAbs) to planktonic and biofilm LAC wild type. (**A**) Planktonic bacteria of LAC WT (AH1263) were grown to exponential phase and incubated with a concentration range of IgG3 mAbs. mAb binding was detected using APC-labeled anti-human IgG antibodies and flow cytometry and plotted as geoMFI of the bacterial population. (**B**) LAC WT (AH1263) biofilm was grown for 24 hr and incubated with a concentration range of IgG3 mAbs. mAb binding was detected using APC-labeled anti-human IgG antibodies and a plate reader. Data represent mean + SD of three independent experiments. One-way ANOVA followed by Dunnett test was performed to test for differences in antibody binding versus control and displayed only when significant as *p≤0.05, **p≤0.01, ***p≤0.001, or ****p≤0.0001.

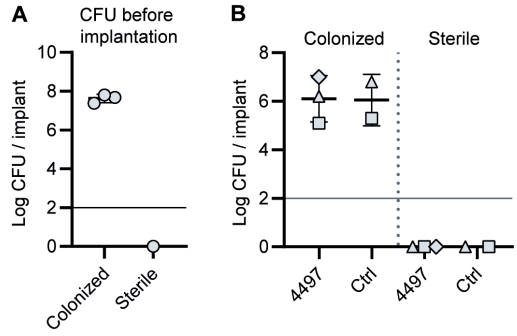

Figure S12. CFU count before implantation and after implantation. (**A**) 5 mm PU catheter segments were inoculated with LAC. After 48 hr of incubation, catheters were washed and sonicated and viable CFU counts recovered were determined. Each data point represents an independent experiment. (**B**) Mice received subcutaneous pre-colonized and sterile catheters and 2 days later were injected with [^{111}In]In-4497-IgG1 (n = 3) or [^{111}In]In-palivizumab (n = 2). At time point 120 hr, mice were sacrificed and catheters were removed to determine CFU counts. Horizontal lines indicate detection limit.

A

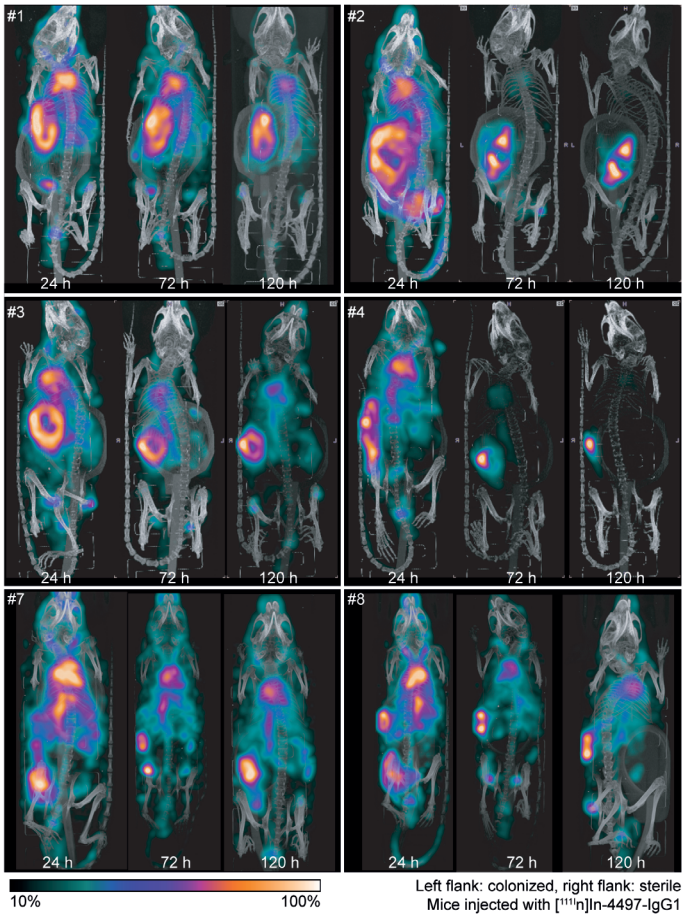

B

24h		
Mouse nr	% colonized	% sterile
1	9,7	1,3
2	10,8	0,0
3	11,2	0,3
4	11,3	2,3
7	1,2	2,0
8	3,5	0,1
9 (Fig 7)	6,1	1,8

72h		
Mouse nr	% colonized	% sterile
1	6,1	0,2
2	16,2	0,1
3	7,5	0,2
4	11,7	2,6
7	1,3	0,3
8	4,0	0,2
9 (Fig 7)	9,5	1,1

120h		
Mouse nr	% colonized	% sterile
1	3,8	0,0
2	13,9	0,3
3	3,5	0,0
4	8,5	0,0
7	3,0	0,3
8	2,8	0,2
9 (Fig 7)	9,1	0,7

Figure S13. Localization of [^{111}In]In-4497-IgG1 to subcutaneous implant pre-colonized with biofilm in a mouse model. (**A**) Maximum intensity projections of [^{111}In]In-4497-IgG1 injected in mice subcutaneously bearing pre-colonized (left flank) and sterile (right flank) catheters. Implantation of colonized and sterile implants was randomized; however, for clarity, we here display all colonized implants on the left. (**B**) Corresponding percentages in regions of interest (ROIs) per mouse.

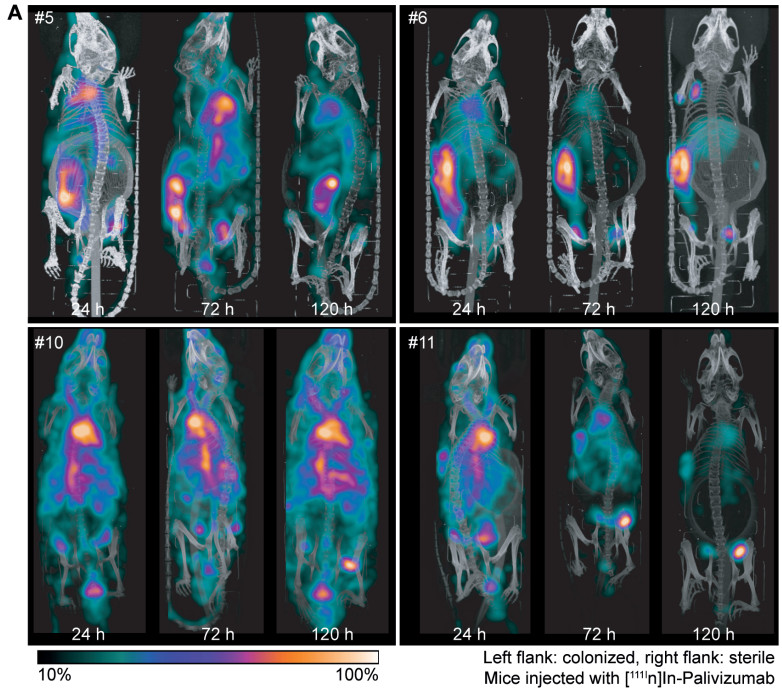

B

24h		
Mouse nr	% colonized	% sterile
5	5,9	0,5
6	11,2	3,1
10	2,0	1,3
11	0,9	0,8

72h		
Mouse nr	% colonized	% sterile
5	4,0	0,5
6	13,7	0,0
10	1,6	0,2
11	1,8	0,8

120h		
Mouse nr	% colonized	% sterile
5	2,9	0,0
6	7,3	0,0
10	0,7	0,2
11	1,3	0,7

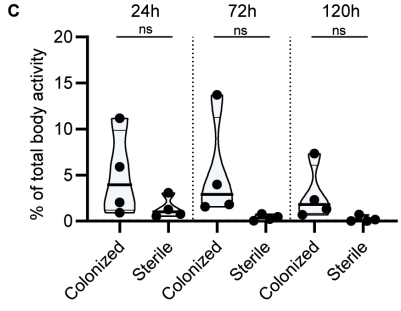

Figure S14. Localization of [^{111}In]In-palivizumab to a subcutaneous implant pre-colonized with biofilm. (**A**) Maximum intensity projections (corrected for decay) of mice subcutaneously bearing pre-colonized (left flank) and sterile (right flank) catheters. Two days after implantation, mice were injected with 7.5 MBq [^{111}In]In-palivizumab (n = 4) and imaged at 24 hr, 72 hr, and 120 hr after injection. Implantation of colonized and sterile implants was randomized, but for display all colonized implants are shown at the left flank. (**B**) Corresponding percentages in regions of interest (ROIs) per mouse. (**C**) The activity detected in regions of interests was expressed as a percentage of total body activity. Each data point represents one mouse. A two-tailed paired t-test was performed to test for differences in activity in sterile versus colonized implants.

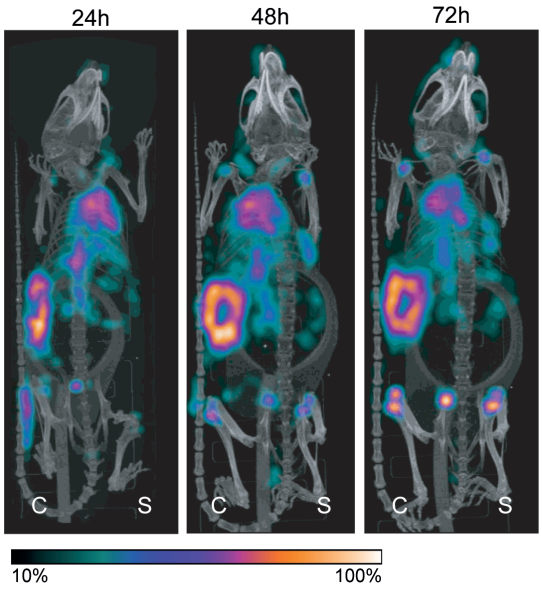

Figure S15. Pilot study for localization of [^{111}In]In-4497-IgG1 to subcutaneous implant-associated biofilm in a mouse model. One mouse received subcutaneous pre-colonized and sterile catheters and 2 days later was injected with 4 MBq [^{111}In]In-4497-IgG1. The same mouse was imaged at 24 hr, 48 hr, and 72 hr. Maximum intensity projections of [^{111}In]In-4497-IgG1 injected in mice subcutaneously pre-colonized (left flank) and sterile (right flank) catheters.

Supplementary tables

Supplementary File 1. Protein sequences used for human monoclonal antibody production.

Clone, *target*	Sequence	Reference
VH variable heavy chain		
G2a2, *Anti-DNP*	DVRLQESGPGLVKPSQSLSLTCSVTGYSITNSYYWNWIRQFPGN-KLEWMVYIGYDGSNNYNPSLKNRISITRDTSKNQFFLKLNSVT-TEDTATYYCARATYYGNYRGFAYWGQGTLVTVSA	Gonzalez 2003 [41]
B12, *Anti-gp120*	QVQLVQSGAEVKKPGASVKVSCQASGYRFSNFVIHWVRQA-PGQRFEWMGWINPYNGNKEFSAKFQDRVTFTADTSAN-TAYMELRSLRSADTAVYYCARVGPYSWDDSPQDNYYMDVWGKGT-TVIVSS	Barbas 1993 [42] Saphire 2001 [43]
4461, *Anti-WTA(α)*	QVQLVQSGAEVRKPGASVKVSCKASGYSFTDYYMHWVRQAPGQ-GLEWMGWINPKSGGTNYAQRFQGRVTMTGDTSISAAYMDLASLTS-DDTAVYYCVKDCGSGGLRDFWGQGTTVTVSS	WO/2014/193722 A1
4497, *Anti-WTA(β)*	EVQLVESGGGLVQPGGSLRLSCSASGFSFNSFWMHWVRQVP-GKGLVWISFTNNEGTTTAYADSVRGRFIISRDNAKNTLYLEMNNL-RGEDTAVYYCARGDGGLDDWGQGTLVTVSS.	WO/2014/193722 A1 Lehar 2015 [38] Fong 2018 [39]
CR5132	EVLESGGGLVQPGGSLRLSCSDSGFSFNNYWMTWVRQAPGK-GLEWVANINRDGSDKYHVDSVEGRFTISRDNSKNSLYLQMNNLRAD-DAA VYFCARGGRTTSWYWRNWGQGTLVTVSS	US 2012/0141493 A1
F598, *Anti-PNAG*	QVQLQESGPGLVKPSETLSLTCTVSGGSISGYYWSWIRQPPGK-GLEWIGYIHYSRSTNSNPALKSRVTISSDTSKNQLSLRLSSVTAAD-TAVYYCARDTYYYDSGDYEDAFDIWGQGTMVTVSS	US/2006/0115486 A1 Seq25 Kelly-Quintos 2006 [74] Soliman 2018 [21]
rF1, *Anti-GlcNac pan-SDR*	EVQLVESGGGLVQPGGSLRLSCAASGFTLSRFAMSWVRQAP-GRGLEWVASINSGNNPYYARSVQYRFTVSRDVSQNTVSLQMNNL-RAEDSATYFCAKDHPSSGWPTFDSWGPGTLVTVSS	WO/2016/090040 Seq13 Hazenbos 2013 [40]
T1-2, *Anti-ClfA*	QVQLKESGPGLVAPSQSLSITCAISGFSLSRYSVHWVRQPPGK-GLEWLGMIWGGGNTDYNSALKSRLSISKDNSKSQVFLKMNSLQTD-DTAMYYCARKGEFYYGYDGFVYWGQGTLVTVSA	WO 02072600 A2
A120, *Anti-LTA*	EVMLVESGGGLVQPKGSLKLSCAASGFTFNTYAMNWVRQAPGK-GLEWVARIRSKSNNYATYYADSVKDRFTISRDDSQSMLYLQMNNLK-TEDTAMYYCVRRGGKETDYAM DYWGQGTSVT VSS	WO 03/059259
10919 *Anti-SpA*	EVQLVQSGAEVKKPGASVKVSCKASGYTFTSYYMHWVRQA-PGQGLEWMGIINPRVGSTSYAQKFQGRVTMTRDTSTST-VYMELSSLRSEDTAVYYCARGRPLSGTGGHHYFDYWGQGTLVT-VSS	US2018/0105584
VL variable light chain		
G2a2, *Anti-DNP*	DIRMTQTTSSLSASLGDRVTISCRASQDISNYLNWYQQKPDGT-VKLLIYYTSRLHSGVPSRFSGSGSGTDYSLTISNLEQEDIATYFC-QQGNTLPWTFGGGTKLEIK	Gonzalez 2003 [41]
B12, *Anti-gp120*	EIVLTQSPGTLSLSPGERATFSCRSSHSIRSRRVAWYQHKPGQA-PRLVIHGVSNRASGISDRFSGSGSGTDFTLTITRVEPEDFALYYC-QVYGASSYTFGQGTKLERK	Barbas 1993 [42] Saphire 2001 [43]
4461, *Anti-WTA(α)*	DIQMTQSPDSLAVSLGERATINCKSSQSVLSRANNNYYVAWYQHKP-GQPPKLLIYWASTREFGVPDRFSGSGSGTDFTLTINSLQAEDVAVYY-CQQYYTSRRTFGQGTKVEIK	WO/2014/193722 A1
4497, *Anti-WTA(β)*	DIQLTQSPDSLAVSLGERATINCKSSQSIFRTSRNKNLLNWYQQRP-GQPPRLLIHWASTRKSGVPDRFSGSGFGTDFTLTITSLQAEDVAIYY-CQQYFSPPYTFGQGTKLEIK	WO/2014/193722 A1 Lehar 2015 [38] Fong 2018 [39]
CR5132	STDIQMTQSPSTLSASVGDRVTITCRASQSISSWLAWYQQKPG-KAPKLLIYKASSLESGVPSRFSGSGSGTEFTLTISSLQPDDFATYYC QQYNSYPLTFGGGTKLEIK	US 2012/0141493 A1

Supplementary File 1. Protein sequences used for human monoclonal antibody production. ()

Clone, *target*	Sequence	Reference
F598, *Anti-PNAG*	QLVLTQSPSASASLGASVKLTCTLSSGHSNYAIAWHQQQPGKG-PRYLMKVNRDGSHIRGDGIPDRFSGSTSGAERYLTISSLQSEDEAD-YYCQTWGAGIRVFGGGTKLTVLG	US/2006/0115486 A1 Seq 26 Kelly-Quintos 2006 [74] Soliman 2018 [21]
rF1, *Anti-GlcNac pan-SDR*	DIQLTQSPSALPASVGDRVSITCRASENVGDWLAWYRQKPGKAPNL-LIYKTSILESGVPSRFSGSGSGTEFTLTISSLQPDDFATYYCQHYMRF-PYTFGQGTKVEIK	WO/2016/090040_ Seq14 Hazenbos 2013 [40]
T1-2, *Anti-ClfA*	NIMMTQSPSSLAVSAGEKVTMSCKSSQSVLYSSNQKNYLAWY-QQKPGQSPKLLIYWASTRESGVPDRFTGSGSGTDFTLTISSVQAED-LAVYYCHQYLSSYTFGGGTKLEIK	WO 02072600 A2
A120, *Anti-LTA*	DIVLSQSPAILSASPGEKVTMTCRASSSVSYMHWYQQKPGSSP-KPWIYATSNLASGVPARFSGSGSGTSYSLTISRVEAEDAATYYC-QQWSSNPPTFGGGTKLEIK	WO 03/059259
10919 *Anti-SpA*	EIVLTQSPATLSVSPGERATLSCQASQDISNYLNWYQQKPGQAPRL-LIYDASNLETGIPARFSGSGSGTEFTLTISSLQSEDFAVYYCQQVY-ALPPWTFGGGTKVEIK	US2018/0105584
HC constant regions		
IgG1	ASTKGPSVFPLAPSSKSTSGGTAALGCLVKDYFPEPVTVSWNS-GALTSGVHTFPAVLQSSGLYSLSSVVTVPSSSLGTQTYICNVNH-KPSNTKVDKKVEPKSCDKTHTCPPCPAPELLGGPSVFLFPPKP-KDTLMISRTPEVTCVVVDVSHEDPEVKFNWYVDGVEVHNAKTK-PREEQYNSTYRVVSVLTVLHQDWLNGKEYKCKVSNKALPAPIEK-TISKAKGQPREPQVYTLPPSREEMTKNQVSLTCLVKGFYPSDIA-VEWESNGQPENNYKTTPPVLDSDGSFFLYSKLTVDKSRWQQGNVF-SCSVMHEALHNHYTQKSLSLSPGK	Kabat 1991 [44]
IgG3	ASTKGPSVFPLAPCSRSTSGGTAALGCLVKDYFPEPVTVSWNS-GALTSGVHTFPAVLQSSGLYSLSSVVTVPSSSLGTQTYTCNVNHK-PSNTKVDKRVELKTPLGDTTHTCPRCPEPKSCDTPPPCPRCPEPK-SCDTPPPCPRCPEPKSCDTPPPCPRCPAPELLGGPSVFLFPPKPK-DTLMISRTPEVTCVVVDVSHEDPEVQFKWYVDGVEVHNAKTKPRE-EQYNSTFRVVSVLTVLHQDWLNGKEYKCKVSNKALPAPIEKTISKT-KGQPREPQVYTLPPSREEMTKNQVSLTCLVKGFYPSDIAVEWESS-GQPENNYNTTPPMLDSDGSFFLYSKLTVDKSRWQQGNIFSCS-VMHEALHNRFTQKSLSLSPGK	Derived from pFuse vector (Invivogen)
LC constant regions		
Kappa class	RTVAAPSVFIFPPSDEQLKSGTASVVCLLNNFYPREAKVQWKVD-NALQSGNSQESVTEQDSKDSTYSLSSTLTLSKADYEKHKVYACEV-THQGLSSPVTKSFNRGEC	Kabat 1991 [44]

CHAPTER 3

Development of Fab fragment-enzyme conjugates to degrade *Staphylococcus aureus* biofilm

Lisanne de Vor, Carla J.C. de Haas, Piet C. Aerts, Jos A.G. van Strijp, Kok P.M. van Kessel, Suzan H.M. Rooijakkers

Department of Medical Microbiology, University Medical Center Utrecht, Utrecht University, Utrecht, The Netherlands

Manuscript in preparation

Abstract

Staphylococcus aureus is a common cause of implant related infections. These infections are difficult to treat because they often involve biofilm formation. Bacteria in a biofilm are protected from antimicrobial agents by a self-made extracellular polymeric substance (EPS), composed of extracellular DNA, polysaccharides and proteins. By degrading the EPS and releasing *S. aureus* from the biofilm, bacteria can become susceptible to antibiotics and the immune system. Therefore, the EPS is an attractive target for anti-biofilm therapy. Enzymes such as DNase I (hydrolyzing DNA) and Dispersin B (hydrolyzing polysaccharide PNAG) have been shown to be effective for easily accessible infections, but delivery of the enzymes to the site of infection via intravenous (IV) injection is challenging. One way to enhance delivery of enzymes is by conjugating them to monoclonal antibodies. We recently described clone 4497-IgG1, recognizing the abundant surface glycopolymer WTA, to localize specifically to biofilm in a mouse model. In this study, we used clone 4497 to produce 4497-Fab-huDNase I and 4497-Fab-DspB and characterized their functionality *in vitro*. First, resulting fusion proteins retained their ability to specifically bind bacteria. Second, the fusion of DNase I or DspB to Fab fragments yielded products with specific enzymatic activity. Furthermore, the fusion proteins were shown to prevent *S. aureus* biofilm formation and to degrade preformed biofilm *in vitro*. Further research needs to address the benefit of a specific antibody compared to an enzyme coupled to control antibody or an enzyme alone.

Introduction

Staphylococcus aureus is a common cause of hospital acquired infections [1,2]. Due to the increasing use of medical implants, 25% of healthcare associated infections are related to implants such as heart valves, intravenous catheters and prosthetic joints [3]. These types of infections are difficult to treat because they often involve biofilm formation. *S. aureus*, known for its ability to form biofilm [4,5], causes one third of all implant related infections in Europe and the United States [6,7]. Bacteria in a biofilm produce a self-made extracellular polymeric substance (EPS) including extracellular DNA, polysaccharides and proteins [5,8]. This EPS forms a barrier for many antimicrobial agents and thereby makes biofilm related infections difficult to treat.

Over the past years, many studies have explored agents that destroy or destabilize EPS [9–11] . The rationale is that detaching bacterial cells from their EPS renders bacteria more susceptible for antimicrobial agents and the host immune system [11–14]. One class of agents that promote biofilm degradation is EPS degrading enzymes such as deoxyribonuclease I (DNase I) and Dispersin B (DspB). DNase I degrades extracellular DNA, which forms an important component of the *S. aureus* EPS [15]. DspB degrades poly-(β-1,6)-*N*-acetylglucosamine (PNAG, also known as PIA; [16], an extracellular polysaccharide that forms the major EPS component in 1/3 of *S. aureus* clinical isolates [17–23]. Many studies show that DNase I can disperse *S. aureus* from *in vitro* biofilm [14,24] and sensitize bacteria to antibiotics including tobramycin and ampicillin [25,26]. *In vitro* treatment of *S. aureus* biofilm with DspB also detaches and sensitizes bacteria to antibiotics [11,25]. Furthermore, a coating of DspB in combination with triclosan on medical implants decreased *S. aureus* colonization on these implants in rabbits [27]. A combination of DNase I and DspB was also shown effective in decolonizing pig skin from *S. aureus* after topical application [28].

DNase I and DspB are currently being developed into drugs and tested in clinical trials. Recombinant human DNase I (rhDNase I) is manufactured as Pulmozyme® by Genentech Inc. [29]. It is used for the treatment of *P. aeruginosa* infections in cystic fibrosis patients [30] and is administered via inhalation. One clinical trial with aerosolized DNase I given to cystic fibrosis patients next to the standard of care yielded a drastic reduction in the prevalence of several pathogens (especially *S. aureus*) in the lungs [31]. DspB is being formulated by Kane Biotech as a hydrogel and wound gel spray for treatment of chronic wounds and is still in preclinical stages of development. Although these results are promising, non-topological delivery of DspB or DNase I to the site of infection via IV injection is still challenging, and the use of DspB or DNase I to remove preformed biofilm in less accessible locations in the body has not been reported yet. In cancer and

sepsis models IV injection of DNAse I has been shown to be safe and successful [32–37], and proved to be active in the blood but not in the tissues. Pharmacokinetic studies show that after IV administration, majority of rhDNase I is cleared from systemic circulation within hours due to its small size, without accumulation in tissues [38].

One way to enhance delivery of drugs (e.g., cytokines, antibiotics, enzymes) to the site of action is by using the specific binding capacity of monoclonal antibodies. This results in less side effects of the drug towards healthy tissue and/or less immunogenic response to the protein drug itself [39]. We previously reported binding of several human IgG1 monoclonal antibodies (mAbs) to *S. aureus* biofilm [17]. Here we used one of these mAbs, clone 4497 which recognizes β-GlcNAc Wall Teichoic Acid, as Fab fragments fused to huDNase I or DspB and characterized their functionality of these fusion proteins *in vitro*. First, resulting fusion proteins retained their ability to specifically bind bacteria. Second, the fusion of DNase I or DspB to Fab fragments yielded products with specific enzymatic activity. Furthermore, the fusion proteins were shown to prevent *S. aureus* biofilm formation and to degrade preformed biofilm in vitro.

Results

Construct of anti-WTA-Fab-DNase I and anti-WTA-Fab-DspB fusion proteins.

We selected the 4497 clone for production of the Fab-enzyme fusion proteins, because it fulfilled several criteria. First, the target (β-GlcNAc-WTA) is highly abundant on *S. aureus in vitro* [40,41]. It was estimated that about 50 000 binding sites are present on one *S. aureus* [40]. Moreover, the target is not present on human cells. Second, nearly all sequenced *S. aureus* strains contain the TarS gene, coding for the glycosyltransferase responsible for the β-GlcNAc modification [42]. In our previous study, the 4497 mAb was shown to bind the two most relevant biofilm phenotypes (PNAG-negative and PNAG-positive) in the clinic [18–23]. Third, we showed previously that 4497-IgG1 has the capacity to specifically localize to biofilm coated implants in vivo [17]. Instead of using the full length IgG1 (150 kDa) described in de Vor *et al.* [17], we used Fab fragments (50 kDa) which lack the Fc region, because smaller antibody fragments may have an advantage when tissue penetration is required [39].

Because Fab fragments are monovalent binders and IgG1 molecules are bivalent binders, we first tested whether monovalent 4497 Fab fragments were able to recognize PNAG-negative and PNAG-positive biofilm. Therefore, we produced 4497-Fab fragments and nonspecific control b12(anti-HIV-gp120)-Fab fragments. The variable heavy

(VH) and light chain (VL) regions of 4497 or b12 were cloned separately into expression vectors containing the human constant heavy Fab (CH1) or the human constant light (CL-kappa) chain backbone. After expression in HEK cells and isolation via the His-tag coupled to the CH1 region, we tested the binding of 4497-Fab fragments and b12-Fab fragments to PNAG-negative (LAC spa-sbi- [17,43–45]) **(Figure 1A)** and PNAG-positive (Wood46 [17,46,47]) **(Figure 1B)** *S. aureus* biofilm, using an Alexa647 labeled anti-kappa for detection in a plate reader. Indeed, 4497-Fab fragments showed binding to both types of biofilms, indicating that converting full length 4497-IgG1 to Fab fragments did not affect the target specificity.

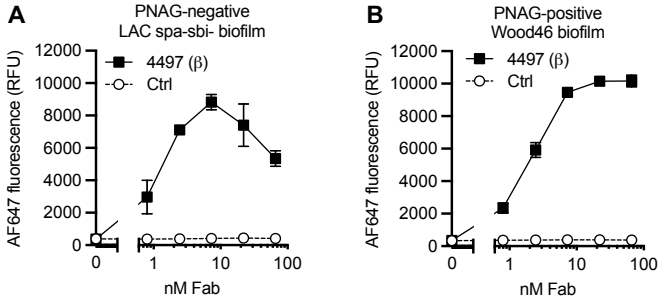

Figure 1. 4497-Fab fragments binding to PNAG-positive and PNAG-negative biofilms. (A,B) Biofilm of Wood46 (A) and LAC (B) were grown for 24h and incubated with a concentration range starting from 66 nM 4497 Fab-fragments or Ctrl Fab-fragments (b12). Fab binding was detected using Alexa Fluor-647-labeled anti-human kappa antibodies and a plate reader and plotted as fluorescence intensity per well. Data represent mean + SD of 2 (Wood46) and 3 (LAC) independent experiments.

We used a genetic coupling method where one DspB/DNase I molecule was conjugated at a fixed position on the Fab fragment, because random chemical labeling can affect epitope binding of Fab fragments. To produce Fab-enzyme fusion proteins, the huDNase I or DspB enzyme sequences were cloned downstream the CL-kappa sequence, separated by a semiflexible linker sequence (78 amino acids) that was designed to have sufficient flexibility and rigidity to allow for a large enzyme sweeping radius **(Figure 2A, Table S1)**[48]. The CH1 vector to produce Fab-enzyme fusion proteins was identical to the one used to produce wild type Fab fragments **(Figure 2B)**. **Figure 2C** shows a schematic representation of the resulting fusion proteins. After transducing the resulting CH1 and CL-kappa vectors in HEKT293 cell lines, supernatants were checked for expression with SDS-page **(Figure 2D**. A clear band was seen at the expected MW of 4497-Fab-DspB (97 kDa), indicating good expression. 4497-Fab-DNase I (expected MW 85 kDa) was expressed less well, but we were able to isolate sufficient amounts to perform experiments. Next to 4497-DNase I and 4497-Fab-DspB, we produced b12-Fab-DNase I as a control for 4497-Fab-DNase I. Because of production issues, we produced G2a2(anti-di-nitrophenol)-Fab-DspB as a control for 4497-Fab-DspB. Next

to 4497-Fab-DspB and 4497-Fab-Dnase I, we produced a 4497 Fab fragment fused to proteinase K, which can also degrade *S. aureus* biofilm [10]. However, we could not detect any protein in the 4497-Fab-proteinase K supernatant, indicating that proteinase K was active and cleaved all proteins produced, including the antibody.

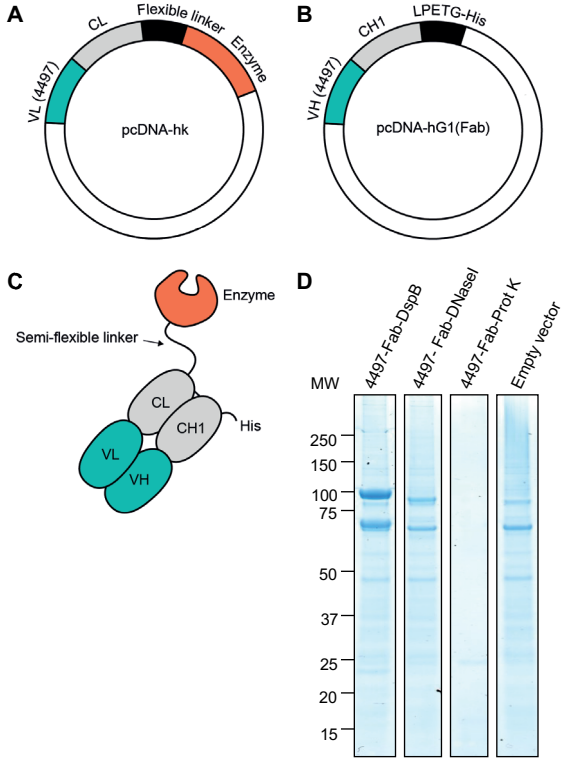

Figure 2. Production of 4497-Fab-DNase I and 4497-Fab-DspB. (A) Schematic representation of light chain expression vector. Variable light (VL) chain sequences were cloned upstream into pcDNA vectors containing the human kappa backbone. A semi-flexible linker sequence and the hDNase I or DspB enzyme sequences were cloned downstream the kappa sequence. (B) Schematic representation of heavy chain expression vector. Variable heavy (VH) chain sequences were cloned upstream into pcDNA vectors containing the human IgG1 (Fab) backbone. An LPETG sequence and a His-tag for isolation were cloned downstream the human IgG1 (Fab) sequence. (C) Schematic representation of Fab-enzyme constructs. (D) SDS page gel with expression supernatants (without DTT). Abbreviations: VL: variable light, VH: variable heavy, CL: constant light (kappa), CH: constant heavy, hk: human kappa, G1 (Fab): IgG1 subclass Fab sequence, MW: molecular weight.

4497-Fab-DNase I and 4497-Fab-DspB bind *S. aureus* and show enzymatic activity.

Next, we tested the Fab-enzyme fusion proteins for their functionality. First, binding of 4497-Fab-DNase I and 4497-Fab-DspB to planktonic *S. aureus* was compared with wild type 4497-Fabs. We compared the Fab binding to planktonic *S. aureus* because degradation of biofilm could complicate the detection of binding Fab fragments. After

incubation of planktonic *S. aureus* with the different Fab fragments, we detected binding using flow cytometry and a fluorescent anti-kappa detection antibody. 4497-Fab-DNase I and 4497-Fab-DspB showed comparable binding to 4497-Fab **(Figure 3A)**, indicating that fusion of DNase and DspB to Fab fragments did not influence binding of the Fab fragments to planktonic bacteria.

Second, we tested whether genetic fusion of enzymes to Fab fragments yielded fusion proteins with enzymatic activity. To measure DspB activity, we measured cleavage of pNitroPhenol-GlcNAC (pNPGlcNAc), which results in a yellow color that can be measured with a plate reader [49]. As expected, both 4497-Fab-DspB and G2a2-Fab-DspB could convert pNPGlcNAc **(Figure 3B)**, while the others could not. There was no significant difference in activity between 4497-Fab-DspB and G2a2-Fab-DspB. Similarly, we detected DNase I activity in a PicoGreen fluorescence assay [50], where a starting amount of substrate DNA is labeled with PicoGreen and a decrease in PicoGreen fluorescence can be detected over time after DNA cleavage. Compared to b12-Fab and 4497-Fab, only 4497-Fab-DNase I and b12-Fab-DNase I could cleave substrate DNA **(Figure 3C)**. The Area Under the Curve (AUC) was calculated to quantify DNAse activity **(Figure 3D)** for statistical analysis and no difference was found between 4497-Fab-DNase I and b12-Fab-DNase I. In conclusion, fusion of DNase and DspB to Fab fragments did not influence binding of the Fab fragments to bacteria and yields products with specific enzymatic activity.

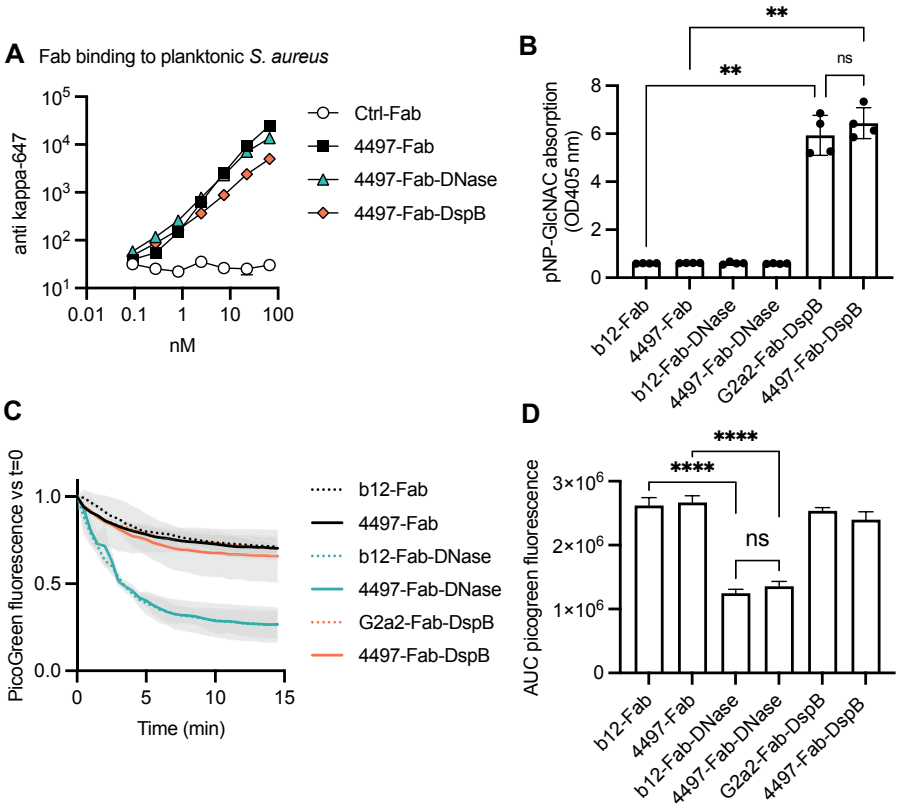

Figure 3. Binding and activity of Fab-enzyme conjugates. (A) Planktonic Wood46 were grown to exponential phase and incubated with a concentration range starting from 66 nM 4497-Fab, b12-Fab, 4497-Fab-DNas I or 4497-Fab-DspB. Fab binding was detected using Alexa Fluor-647-labeled anti-human kappa antibodies and flow cytometry and plotted as geoMFI of the bacterial population. Data represent mean + SD of 2 independent experiments. (B) Conversion of pNPGlcNAc by DspB. 500 nM Fab fragments were incubated with 10 mM pNPGlcNAc for 15 minutes. To quantify substrate conversion, the optical density at 405 nm was measured using a plate reader. Data represent mean + SD of 4 independent experiments. One-way ANOVA followed by Tukey test was performed to test for differences in antibody binding versus control and displayed only when significant as *P ≤ 0.05, **P ≤ 0.01, ***P ≤ 0.001, or ****P ≤ 0.0001. (C) Conversion of DNA by DNase I. 25 nM Fab fragments were incubated with 20 ng dsDNA for 15 minutes in presence of PicoGreen. PicoGreen fluorescence was measured every 30 seconds. Data is normalized against t=0 minutes. Data represent mean + SD of 4 independent experiments. SD is plotted as grey area. (D) Data of (C) were expressed as AUC of the curve (mean + SEM) of 3 independent experiments. One-way ANOVA followed by Tukey test was performed to test for differences in antibody binding versus control and displayed only when significant as *P ≤ 0.05, **P ≤ 0.01, ***P ≤ 0.001, or ****P ≤ 0.0001.

4497-Fab-DspB and 4497-Fab-DNase I prevent biofilm formation in vitro.

Next, we tested the ability of the different Fab fragments to prevent biofilm formation by *S. aureus*. After 24 hours of biofilm formation in the presence of Fab fragments, we measured the biofilm biomass attached to surface of the 96-wells plate by crystal violet staining and measuring the optical density at 595 nm. As expected, the formation of PNAG-negative (i.e., DNA dependent) biofilm could be prevented by 4497-Fab-DNase I and not by DspB coupled Fab fragments **(Figure 4A)**. Interestingly, b12-Fab-DNase could also prevent PNAG-negative biofilm formation, indicating that the DNase I domain could target biofilm DNA without specific binding of the Fab domain. Similarly, wild type 4497-Fab, b12-Fab, 4497-Fab-DNase I and b12-Fab-DNase I did not affect PNAG-positive biofilm formation **(Figure 4B)**, while the formation of PNAG-positive biofilm could be prevented by 4497-Fab-DspB and G2a2-Fab-DpsB. Thus, we show that the Fab-enzyme fusion proteins are active against biofilm formation *in vitro*.

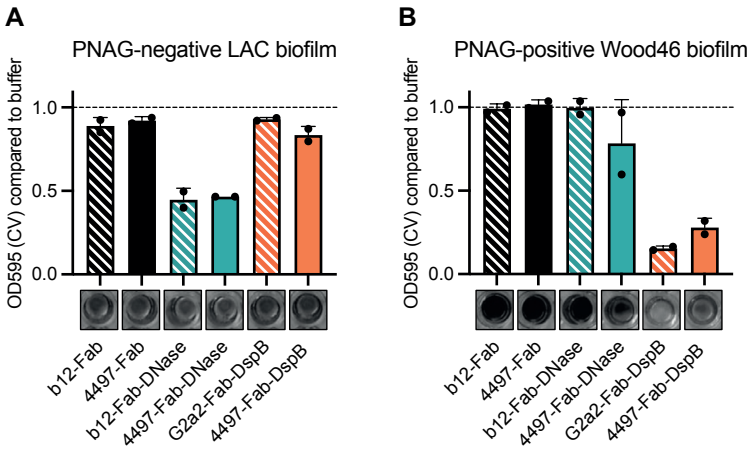

Figure 4. Ability of Fab fragments to prevent biofilm formation. (A,B) Biofilm of strain LAC (A) and Wood46 (B) was grown for 24 h with buffer or Fab-fragments (100 nM). After washing, adherent biofilm biomass was measured by crystal violet staining. Representative pictures of wells after CV staining are shown below the graph. Data is expressed as relative biomass by dividing the OD595 of treated samples by the OD595 of control (buffer) samples. Data represent mean + SD of 2 independent experiments.

4497-Fab-DspB and 4497-Fab-DNase I can degrade preformed biofilm

Next, we assessed whether the Fab fragments could degrade preformed biofilms. After 24 hours of biofilm growth, Fab fragments were added to the preformed biofilm culture for 3 hours. After washing to remove the detached material, the biofilm biomass attached to the plate surface was detected with a crystal violet staining. Compared to buffer, treatment with 4497-Fab-DspB and G2a2-Fab-DspB could remove PNAG-positive biofilm from the surface **(Figure 5B)**. Combining 4497-Fab-DspB and 4497-Fab-DNase I did not result in an additive effect, indicating that PNAG is the main factor stabilizing PNAG-

positive biofilm. On the other hand, 4497-Fab-DNase I and b12-Fab-DNase I resulted in significant removal of PNAG-negative biofilm **(Figure 5A)**. Interestingly 4497-Fab-DspB also slightly degrade biofilm, but a combination of 4497-Fab-DNase I and 4497-Fab-DspB did not enhance the effect compared to 4497-Fab-DNase I alone. Although we expected that 4497-Fab-DNase I and 4497-Fab-DspB would have increased concentrations at the biofilm surface compared to control Fabs because of target specificity, we could not detect a difference in the biofilm degrading effect of specific Fab fragments versus nonspecific Fab fragments. To remove unbound control Fabs, we introduced a washing step in the experimental setup by first incubation preformed biofilm with a concentration range of 4497-Fab-DspB and G2a2-Fab-DspB at 4°C to allow Fab binding. After washing, the biofilm was further incubated at 37°C for enzymatic activity of the bound antibodies. In this setup, we could still not detect a difference between specific and nonspecific Fab fragments **(Figure S1)** even at low Fab-fragment concentrations where we expected a beneficial effect of specific Fab binding to the biofilm surface. It is possible that DspB was active at 4°C and removed the biofilm in the first Fab fragment binding step at 4°C. Therefore, more sophisticated assays need to be performed to test the additive effect of coupling enzymes to WTA specific Fab fragments compared to

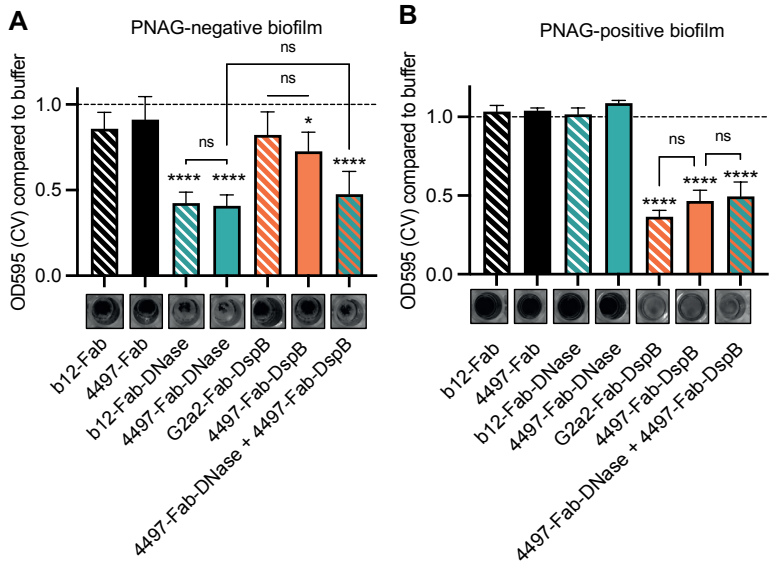

Figure 5. anti-biofilm effect of Fab fragments on preformed biofilm. (A,B) Biofilm of strain LAC (A) and Wood46 (B) was grown for 24 h. Buffer or Fab-fragments (100 nM) were added for 3 hours. After washing, adherent biofilm biomass was measured by crystal violet staining. Representative pictures of wells after CV staining are shown below the graph. Data represent mean + SD of 4 independent experiments. Data is expressed as relative biomass by dividing the OD595 of treated samples by the OD595 of control (buffer) samples. One-way ANOVA followed by Tukey test was performed to test for differences in biofilm biomass and displayed only when significant as *P ≤ 0.05, **P ≤ 0.01, ***P ≤ 0.001, or ****P ≤ 0.0001.

control Fab fragments. In all, we show that huDNase I and DspB genetically fused to Fab fragments can actively degrade preformed *S. aureus* biofilm.

Discussion

Antibody-enzyme conjugates have been widely reported in cancer research [51]. Monoclonal antibodies directed against tumor associated antigens are used to deliver either enzymes that cleave prodrugs or enzymes that are toxic to tumor cells. The use of enzymes in bacterial infections has also been proposed [10], but delivery of the enzymes to site of infection is a challenge. While the concept of coupling enzymes to full length antibodies or antibody fragments is not new [52–54], the testing of antibody-enzyme fusion proteins for bacterial infections has not been reported yet. Here we provide as a first step the coupling of anti-*S. aureus* biofilm enzymes to anti-*S. aureus* Fab fragments, which yield functional fusion proteins. We produced two Fab-enzyme fusion proteins, one anti-*S. aureus* Fab fragment coupled to PNAG-degrading enzyme DspB (4497-Fab-DspB) and one to DNA degrading enzyme DNase I (4497-Fab-DNase I). Because random chemical labeling of antibodies can affect the epitope binding, we used a genetic coupling method where one DspB/DNase I molecule was conjugated at a fixed position on the Fab fragment. This way, we produced Fab fragment-enzyme conjugates that retained similar binding to *S. aureus* as wild type 4497 Fab-fragments, could cleave their substrates efficiently and were active against *S. aureus* biofilm.

Our data is in line with previous reports describing the existence of two types of *S. aureus* biofilm: PNAG-negative and PNAG-positive [19–23,55]. However, we also unexpectedly observed a slight, although not significant, degrading of LAC (PNAG-negative) biofilm after incubation with 4497-Fab-DspB. This could be explained by a recent report describing that PNAG and eDNA/protein biofilm are not mutually exclusive and that PNAG and eDNA can interact to form a stable biofilm EPS [18]. Although we could not detect binding of anti-PNAG-IgG1 (F598) to or degradation of LAC biofilm by DspB in previous work [17], a low amount of PNAG could be present in LAC biofilm. Interestingly, the degrading effect was only observed for 4497-Fab-DspB but not G2a2-Fab-DspB. We hypothesize that the specificity of the 4497 Fab-fragments could localize DspB near its substrate and thereby enhance the anti-biofilm effect compared to G2a2-Fab-DspB **(Figure 4a)** or DspB alone [17]. As a proof of principle, we produced Fab fragments fused to one DNase I or DspB molecule via the CL-kappa chain. To possibly enhance the effectivity, an additional enzyme molecule could be fused to the CH-Fab chain, yielding Fab fragments coupled to two identical enzymes or mixed enzymes. It would

be interesting to test such mixed Fab-enzyme fusion proteins on strains with a “mixed” EPS phenotype [18].

The obtained *in vitro* results with 4497-Fab-DspB and 4497-Fab-DNase I indicate that the Fab-enzymes may hold promise for the use against *S. aureus* biofilm, although the benefit of the *S. aureus* specific Fab fragment as a vehicle needs to be determined. For example, studying 4497-Fab-DspB and 4497-Fab-DNase I in a flow chamber biofilm or an *in vivo* model could allow us to incorporate an experimental step where binding of specific Fab fragments may facilitate interaction between enzymes and substrates. We speculate an enhancement in half life and effectivity of specific versus nonspecific Fab-enzyme fragments if the specific Fab fragments retain the enzymes at the biofilm site. Other important points that need to be addressed would be 1) the immunogenicity of the conjugates, as repeated administration of Fab-enzyme conjugates would require non-immunogenicity, and 2) the half-life in serum, as coupling the small enzymes to larger fab-fragments could lead to a longer half-life. Moreover, the use of Fab fragments instead of IgG1 could decrease half-life due to the loss of interaction with FcRn. A great concern of using enzyme-based detachment of bacteria from the biofilm during infections is that it may induce bloodstream infections or disseminate infections to distant sites. As these enzymes do not kill or affect planktonic growth of *S. aureus*, enzyme-based biofilm degrading strategies should always be performed in combination with other antimicrobial agents, where they sensitize the bacteria to antimicrobials and the immune system.

In conclusion, we here provide a proof of principle for the genetic fusion of *S. aureus* biofilm degrading enzymes to *S. aureus* biofilm specific Fab fragments, yielding fully functional fusion proteins that may hold promise for the use against *S. aureus* biofilm.

Methods

Generation of Fab-enzyme fusion proteins

To produce Fab fragments, the constant heavy (CH) and light chain (CL) regions were cloned separately into pcDNA3.4 expression vectors (Thermo Fisher Scientific) containing the human IgG1 (Fab) backbone or the human Kappa backbone. A short linker, LPETG sequence and a His-tag for purification were cloned downstream the CH sequence. A semi-flexible linker sequence and the enzyme sequence (huDNAse I, DspB or Proteinase K) were cloned after the CL sequence. The variable heavy (VH) and variable light (VL) sequences containing codon-optimized genes with an upstream KOZAK and HAVT20 signal peptide (MACPGFLWALVISTCLEFSMA) were ordered as

gBlocks (Integrated DNA Technologies, IA, USA) and cloned upstream the CH and CL regions of the expression vector, respectively, using Gibson assembly (Bioke). Constant CH (human IgG1-Fab), CL (human Kappa), VH, VL, semi flexible linker, hDNase I, proteinase K and DspB sequences were derived from literature **(Table S1)**. Expression vector plasmids were amplified in TOP10F' E. coli. After sequence verification, plasmids were isolated using NucleoBond Xtra Midi plasmid DNA purification (Machery-Nagel). Then 2 x 10^6 EXPI293F cells/ml (Life Technologies) were transfected with 1 µg DNA/ml in a 3:2 (light chain:heavy chain) ratio using polyethylenimine HCl MAX (Polysciences). After 4 to 5 days, cells were harvested, supernatant collected and dialyzed for 2 days, including an extra buffer exchange, against 50 mM Tris/500 mM NaCl, pH8.0. From this, Fab fragments were isolated using HISTrap FF columns (Cytiva, GE Healthcare) in the Äkta Pure protein chromatography system (GE Healthcare). All Fab fractions were dialyzed overnight against PBS and filter-sterilized through 0.22 µm SpinX-filters. Size exclusion chromatography (SEC), using a Superdex 200 Increase 10/300 GL column (Cytiva, GE Healthcare), was performed to check for homogeneity, and the monomeric fraction was separated when aggregation levels exceeded 5%. Final Fab concentration was determined by measuring the absorbance at 280 nm and antibodies were stored at -80 °C and 4°C. The predicted weight of all conjugates and controls can be found in **Table S2**.

Antibody binding to biofilm cultures

To determine Fab binding capacity to biofilm, wells containing 24 h biofilm were blocked for 30 min with 4% BSA in PBS. After washing with PBS, wells were incubated with a concentration range of Fab fragments in PBS-BSA (1%) for 1 h at 4°C, statically. After washing two times with PBS, samples were further statically incubated for 1 h at 4°C with Alexa Fluor 647 conjugated goat-anti-human-kappa $F(ab')_2$ antibody (Southern Biotech, 1:500). After washing, fluorescence per well was measured using a CLARI-Ostar plate reader (BMG LABTECH). Excitation and emission wavelengths used were 625-30 nm and 680–30 nm.

Antibody binding to planktonic cultures

To determine Fab-enzyme binding capacity, planktonic Wood46 cultures were suspended and washed in PBS containing 0.1% BSA (Serva) and mixed with a concentration range of Fabs in a round-bottom 96-well plate in PBS-BSA. Each well contained 2.5 x 10^6 bacteria in a total volume of 55 µl. Samples were incubated for 30 min at 4°C, shaking (~700 rpm) and washed once with PBS-BSA. Samples were further incubated for another 30 min at 4°C, shaking (~700 rpm), with Alexa Fluor 647 conjugated goat-anti-human-kappa $F(ab')_2$ antibody (1:500). After washing, samples were fixed for 30 min with cold 1% paraformaldehyde. Fluorescence per bacterium was measured on a

flow cytometer (FACSVerse, BD). Control bacteria were used to set proper FSC and SSC gate definitions to exclude debris and aggregated bacteria. Data were analyzed with FlowJo (version 10).

DNAse activity assay

DNase activity was measured in a DNA conversion assay based on Sheppard *et al.* [50]. In a black flat bottom 96 well plate, we mixed 10 µL dsDNA substrate (final concentration 2 ng/µL), 50 µL Quant-iT PicoGreen (1:200, Invitrogen™), 5 µL DNase (final concentration 25 nM). The assay was performed in DNase buffer (10 mM Tris-HCl,2,5 mM MgCl2, 0.5 mM CaCl2), which was also added to bring the reaction volume to 100 µL. A CLARIOstar microplate reader (BMG labtech) was pre-heated to 37 °C. Samples were read every 30 s for 60 mins. Excitation and emission wavelengths used were 483–15 nm and 530–30 nm, with a shake before each read.

DspB activity assay

DspB activity was measured in a pNitroPhenol-GlcNAC (pNPGlcNAc) conversion assay. pNPGlcNAc is a substrate for hexosaminidases such as DspB. Hydrolysis of pNPGlcNAc into p-nitrophenol and N-acetylglucosamine results in the development of a yellow color [49]. pNPGlcNAc (10 mM) and Fab fragments (500 nM) were mixed in a total volume of 100 uL phosphate buffer (pH 5.8). After incubation for 15 minutes at 37°C, the reaction was stopped by adding 2 uL 2.5 M NaOH. To quantify substrate conversion, the optical density at 405 nm was measured using a CLARIOstar plate reader (BMG LABTECH).

Bacterial strains and growth conditions

S. aureus strains Wood46 (ATCC 10832) [46,47,56], USA300 LAC (AH1263) [57] and USA300 LAC Δ*spa, sbi*::Tn (AH4116) [17] were used in this study. Strains were grown overnight on sheep blood agar (SBA) at 37°C and were cultured overnight in Tryptic Soy Broth (TSB) before each experiment. For exponential phase planktonic cultures, overnight cultures were sub-cultured in fresh TSB for 2 h.

Biofilm culture

For PNAG-negative biofilm, overnight cultures of LAC or LAC Δ*spa sbi*::Tn (AH4116) were diluted to an OD_{600} of 1 and then diluted 1:1000 in fresh TSB containing 0.5% (wt/vol) glucose and 3% (wt/vol) NaCl. 200 µl was transferred to wells in a flat bottom 96 wells plate (Corning costar 3598, Tissue Culture treated) and incubated statically for 24 h at 37°C. To facilitate attachment of PNAG-negative bacteria to the wells, plates were precoated with 20% human plasma (Sigma) in 0.1M carbonate – bicarbonate buffer (pH 9.6) overnight at 4°C before inoculation. PNAG-positive Wood46 biofilms were grown

similarly, except that no coating was used, and growth medium was TSB supplemented with 0.5% (wt/vol) glucose.

Crystal violet assay

To determine the ability to prevent biofilm formation, Fab fragments (100 nM) were added at the same time as inoculation and incubated during biofilm formation for 24 h. To determine activity against preformed biofilm, Fab fragments (100 nM) were added to 24 h biofilm and incubated statically for 3 hours at 37°C. Biofilm adherence after treatment with Fab fragments compared to untreated controls was analyzed as follows. Wells were washed once with PBS and adherent cells where fixed by drying plates at 60°C for 1 hour. Adherent material was stained with 0.1% crystal violet for 5 min and excess stain was removed by washing with distilled water. Remaining dye was solubilized in 33% acetic acid and biofilm formation was quantified by measuring the optical density at 595 nm using a CLARIOstar plate reader (BMG LABTECH).

Acknowledgements

The project was co-funded by the PPP Allowance made available by Health~Holland (LSHM17026), Top Sector Life Sciences & Health, to stimulate public-private partnerships. The authors would like to acknowledge Sjors van der Lans for critical reading of the manuscript.

References

1. Lowy, F. D. Medical progress: *Staphylococcus aureus* infections. *N. Engl. J. Med.* **339**, 520–532 (1998).
2. Tong, S. Y. C., Davis, J. S., Eichenberger, E., Holland, T. L. & Fowler, V. G. *Staphylococcus aureus* infections: Epidemiology, pathophysiology, clinical manifestations, and management. *Clin. Microbiol. Rev.* **28**, 603–661 (2015).
3. Magill, S. S. *et al.* Multistate point-prevalence survey of health care-associated infections. *N. Engl. J. Med.* **370**, 1198–1208 (2014).
4. Arciola, C. R., Campoccia, D. & Montanaro, L. Implant infections: Adhesion, biofilm formation and immune evasion. *Nat. Rev. Microbiol.* **16**, 397–409 (2018).
5. Otto, M. Staphylococcal Biofilms. *Microbiol. Spectr.* **6**, (2018).
6. Aggarwal, V. K. *et al.* Organism profile in periprosthetic joint infection: pathogens differ at two arthroplasty infection referral centers in Europe and in the United States. *J. Knee Surg.* **27**, 399–406 (2014).
7. Arciola, C. R., An, Y. H., Campoccia, D., Donati, M. E. & Montanaro, L. Etiology of implant orthopedic infections: A survey on 1027 clinical isolates. *Int. J. Artif. Organs* **28**, 1091–1100 (2005).
8. Schilcher, K. & Horswill, A. R. Staphylococcal Biofilm Development: Structure, Regulation, and Treatment Strategies. *Microbiol. Mol. Biol. Rev.* **84**, (2020).
9. Suresh, M. K., Biswas, R. & Biswas, L. An update on recent developments in the prevention and treatment of *Staphylococcus aureus* biofilms. *Int. J. Med. Microbiol.* **309**, 1–12 (2019).
10. Bhattacharya, M., Wozniak, D. J., Stoodley, P. & Hall-Stoodley, L. Prevention and treatment of *Staphylococcus aureus* biofilms. *Expert Rev. Anti. Infect. Ther.* **13**, 1499–1516 (2015).
11. Hogan, S. *et al.* Potential use of targeted enzymatic agents in the treatment of *Staphylococcus aureus* biofilm-related infections. *J. Hosp. Infect.* **96**, 177–182 (2017).
12. Izano, E. A., Amarante, M. A., Kher, W. B. & Kaplan, J. B. Differential roles of poly-N-acetylglucosamine surface polysaccharide and extracellular DNA in *Staphylococcus aureus* and *Staphylococcus epidermidis* biofilms. *Appl. Environ. Microbiol.* **74**, 470–476 (2008).
13. Kaplan, J. B. *et al.* Detachment of Actinobacillus actinomycetemcomitans Biofilm Cells by an Endogenous β-Hexosaminidase Activity. *J. Bacteriol.* **185**, 4693 LP – 4698 (2003).
14. Kaplan, J. B. *et al.* Recombinant human DNase i decreases biofilm and increases antimicrobial susceptibility in staphylococci. *J. Antibiot. (Tokyo).* **65**, 73–77 (2012).
15. Dengler, V., Foulston, L., DeFrancesco, A. S. & Losick, R. An electrostatic net model for the role of extracellular DNA in biofilm formation by *Staphylococcus aureus*. *J. Bacteriol.* **197**, 3779–3787 (2015).
16. Otto, M. Staphylococcal Biofilms. in *Current Topics in Microbiology and Immunology* vol. 322 207–228 (2008).
17. de Vor, L. *et al.* Human monoclonal antibodies against *Staphylococcus aureus* surface antigens recognize in vitro and in vivo biofilm. *Elife* **11**, 1–25 (2022).
18. Mlynek, K. D. *et al.* Genetic and biochemical analysis of cody-mediated cell aggregation in *staphylococcus aureus* reveals an interaction between extracellular DNA and polysaccharide in the extracellular matrix. *J. Bacteriol.* **202**, 1–21 (2020).

19. Rohde, H. *et al.* Polysaccharide intercellular adhesin or protein factors in biofilm accumulation of *Staphylococcus epidermidis* and *Staphylococcus aureus* isolated from prosthetic hip and knee joint infections. *Biomaterials* **28**, 1711–1720 (2007).
20. O'Neill, E. *et al.* Association between methicillin susceptibility and biofilm regulation in *Staphylococcus aureus* isolates from device-related infections. *J. Clin. Microbiol.* **45**, 1379–1388 (2007).
21. O'Neill, E. *et al.* A novel *Staphylococcus aureus* biofilm phenotype mediated by the fibronectin-binding proteins, FnBPA and FnBPB. *J. Bacteriol.* **190**, 3835–3850 (2008).
22. Sugimoto, S. *et al.* Broad impact of extracellular DNA on biofilm formation by clinically isolated Methicillin-resistant and -sensitive strains of *Staphylococcus aureus*. *Sci. Rep.* **8**, 2254 (2018).
23. McCarthy, H. *et al.* Methicillin resistance and the biofilm phenotype in *staphylococcus aureus*. *Front. Cell. Infect. Microbiol.* **5**, 1–9 (2015).
24. Kiedrowski, M. R. *et al.* Nuclease modulates biofilm formation in community-associated methicillin-resistant *staphylococcus aureus*. *PLoS One* **6**, e26714 (2011).
25. Waryah, C. B. *et al.* In Vitro Antimicrobial Efficacy of Tobramycin Against *Staphylococcus aureus* Biofilms in Combination With or Without DNase I and/or Dispersin B: A Preliminary Investigation. *Microb. Drug Resist.* **23**, 384–390 (2017).
26. Tetz, G. V., Artemenko, N. K. & Tetz, V. V. Effect of DNase and Antibiotics on Biofilm Characteristics. *Antimicrob. Agents Chemother.* **53**, 1204–1209 (2009).
27. Darouiche, R. O., Mansouri, M. D., Gawande, P. V. & Madhyastha, S. Antimicrobial and antibiofilm efficacy of triclosan and DispersinB(R) combination. *J. Antimicrob. Chemother.* **64**, 88–93 (2009).
28. Kaplan, J. B. *et al.* Extracellular polymeric substance (EPS)-degrading enzymes reduce staphylococcal surface attachment and biocide resistance on pig skin in vivo. *PLoS One* **13**, e0205526 (2018).
29. Alekseeva, L., Sen'kova, A., Savin, I., Zenkova, M. & Mironova, N. Human Recombinant DNase I (Pulmozyme®) Inhibits Lung Metastases in Murine Metastatic B16 Melanoma Model That Correlates with Restoration of the DNase Activity and the Decrease SINE/LINE and c-Myc Fragments in Blood Cell-Free DNA. *Int. J. Mol. Sci.* **22**, 12074 (2021).
30. Shak, S., Capon, D. J., Hellmiss, R., Marsters, S. A. & Baker, C. L. Recombinant human DNase I reduces the viscosity of cystic fibrosis sputum. *Proc. Natl. Acad. Sci.* **87**, 9188–9192 (1990).
31. Frederiksen, B., Pressler, T., Hansen, A., Koch, C. & Høiby, N. Effect of aerosolized rhDNase (Pulmozyme®) on pulmonary colonization in patients with cystic fibrosis. *Acta Paediatr.* **95**, 1070–1074 (2006).
32. Sugihara, S. *et al.* Deoxyribonuclease treatment prevents blood-borne liver metastasis of cutaneously transplanted tumour cells in mice. *Br. J. Cancer* **67**, 66–70 (1993).
33. Tokita, K. *et al.* Effects of serine protease and deoxyribonuclease on intravascular tumor cell arrest in rat blood-borne lung metastasis. *Invasion Metastasis* **15**, 46–59 (1995).
34. Gao, X. *et al.* Neutrophil extracellular traps contribute to the intestine damage in endotoxemic rats. *J. Surg. Res.* **195**, 211–218 (2015).
35. Mai, S. H. C. *et al.* Delayed but not Early Treatment with DNase Reduces Organ Damage and Improves Outcome in a Murine Model of Sepsis. *Shock* **44**, 166–172 (2015).
36. Meng, W. *et al.* Depletion of neutrophil extracellular traps in vivo results in hypersusceptibility to polymicrobial sepsis in mice. *Crit. Care* **16**, R137 (2012).

37. Lauková, L. *et al.* Exogenous deoxyribonuclease has a protective effect in a mouse model of sepsis. *Biomed. Pharmacother.* **93**, 8–16 (2017).
38. Green, J. D. Pharmaco-toxicological expert report Pulmozyme rhDNase Genentech, Inc. *Hum. Exp. Toxicol.* **13 Suppl 1**, S1-42 (1994).
39. Joosten, V., Lokman, C., van den Hondel, C. A. M. J. J. & Punt, P. J. The production of antibody fragments and antibody fusion proteins by yeasts and filamentous fungi. *Microbial Cell Factories* vol. 2 at https://doi.org/10.1186/1475-2859-2-1 (2003).
40. Lehar, S. M. *et al.* Novel antibody-antibiotic conjugate eliminates intracellular *S. aureus*. *Nature* **527**, 323–328 (2015).
41. Kurokawa, K. *et al.* Glycoepitopes of Staphylococcal Wall Teichoic Acid Govern Complement-mediated Opsonophagocytosis via Human Serum Antibody and Mannose-binding Lectin. *J. Biol. Chem.* **288**, 30956–30968 (2013).
42. Winstel, V. *et al.* Wall Teichoic Acid Glycosylation Governs *Staphylococcus aureus* Nasal Colonization. *MBio* **6**, (2015).
43. Kennedy, A. D. *et al.* Epidemic community-associated methicillin-resistant *Staphylococcus aureus*: Recent clonal expansion and diversification. *Proc. Natl. Acad. Sci. U. S. A.* **105**, 1327–1332 (2008).
44. Voyich, J. M. *et al.* Insights into Mechanisms Used by *Staphylococcus aureus* to Avoid Destruction by Human Neutrophils . *J. Immunol.* **175**, 3907–3919 (2005).
45. Montgomery, C. P. *et al.* Comparison of Virulence in Community-Associated Methicillin-Resistant *Staphylococcus aureus* Pulsotypes USA300 and USA400 in a Rat Model of Pneumonia . *J. Infect. Dis.* **198**, 561–570 (2008).
46. Balachandran, M., Riley, M. C., Bemis, D. A. & Kania, S. A. Complete Genome Sequence of *Staphylococcus aureus* Strain Wood 46. *Genome Announc.* **5**, (2017).
47. Balachandran, M., Giannone, R. J., Bemis, D. A. & Kania, S. A. Molecular basis of surface anchored protein A deficiency in the *Staphylococcus aureus* strain Wood 46. *PLoS One* **12**, e0183913 (2017).
48. Van Rosmalen, M., Krom, M. & Merkx, M. Tuning the Flexibility of Glycine-Serine Linkers to Allow Rational Design of Multidomain Proteins. *Biochemistry* **56**, 6565–6574 (2017).
49. Manuel, S. G. A. *et al.* Role of active-site residues of dispersin B, a biofilm-releasing β-hexosaminidase from a periodontal pathogen, in substrate hydrolysis. *FEBS J.* **274**, 5987–5999 (2007).
50. Sheppard, E. C., Rogers, S., Harmer, N. J. & Chahwan, R. A universal fluorescence-based toolkit for real-time quantification of DNA and RNA nuclease activity. *Sci. Rep.* **9**, 1–14 (2019).
51. Sharma, S. K. & Bagshawe, K. D. Translating antibody directed enzyme prodrug therapy (ADEPT) and prospects for combination. *Expert Opin. Biol. Ther.* **17**, 1–13 (2017).
52. Bagshawe, K. Antibody directed enzymes revive anti-cancer prodrugs concept. *Br. J. Cancer* **56**, 531–532 (1987).
53. Bagshawe, K. *et al.* A cytotoxic agent can be generated selectively at cancer sites. *Br. J. Cancer* **58**, 700–703 (1988).
54. Senter, P. D. *et al.* Anti-tumor effects of antibody-alkaline phosphatase conjugates in combination with etoposide phosphate. *Proc. Natl. Acad. Sci.* **85**, 4842–4846 (1988).
55. Fitzpatrick, F., Humphreys, H. & O'Gara, J. P. Evidence for icaADBC-independent biofilm development mechanism in methicillin-resistant *Staphylococcus aureus* clinical isolates. *J. Clin. Microbiol.* **43**, 1973–1976 (2005).

56. Amend, A., Chhatwal, G. S., Schaeg, W. & Blobel, H. Characterization of immunoglobulin G binding to *Staphylococcus aureus* strain Wood 46. *Zentralblatt fur Bakteriol. Mikrobiol. und Hyg. - Abt. 1 Orig. A* **258**, 472–479 (1984).
57. Boles, B. R., Thoendel, M., Roth, A. J. & Horswill, A. R. Identification of Genes Involved in Polysaccharide-Independent *Staphylococcus aureus* Biofilm Formation. *PLoS One* **5**, e10146 (2010).

Supplementary information

Supplementary figures

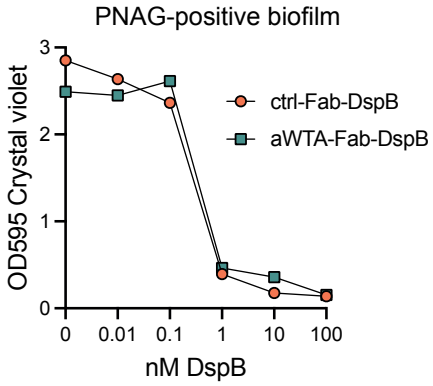

Figure S1. anti-biofilm effect of Fab fragments on preformed biofilm. Biofilm of strain Wood46 was grown for 24 h. A concentration range of Fab fragments was added for 30 minutes at 4°C. After washing, biofilm was further incubated at 37°C. After washing, adherent biofilm biomass was measured by crystal violet staining. Data represent 1 independent experiment.

Supplementary tables

Table S1. Protein sequences used for Fab-enzyme production.

	Sequence	Patent number or reference
VH: variable region heavy chain		
G2a2, *Anti-DNP*	DVRLQESGPGLVKPSQSLSLTCSVTGYSITNSYYWNWIRQF-PGNKLEWMVYIGYDGSNNYNPSLKNRISITRDTSKNQF-FLKLNSVTTEDTATYYCARATYYGNYRGFAYWGQGTLVT-VSA	[1]
B12, *Anti-gp120*	QVQLVQSGAEVKKPGASVKVSCQASGYRFSNFVIHWVRQA-PGQRFEWMGWINPYNGNKEFSAKFQDRVTFTADTSAN-TAYMELRSLRSADTAVYYCARVGPYSWDDSPQDNYYMD-VWGKGTTVIVSS	[2] [3]
4497, *Anti-WTA(β)*	EVQLVESGGGLVQPGGSLRLSCSASGFSFNSFWMH-WVRQVPGKGLVWISFTNNEGTTTAYADSVRGRFIISRD-NAKNTLYLEMNNLRGEDTAVYYCARGDGGLDDWGQGTLVT-VSS.	WO/2014/193722 A1 [4] [5]
VL: variable region light chain		
G2a2, *Anti-DNP*	DIRMTQTTSSLSASLGDRVTISCRASQDISNYLNWYQQKP-DGTVKLLIYYTSRLHSGVPSRFSGSGSGTDYSLTISNLEQE-DIATYFCQQGNTLPWTFGGGTKLEIK	[1]
B12, *Anti-gp120*	EIVLTQSPGTLSLSPGERATFSCRSSHSIRSRRVAWYQHKP-GQAPRLVIHGVSNRASGISDRFSGSGSGTDFTLTITRVEPED-FALYYCQVYGASSYTFGQGTKLERK	[2] [3]
4497, *Anti-WTA(β)*	DIQLTQSPDSLAVSLGERATINCKSSQSIFRTSRNKNLLNWY-QQRPGQPPRLLIHWASTRKSGVPDRFSGSGFGTDFTLTIT-SLQAEDVAIYYCQQYFSPPYTFGQGTKLEIK	WO/2014/193722 A1 [4] [5]
CH: constant regions heavy chain		
IgG1-Fab	ASTKGPSVFPLAPSSKSTSGGTAALGCLVKDYFPEPVT-VSWNSGALTSGVHTFPAVLQSSGLYSLSSVVTVPSSSLGTQ-TYICNVNHKPSNTKVDKKVEPKSC	[6] [7]
CL: constant regions light chain		
Kappa class	RTVAAPSVFIFPPSDEQLKSGTASVVCLLNNFYPREAK-VQWKVDNALQSGNSQESVTEQDSKDSTYSLSSTLTLSKA-DYEKHKVYACEVTHQGLSSPVTKSFNRGEC	[7]
Linkers		
Semi flexible linker	GSGGSGGSGGSGGSGGSGGSGGSGEFAEAAAKEAAAKEAAAK EAAAKEAAAKEAAAKAEFGGSGGSGGSGGSGGSGGSGGT	[8]
Linker-LPETG-His tag	GGGGSLPETGGHHHHHH	

Table S1. Protein sequences used for Fab-enzyme production. ()

	Sequence	**Patent number or reference**
Enzymes		
huDNase I	LKIAAFNIQTFGETKMSNATLVSYIVQILSRYDIALVQEVRDSH-LTAVGKLLDNLNQDAPDTYHYVVSEPLGRNSYKERYLFVYR-PDQVSAVDSYYYDDGCEPCGNDTFNREPAIVRFFSRFTE-VREFAIVPLHAAPGDAVAEIDALYDVYLDVQEKWGLED-VMLMGDFNAGCSYVRPSQWSSIRLWTSPTFQWLIPDSADT-TATPTHCAYDRIVVAGMLLRGAVVPDSALPFNFQAAYGLS-DQLAQAISDHYPVEVMLK	[9]
DspB	NCCVKGNSIYPQKTSTKQTGLMLDIARHFYSPEVIKS-FIDTISLSGGNFLHLHFSDHENYAIESHLLNQRAENAVQG-KDGIYINPYTGKPFLSYRQLDDIKAYAKAKGIELIPELD-SPNHMTAIFKLVQKDRGVKYLQGLKSRQVDDEIDITNADSIT-FMQSLMSEVIDIFGDTSQHFHIGGDEFGYSVESNHEFITY-ANKLSYFLEKKGLKTRMWNDGLIKNTFEQINPNIEITYWSY-DGDTQDKNEAAERRDMRVSLPELLAKGFTVLNYNSYYLY-IVPKASPTFSQDAAFAAKDVIKNWDLGVWDGRNTKNRVQN-THEIAGAALSIWGEDAKALKDET IQKNTKSLLEAVIHKTNGDE	WO2009/121183 [10]
Proteinase K	APAVEQRSEAAPLIEARGEMVANKYIVKFKEGSAL-SALDAAMEKISGKPDHVYKNVFSGFAATLDENMVRVLRAHP-DVEYIEQDAVVTINAAQTNAPWGLARISSTSPGTSTYYYDE-SAGQGSCVYVIDTGIEASHPEFEGRAQMVKTYYYS-SRDGNGHGTHCAGTVGSRTYGVAKKTQLFGVKVLDDNGS-GQYSTIIAGMDFVASDKNNRNCPKGVVASLSLGGGYSSS-VNSAAARLQSSGVMVAVAAGNNNADARNYSPASEPSVCT-VGASDRYDRRSS FSNYGSVLDIFGPGTSILSTWIGGSTRSISGTSMATPHVA-GLAAYLMTLGKTTAASACRY IADTANKGDLSNIPFGTVNLLAYNNYQA	WO2009/121183 [10]

Table S2. Predicted molecular weight (kDa) of Fab-controls and Fab-enzyme conjugates.

Fab-enzyme fusion	Predicted MW (kDa)
B12-Fab-DNase	86
4497-Fab-DNase	85
aDNP-Fab-DspB	97
4497-Fab-DspB	97
B12-Fab	50
4497-Fab	49

References

1. Gonzalez, M. L., Frank, M. B., Ramsland, P. A., Hanas, J. S. & Waxman, F. J. Structural analysis of IgG2A monoclonal antibodies in relation to complement deposition and renal immune complex deposition. *Mol. Immunol.* **40**, 307–317 (2003).
2. Barbas, C. F. *et al.* Molecular profile of an antibody response to HIV-1 as probed by combinatorial libraries. *J. Mol. Biol.* **230**, 812–823 (1993).
3. Saphire, E. O. *et al.* Crystal structure of a neutralizing human IgG against HIV-1: A template for vaccine design. *Science (80-.).* **293**, 1155–1159 (2001).
4. Lehar, S. M. *et al.* Novel antibody-antibiotic conjugate eliminates intracellular *S. aureus*. *Nature* **527**, 323–328 (2015).
5. Fong, R. *et al.* Structural investigation of human *S. aureus*-targeting antibodies that bind wall teichoic acid. *MAbs* **10**, 979–991 (2018).
6. Cruz, A. R. *et al*. Staphylococcal protein A inhibits complement activation by interfering with IgG hexamer formation. *Proc. Natl. Acad. Sci. U. S. A.* **118**, (2021).
7. Kabat, E. A., Wu, T. T., Perry, H. M., Gottesman, K. S. & Foeller, C. *Sequences of proteins of immunological interest*. *Analytical Biochemistry* vol. 138 (1984).
8. Van Rosmalen, M., Krom, M. & Merkx, M. Tuning the Flexibility of Glycine-Serine Linkers to Allow Rational Design of Multidomain Proteins. *Biochemistry* **56**, 6565–6574 (2017).
9. Kaplan, J. B. *et al.* Recombinant human DNase i decreases biofilm and increases antimicrobial susceptibility in staphylococci. *J. Antibiot. (Tokyo).* **65**, 73–77 (2012).
10. Ramasubbu, N., Thomas, L. M., Ragunath, C. & Kaplan, J. B. Structural analysis of dispersin B, a biofilm-releasing glycoside hydrolase from the periodontopathogen Actinobacillus actinomycetemcomitans. *J. Mol. Biol.* **349**, 475–486 (2005).

CHAPTER 4

Monoclonal antibodies effectively potentiate complement activation and phagocytosis of *Staphylococcus epidermidis* in neonatal human plasma

Lisanne de Vor[1#], Coco Beudeker[2#], Anne Flier[1], Lisette Scheepmaker[1], Piet C. Aerts[1], Daniel Vijlbrief[3], Mireille Bekker[4], Frank J. Beurskens[5], Kok P.M. van Kessel[1], Carla J.C. de Haas[1], Suzan H.M. Rooijakkers[1$], Michiel van der Flier[2$*]

1. Department of Medical Microbiology, University Medical Center Utrecht, Utrecht University, Utrecht, The Netherlands
2. Department of Paediatric Infectious Diseases and Immunology, University Medical Center Utrecht, Utrecht University, Utrecht, Netherlands
3. Department of Neonatology, University Medical Center Utrecht, Utrecht University, Utrecht, Netherlands
4. Department of Obstetrics, University Medical Center Utrecht, Utrecht University, Utrecht, Netherlands
5. Genmab, Utrecht, The Netherlands

[#] *These authors contributed equally to this work as first authors.*

[$] *these authors shared supervision of this study*

Published in Frontiers Immunology, 2022 Jul 29; doi:10.3389/fimmu.2022.933251

Abstract

Central line associated bloodstream infections (CLABSI) with *Staphylococcus epidermidis* are a major cause of morbidity in neonates, who have an increased risk of infection because of their immature immune system. As especially preterm neonates suffer from antibody deficiency, clinical studies into preventive therapies have thus far focused on antibody supplementation with pooled intravenous immunoglobulins from healthy donors (IVIG) but with little success. Here we study the potential of monoclonal antibodies (mAbs) against *S. epidermidis* to induce phagocytic killing by human neutrophils. Nine different mAbs recognizing Staphylococcal surface components were cloned and expressed as human IgG1s. In binding assays, clones rF1, CR5133 and CR6453 showed the strongest binding to *S. epidermidis* ATCC14990 and CR5133 and CR6453 bound the majority of clinical isolates from neonatal sepsis (19 out of 20). To study the immune activating potential of rF1, CR5133 and CR6453, bacteria were opsonized with mAbs in the presence or absence of complement. We observed that activation of the complement system is essential to induce efficient phagocytosis of *S. epidermidis*. Complement activation and phagocytic killing could be enhanced by Fc mutations that improve IgG1 hexamerization on cellular surfaces. Finally, we studied the ability of the mAbs to activate complement in r-Hirudin neonatal plasma conditions. We show that classical pathway complement activity in plasma isolated from neonatal cord blood is comparable to adult levels. Furthermore, mAbs could greatly enhance phagocytosis of *S. epidermidis* in neonatal plasma. Altogether, our findings provide insights that are crucial for optimizing anti-*S. epidermidis* mAbs as prophylactic agents for neonatal CLABSI.

Introduction

Neonatal sepsis is a major cause of mortality and morbidity [1,2]. Due to the use of indwelling medical devices, more than half of all late onset sepsis episodes (occurring after more than 7 days of age) are caused by central line associated bloodstream infections (CLABSI) [3]. The incidence of CLABSI is highest in preterm neonates (gestational age (GA) < 37 weeks) compared to term neonates (≥ 37 weeks GA) and children admitted to pediatric intensive care units [4–6]. The most common pathogens found in CLABSI are coagulase negative staphylococci, with *Staphylococcus epidermidis* being the predominant species [7,8]. Currently, no effective strategy exists to prevent late onset sepsis in neonates.

The high risk of CLABSI in neonates compared to older children is likely related to transient immunodeficiency of immaturity [9–15]. Three elements that are crucial for immune protection against Gram-positive bacteria, namely neutrophils [16], antibodies and the complement system, have been reported to be impaired in neonates. First, neonates have low levels of circulating neutrophils [14]. Neutrophils are highly specialized immune cells that circulate in the blood and are attracted to the site of infection to phagocytose bacteria. Following uptake by neutrophils, bacteria are subjected to high levels of reactive oxygen species (ROS) and degranulation of antimicrobial products that are destructive to staphylococci, this makes phagocytosis an efficient way to eliminate *S. epidermidis* [17,18]. Second, neonates have low levels of circulating antibodies. Because endogenous antibody synthesis only begins at birth, neonates depend on passive transfer of maternal antibodies over the placenta which mainly occurs in the final trimester of pregnancy. As a result, preterm neonates have low IgG levels [19]. IgM and IgA are not transported over the placenta, thus all neonates newborns are IgM/IgA deficient at birth [9,10]. Third, the complement system is less active in neonates when compared to adults, but it can be activated in the presence of infection [11–13,15]. Both antibodies and complement concentrations in neonatal plasma increase with gestational age, meaning that extremely preterm neonates are more at risk than term neonates. Antibodies and complement components are important opsonins that are needed to label bacteria for efficient phagocytosis. Antibodies consist of two functional domains: the fragment antigen binding (Fab) region confers antigen specificity, while the crystallizable fragment (Fc) region drives interaction with other components of the immune system [20]. After binding to the bacterial surface, IgG and IgA antibodies can directly induce phagocytosis via interaction with Fc receptors on neutrophils. IgG and IgM antibodies are both able to activate the classical pathway of the complement system which leads to deposition of C3b on the bacterial surface. C3b is recognized by complement receptors on neutrophils and leads to phagocytosis of the pathogen

[21]. Thus, antibodies play a central role in the immune response against Gram-positive bacteria such as *S. epidermidis.*

Clinical trials have assessed if antibody supplementation therapy with pooled intravenous immunoglobulins from healthy donors (IVIG) can ameliorate neonatal antibody deficiency and prevent or treat neonatal sepsis. These studies show only a 3% reduction in sepsis incidence in neonates and no improvement in mortality [22]. We hypothesize that the disappointing efficacy of IVIG therapy in neonatal infections could be caused by low concentration of antibodies specific to the relevant neonatal pathogens.

In this study, we wondered whether pathogen specific monoclonal antibodies (mAbs), which have a sole specificity for one target, can be more effective than IVIG. Therefore, we cloned and expressed nine different mAbs recognizing staphylococcal surface components as human IgG1s. Of the three best binders (rF1, CR5133 and CR6453), we tested the ability to recognize a panel of 20 clinical *S. epidermidis* isolates from neonatal sepsis and showed that CR5133 and CR6453 bound to the majority (19 out of 20) of isolates. We then studied the immune activating potential of rF1-, CR5133- and CR6453-IgG1 and found that activation of the complement system is essential to induce efficient phagocytosis of *S. epidermidis*. As shown before on *Staphylococcus aureus* [23] and *Streptococcus pneumoniae* [24], phagocytosis and killing of *S. epidermidis* could be further enhanced by Fc mutations that improve IgG hexamerization, which is needed for efficient activation of the classical pathway [25–27]. Finally, we collected human cord blood from neonates to study the ability of the mAbs to activate the neonatal complement system. In contrast to what is reported [11–13,15,28], plasma isolated from preterm and term neonatal cord blood showed classical pathway complement activity comparable to adult levels. Furthermore, we demonstrate that pathogen specific monoclonal antibodies with hexamer enhancing mutations greatly enhanced phagocytosis of *S. epidermidis* in neonatal plasma by healthy donor neutrophils. Altogether, our findings provide insights that are crucial for optimizing anti-*S. epidermidis* mAbs as prophylactic or therapeutic agents for neonatal sepsis.

Results

Production and identification of human monoclonal antibodies against *S. epidermidis*

First, we produced a panel of nine mAbs by cloning the variable light chain (VL) and heavy chain (VH) sequences derived from scientific publications or patents **(Table S1)** into expression vectors to produce full length human IgG1 antibodies. We selected

clones rF1 (binding surface proteins of the SDR family [38]), M130 (binding peptidoglycan [US20030228322A]), A120 (binding LTA [WO-03059260-A3]), CR5132 (possible target LTA [2012/0141493 A1] or Wall Teichoic Acid [31], CR5133 (possible target LTA [2012/0141493 A1]) and CR6453 (possible target LTA [2012/0141493 A1]) that have already been described to bind and induce opsonophagocytic killing of different *S. epidermidis* strains, but not to our model strain ATCC 14990 [33]. We also included clones CR6166, CR6171 and CR6176, that are related to CR6453 and were screened for cross reactivity because they bind *S. aureus* [2012/0141493 A1]. As a negative control, we produced one antibody recognizing the hapten dinitrophenol (DNP) (G2a2-IgG1) [39].

Next, we compared the binding of the panel of IgG1 mAbs to the sequenced common laboratory strain *S. epidermidis* ATCC 14990 [33], using flow cytometry. Compared to the negative control antibody (aDNP-IgG1) which does not recognize a bacterial component, only three antibodies (CR5133-IgG1, CR6453-IgG1 and rF1-IgG1) significantly bound to ATCC 14990 **(Figure 1A)**. Although binding to other *S. epidermidis* strains has been described, we could not detect significant binding of IgG1 mAbs M130 and A120 to ATCC 14990. Our results indicate that CR5132 also specifically binds ATCC14490, although not significant. As CR5132 has been described to bind the same target as CR5133, which does show stronger and significant binding, we selected CR5133 instead of CR5132 for further characterization. After titration, we detected a higher binding signal at lower concentrations for rF1-IgG1 compared to CR5133- and CR6453-IgG1 **(Figure 1B)**, indicating that rF1-IgG1 is the best binding mAb in the panel.

We also compared the strength and broad specificity of mAb binding and IVIG binding to *S. epidermidis*. We could measure binding of IVIG antibodies to ATCC 14990, but this required higher concentrations (10 µg/mL IVIG vs 0.004 µg/mL rF1-IgG1 or 0.37 µg/mL CR5133- and CR6453-IgG1) to reach a similar binding level. One advantage of the polyclonal nature of IVIG is that it may be possible to target a broad range of isolates. As mAbs recognize one unique target, it is important that this target is present on the majority of *S. epidermidis* isolates found in the clinic. To test the broad specificity of rF1-, CR5133- and CR6453-IgG1 when compared to IVIG, we collected a set of twenty clinical *S. epidermidis* isolates from neonatal sepsis cases. Indeed, we could detect binding of IVIG to all clinical isolates in the panel **(Figure 1C)**. CR5133- and CR6453-IgG1 bound 19/20 isolates and rF1 bound 11/20 isolates with good capacity (classified as at least 10x binding compared to ctrl-IgG1) **(Figure 1D)**. Thus, although CR5133- and CR6453-IgG1 bind less well to ATCC 14990, overall, they bind a larger fraction of clinical isolates compared to rF1-IgG1.

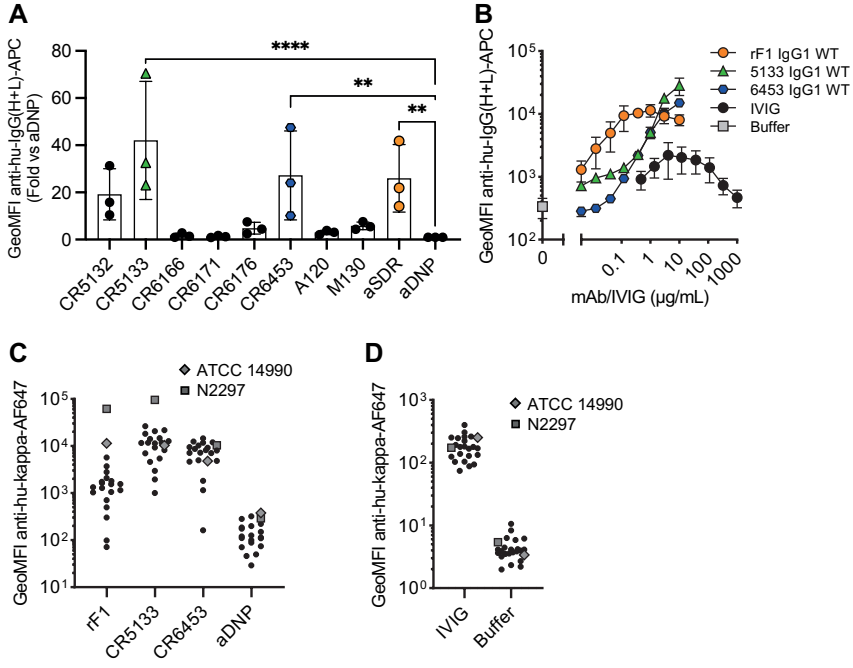

Figure 1. Identifying mAbs that bind *S. epidermidis* neonate isolates. (A) Screening mAb binding to ATCC 14990. Bacteria were incubated with 2 µg/mL IgG1. MAb binding was detected using goat anti-hu-IgG(H+L)-APC and using flow cytometry. Data represent GeoMFI ± SD normalized to aDNP (ctrl)-IgG1 of three independent experiments. One-way ANOVA followed by Dunnett test was performed to test for differences in antibody binding versus aDNP and displayed only when significant as *P ≤ 0.05, **P ≤ 0.01, ***P ≤ 0.001 and ****P ≤ 0.0001. **(B)** Titration of binding mAbs. FITC labeled ATCC 14990 were incubated in a 3-fold dilution range from 1000 µg/mL for IVIG and from 10 µg/mL for rF1-IgG1, CR5133-IgG1 or CR6453-IgG1. MAb binding detected with donkey anti-hu-IgG(H+L)-APC and analyzed with flow cytometry. Data represent GeoMFI ± SD of three independent experiments. Histograms of flow cytometry analysis are included in **figure S2**. **(C)** IVIG binding to clinical isolates. 20 clinical isolates and ATCC 14990, were incubated with 25 µg/mL IVIG. IVIG binding was detected with goat anti-hu-kappa-AF647. Data points are represented as mean AF647 GeoMFI of one experiment. **(D)** mAb binding to clinical isolates. 20 clinical isolates and ATCC 14990, were incubated with 2 µg/mL nM rF1-, CR5133-, CR6453- and aDNP-IgG1. mAb binding was detected with goat anti-hu-kappa-AF647. Data points are represented as mean AF647 GeoMFI of two independent experiments.

Activation of the complement system greatly enhances phagocytosis by mAbs.

We then evaluated whether the selected IgG1 mAbs could induce phagocytosis of *S. epidermidis* by human neutrophils. First, we studied their capacity to directly engage Fc gamma receptors in the absence of the complement system. To study this, we incubated freshly isolated neutrophils together with *S. epidermidis* ATCC 14990 opsonized with mAb at a multiplicity of infection (MOI) of 10:1. CR5133-IgG1, CR6453-IgG1 and the negative control aDNP-IgG1 could not induce Fc gamma mediated phagocytosis after 15 minutes of co incubation **(Figure 2A)**. Only rF1-IgG1 was capable of inducing phagocytosis in absence of the complement system. When 1% normal human serum

depleted of IgG and IgM (ΔNHS) as complement source was added, phagocytosis was enhanced **(Figure 2B)**, with rF1-IgG1 reaching high phagocytosis levels from a concentration above 0.1 µg/mL. Phagocytosis induced by CR5133-IgG1 and CR6453-IgG1 was also enhanced, but these antibodies were less efficient than rF1-IgG1 because higher concentrations were needed to reach similar phagocytosis levels as rF1-IgG1. This observation was very consistent with the ability of the mAbs to induce complement deposition on the bacterial surface, measured using a fluorescent mAb recognizing a neoepitope in C3b [35] and flow cytometry **(Figure 2C)**. RF1-IgG1 was the most efficient, followed by CR5133-IgG1 and CR6453-IgG1. At a fixed concentration of 10 µg/mL, we observed large differences between phagocytosis induced in absence or presence of complement, showing that mAb binding and the complement system are essential for efficient phagocytosis **(Figure 2D)**. Finally, we tested the ability of mAbs to induce phagocytic killing, measured as a reduction in colony forming units (CFU) after prolonged incubation (90 minutes) with neutrophils at an MOI of 1:1. Consistent with the phagocytosis data showing that only rF1-IgG1 can induce Fc-mediated phagocytosis **(Figure 2A)**, we observed that rF1-IgG1, but not CR5133-IgG1 and CR6453-IgG1, could induce phagocytic killing in absence of complement **(Figure 2E)**. Also, in the presence of complement, killing by rF1-IgG1 was more efficient than in the absence of complement. CR5133-IgG1 and CR6453-IgG1 seemed to perform better in the presence of complement, although no significant killing compared to buffer treated samples was observed **(Figure 2E)**. Overall, there are potent mAbs (rF1-IgG1) and less potent mAbs (CR5133- and CR6453-IgG1), and complement enhances phagocytic uptake and killing.

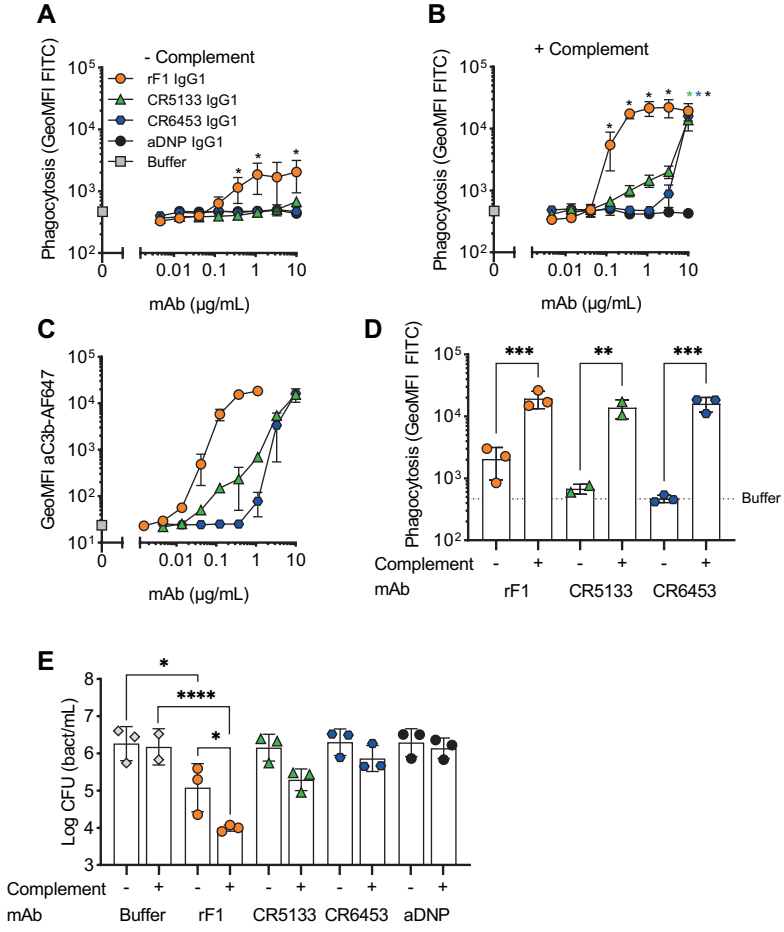

Figure 2. Activation of the complement system greatly enhances phagocytosis and killing with mAbs. **(A,B)** Phagocytosis of ATCC 14990 by human neutrophils ((t=15 min), MOI 10:1) in **(A)** absence or **(B)** presence of complement. FITC labeled bacteria were incubated in **(A)** RPMI-HSA or **(B)** 1% IgG/IgM-depleted normal human serum (ΔNHS) supplemented with a concentration range of rF1, CR5133, CR6453, aDNP IgG1 or buffer. Phagocytosis was quantified by flow cytometry and plotted as FITC GeoMFI of the neutrophil population. The gating strategy at 1 µg/mL mAb is shown in **Figure S3.** Data represent mean ± SD of three independent experiments. One-way ANOVA followed by Bonferroni correction was used to test the effect of mAb addition compared to aDNP-IgG1. Test results were displayed only when significant as *P ≤ 0.05 (black for rF1, green for CR5133, blue for CR6453). **(C)** C3b deposition by mAbs. FITC labeled ATCC 14990 were incubated in 1% ΔNHS supplemented with a concentration range of mAb. C3b deposition was detected by flow cytometry using an anti-neoC3b-AF647 antibody conjugate and plotted as AF647 GeoMFI of the FITC+ve bacterial population. Data represent mean ± SD of three independent experiments. **(D)** Comparison of mAb (10 µg/mL) induced phagocytosis in absence and presence of complement. One-way ANOVA was performed to test for the effect of complement addition on phagocytosis and displayed as *P ≤ 0.05, **P ≤ 0.01, ***P ≤ 0.001 and ****P ≤ 0.0001. **(E)** Killing of ATCC 14990 by human neutrophils (t=90 min, MOI 1:1) in absence or presence of complement. Bacteria were incubated in 10% heat-inactivated (HI)-ΔNHS (-) or 10% ΔNHS (+) supplemented with buffer (dashed horizontal line) or 14.8 µg/mL (100 nM) rF1-, CR5133-, CR6453- or aDNP-IgG1. Data represent mean ± SD of three independent experiments. One-way ANOVA followed by Bonferroni correction was used to test the effect of mAb addition to HI-ΔNHS, mAb addition to ΔNHS and to test the effect of complement addition for each mAb specifically. Test results were displayed only when significant as *P ≤ 0.05, **P ≤ 0.01, ***P ≤ 0.001 and ****P ≤ 0.0001.

Hexamer enhancing mutations in CR5133- and CR6453-IgG1 enhance phagocytosis and killing of *S. epidermidis*.

For optimal interaction with the six globular headpieces of C1q, target bound IgG molecules require organization into higher order oligomers (IgG hexamers), which occurs via noncovalent Fc-Fc interactions [26,27]. Therefore, we hypothesized that hexamer enhancing mutations can improve complement activation and phagocytosis of *S. epidermidis*. We introduced mutation E345K in the Fc backbone of rF1-IgG1, CR5133-IgG1, CR6453-IgG1. This mutation was selected based on previous results obtained with *Streptococcus pneumoniae* [24]. After confirming that introduction of the E345K-mutations did not affect antibody binding to *S. epidermidis* **(Figure S4)**, we tested their ability to induce C3b deposition **(Figure 3A)**, phagocytosis **(Figure 3B)** and killing **(Figure 3C)**. Introduction of the hexamer enhancing mutation into the already potent rF1-IgG1 could only slightly improve complement deposition **(Figure 3A)**. In contrast, hexamer enhanced variants of CR5133-IgG1 and CR6453-IgG1 induced very potent complement deposition compared to the WT IgG1 mAbs. For CR5133-IgG1 and CR6453-IgG1, increased complement deposition by the IgG1-E345K variants translated into more efficient phagocytosis **(Figure 3B)**, while for rF1-IgG1 we only measured a difference in phagocytosis at the lowest mAb concentrations. Interestingly, rF1-IgG1E E345K at higher concentrations induced less phagocytosis than rF1-IgG1, which did not correlate to C3b deposition. In general, more phagocytosis benefit was gained by alteration of CR5133- and CR6453-IgG1 than by alteration of the already potent rF1-IgG1, shifting the effectiveness to a lower mAb concentration. Finally, we determined the effect of the hexamer enhancing mutation on killing. At the lowest concentration tested (0.147 µg/mL), no additive effects of rF1-IgG1 E345K compared to rF1-IgG1 were observed **(Figure 3C)**, presumably because incubation with 0.147 µg/mL rF1-IgG1 already reached the maximum killing capacity of the assay. In line with this hypothesis, the use of higher concentrations rF1-IgG1 or rF1-IgG1 E345K did not increase killing **(Figure S5A)**. However, we observed a striking increase in killing after introducing the hexamer enhancing mutation in CR5133- and especially in CR6453-IgG1 **(Figure 3C)**. Again, these data show that rF1-IgG1 is a potent mAb that could not be improved further by introducing a hexamer enhancing mutation. Importantly, our data also shows that less potent IgG1 mAbs, such as CR5133 and CR6453, can be greatly improved by introducing hexamer enhancing mutations.

Because antibodies of subclass IgG3 bind C1q more stable than IgG1 [40], we also studied the effect of subclass switching to IgG3. As the molecular weight of IgG3 is slightly different from the molecular weight of IgG1, we compared concentrations in nM instead of µg/mL. Subclass switching of rF1-IgG1 to IgG3 did not change its killing capacity **(Figure S5A)**, again presumably because the maximum killing capacity was already reached by

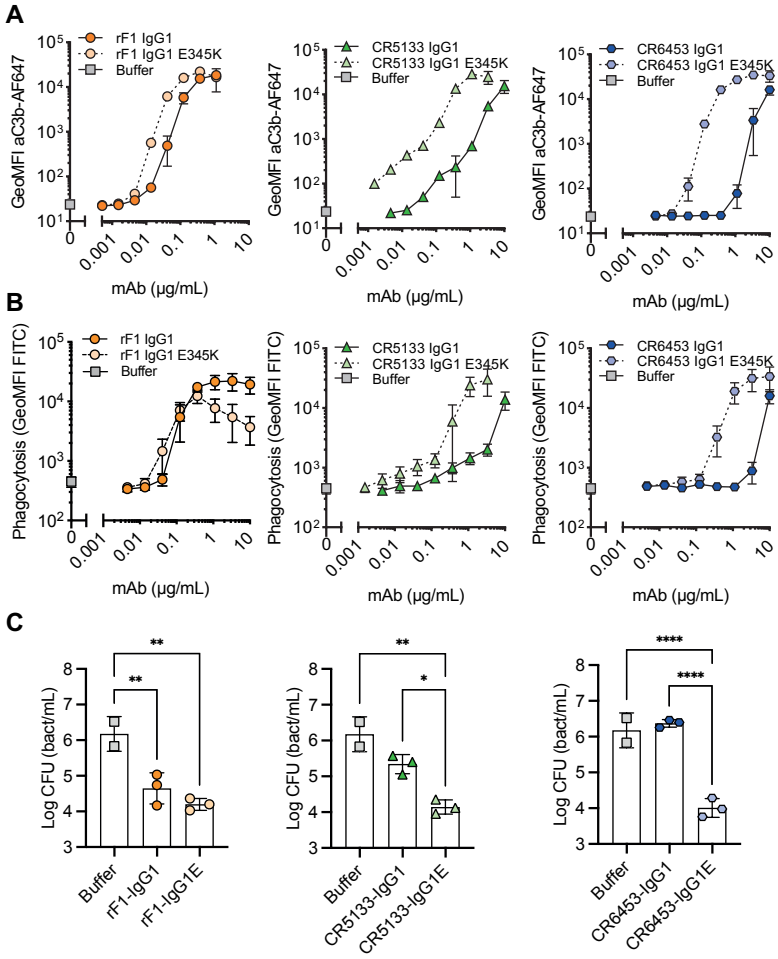

Figure 3. Hexamer enhancing mutations significantly improve effector functions against *S. epidermidis.* **(A)** Effect of introduced hexamer enhancing mutations on deposition of C3b. FITC labeled ATCC 14990 were incubated in 1% ΔNHS supplemented with a concentration range of mAb in IgG1 or IgG1-E345K variant. C3b deposition was detected by flow cytometry using an anti-neoC3b-AF647 antibody conjugate and plotted as AF647 GeoMFI of the FITC+ve bacterial population. Data represent mean ± SD of three independent experiments. **(B)** Phagocytosis of ATCC 14990 by neutrophils (MOI 10:1) in the presence of complement. Bacteria were prepared as in **(A)**. Phagocytosis was assessed by flow cytometry and plotted as FITC GeoMFI of the neutrophil population. Data represent mean ± SD of three independent experiments. Data shown for IgG1 are identical to data shown in **Figure 2B**. **(C)** Killing of ATCC 14990 by neutrophils (MOI 1:1) in presence of complement. Bacteria were incubated in 10% ΔNHS supplemented with 0.148µg/mL (1nM) rF1, 1.48µg/mL (10nM) CR5133 or CR6453. All concentrations tested can be viewed in **Figure S5**. Bacterial survival was quantified after neutrophils lysis by serial dilution and CFU counting. Data represent mean ± SD of three independent experiments. One-way ANOVA followed by Bonferroni correction was used to test the effect of mAb addition in ΔNHS, as well as the difference in bacterial survival of WT vs hexabody, *P ≤ 0.05, **P ≤ 0.01, ***P ≤ 0.001 and ****P ≤ 0.0001.

the IgG1 variant. For mAbs CR5133 and CR6453, the effect of subclass switching to IgG3 was only detectable at a concentration that was 10 times higher (100 nM) than the concentration at which the effect of hexamer enhancing mutations was detectable (10 nM) (**Figure S5BC)**. This indicates that introducing the E345K mutation is more effective than subclass switching to IgG3. Moreover, introduction of the hexamer enhancing mutation in the IgG3 subclass (IgG3E) did not improve killing beyond its IgG1E counterpart.

Plasma isolated from human umbilical cord blood retains classical pathway activity.

Previous studies have reported that the neonatal complement system is less active than in healthy adults [11–13,15]. To investigate if mAbs can also activate the neonatal complement system, we first compared neonatal cord blood plasma samples to adult pooled human plasma in complement activity ELISAs to measure classical (CP), lectin (LP) and alternative (AP) pathway activity. We collected cord blood plasma from neonates (n=5) with a gestational age ranging from 32-42 weeks. Parallel, plasma from healthy adult volunteers was collected in the exact same procedure. To preserve complement activity, all samples were collected in r-Hirudin tubes. Hirudin is a direct thrombin inhibitor, which does not interfere with the complement system, in contrast to other anticoagulants such as heparin or sodium citrate [41,42]. We showed that in all neonatal samples the CP was equally active to adult pooled human plasma **(Figure 4A)**. The LP was decreased in activity compared to pooled human plasma in only one neonatal donor **(Figure 4B)**. On the other hand, the alternative pathway was decreased in all but one neonatal donor **(Figure 4C)**. Thus, although not all complement pathways are equally active in neonatal plasma, we showed that the classical pathway, which is activated by mAbs, is not impaired.

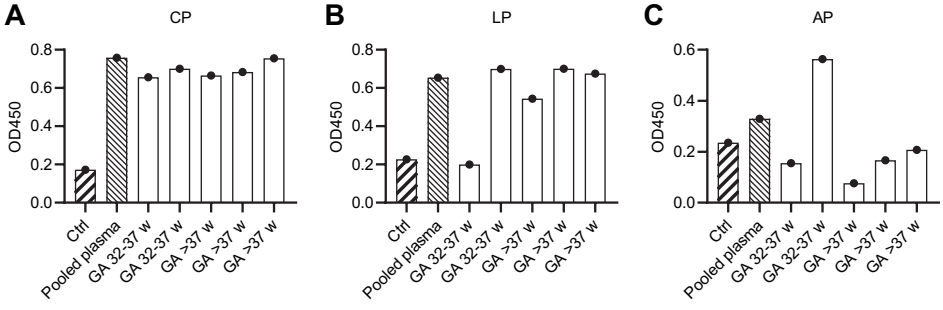

Figure 4. Complement activity of neonatal plasma. Complement activity in pooled human hirudin plasma and neonatal hirudin plasma (n=5) was determined in complement ELISAs, detecting deposition of C3b. Plates were coated with **(A)** IgM and 2% plasma to determine CP activity, **(B)** mannan and 2% plasma to determine LP activity and **(C)** LPS and 30% plasma to determine AP activity. Ctrl wells were uncoated and incubated with pooled adult plasma. CP = Classical pathway, LP = Lectin pathway, AP = Alternative pathway.

Anti-*S. epidermidis* mAbs react with the neonatal complement system.

Finally, we used the same assay to study if neonatal plasma could react with mAbs to opsonize bacteria for phagocytosis. Because umbilical cord blood was collected anonymously, there is a possibility that mothers received prophylaxis against group B streptococci by Amoxicillin/Clavulanic acid (Augmentin®) during labor, which is transferred to the neonatal plasma. Unfortunately, ATCC 14990 was sensitive to this antibiotic. As this could interfere with our assays, we selected a clinical isolate (N2297) that was resistant to Amoxicillin/Clavulanic acid for use in the assays with neonatal plasma. First, we confirmed that all mAbs can bind N2297 and that introduction of the E mutation did not affect mAb binding **(Figure S6)**. We also compared mAb and IVIG binding and again observed that all mAbs showed increased binding compared to IVIG, even at very low concentrations.

As complement activity increases with gestational age [12,13], we divided the donors in two groups of different gestational age; 32-37 weeks GA (n=2) **(Figure 5A)** and >37 weeks GA (n=3) **(Figure 5B)**. Similar to the results on strain ATCC 14990 **(Figure 3B)**, rF1-IgG1 could induce phagocytosis and introduction of the hexamer enhancing mutation in rF1-IgG1 did not result in beneficial effects. CR5133-IgG1 was also capable of inducing phagocytosis in presence of neonatal plasma and CR5133-IgG1 E345K further enhanced phagocytosis. CR6453-IgG1 could not induce phagocytosis, but introduction of the hexamer enhancing mutation greatly enhanced phagocytosis. For all mAbs, the phagocytosis was completely dependent on the neonatal complement system, because when heat inactivated plasma was used, there was no phagocytosis (**Figure 5, S7**). We also compared mAb efficacy to IVIG efficacy. To observe a response in presence of complement, we added a maximum of 1 mg/mL IVIG in 1% plasma. However, this dose is ~10 times higher than clinically relevant, as neonatal clinical trials reach maximum IVIG concentrations of 7-15 mg/mL in 100% plasma [22,43], which corresponds to 70-150 µg/mL in 1% plasma. In absence of complement, IVIG could not induce phagocytosis (**Figure S8**). For CR5133-IgG1 E345K, a concentration of only 0.042 µg/mL was needed to reach a comparable level of phagocytosis as 1000 µg/mL IVIG. For the other mAbs, a concentration of ~1 µg/mL mAb was needed to reach comparable levels to 1000 µg/mL IVIG. We did not observe differences between the two donor groups, thus mAbs can react with the neonate complement system of term (>37 weeks GA) and pre-term (32-37 weeks) infants. Concluding, we show complement activity in term and preterm infant plasma is sufficient to enhance IgG1 mediated opsonophagocytosis by human neutrophils.

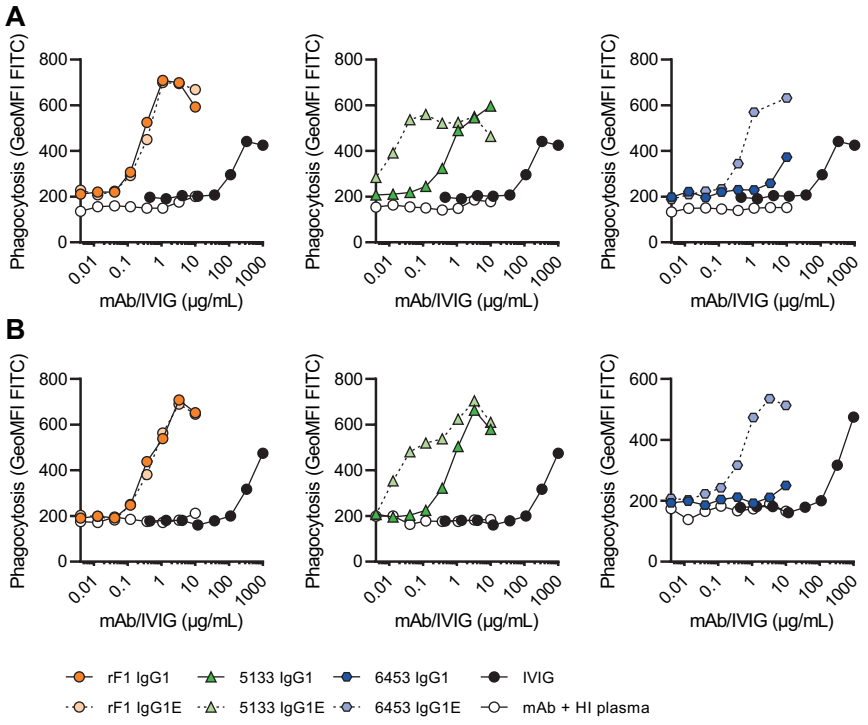

Figure 5. Phagocytosis of FITC labeled N2297 after incubation with mAbs or IVIG in 1% neonatal plasma. Phagocytosis of N2297 by human neutrophils (MOI 10:1) in **(A)** a representative donor of 32-37 weeks GA and **(B)** a representative donor >37 weeks GA. FITC labeled bacteria were incubated in 1% neonatal plasma or 1% HI neonatal plasma supplemented with a concentration range of rF1, CR5133 or CR6453 IgG1 or IgG1 E345K or IVIG. Phagocytosis was quantified by flow cytometry and plotted as FITC GeoMFI of the neutrophil population. Data represent data of one independent experiment. Additional donors (n=5) can be viewed in **Figure S5**. GA = Gestational Age.

Discussion

Staphylococcus epidermidis is the most prevalent causative agent of late onset sepsis in neonates, who are at high risk for infections because of transient immunodeficiency of immaturity [7–15,44]. In this study we show that monoclonal IgG1 antibodies against *S. epidermidis* can boost the neonatal complement system to opsonize bacteria for phagocytosis by neutrophils, which is an efficient way for the immune system to eliminate Gram-positive bacteria such as *S. epidermidis* [18].

Our study highlights that complement is essential for antibody mediated phagocytosis of *S. epidermidis*. For the different IgG1 mAbs we compared, Fc gamma receptor mediated phagocytosis was absent (CR5133 and CR6453) or low (rF1). In the presence of complement, uptake was greatly enhanced. This is in agreement with previous work

on *Streptococcus pneumoniae,* where IgG1 mAbs directed against capsule polysaccharide CPS6 were completely dependent on complement deposition [24]. In contrast, we previously observed that naturally occurring IgG, IVIG [45] and a monoclonal antibody against WTA [23] can induce Fc receptor mediated phagocytosis of *S. aureus* in absence of complement. However, also in these studies, phagocytosis could be improved when complement was added.

Recently, Fc mutations and subclass switching to modify the interaction of a mAbs Fc part with C1q to increase antibody-mediated complement deposition are being explored [46]. This is because for optimal interaction with the six globular headpieces of C1q, target bound IgG molecules require organization into hexamers, which occurs via noncovalent Fc-Fc interactions [26,27]. Hexamer enhancing mutations have already been shown to enhance complement mediated lysis of *Neisseria gonorrhoeae* [47] and tumor cells [26] via the formation of membrane attack complex pores. Together with data on *S. aureus* [23] and *S. pneumoniae* [24], our study provides an important proof of concept that hexamer enhancing mutations can also potentiate opsonization and phagocytic killing of Gram-positive bacteria. This indicates that hexamer enhancing mutations could be applied to a broad range of pathogens and diseases.

Our data also indicates that introducing the hexamer enhancing E345K mutation can enhance mAbs to a similar extent or more than switching to IgG3 subclass. This is an important insight because IgG1 is established to be safe for antibody therapy in other fields than infectious diseases such as oncology and autoimmune diseases [48], is easier to produce and purify than IgG3 [46] and has a longer half life than IgG3 [49].

This study also sheds light on the role of mAb epitopes in efficacy of phagocytosis. We here compared mAbs with an identical Fc backbone but different Fab domains on the same bacterial strain. Our data shows that the use of different Fab domains, which confers binding to epitopes, results in different efficacy between mAbs. This is novel compared to previous publications from our laboratory, in which we either compared mAbs recognizing different bacterial strains (*S. pneumoniae* [24]) or we studied one mAb (4497) with different Fc tails (*S. aureus* [23]). The direct comparison in this work is a strong indication that the epitope is crucial for the efficacy of mAbs to opsonize *S. epidermidis* for phagocytic killing. We hypothesize that the ideal epitope allows for IgG clustering, as literature describes that epitope density can influence hexamerization [26]. Affinity for the epitope may also play a role, as binding with one Fab arm (instead of two) enhances hexamer formation [26,50]. In all, this stresses the importance of identifying the ideal epitope to target with mAb therapy.

Next to being able to trigger complement activation, for application of mAbs it is also important that they react with conserved antigens that are present on the majority of clinical isolates. This made rF1, although being the most potent mAb on our model strain, less ideal because it only bound ~50% of clinical isolates. Interestingly we showed that two mAbs (CR5133 and CR6453) could bind 19/20 clinical isolates. Even if CR5133- and CR6453-IgG1 were less potent in driving phagocytosis than rF1-IgG1, their functionality could be enhanced by hexamer enhancing mutations. The fact that we found two mAbs that bound 95% of clinical isolates indicates that mAb therapy for *S. epidermidis* holds potential, while for other pathogens, such as *S. pneumoniae*, the existence of many different serotypes will pose a challenge [51]. The future of antibacterial preventive or therapeutic mAb therapies may well be in cocktails of multiple mAbs against different strains of a single species or against multiple species of interest [52].

Our study supports the presence of an effective complement system in neonates, enabling effective antibody induced opsonophagocytosis. Previous studies have reported a decreased complement activity and plasma concentrations of complement components in neonates, which is correlated with gestational age [11]. Older studies described that most complement levels are at 50–70% of the adult values, rising to adult concentrations within 6 months after birth [11,12,15]. Recent work describes significantly lower levels for approximately one third of the complement factors measured [28]. We found lower complement activity compared to adults in the alternative pathway but not in the lectin and classical pathway. An explanation could be that we used r-Hirudin tubes to collect plasma in this study, which preserves complement activity the best [36]. Even though alternative pathway activity, which is responsible for the complement amplification loop, was decreased, we showed that mAbs can greatly stimulate phagocytosis in the presence of neonatal complement. This confirms that neonatal complement can be activated by mAbs and that mAb therapy in neonates should be further explored.

As a proof of concept, we here show that mAbs (IgG1 and Fc:Fc enhanced IgG1) can react with the neonatal complement system to potentiate phagocytosis by healthy donor adult neutrophils. Others have shown neonatal neutrophils can efficiently phagocytose and kill *S. epidermidis* when opsonized with adult serum [44]. Therefore, we expect that neonatal neutrophils will respond in the same manner as the adult neutrophils in our assay, although this will need further investigation.

In conclusion, we demonstrate that monoclonal antibodies against *S. epidermidis* can effectively induce opsonophagocytosis in the context of neonatal plasma. Opsonophagocytosis of *S. epidermidis* is dependent on complement activation and hexamer enhancing mutations in IgG effectuate more efficient opsonophagocytosis in neonatal

plasma. Anti-*S. epidermidis* mAbs are a potential future preventive therapy that could be used in the neonatal setting to avoid *S. epidermidis* CLABSI in high risk infants admitted to neonatal intensive care units.

Materials and Methods

Ethics statement

Human blood was obtained from healthy donors after informed consent was given by all subjects in accordance with the Declaration of Helsinki. Approval from the Medical Ethics Committee of the University Medical Center Utrecht was obtained (METC protocol 07-125/C approved on March 1, 2010). Cord blood (CB) was obtained from the umbilical cord after vaginal birth of neonates of different gestational age (GA); 32-37 weeks GA (n=2) and >37 weeks GA (n=3). Samples were collected at the obstetrics department and analyzed and stored anonymously. Written informed consent was obtained from the mother in accordance with the Declaration of Helsinki. The Ethics Committee for Biobanking of the University Medical Center Utrecht approved the collection protocol (TCBio 21/223, approved on June 14th, 2021).

IgG and IgM depletion from human serum

Normal human serum (NHS) from twenty healthy donors was depleted of IgG and IgM as previously described [29]. Briefly, affinity chromatography was used to capture IgG by using HiTrap protein G High Performance column (Cytiva, GE Healthcare) and IgM with Capture Select IgM Affinity Matrix (Thermo Fischer Scientific) from NHS. Complement levels and activity were determined after depletion, using enzyme linked immunosorbent serological assay (ELISA) and classical/alternative pathway hemolytic assays. Although C1q is partially co depleted during the procedure, C1q was not supplemented in IgG/IgM depleted NHS (ΔNHS), because supplementation with 70 µg/ml C1q did not alter complement deposition on *S. epidermidis* **(Figure S1)**, indicating that the amount of C1q left was sufficient.

Generation of human monoclonal antibodies

IgG1 mAbs A120, CR5133, CR6166 and CR6176 were produced by Genmab (Utrecht, the Netherlands) as described previously [WO 2017/198731 Al, [30]. IgG1 clones M130, CR5132, CR6171, CR6453, rF1 and G-2A2 (aDNP) and the subtypes of rF1, CR5133, CR6453 and G-2A2 (IgG3, IgG1 E345K, IgG3 E345K) were produced as described previously [23,31]. For mAb expression, variable heavy (VH) chain and variable light (VL) chain sequences were cloned in expression vectors pcDNA3.3 (Thermo Fisher Scientific) as described in Vink et al. [30] or pcDNA3.4 (Thermo Fisher Scientific) as described in de Vor

et al. [31], containing human IgG1 heavy chain (HC) and light chain (LC) constant regions as indicated in **Table S1**. The E345K single mutation of Glu at position 345 into Lys was introduced in the heavy chain expression vectors by gene synthesis (IDT (Integrated DNA Technologies)). Variable heavy (VH) and light chain (VL) sequences from all antibodies were obtained from scientific publications or patents **(Table S1)**. Antibodies were expressed as IgG1,κ except for CR6166 which was expressed as IgG1,λ. Plasmid DNA mixtures encoding both heavy and light chains of antibodies were transiently transfected in EXPI293F (Life technologies, USA) as described before [3031]. IgG1 antibodies were isolated using HiTrap Protein A High Performance column (Cytiva, GE Healthcare) and IgG3 antibodies were collected using HiTrap Protein G High Performance column (Cytiva, GE Healthcare) in the Äkta Pure protein chromatography system (GE Healthcare). All antibody fractions were dialyzed overnight in PBS and filter sterilized through 0.22 µm SpinX-filters. Size exclusion chromatography (SEC) (Cytiva, GE Healthcare) was performed to check for mAb homogeneity, and the monomeric fraction was separated when aggregation levels exceeded 5%. Final antibody concentration was determined by measuring the absorbance at 280 nm and antibodies were stored at -80 °C or 4°C.

Bacterial strains and growth conditions

S. epidermidis type strain ATCC 14990 [32,33] and twenty clinical bacteremia isolates from neonates admitted to the Wilhelmina Children's hospital (UMC Utrecht) were used in this study. Strains were grown overnight at 37 °C on sheep blood agar (SBA) and were cultured overnight in Tryptic Soy Broth (TSB). Next, they were sub cultured and grown to exponential phase for ± 2.5 hours. For flow cytometry, exponential phase bacteria were washed in PBS and incubated in 250 µg/ml fluorescein isothiocyanate (FITC) (Sigma Aldrich) in PBS for 30 minutes at 4 °C. After washing, FITC labeled bacteria were diluted in RPMI (Gibco) supplemented with 0.05% human serum albumin (HSA) (Sanquin products) and the bacterial concentration was determined by flow cytometry using a MACSQuant analyzer (Miltenyi), counting bacterial events in a defined volume. Bacteria were aliquoted and stored at -20 °C. When indicated, freshly grown exponential cultures were used of which the concentration was determined based on optical density at 600 nm (OD_{600}) (OD 1.0 = 5 x 10^8 bact/ml).

Antibody binding to *S. epidermidis*

For the initial screening of mAb binding to *S. epidermidis*, freshly grown bacteria were washed and diluted in PBS supplemented with 0.1% bovine serum albumin (BSA) (Serva). For all other binding experiments, FITC labeled 14990 and N2297 were used. A total of 150,000 bacteria were incubated with a concentration range of mAbs or IVIG (Nanogam, Sanquin) in PBS-BSA in a round bottom 96-wells plate for 30 minutes at 4 °C, shaking (± 750 rpm). After washing, bacteria were further incubated for 30 minutes at

4 °C, shaking (± 750 rpm) with 30 µl APC-conjugated goat anti-human IgG (H+L) $F(ab')_2$ antibody (Jackson Immunoresearch, 1 µg/ml) or APC-conjugated donkey anti-human IgG (H+L) $F(ab')_2$ antibody (Jackson Immunoresearch, 1:250) to detect both lambda and kappa chains or AlexaFluor647(AF647)-conjugated goat anti-human kappa $F('ab)_2$ antibody (Southern Biotech, 1 µg/ml) to compare binding of IgG1, IgG1 E345K, IgG3 and IgG3 E345K. After incubation with detection antibodies, bacteria were washed and fixed in 1% paraformaldehyde (PFA) (Polysciences) in PBS. Samples were measured by flow cytometry (BD FACSVerse), and data analyzed by FlowJo Software (Version 10). A control sample was used to set FSC-SSC gates to exclude debris and large aggregates of bacteria. In case we used FITC labeled bacteria, only FITC positive events were analyzed. Data are presented as APC or AF647 geometric mean fluorescence intensity (GeoMFI ± SD).

Phagocytosis of *S. epidermidis* by neutrophils

Human neutrophils were isolated from blood of healthy donors by Ficoll-Histopaque gradient centrifugation and suspended in RPMI-HSA [34]. For opsonization, 750,000 FITC labeled bacteria (20 µL) were incubated with 10 µL mAbs or IVIG supplemented with 10 µL ΔNHS or neonatal plasma (final concentration 1%) or buffer, to investigate complement- or Fc receptor mediated phagocytosis, respectively. Bacteria were incubated in a round-bottom 96-wells plate for 15 minutes, at 37 °C, shaking (± 750 rpm). Subsequently, 75,000 neutrophils (10 µL) were added, giving a 10:1 bacteria-to-cell ratio and samples were incubated for 15 minutes at 37 °C, shaking (± 750 rpm). The reaction was stopped with 1% ice cold PFA in RPMI-HSA and FITC fluorescence was measured by flow cytometry (BD FACSVerse). To exclude debris, a neutrophil population incubated in RPMI-HSA alone was used to set FSC-SSC gates. Data were analyzed by FlowJo (version 10) and presented as FITC GeoMFI ± SD of the neutrophil population.

Killing of *S. epidermidis*

Freshly grown, exponential phase *S. epidermidis* was washed with Hanks Balanced Salt Solution (HBSS) (BioWitthaker) supplemented with 0.1% HSA. For opsonization, 850,000 bacteria were incubated with NHS or mAbs and ΔNHS in HBSS-HSA (concentrations indicated in figure legends) in a round bottom 96-deep-well plate for 30 minutes at 37 °C, shaking (± 750 rpm) (final volume: 15 µl). After 30 minutes opsonization, 850,000 neutrophils were added (MOI 1:1) and further incubated for an additional 90 minutes at 37 °C, 5% CO_2 with open cover, shaking (± 750 rpm) (final volume: 100 µl). The reaction was stopped by adding 900 µl of ice-cold, freshly prepared, 0.2 µm sterile filtered 0.3% saponin (w/v, Sigma) in Milli-Q water. Samples were incubated for 5-15 minutes at 4 °C, shaking (± 750 rpm). Total viable bacterial counts were determined by serial dilution and plating. Data are presented as CFU ± SD. The following control

conditions were always included: 10% NHS with neutrophils (positive control for killing), heat-inactivated-ΔNHS with neutrophils (negative control for killing), HBSS-HSA with neutrophils only (sterility control) and HBSS-HSA with bacteria only (reference control for the amount of bacteria added).

Production of anti-C3b AF647 conjugate

2000 µg/ml mouse IgG2a mAb against a neo-epitope C3b (clone Bh6) [35] was incubated with AF647 NHS ester (Life Technologies) (final concentration: 100 µg/ml) and sodium carbonate (pH 9.4, final concentration: 0.1 M) for 70 minutes, room temperature, rotating. The sample was separated from aggregates by spinning through 0.22 µm SpinX filter columns (Corning life Sciences BV) for 2 minutes at 1500x *g*. To remove free AF647 from the mixture, filtrate was transferred to a sterile PBS washed Zeba spin column (Thermo Scientific) and spun for 2 minutes at 1500x *g*. From OD_{280} and OD_{650} Nanodrop (Thermo Scientific) measurements, the degree of labeling (DOL) was determined at 4.14. The conjugate was checked for integrity by SDS-PAGE and fluorescence of antibody conjugate was confirmed using ImageQuant LAS 4000.

Complement deposition on *S. epidermidis*

To determine C3b deposition on *S. epidermidis*, 150,000 FITC labeled bacteria were incubated with mAbs supplemented with 1% ΔNHS in RPMI-HSA for 30 minutes at 37 °C, shaking (± 750 rpm) (final volume: 30 µl). After washing twice with PBS-BSA, bacteria were further incubated for an additional 30 minutes at 4 °C, shaking (± 750 rpm) with 15 µl anti-C3b AF647 detection antibody (3 µg/ml) in PBS-BSA. Bacteria were washed with PBS-BSA and fixed in 1% PFA in PBS-BSA for at least 30 minutes at 4 °C, shaking (± 750 rpm) after which fluorescence was measured by flow cytometry (BD FACSVerse). To exclude debris and large aggregates of bacteria, control bacteria incubated in RPMI-HSA alone were used to set FSC-SSC gates, only FITC-positive events were analyzed. Data were analyzed by FlowJo Software (Version 10) and presented as AF647 GeoMFI ± SD.

Collection of plasma samples

Cord blood or peripheral venous blood of healthy human donors was collected in S-Monovette r-Hirudin tubes (Sarstedt) to preserve complement activity [36]. The blood was centrifuged at 1000x g for 5 minutes and plasma was removed and stored immediately at -80°C. Plasma of 27 healthy donors was pooled before freezing and cord blood plasma was stored individually. For complement inactivation, the plasma was heat inactivated for 30 minutes at 56°C.

Complement ELISAs

Complement ELISAs were performed as previously described [37] with minor modifications. Briefly, microtiter plates (Nunc maxisorp) were precoated with 3 µg/mL IgM (Sigma) for classical pathway (CP) ELISA, with 20 µg/ml LPS (from *Salmonella enteriditis*, Sigma) for alternative pathway (AP) ELISA and with 20 µg/mL mannan (from *Saccharomyces cerevisiae*, Sigma) for lectin pathway (LP) ELISA. All coatings were prepared in 0.1 M carbonate buffer (pH 9) and incubated overnight at room temp. Plasma samples were diluted in Veronal Buffered Saline (VBS) + 0.1% gelatin + 5 mM $MgCl_2$ + 10 mM EGTA for AP ELISA and in VBS + 0.1% gelatin + 0.5 mM $CaCl_2$ + 0.25 mM $MgCl_2$ for CP ELISA and LP ELISA. After washing the plates with PBS 0.05% Tween-20, wells were blocked with 4% BSA in PBS-Tween. Then, plasma samples were added for 1 hour at 37°C in the appropriate buffer and dilutions. After additional washing, deposited C3b was detected using DIG-labeled mouse anti C3 antibody (WM1, 0.1 µg/mL) followed by Peroxidase conjugated sheep anti-DIG-Fab fragments (1:8000, Roche 11207733910). Finally, the plates were washed and developed using 3,3',5,5'-tetramethylbenzidine (Thermo Fisher). The reaction was stopped by addition of 1 N H_2SO_4. Absorption at 450nm was measured using a microplate reader (Biorad).

Statistical analysis

Statistical analyses were performed in Prism software (version 8.3; Graphpad). The tests used to calculate P-values are indicated in the figure legends. The number of independent biological repeats per graph is indicated in the figure legends.

Acknowledgements

The authors greatly thank J.T. van der Bruggen for providing *S. epidermidis* clinical isolates; prof. T. Mollnes and prof. P. Garred for providing clone Bh6 cells. This project was financially supported by a grant from the Wilhelmina Children's Hospital Fund (MvdF) and by a PPP Allowance made available by Health~Holland (LSHM17026), Top Sector Life Sciences & Health, to stimulate public-private partnerships.

References

1. James, S. L. *et al.* Global, regional, and national incidence, prevalence, and years lived with disability for 354 Diseases and Injuries for 195 countries and territories, 1990-2017: A systematic analysis for the Global Burden of Disease Study 2017. *Lancet* **392**, 1789–1858 (2018).
2. Fleischmann, C. *et al.* Global incidence and mortality of neonatal sepsis: A systematic review and meta-analysis. *Arch. Dis. Child.* **106**, 745–752 (2021).
3. Dong, Y., Speer, C. P. & Glaser, K. Beyond sepsis: *Staphylococcus epidermidis* is an underestimated but significant contributor to neonatal morbidity. *Virulence* **9**, 621–633 (2018).
4. Kollmann, T. R., Kampmann, B., Mazmanian, S. K., Marchant, A. & Levy, O. Protecting the Newborn and Young Infant from Infectious Diseases: Lessons from Immune Ontogeny. *Immunity* **46**, 350–363 (2017).
5. Hsu, H. E. *et al.* Health Care–Associated Infections Among Critically Ill Children in the US, 2013-2018. *JAMA Pediatr.* **174**, 1176 (2020).
6. Watson, R. S. *et al.* The Epidemiology of Severe Sepsis in Children in the United States. *Am. J. Respir. Crit. Care Med.* **167**, 695–701 (2003).
7. Claessens, L. C., Zonnenberg, I. A., Van Den Dungen, F. A. M., Vermeulen, R. J. & Van Weissenbruch, M. M. Cerebral ultrasound abnormalities in preterm infants caused by late-onset sepsis. *PLoS One* **12**, 1–10 (2017).
8. Isaacs, D. A ten year, multicentre study of coagulase negative staphylococcal infections in Australasian neonatal units. *Arch. Dis. Child. Fetal Neonatal Ed.* **88**, 89–93 (2003).
9. Palmeira, P., Quinello, C., Silveira-Lessa, A. L., Zago, C. A. & Carneiro-Sampaio, M. IgG Placental Transfer in Healthy and Pathological Pregnancies. *Clin. Dev. Immunol.* **2012**, 1–13 (2012).
10. Malek, A., Sager, R., Kuhn, P., Nicolaides, K. H. & Schneider, H. Evolution of maternofetal transport of immunoglobulins during human pregnancy. *Am. J. Reprod. Immunol.* **36**, 248–255 (1996).
11. McGreal, E. P., Hearne, K. & Spiller, O. B. Off to a slow start: Under-development of the complement system in term newborns is more substantial following premature birth. *Immunobiology* **217**, 176–186 (2012).
12. Notarangelo, L. D. *et al.* Activity of classical and alternative pathways of complement in preterm and small for gestational age infants. *Pediatr. Res.* **18**, 281–285 (1984).
13. Grumach, A. S., Ceccon, M. E., Rutz, R., Fertig, A. & Kirschfink, M. Complement profile in neonates of different gestational ages. *Scand. J. Immunol.* **79**, 276–281 (2014).
14. Prosser, A. *et al.* Phagocytosis of neonatal pathogens by peripheral blood neutrophils and monocytes from newborn preterm and term infants. *Pediatr. Res.* **74**, 503–510 (2013).
15. Høgåsen, A. K. M. *et al.* The analysis of the complement activation product SC5 b-9 is applicable in neonates in spite of their profound C9 deficiency. *J. Perinat. Med.* **28**, (2000).
16. Lawrence, S. M., Corriden, R. & Nizet, V. Age-Appropriate Functions and Dysfunctions of the Neonatal Neutrophil. *Front. Pediatr.* **5**, (2017).
17. Rigby, K. M. & DeLeo, F. R. Neutrophils in innate host defense against *Staphylococcus aureus* infections. *Semin. Immunopathol.* **34**, 237–259 (2012).
18. Segal, A. W. How neutrophils kill microbes. *Annu. Rev. Immunol.* **23**, 197–223 (2005).

19. Bayram, R. O., Özdemir, H., Emsen, A., Türk Dağı, H. & Artaç, H. Reference ranges for serum immunoglobulin (Igg, iga, and igm) and igg subclass levels in healthy children. *Turkish J. Med. Sci.* **49**, 497–505 (2019).
20. Lu, L. L., Suscovich, T. J., Fortune, S. M. & Alter, G. Beyond binding: Antibody effector functions in infectious diseases. *Nat. Rev. Immunol.* **18**, 46–61 (2018).
21. Dustin, M. L. Complement Receptors in Myeloid Cell Adhesion and Phagocytosis. *Microbiol. Spectr.* **4**, (2016).
22. Ohlsson, A. & Lacy, J. B. Intravenous immunoglobulin for suspected or proven infection in neonates. *Cochrane Database Syst. Rev.* **2020**, (2020).
23. Zwarthoff, S. A. *et al.* C1q binding to surface-bound IgG is stabilized by C1r 2 s 2 proteases. *Proc. Natl. Acad. Sci.* **118**, (2021).
24. Aguinagalde, L. *et al.* Promoting Fc-Fc interactions between anti-capsular antibodies provides strong complement-dependent immune protection against Streptococcus pneumoniae *bioRxiv* 2022.01.21.477211 (2022) doi:10.1101/2022.01.21.477211.
25. Wang, G. *et al.* Molecular Basis of Assembly and Activation of Complement Component C1 in Complex with Immunoglobulin G1 and Antigen. *Mol. Cell* **63**, 135–145 (2016).
26. Diebolder, C. A. *et al.* Complement Is Activated by IgG Hexamers Assembled at the Cell Surface. *Science (80-.).* **343**, 1260–1263 (2014).
27. de Jong, R. N. *et al.* A Novel Platform for the Potentiation of Therapeutic Antibodies Based on Antigen-Dependent Formation of IgG Hexamers at the Cell Surface. *PLOS Biol.* **14**, e1002344 (2016).
28. Willems, E. *et al.* Biosynthetic homeostasis and resilience of the complement system in health and infectious disease. *EBioMedicine* **45**, 303–313 (2019).
29. Zwarthoff, S. A., Magnoni, S., Aerts, P. C., van Kessel, K. P. M. & Rooijakkers, S. H. M. Method for Depletion of IgG and IgM from Human Serum as Naive Complement Source. in *Methods in molecular biology (Clifton, N.J.)* vol. 2227 21–32 (2021).
30. Vink, T., Oudshoorn-Dickmann, M., Roza, M., Reitsma, J.-J. & de Jong, R. N. A simple, robust and highly efficient transient expression system for producing antibodies. *Methods* **65**, 5–10 (2014).
31. de Vor, L. *et al.* Human monoclonal antibodies against *Staphylococcus aureus* surface antigens recognize in vitro and in vivo biofilm. *Elife* **11**, 1–25 (2022).
32. Hugh, R. & Ellis, M. A. The neotype strain for *Staphylococcus epidermidis* (Winslow and Winslow 1908) Evans 1916. *Int. J. Syst. Bacteriol.* **18**, 231–239 (1968).
33. Putonti, C. *et al.* Draft Genome Sequence of *Staphylococcus epidermidis* (Winslow and Winslow) Evans (ATCC 14990). *Genome Announc.* **5**, (2017).
34. Bestebroer, J. *et al.* Staphylococcal superantigen-like 5 binds PSGL-1 and inhibits P-selectin–mediated neutrophil rolling. *Blood* **109**, 2936–2943 (2007).
35. Garred, P., Mollnes, T. E., Lea, T. & Fischer, E. Characterization of a Monoclonal Antibody MoAb bH6 Reacting with a Neoepitope of Human C3 Expressed on C3b, iC3b, and C3c. *Scand. J. Immunol.* **27**, 319–327 (1988).
36. Bexborn, F. *et al.* Hirudin versus heparin for use in whole blood *in vitro* biocompatibility models. *J. Biomed. Mater. Res. Part A* **89A**, 951–959 (2009).
37. Seelen, M. A. *et al.* Functional analysis of the classical, alternative, and MBL pathways of the complement system: standardization and validation of a simple ELISA. *J. Immunol. Methods* **296**, 187–198 (2005).

38. Hazenbos, W. L. W. *et al.* Novel Staphylococcal Glycosyltransferases SdgA and SdgB Mediate Immunogenicity and Protection of Virulence-Associated Cell Wall Proteins. *PLoS Pathog.* **9**, e1003653 (2013).
39. Gonzalez, M. L., Frank, M. B., Ramsland, P. A., Hanas, J. S. & Waxman, F. J. Structural analysis of IgG2A monoclonal antibodies in relation to complement deposition and renal immune complex deposition. *Mol. Immunol.* **40**, 307–317 (2003).
40. Vidarsson, G., Dekkers, G. & Rispens, T. IgG Subclasses and Allotypes: From Structure to Effector Functions. *Front. Immunol.* **5**, 520 (2014).
41. van der Maten, E., de Jonge, M. I., de Groot, R., van der Flier, M. & Langereis, J. D. A versatile assay to determine bacterial and host factors contributing to opsonophagocytotic killing in hirudin-anticoagulated whole blood. *Sci. Rep.* **7**, 42137 (2017).
42. Chang, J.-Y. The functional domain of hirudin, a thrombin-specific inhibitor. *FEBS Lett.* **164**, 307–313 (1983).
43. Ohlsson, A. & Lacy, J. B. Intravenous immunoglobulin for preventing infection in preterm and/or low birth weight infants. *Cochrane database Syst. Rev.* **1**, CD000361 (2020).
44. Wolach, B. *et al.* Some aspects of the humoral immunity and the phagocytic function in newborn infants. *Isr. J. Med. Sci.* **30**, 331–5 (1994).
45. Boero, E. *et al.* Use of Flow Cytometry to Evaluate Phagocytosis of *Staphylococcus aureus* by Human Neutrophils. *Front. Immunol.* **12**, 1–15 (2021).
46. Chu, T. H., Patz, E. F. & Ackerman, M. E. Coming together at the hinges: Therapeutic prospects of IgG3. *MAbs* **13**, (2021).
47. Gulati, S. *et al.* Complement alone drives efficacy of a chimeric antigonococcal monoclonal antibody. *PLOS Biol.* **17**, e3000323 (2019).
48. Castelli, M. S., McGonigle, P. & Hornby, P. J. The pharmacology and therapeutic applications of monoclonal antibodies. *Pharmacol. Res. Perspect.* **7**, (2019).
49. Morell, A., Terry, W. D. & Waldmann, T. A. Metabolic properties of IgG subclasses in man. *J. Clin. Invest.* **49**, 673–680 (1970).
50. Wang, B. *et al.* Regulation of antibody-mediated complement-dependent cytotoxicity by modulating the intrinsic affinity and binding valency of IgG for target antigen. *MAbs* **12**, (2020).
51. Bentley, S. D. *et al.* Genetic Analysis of the Capsular Biosynthetic Locus from All 90 Pneumococcal Serotypes. *PLoS Genet.* **2**, e31 (2006).
52. Frandsen, T. P. *et al.* Consistent manufacturing and quality control of a highly complex recombinant polyclonal antibody product for human therapeutic use. *Biotechnol. Bioeng.* **108**, 2171–2181 (2011).

Supplementary information

Supplementary figures

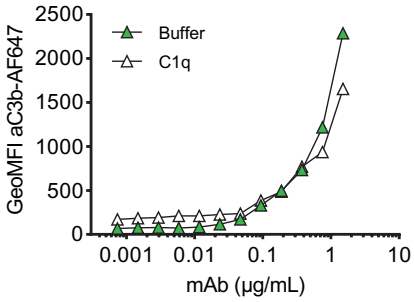

Figure S1. Effect of C1q supplementation in IgG/IgM depleted NHS on deposition of C3b. FITC labeled ATCC 14990 were incubated in 1% ΔNHS supplemented with buffer or C1q and a concentration range of CR5133-IgG1. C3b deposition was detected by flow cytometry using an anti-neoC3b-AF647 antibody conjugate and plotted as AF647 GeoMFI of the FITC+ve bacterial population.

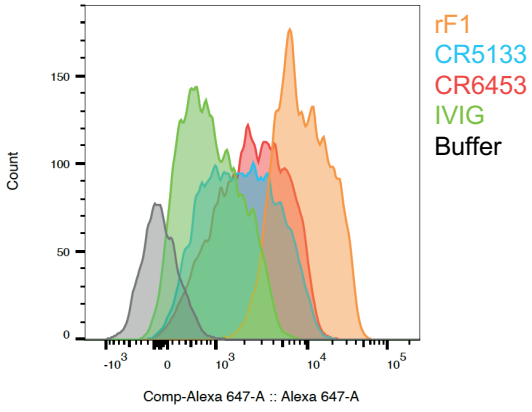

Figure S2. Flow cytometry histograms for Figure 1B. Representative of n=3.

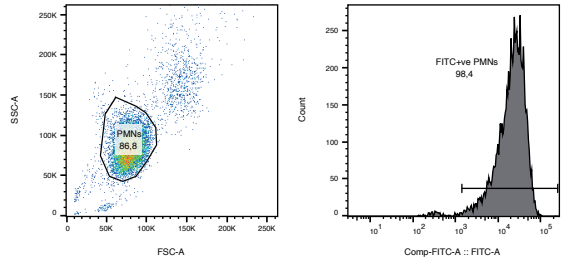

1 µg/mL rF1-IgG1 in 1% IgG/IgM dNHS

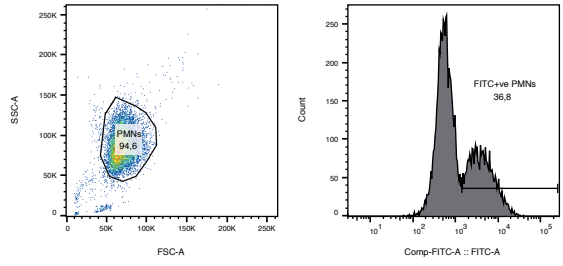

1 µg/mL CR5133-IgG1 in 1% IgG/IgM dNHS

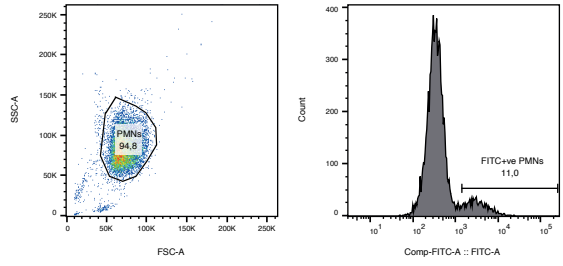

1 µg/mL CR6453-IgG1 in 1% IgG/IgM dNHS

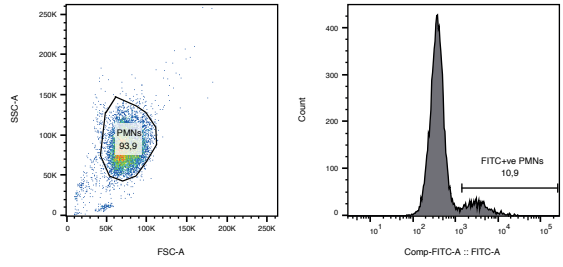

1 µg/mL aDNP-IgG1 in 1% IgG/IgM dNHS

Figure S3. Gating strategy for phagocytosis. Representative of n=3. A neutrophil population was gated based on FSC-SSC and GeoMFI of neutrophil in the FITC channel was analyzed.

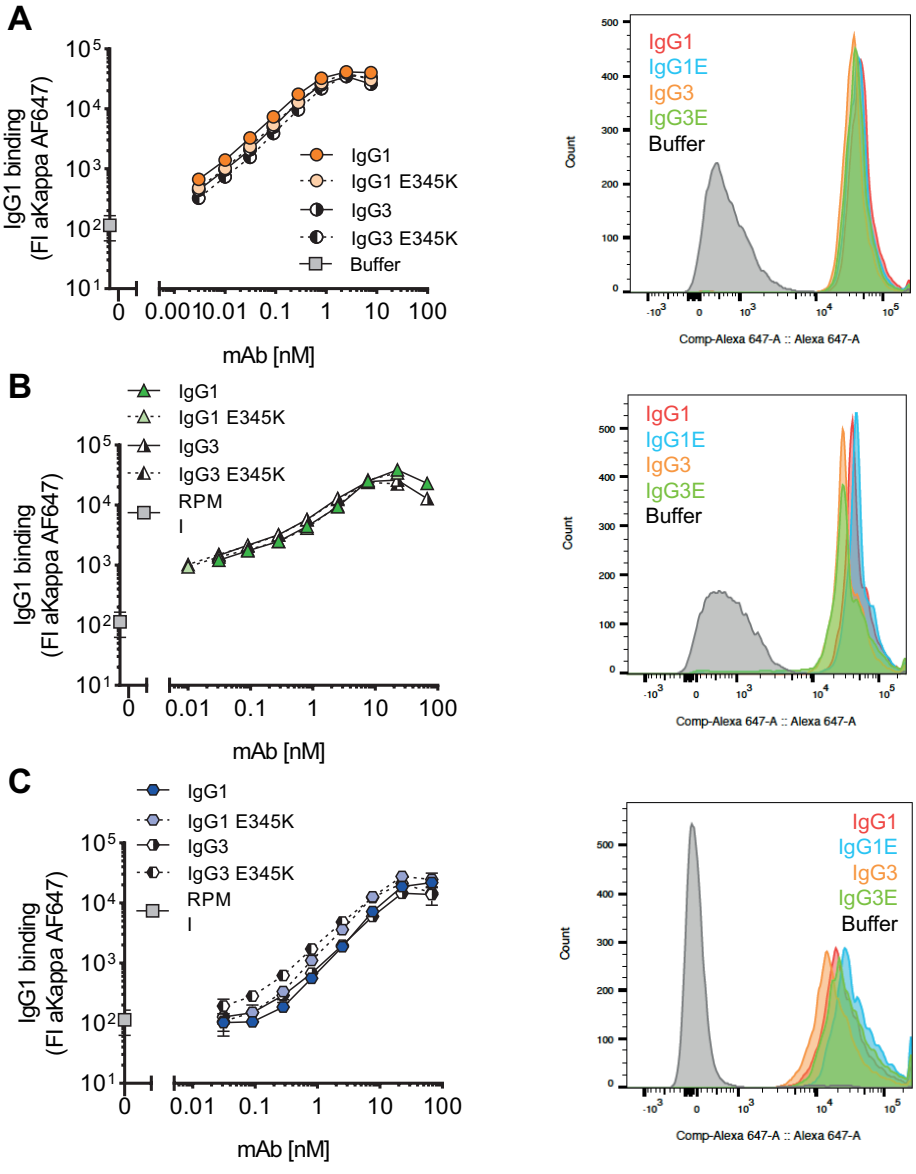

Figure S4. Titration of mAb variants. FITC labeled ATCC 14990 were incubated in a concentration range of rF1 **(A)**, CR5133 **(B)**, CR6453 **(C)** in IgG1, IgG1E, IgG3 or IgG3E variant. Flow cytometry histograms of 2.5 nM rF1, 22.7 nM CR5133 and 22.7 nM CR6453 are shown in the right panel. MAb binding detected with anti-kappa-AF647 and analyzed with flow cytometry. Data represent GeoMFI ± SD of three independent experiments.

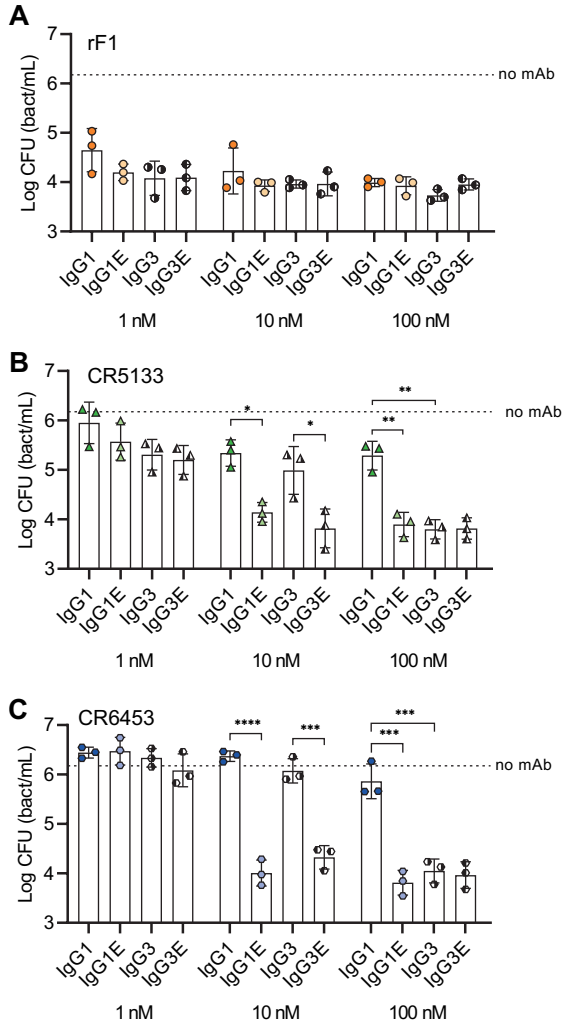

Figure S5. Killing at all concentrations of mAb variants tested. Killing of ATCC 14990 by neutrophils (MOI 1:1) in presence of complement. Bacteria were incubated in 10% ΔNHS supplemented with different rF1 **(A)**, CR5133 **(B)**, CR6453 **(C)** concentrations. Bacterial survival was quantified after neutrophils lysis by serial dilution and CFU counting. Data represent mean ± SD of three independent experiments. One-way ANOVA followed by Bonferroni correction was used to test the effect of mAb addition in ΔNHS, as well as the difference in bacterial survival of WT vs hexabody variant and the difference in effect between IgG1 and IgG3, *P ≤ 0.05, **P ≤ 0.01, ***P ≤ 0.001 and ****P ≤ 0.0001.

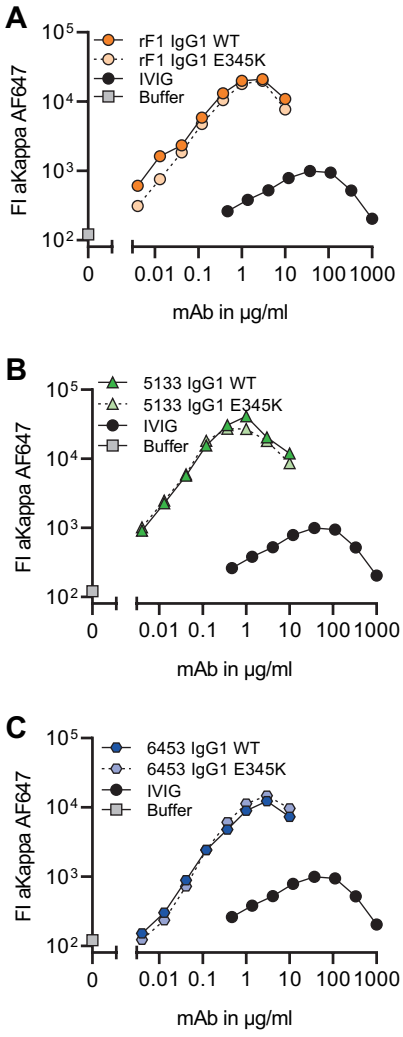

Figure S6. mAb binding to N2297. FITC labeled N2297 were incubated in a concentration range of IVIG, (A) rF1, (B) CR5133, (C) CR6453 IgG1. MAb binding detected with goat anti-hu-kappa-AF647 and analyzed with flow cytometry. Data represent GeoMFI one experiment.

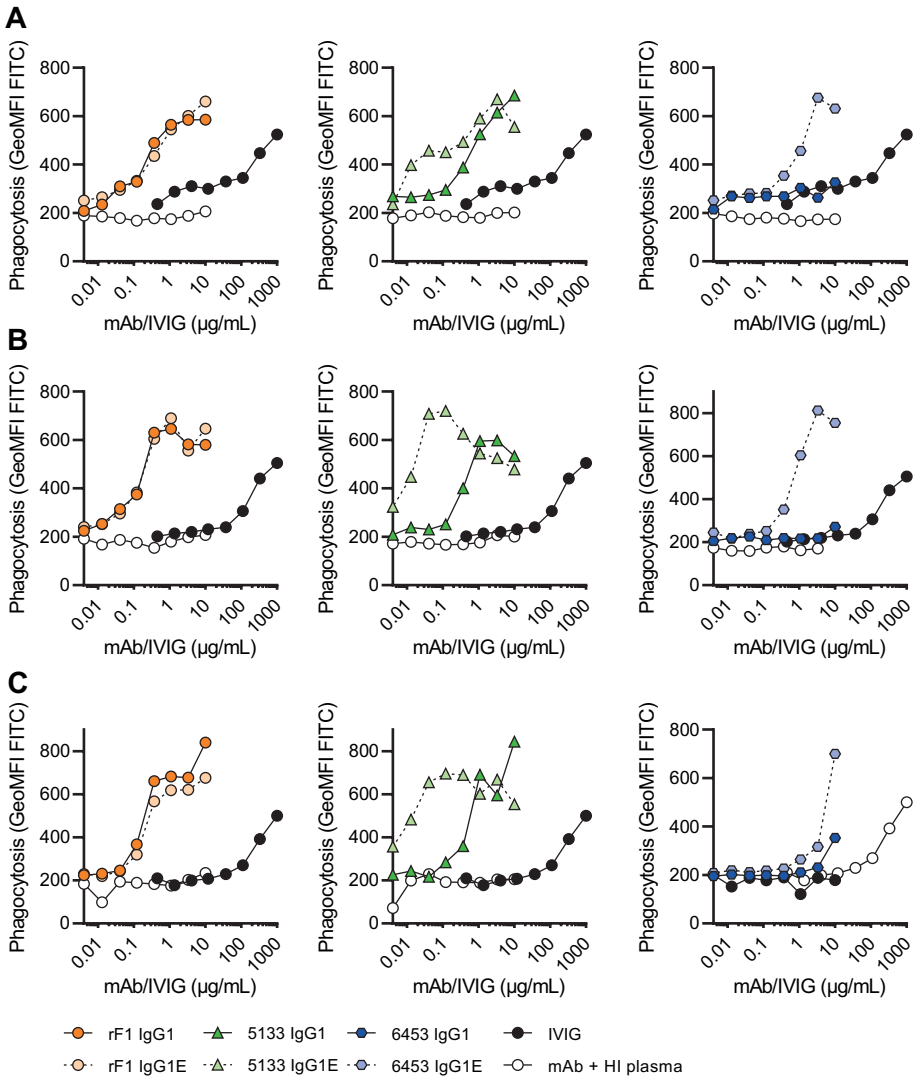

Figure S7. Phagocytosis of FITC labeled N2297 after incubation with mAbs or IVIG in 1% neonatal plasma. Phagocytosis of N2297 by human neutrophils (MOI 10:1) in **(A)** a donor of 32-37 weeks GA and **(B, C)** 2 donors of >37 weeks GA. FITC labeled bacteria were incubated in 1% neonatal plasma or 1% HI neonatal plasma supplemented with a concentration range of rF1, CR5133 or CR6453 IgG1 or IgG1 E345K or IVIG. Phagocytosis was quantified by flow cytometry and plotted as FITC GeoMFI of the neutrophil population. Data represent data of one independent experiment. All donors (n=5) can be viewed in **Figure 5**. GA = Gestational Age

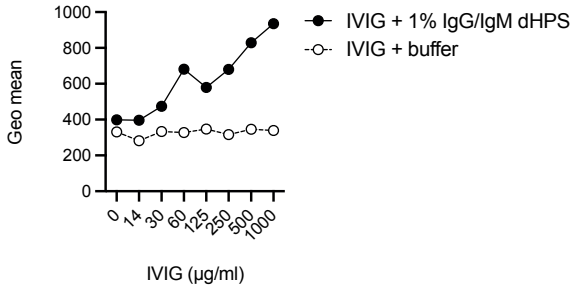

Figure S8. Phagocytosis of FITC labeled N2297 after incubation with mAbs or IVIG in 1% neonatal plasma. Phagocytosis of N2297 by human neutrophils (MOI 10:1). FITC labeled bacteria were incubated in 1% IgG/IgM depleted NHS or buffer supplemented with a concentration range of IVIG. Phagocytosis was quantified by flow cytometry and plotted as FITC GeoMFI of the neutrophil population. Data represent data of one independent experiment.

Supplementary tables

Table S1. Protein sequences used for human monoclonal antibody production.
Variable and constant heavy chain and light chain amino acid sequences used for antibody production. Residues E345K are highlighted in yellow. All antibodies were of kappa class, except otherwise indicated.

Antibody clone	Sequence	Patent number or reference
VH: variable region heavy chain		
rF1	EVQLVESGGGLVQPGGSLRLSCAASGFTLSRFAMSWVRQAP-GRGLEWVASINSGNNPYYARSVQYRFTVSRDVSQNTVSLQMNN-LRAEDSATYFCAKDHPSSGWPTFDSWGPGTLVTVSS	WO/2016/090040 A1 (1)
M130	QVQLQQSGPGILQPSQTLSLTCSFSGFSLSTSGMSVSWIRQPS-GKGLEWLAHIFWDDDKRYNPSLKSRLTVSKDTSSNQVFLKITS-VGTADTATYYCARNYDYDWFVYWGQGTLVTVSA	US 2002/041033 (2)
CR5132	EVLESGGGLVQPGGSLRLSCSDSGFSFNNYWMTWVRQAPGK-GLEWVANINRDGSDKYHVDSVEGRFTISRDNSKNSLYLQMNNL-RADDAA VYFCARGGRTTSWYWRNWGQGTLVTVSS	US 2012/0141493 A1 (3)
CR5133	EVQLVETGGGLVKPGGSLRLSCSASRFSFRDYYMTWIRQAPG-KGPEWVSHISGSGSTIYYADSVRGRFTISRDNAKSSLYLQMD-SLQADDTAVYYCARGGRATSYYWVHWGPGTLVTVSS	US 2012/0141493 A1 (3)
CR6453	EVQLVESGGGLVQPGGSLRVSCAASGFTFSSYWMTWVRQAPG-KGLEWVANIKKDGSEKYYVDSVKGRFSISRDNAKDSLYLQMSSL-RAEDTAVYYCARGGSSSSFYWWLWGKGTTVTVSS	US 2012/0141493 A1 (3)
A120	EVMLVESGGGLVQPKGSLKLSCAASGFTFNTYAMN-WVRQAPGKGLEWVARIRSKSNNYATYYADSVKDRFT-ISRDDSQSMLYLQMNNLKTEDTAMYYCVRRGGKETDYAMDY-WGQGTSVTVSS	WO/03/059259 A2 (4)
CR6166 (Lambda)	QVQLVQSGAEVKKPGESLKISCKGSGYSFTSYWIGWVRQMP-GKGLEWMGIIYPGDSDTRYSPSFQGQVTISADKSISTAY-LQWSSLKASDTAMYYCARRASIVGATHFDYWGQGTLVTVSS	US 2012/0141493 A1 (3)
CR6171	EVQLVETGGVAVQPGRSLRLSCAASGFSFRDYGMHWVRQA-AGKGLEWVAFIWPHGVNRFYADSMEGRFTISRDDSKNMLYL-EMNNLRTEDTALYYCTRDQDYVPRKYFDLWGRGTLVTVSS	US 2012/0141493 A1 (3)
CR6176	VQLQESGPRLVKPSETLSLTCNVSDDSITSYGYYWGWIRQP-PGEALEWIGNVFYSGMAYYNPSLKSRVTILIDTSKKQFSLRLNS-VTAADTAIYYCARVPFLMFRVKIVQGTGAFDIWGQGTMVTVSS	US 2012/0141493 A1 (3)
G2a2	DVRLQESGPGLVKPSQSLSLTCSVTGYSITNSYYWNWIRQFPGN-KLEWMVYIGYDGSNNYNPSLKNRISITRDTSKNQFFLKLNSVT-TEDTATYYCARATYYGNYRGFAYWGQGTLVTVSA	(5)
VL: variable region light chain		
rF1	DIQLTQSPSALPASVGDRVSITCRASENVGDWLAWYRQKPG-KAPNLLIYKTSILESGVPSRFSGSGSGTEFTLTISSLQPDDFATYY-CQHYMRFPYTFGQGTKVEIK	WO/2016/090040 A1 (1)
M130	DIKMTQSPLTLSVTIGQPASISCKSSQSLLDSDGKTYLNWLLQR-PGQSPKRLIYLVSKLDSGVPDRFAGSGSGTDFTLKISRVEAEDL-GVYYCWQGTHFPLTFGAGTKLELK	US 2002/041033 (2)

Table S1. Protein sequences used for human monoclonal antibody production.
Variable and constant heavy chain and light chain amino acid sequences used for antibody production. Residues E345K are highlighted in yellow. All antibodies were of kappa class, except otherwise indicated. (*continued*)

Antibody clone	Sequence	Patent number or reference
CR5132	STDIQMTQSPSTLSASVGDRVTITCRASQSISSWLAWYQQKP-GKAPKLLIYKASSLESGVPSRFSGSGSGTEFTLTISSLQPDDFA-TYYC QQYNSYPLTFGGGTKLEIK	US 2012/0141493 A1 (3)
CR5133	STEIVLTQSPATLSLSPGERATLSCRASQSVSGYLGWYQQKP-GQAPRLLIYGASSRATGIPDRFSGSGSGTDFTLTISRLEPEDFA-VYYCQQYGSSPLTFGGGTKLEIK	US 2012/0141493 A1 (3)
CR6453	EIVLTQSPGTLSLSPGERATLSCRASQSVSSNYLAWYQQKPGQA-PRLLVYGASSRATGIPDRFSGSGSGTDFTLTISRLEPEDFAVYHC-QQYAGSPWTFGQGTKVEIK	US 2012/0141493 A1 (3)
A120	DIVLSQSPAILSASPGEKVTMTCRASSSVSYMHWYQQKPGSSP-KPWIYATSNLASGVPARFSGSGSGTSYSLTISRVEAEDAATYYC-QQW SSNPPTFGGGTKLEIK	WO/03/059259 A2 (4)
CR6166 (Lambda)	QSALTQPPSASGSPGQSVTISCTGTSSDVGGYNYVSWYQQH-PGKAPKLMIYEVSKRPSGVPDRFSGSKSGNTASLTVSGLQA-EDEADYYCSSYAGSNNLVFGGGTKLTVLG	US 2012/0141493 A1 (3)
CR6171 (Lambda)	QSVLTQPPSLSVSPGQTASISCSGDKLGDKYVSWYQQRP-GQSPVLVIYHDTKRPSGIPERFSGTNSGNTATLTISGTQILDEADY-YCQVWDRSTVVFGGGTQLTVL	US 2012/0141493 A1 (3)
CR6176	EIVLTQSPGTLSLSPGERATLSCRASQSVSSSYLAWYQQKPGQA-PRLLIYGASSRATGIPDRFSGSGSGTDFTLTISSLEPEDFAVYYC-QQYGSSSITFGQGTRLEIK	US 2012/0141493 A1 (3)
G2a2	DIRMTQTTSSLSASLGDRVTISCRASQDISNYLNWYQQKPDGT-VKLLIYYTSRLHSGVPSRFSGSGSGTDYSLTISNLEQEDIATYFC-QQGNTLPWTFGGGTKLEIK	(5)
CH: constant regions heavy chain		
IgG1	ASTKGPSVFPLAPSSKSTSGGTAALGCLVKDYFPEPVTVSWNS-GALTSGVHTFPAVLQSSGLYSLSSVVTVPSSSLGTQTYICNVN-HKPSNTKVDKKVEPKSCDKTHTCPPCPAPELLGGPSVFLFP-PKPKDTLMISRTPEVTCVVVDVSHEDPEVKFNWYVDGVEVH-NAKTKPREEQYNSTYRVVSVLTVLHQDWLNGKEYKCKVSNKAL-PAPIEKTISKAKGQPREPQVYTLPPSREEMTKNQVSLTCLVKG-FYPSDIAVEWESNGQPENNYKTTPPVLDSDGSFFLYSKLTVDK-SRWQQGNVFSCSVMHEALHNHYTQKSLSLSPGK	(6) (7)

Table S1. Protein sequences used for human monoclonal antibody production.
Variable and constant heavy chain and light chain amino acid sequences used for antibody production. Residues E345K are highlighted in yellow. All antibodies were of kappa class, except otherwise indicated. (*continued*)

Antibody clone	Sequence	Patent number or reference
IgG3	ASTKGPSVFPLAPCSRSTSGGTAALGCLVKDYFPEPVTVSWNS- GALTSGVHTFPAVLQSSGLYSLSSVVTVPSSSLGTQTYTCNVN- HKPSNTKVDKRVELKTPLGDTTHTCPRCPEPKSCDTPPPCPRC- PEPKSCDTPPPCPRCPEPKSCDTPPPCPRCPAPELLGGPSVFLF- PPKPKDTLMISRTPEVTCVVVDVSHEDPEVQFKWYVDGVEVH- NAKTKPREEQYNSTFRVVSVLTVLHQDWLNGKEYKCKVSNK- ALPAPIEKTISKTKGQPREPQVYTLPPSREEMTKNQVSLTCLVK- GFYPSDIAVEWESSGQPENNYNTTPPMLDSDGSFFLYSKLTVDK- SRWQQGNIFSCSVMHEALHNRFTQKSLSLSPGK	(6) (7)
CL: constant regions light chain		
Kappa class	RTVAAPSVFIFPPSDEQLKSGTASVVCLLNNFYPREAKVQWKVD- NALQSGNSQESVTEQDSKDSTYSLSSTLTLSKADYEKHKVY- ACEVTHQGLSSPVTKSFNRGEC	(7)
Lambda class	GQPKAAPSVTLFPPSSEELQANKATLVCLISDFYPGAVT- VAWKADSSPVKAGVETTTPSKQSNNKYAASSYLSLTPEQWK- SHRSYSCQVTHEGSTVEKTVAPTECS	(7)

Supplementary references

1. Hazenbos WLW, Kajihara KK, Vandlen R, Morisaki JH, Lehar SM, Kwakkenbos MJ, et al. Novel Staphylococcal Glycosyltransferases SdgA and SdgB Mediate Immunogenicity and Protection of Virulence-Associated Cell Wall Proteins. PLoS Pathog. 2013;9(10).
2. Schuman RF, Kokai-kun JF, Foster SJ, Stinson JR, Fischer GW. Multifunctional monoclonal antibodies directed to peptidoglycan of gram-positive bacteria. 2007.
3. Throsby M, Geuijen C, Kruif C. Human binding molecules having activity against staphylococci and uses thereof. 2012.
4. Stinson JR, Schuman RF, Mond JJ, Lees A, Fischer GW. Opsonic monoclonal and chimeric antibodies specific for lipoteichoic acid of Gram positive bacteria. 2007.
5. Gonzalez ML, Frank MB, Ramsland PA, Hanas JS, Waxman FJ. Structural analysis of IgG2A monoclonal antibodies in relation to complement deposition and renal immune complex deposition. Mol Immunol. 2003;40(6):307–17.
6. Cruz AR, den Boer MA, Strasser J, Zwarthoff SA, Beurskens FJ, de Haas CJC, et al. Staphylococcal protein A inhibits complement activation by interfering with IgG hexamer formation. Proc Natl Acad Sci U S A. 2021;118(7).
7. Kabat EA, Wu TT, Perry HM, Gottesman KS, Foeller C. Sequences of proteins of immunological interest. Vol. 138, Analytical Biochemistry. 1984. 265 p.

CHAPTER 5

Classical pathway mediated complement activation hinders interaction of target bound IgG molecules with Fc gamma receptor CD32

Lisanne de Vor, Seline Zwarthoff, Maartje Ruyken, Anne Flier, Piet Aerts, Carla de Haas, Jos van Strijp, Kok van Kessel, Suzan Rooijakkers

Department of Medical Microbiology, University Medical Center Utrecht, Utrecht University, Utrecht, The Netherlands

Manuscript in preparation

Abstract

Fc gamma receptors (FcγRs) are membrane associated molecules that activate different immune processes, such as tumor clearance by NK cells and bacterial killing via neutrophils. To trigger these responses, FcγRs should directly interact with the Fc tail of target bound immunoglobulin G (IgG) antibodies. Besides interacting with FcγRs, target bound IgG molecules can also induce activation of the complement system which further labels the surface with complement derived opsonins recognized by complement receptors (CRs). Previously, others and we demonstrated that complement labeling strongly enhances phagocytosis of bacteria in human immune sera. Here we report on a dual role of complement in steering phagocytic uptake of antibody coated bacteria. Using monoclonal antibodies (mAbs) recognizing *S. aureus*, we show that antibody labeled bacteria can drive phagocytosis via FcyRs and interact with FcyRIIA expressing cell lines. While the addition of complement could enhance the phagocytosis of antibody labeled *S. aureus* in total, it negatively influences the contribution of FcyRs to this process. Using CD32 (FcyRIIA) expressing cell lines, we demonstrate that complement activation directly blocks the interaction between bacterium bound IgG molecules and FcyRIIA. Complement inhibition of IgG:CD32 interaction was observed for IgG molecules with different Fab regions and was independent of the IgG subclasses. Using Fc engineering, we found that inhibition of FcyR binding is dependent on the ability of IgG molecules to form IgG hexamers and activate complement. Mechanistic studies suggest that not only the binding of antibody recognition molecule C1, but also downstream surface deposition of C3b molecules, reduces efficient binding of FcyR to IgG molecules. Altogether, this study provides fundamental insights into the mechanisms of antibody dependent immunity against infections and development of antibody therapeutics.

Introduction

Immunoglobulin Fc gamma receptors (FcγRs) are membrane associated molecules that recognize the Fc region of different immunoglobulin G (IgG) subclasses. FcγRs are expressed by many types of immune cells, including neutrophils, macrophages, dendritic cells, eosinophils, basophils, mast cells and NK cells. As a result, FcγRs are involved in many different immune processes, such as phagocytosis, antibody dependent cell mediated cytotoxicity (ADCC) and release of inflammatory mediators and cytokines [1,2]. Therefore, the interaction between IgG and FcγRs (IgG-Fc:FcγR) plays an important role in the clearance of infections and tumor cells.

Besides interacting with FcγRs, target bound IgG molecules can also activate the classical pathway of the complement system [3]. This requires the recruitment of C1 (or $C1qr_2s_2$), a large complex (766 kDa)) comprised of antibody recognition protein C1q and a heterotetramer of proteases C1r and C1s ($C1r_2s_2$). For efficient docking of C1q, IgG molecules require organization into hexamers that are held together by noncovalent Fc-Fc interactions [4]. Then, C1q associated proteases $C1r_2s_2$ initiate a proteolytic cascade that results in the formation of enzymatic complexes. These so-called C3 convertases $(C4b2b)^5$ catalyze the cleavage of C3 into C3a and C3b, which covalently deposits onto the target surface via a reactive thioester [6]. Convertase mediated C3 cleavage results in the massive labelling of target surfaces with C3b molecules that can, together with inactivation product iC3b, opsonize the surface for phagocytosis *via* complement receptors (CRs) [7,8].

In the past years, our lab has examined phagocytosis of *Staphylococcus aureus* by human neutrophils [9–11], a process that is eminent for immune clearance of this important pathogen [12]. Besides its importance in health care infections [13], *S. aureus* is also an ideal model pathogen to study human antibody responses. An important advantage is that all healthy individuals have pre-existing antibodies against *S. aureus* because of common exposure during nasal carriage [14]. Upon using human immune sera to study phagocytosis, we previously noticed a dual effect of complement in steering phagocytosis [11]. While complement typically enhances phagocytosis of *S. aureus* [9,10], it also diminishes the relative role of FcγRs in the phagocytic process [11]. Specifically, Stemerding *et al.* identified the staphylococcal Flipr-Like molecule (FLL/denoted as FcγR inhibitor) [15] as a potent antagonist of FcγRs [11]. In their study, it was observed that FLL could potently inhibit phagocytosis via pre-existing antibodies, but only in conditions where complement was absent [11]. In this paper, we further investigated the mechanism behind this yet unexplained role of complement in FcγR-mediated phagocytosis.

Results

Complement reduces FcγR mediated phagocytosis of *S. aureus* via polyclonal and monoclonal antibodies

Before studying the mechanism in more detail, we first confirmed the observations by Stemerding *et al.* but using a slightly different assay setup. Most important is that we used a *S. aureus* strain that lacks surface bound IgG molecules protein A and Sbi which can both influence the orientation of IgG molecules on the bacterial surface [16,17]. After incubation of fluorescent *S. aureus* Newman Δ*spa*/*sbi* with human serum and co-incubation with human neutrophils, we measured uptake using flow cytometry. To measure phagocytosis of *S. aureus* in the presence of naturally occurring antibodies but without complement activation, we used heat-inactivated serum (△complement serum), in which thermosensitive complement components are inactivated. Opsonizing *S. aureus* with increasing △complement serum concentrations resulted in an increasing percentage of neutrophils involved in phagocytosis, with a plateau of ~39% of the neutrophil population compared to ~7% of the neutrophils interacting with bacteria in absence of opsonins (0% serum) **(Figure S1A)**. In the presence of the FcγR inhibitor, phagocytosis of △complement serum opsonized bacteria was completely reduced to baseline levels **(Figure S1A)**. At a fixed concentration of 5% △complement serum, we observed large differences in phagocytosis by FcγR inhibitor treated neutrophils versus untreated neutrophils **(Figure S1B)**, showing that △complement serum opsonized bacteria are taken up *via* FcγR mediated phagocytosis. In contrast, opsonizing bacteria with serum (antibodies and complement) led to the involvement of ~90% of the neutrophil population **(Figure S1B)** from a concentration of 1% serum (**Figure S1C**). This coincided with C3b deposition which was verified with an anti-C3b fluorescent antibody and flow cytometry **(Figure S1D)**. Thus, the complement system greatly enhances phagocytosis of *S. aureus* by human neutrophils, as observed before [9,11]. Like the observations in Stemerding *et al.*, we could not observe a decrease in the uptake of serum opsonized bacteria by neutrophils blocked with the FcγR inhibitor. Thus also for strain Newman Δ*spa*/*sbi* used in this study, the phagocytic process operates mainly via complement receptors under conditions with sufficient serum (>0.1%).

Next, we wondered whether complement dependent inhibition of FcγR mediated phagocytosis is also observed in the presence of monoclonal antibodies. Therefore, we made use of a panel of well identified monoclonal IgG1 antibodies against *S. aureus* surface antigen Wall Teichoic Acid (WTA, clone 4497) [10,18], GlcNAc SDR proteins (clone rF1) [19], against LTA (clone CR5132) [US 2012/0141493 A1] and as a control against hapten DNP (clone G2a2). Binding of these mAbs to *S. aureus* strain USA300 LAC was described before [12] and binding to strain Newman Δ*spa*/*sbi* was verified here (**Figure**

S2A-D). Opsonizing bacteria with IgG1 alone induced phagocytosis in a concentration dependent manner **(Figure 1A)**. MAb rF1-IgG1 was more efficient than 4497-IgG1 in inducing FcγR mediated phagocytosis, reaching high percentages of involved neutrophils at lower antibody concentrations. CR5132-IgG1 required slightly higher concentrations than 4497-IgG1 to induce FcγR mediated phagocytosis. For all three mAbs, phagocytosis could completely be blocked with the FcγR inhibitor. In the presence of 1% serum depleted from IgG and IgM (ΔIgG/IgM serum) as complement source [20], we observed more efficient phagocytosis that could not be blocked by the FcγR inhibitor **(Figure 1B)**, again indicating that FcγRs are not involved in phagocytosis in the presence of complement activation. Only phagocytosis induced by rF1-IgG1 could slightly be blocked with the FcγR inhibitor at lower mAb concentrations, indicating that FcγRs still play a small role in phagocytosis. As a control, opsonizing bacteria with aDNP-IgG1 in the absence

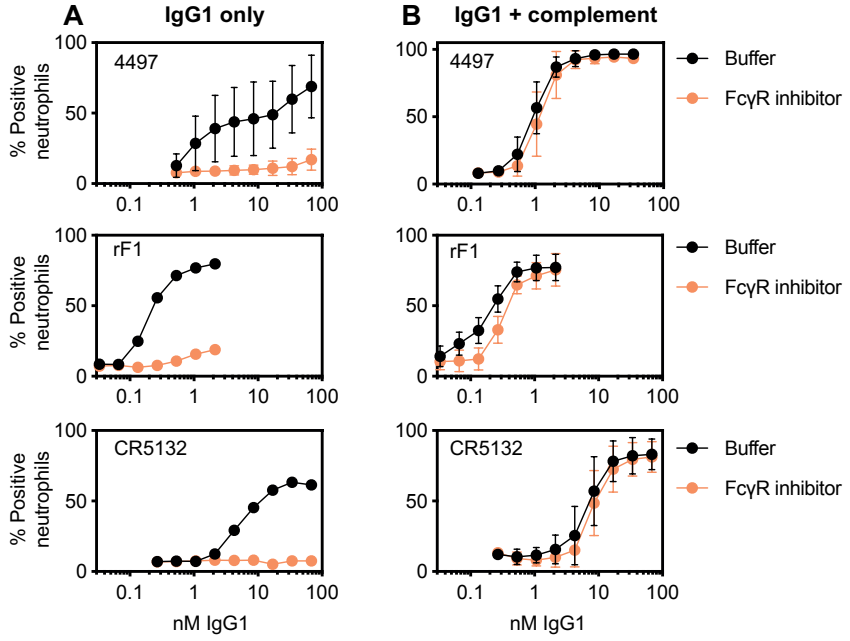

Figure 1. FcγR mediated phagocytosis by human neutrophils induced by different mAb clones is reduced in the presence of complement. (A,B) Phagocytosis of Newman Δ/ by human neutrophils (MOI 10:1) in **(A)** absence or **(B)** presence of complement. MAmetrine expressing bacteria were incubated with a concentration range of 4497, rF1 or CR5132 in (**A)** buffer (IgG1 only) or **(B)** 1% IgG/IgM-depleted normal human serum (IgG1+complement). Neutrophils were incubated with buffer or 10 µg/mL FLIPr-like (FcγR inhibitor). Phagocytosis was quantified by flow cytometry and plotted as percentage mAmetrine positive events of the neutrophil population. Data represent mean ± SD of n=6 (4496-IgG1), n=1 (rF1 only, CR5132 only) and n=2 (rF1 + complement, CR5132 + complement) independent experiments.

or presence of complement did not induce any phagocytosis **(Figure S2E)**. Altogether, we observed that the complement reaction can inhibit FcγR mediated uptake of not only bacteria coated with natural antibodies in serum, but also bacteria coated with monoclonal antibodies.

Complement inhibition of FcγR mediated phagocytosis is independent of the IgG subclass.

To study whether the observed effect is dependent on the IgG subclass, we used 4497-IgG2 **(Figure 2A)** and 4497-IgG3 **(Figure 2B)** to opsonize *S. aureus* in absence or presence of complement, after confirming binding to the bacterial surface **(Figure S2F)**. In line with previous results [10] 4497-IgG2 did not potently induce FcγR mediated phagocytosis of *S. aureus* and this could completely be blocked by FcγR inhibitor **(Figure 2A)**. However, in the presence of complemet, phagocytosis of IgG2 opsonized bacteria was strongly promoted and could not be blocked by FcγR inhibitor. FcγR mediated uptake of IgG3 labeled bacteria was very efficient and could not completely be blocked by FcγR inhibitor **(Figure 2B)**, indicating that the FcγR inhibitor is not able to fully compete with the strong interaction between FcγRs and IgG3 [21]. In the presence of complement **(Figure 2B)**, FcγR inhibitor was able to block phagocytosis at lower IgG3 concentrations but not at higher IgG3 concentrations. An explanation could be that at lower IgG3 concentrations, there is no sufficient complement activation yet while phagocytosis is efficient via FcγRs. Moreover, we observed the same results for the bacterium *Staphylococcus epidermidis* (**Figure S3)**. After opsonizing fluorescent *S. epidermidis* ATCC 14990 with rF1-IgG1, that binds to and induces FcγR mediated phagocytosis of *S. epidermidis* (Chapter 3), we observed blockage of phagocytosis by FcγR inhibitor. When complement was present, the FcγR inhibitor was unable to block phagocytosis **(Figure S3)**. Thus, the complement reaction can inhibit FcγR mediated uptake of bacteria coated with IgG molecules of different subclasses.

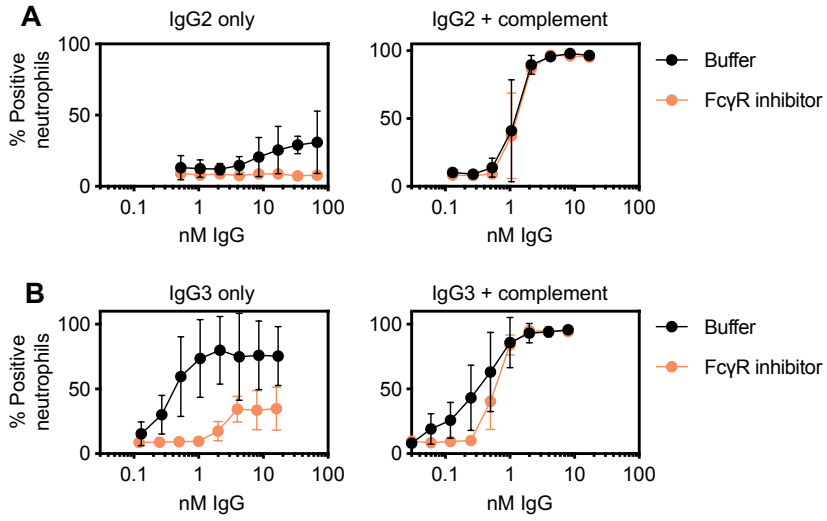

Figure 2. FcγR mediated phagocytosis by human neutrophils induced by different IgG subclasses is reduced in the presence of complement. MAmetrine expressing bacteria were incubated with a concentration range of 4497-IgG2 **(A)** or 4497-IgG3 **(B)** in buffer (IgG2/3 only) or 1% IgG/IgM-depleted normal human serum (IgG2/3+complement). Neutrophils were incubated with buffer or 10 µg/mL FLIPr-like (FcγR inhibitor). Phagocytosis was quantified by flow cytometry and plotted as percentage mAmetrine positive events of the neutrophil population. Data represent mean ± SD of n=2 (IgG2) and n=4 (IgG3) independent experiments.

Complement deposition on the bacterial surface reduces the interaction of IgG-Fc with CD32A but enables the engagement of CR3.

Next, we studied whether complement reduces the direct interaction of IgG molecules with FcγRs. As neutrophils are primary cells isolated from donors and they express different types of opsonic receptors, it is difficult to study the interaction between opsonized bacteria and FcγR or CRs alone. To study receptor binding in its natural environment, the cell membrane, we used non-phagocytic Chinese hamster ovary (CHO) cell lines stably expressing CD32A (allotype R131) [22] and HEK293T cell lines expressing CR3. Like the phagocytosis assay, the cell lines were incubated with opsonized, fluorescent bacteria and the percentage of fluorescence positive cells was measured with flow cytometry. Using increasing concentrations of △complement serum, we detected an increasing percentage of CD32A cells interacting with opsonized bacteria **(Figure 3A)**. We also detected interaction with cells expression CD32 allotype H131 **(Figure S4A)** but not with empty CHO cells **(Figure S4B)**. The interaction with the R131 and H131 allotypes was completely dependent on CD32A because it could be blocked with the FcγR inhibitor **(Figure S4CD)**. After opsonization with serum, the percentage of positive CD32A cells first increased in a concentration dependent manner, but from a concentration of 0.1% serum, which coincides with complement activation **(Figure S1D)**, the percentage dropped to almost 0% serum level **(Figure 3A)**. On the other hand, the

binding of serum opsonized bacteria to CR3 cells increased from a concentration of 0.1% serum **(Figure 3B)**.

To further confirm these observations, we also used soluble FcγRIIA/CD32A (sCD32A) to measure FcγR receptor binding to IgG1-coated bacteria. Dose related binding of sCD32A was detected after incubation of bacteria with increasing concentrations 4497-IgG1 and sCD32A binding decreased after the addition of complement **(Figure 3C)**. In all, these data indicate that at concentrations lower than 0.1% serum, natural antibodies bind to the surface of bacteria and interact with CD32A. At concentrations higher than 0.1% serum, complement deposition takes place on the bacterial surface, which blocks the interaction with CD32A but enables the engagement of CR3 receptors. Bacteria opsonized with increasing concentrations of 4497-IgG1 also efficiently associated with CD32A cells **(Figure 3D)**. When complement was added, a drop in CD32A binding was observed from a concentration of 0.1 nM 4497-IgG1 and higher, coinciding with CR3 binding **(Figure 3E)** and C3b deposition **(Figure 3F)**. We also observed a drop in CD32A binding coinciding with an increase of CR3 binding for mAb clones rF1-IgG1 **(Figure S5A)** and CR5132-IgG1 **(Figure S5B)**. Concluding, we show that complement activation by IgG1 mAbs blocks the interaction of monoclonal IgG1 with CD32A but enables recognition of bacteria via the interaction of complement with CR3.

Blocking IgG-Fc:CD32A interaction is dependent on the ability of IgG to form IgG hexamers

Next, we wondered whether the interference of complement with CD32A binding was related to the ability of IgG molecules to induce complement deposition onto the bacterial surface. To study this in more detail, we produced two variants of 4497-IgG1 with single amino acid mutations in the Fc tail that influence C1q binding but not FcγR binding [4,23,24]. Introduction of the E345K mutation enhances Fc dependent hexamerization of IgG1 molecules, which is needed for C1q docking and thus results in enhanced C1q binding and subsequent complement deposition [4,23,24]. On the other hand, introduction of the S440K mutation results in charge repulsion and reduces hexamerization, thereby decreasing C1q binding and complement deposition [4,25].

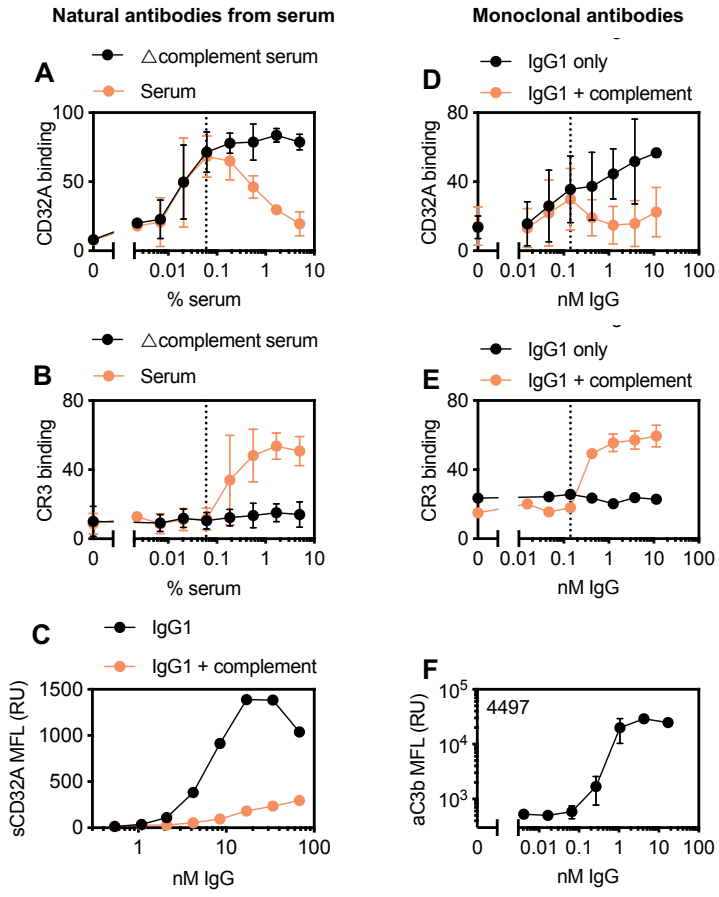

Figure 3. Complement deposition on the bacterial surface reduces the interaction with CD32A but enables the engagement of CR3. Binding of Newman Δspa/sbi to CD32A expressing CHO cells **(A,D)** or CR3 expressing HEK cells **(B,E)** (MOI 10:1) induced by **(A,B)** natural antibodies or **(D,E)** monoclonal antibodies. MAmetrine expressing bacteria were incubated with a concentration range of **(A,B)** serum/serum Δ complement or **(D,E)** 4497-IgG1 in buffer (IgG1 only) or 1% ΔIgG/IgM serum (IgG1+complement). Binding to cell lines was quantified by flow cytometry and plotted as percentage mAmetrine positive events of the cell line population. Data represent mean ± SD of n=3 (natural antibodies) and n=4 (4497-IgG1, except for 4497-IgG1 only with CR3 cells (n=1)) independent experiments. **(C)** Soluble CD32 (sCD32) binding to 4497-IgG1 opsonized bacteria. MAmetrine expressing Newman Δspa/sbi were incubated in a concentration range of 4497-IgG1 in buffer (IgG1 only) or 1% IgG/IgM-depleted normal human serum (IgG1+complement) and further incubated with 1 µg/mL Hu CD32 H167 His. sCD32 deposition was detected by flow cytometry using an mouse anti-HIS and goat anti-mouse-Ig-APC and plotted as APC GeoMFI of the mAmetrine positive bacterial population. Data represent n=1 independent experiments. **(F)** C3b deposition induced by 4497-IgG1. MAmetrine expressing Newman Δspa/sbi were incubated in a concentration range of 4497-IgG1 in 1 % IgG/IgM-depleted normal human serum. C3b deposition was detected by flow cytometry using an anti-neoC3b-AF647 antibody conjugate and plotted as AF647 GeoMFI of the mAmetrine positive bacterial population. Data represent mean ± SD of three independent experiments.

We compared the result of the 4497-IgG1-WT **(Figure 3DE)** with the hexamer enhancing (4497-IgG1-E345K) and reducing (4497-IgG1 S440K) variants under the same conditions as in **Figure 3DE**. We observed comparable CD32A cell binding of bacteria coated with 4497-IgG1-WT and bacteria coated with 4497-IgG1-E345K **(Figure S6A)**. However, binding of 4497-IgG1-S440K coated bacteria was slightly reduced at lower IgG concentrations. Therefore, the reduction in CD32A cell binding after addition of 1% ΔIgG/IgM serum was normalized against the buffer control. We compared the CD32A cell binding of IgG coated bacteria at 0.13 nM, 0.42 nM and 3.77 nM and observed that in the presence of complement, the interaction between 4497-IgG1-E345K is already blocked at much lower concentrations (0.13 nM **(Figure 4A)**), as compared to 4497-IgG1-WT (0.42 nM **(Figure 4B)**. This is caused by 4497-IgG1-E345K's enhanced ability to activate complement deposition, as indicated by binding to CR3 cells **(Figure S8B)** starting at lower concentrations compared to WT IgG1. On the other hand, the hexamer reducing mutation S440K showed the opposite effect and inhibition by 1% ΔIgG/IgM serum required almost 10 times higher IgG concentrations than IgG1-WT (3.77 nM **(Figure 4C)**), with less reduction in binding. This again coincided with less efficient binding to CR3 cells **(Figure S8B)**. In all, we show here that the interference of complement with the IgG-Fc:CD32A interaction was related to the ability of IgG molecules to induce complement deposition onto the bacterial surface.

C1 can partially block IgG-Fc:CD32A interaction and subsequent classical pathway mediated complement deposition further blocks the interaction.

Because FcγRs [26] and C1q [27] both bind to the same location on the IgG Fc tail, we wondered whether the interference with FcγR binding was caused by the direct binding of C1 complex to IgG1. Moreover, the covalent deposition of other complement components in proximity to IgG molecules could interfere with FcγR binding. To unravel the mechanism, we used purified complement proteins, added one-by-one in a physiologically relevant ratio to each other. This allowed us to study the role of each additional factor in de classical pathway cascade, shown in **Figure 5A**. We first validated this system by measuring C3b deposition after opsonizing bacteria with 8.5 nM 4497-IgG1 and a concentration range of purified classical pathway components (denoted as % serum equivalent). Like the assay in serum, C3b deposition **(Figure S7)** could be measured at a concentration of 0.1% serum equivalent and higher. Incubation with a control mAb (aDNP-IgG1) did not result in C3b deposition.

Then, we incubated bacteria with 34 nM 4497-IgG1 and the subsequential purified complement components at a concentration of 5% serum equivalent after which binding to CD32A cells was determined. After addition of only purified C1, the binding of bacteria opsonized with WT 4497-IgG1 was reduced from 60% to 40% **(Figure 5B)**.

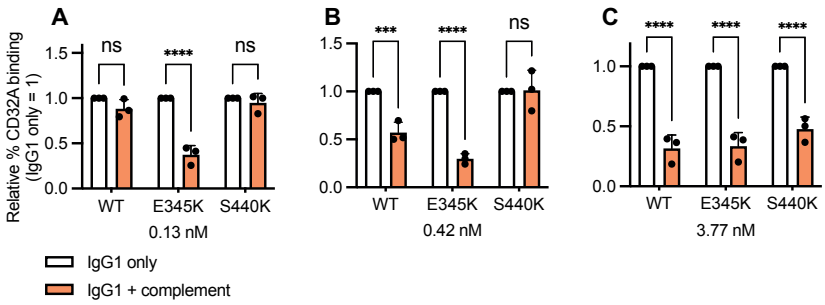

Figure 4. Blocking IgG-Fc:CD32A interaction is dependent on ability of IgG to induce complement activation. Binding of Newman Δspa/sbi to CD32A expressing CHO cells (MOI 10:1) induced by 4497-IgG1 WT (same data as **Figure 3D**), 4497-IgG1 E345K or 4497-IgG1 S440K monoclonal antibodies. MAmetrine expressing bacteria were incubated with 0.13 nM **(A)**, 0.42 nM **(B)** or 3.77 nM **(C)** mAb in buffer (IgG1 only) or 1% ΔIgG/IgM serum (IgG1+complement). Binding to cell lines was quantified by flow cytometry and plotted as binding compared to mAb only in buffer (100%). Data represent mean ± SD of n=4 (4497 IgG1 WT, 4497-IgG1 S440K) and n=3 (4497-IgG1 E345K) independent experiments.

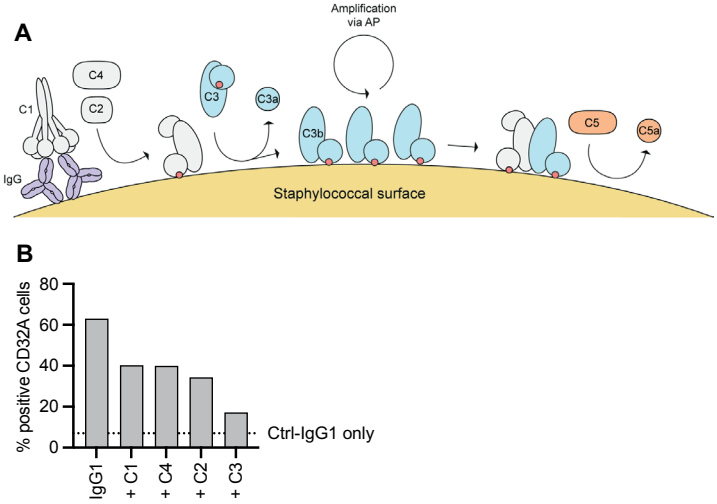

Figure 5. Purified complement components block IgG-Fc:CD32A interaction. (A) Schematic representation of the activation of the classical pathway by IgG molecules. **(B)** Binding of Newman Δspa/sbi to CD32A expressing CHO cells (MOI 10:1) induced by 4497-IgG1. MAmetrine expressing bacteria were incubated with a concentration range of 4497-IgG1 in buffer (IgG1 only) or with purified complement components. Binding to cell lines was quantified by flow cytometry and plotted as percentage mAmetrine positive events of the cell line population. Data represent results of n=1 experiment.

This indicates that the direct binding of C1 to the Fc tail of IgG1 hampers the interaction with CD32A. After the addition of C1 plus C4, or C1 plus C4 and C2, there was no additional blocking. Thus, subsequent activation of C4 and C2 and their deposition on the bacterial surface did not influence the IgG-Fc:CD32A interaction. However, after addition of C1, C4, C2 and C3 we observed almost complete blocking of the binding of opsonized bacteria to CD32A cells. These experiments indicate that the transient interaction between C1 and IgG1 hexamers by itself can hinder CD32A binding. Sufficient covalent C3b deposition on the bacterial surface further obscures efficient IgG-Fc:CD32A interactions.

Discussion

Fc-mediated antibody effector functions play an important role in shaping the immune response. In this project, we studied the contribution of the IgG-Fc:FcγR interaction to phagocytosis of antibody coated *Staphylococcus aureus* by neutrophils in the presence and absence of complement. We show that, while classical pathway mediated complement deposition enhances bacterial uptake, it significantly reduces the contribution of FcγRs to the phagocytic process by directly blocking the IgG-Fc:FcγR interaction. This dual role of complement in steering phagocytic uptake of antibody coated targets is crucial information for understanding antibody dependent immunity against infections and for development of antibody therapeutics.

The major players that prevent the IgG-Fc: FcγR interaction we found were C1 and C3. Since the binding sites of C1q [27] and FcγR [26] on the IgG-Fc partially overlap, it is likely that C1 sterically prevents a direct interaction between IgG-Fc and FcγR. Indeed, our findings with purified complement components indicate a role for C1 and experiments with IgG hexamer reducing and -enhancing mutants [4,23,24] revealed a dependency on the ability of IgG molecules to interact with C1. Furthermore, full prevention of interaction between IgG-Fc and FcγR could be reached after C3b deposition. Looking at the molecular weight and height of antibodies, it could be that deposition of C3b (16 nm height, 177 kDa [PDB: 2I07, [6,28]] in proximity of the antibody, sterically hinders FcγR (4 nm height [29]) from reaching the IgG Fc tail (6-7 nm height, 150 kDa [30]. It is proposed that C3b molecules deposit on the surface within a 200 nm radius around the C3 convertase [31], giving the possibility that C3b molecules affect the recognition of neighboring antibodies by FcγRs. Further research should further explore the exact mechanisms.

This study sheds light on the natural immune response against *S. aureus*. We find that in presence of complement, antibody mediated complement deposition leads to a switch

from FcγR to CR mediated phagocytosis. Interestingly, CR-mediated phagocytosis is different from FcγR-mediated phagocytosis. In macrophages, CR-mediated phagocytosis is mainly characterized by a more passive “sinking” of the target particle into the cell membrane and only a small proportion involves active formation of pseudopods as observed during FcγR-mediated phagocytosis [32–34]. Recent work using macrophages and IgG/C3b opsonized red blood cells has indicated that FcγRs and CR3 can cooperate, for example, CR3 can signal via FcγR ITAM domains in absence of IgG [33]. Although the implications of CR-mediated phagocytosis versus FcγR-mediated phagocytosis are not yet fully understood, the manner of phagocytosis could have a major impact on how the pathogen is engulfed and killed by neutrophils.

We showed that our findings with antibodies against the highly abundant WTA epitope on *S. aureus* could be translated to other pathogenic surfaces, namely the closely related *S. epidermidis*. Moreover, there is a strong indication from literature that complement also blocks IgG:FcγR interactions on viruses *in vitro* and *in vivo*. This evidence stems from a paper by Mehlhop *et al* (2007) that studied the mechanisms of antibody dependent enhancement (ADE), a notorious and unwanted side effect of antibodies in viral immunity [35]. It is well established that viruses can misuse the Fc portion of surface bound antibodies to infect FcγR expressing immune cells. Mehlhop *et al* showed that ADE by flavivirus is blocked by C1q in vivo. Furthermore, they found that C1q (but not C3) in human serum blocked viral uptake in FcγR expressing cells. The authors hypothesized that the mechanism could be interference with binding to FcγRs or the subsequent signalling and internalization of viral particles. Our study provides important proof-of-concept that C1 can block IgG:FcγR interactions. Since ADE is an important cause of pathology by flaviviruses, Dengue, Ebola and Coronaviruses (MERS and SARS-CoV1) [36], insights into potential mechanism of inhibition of ADE by the complement system could hold important information for development of antibody based drug therapies and vaccines against emerging viruses. Furthermore, complement deposition on IgG coated target surfaces could also affect phagocytosis by other phagocytic cells such as dendritic cells and macrophages and other immune processes that depend on FcγR, such as ADCC by NK cells, antigen presentation by DCs or B cell responses [1]. Altogether, these new insights into the dual role of complement after binding to surface bound IgG molecules could be important for optimal design of antibody therapies.

Methods

Production of human monoclonal antibodies

IgG1 clones 4497, CR5132, rF1 and G-2A2 (aDNP) and the subtypes of 4497 (IgG2, IgG3, IgG1 E345K, IgG1 S440K) were produced as described previously [10,12]. For mAb expression, variable heavy (VH) chain and variable light (VL) chain sequences were cloned in expression vector pcDNA3.4 (Thermo Fisher Scientific) as described in de Vor et al. [12], containing human IgG1 heavy chain (HC) and light chain (LC) constant regions as indicated in **Table S1**. The E345K and S440K single mutation were introduced in the heavy chain expression vectors by gene synthesis (IDT (Integrated DNA Technologies)). Variable heavy (VH) and light chain (VL) sequences from all antibodies were obtained from scientific publications or patents **(Table S1)**. Antibodies were expressed as IgG1/2/3,κ. Plasmid DNA mixtures encoding both heavy and light chains of antibodies were transiently transfected in EXPI293F cells (Life technologies, USA) as described in de Vor et al. [12]. IgG1 and IgG2 antibodies were isolated using HiTrap Protein A High Performance column (Cytiva, GE Healthcare) and IgG3 antibodies were collected using HiTrap Protein G High Performance column (Cytiva, GE Healthcare) in the Äkta Pure protein chromatography system (GE Healthcare). All antibody fractions were dialyzed overnight in PBS and filter sterilized through 0.22 µm SpinX-filters. Size exclusion chromatography (SEC) (Cytiva, GE Healthcare) was performed to check for mAb homogeneity, and the monomeric fraction was separated when aggregation levels exceeded 5%. Final antibody concentration was determined by measuring the absorbance at 280 nm and antibodies were stored at -80 °C or 4°C.

Production of anti-C3b AF647 conjugate

2000 µg/ml mouse IgG2a mAb against a neo-epitope C3b (clone Bh6) [37] was incubated with AF647 NHS ester (Life Technologies) (final concentration: 100 µg/ml) and sodium carbonate (pH 9.4, final concentration: 0.1 M) for 70 minutes, room temperature, rotating. The sample was separated from aggregates by spinning through 0.22 µm SpinX filter columns (Corning life Sciences BV) for 2 minutes at 1500x *g*. To remove free AF647 from the mixture, filtrate was transferred to a sterile PBS washed Zeba spin column (Thermo Scientific) and spun for 2 minutes at 1500x *g*. From OD_{280} and OD_{650} Nanodrop (Thermo Scientific) measurements, the degree of labelling (DOL) was determined at 4.14. The conjugate was checked for integrity by SDS-PAGE and fluorescence of antibody conjugate was confirmed using ImageQuant LAS 4000.

Bacterial strains and culture conditions

GFP-labeled *S. aureus* Newman Δ*spa*/*sbi* (knock-out of Protein A and the second immunoglobulin-binding protein (Sbi) [38]), mAmetrine (mAm)-labeled *S. aureus* Newman

Δ*spa*/*sbi* and Newman WT were constructed as described before [9]. Briefly, to construct GFP- and mAm-labeled *S. aureus* strains, bacteria were transformed with a pCM29 plasmid that constitutively and robustly expresses superfolder green fluorescent protein (sGFP) or a codon optimized mAm protein (GenBank: KX759016) [39] from the sarAP1 promoter [40]. Bacteria were grown overnight in Todd Hewitt broth (THB) plus 10 µg/mL chloramphenicol, diluted to an OD600 = 0.05 in fresh THB plus chloramphenicol, and cultured until midlog phase (OD600 = 0.5). Bacteria were then washed and resuspended in RPMI-H medium (Roswell Park Memorial Institute medium [RPMI], 0.05% HSA) and stored until use at −20 °C.

Depletion of IgG/IgM from human serum

Normal human serum (NHS) from twenty healthy donors was depleted of IgG and IgM as previously described [20]. Briefly, affinity chromatography was used to capture IgG by using HiTrap protein G High Performance column (Cytiva, GE Healthcare) and IgM with Capture Select IgM Affinity Matrix (Thermo Fischer Scientific) from NHS. Complement levels and activity were determined after depletion, using enzyme-linked immunosorbent serological assay (ELISA) and classical/alternative pathway hemolytic assays.

Phagocytosis of *S. aureus* by neutrophils

Human neutrophils were isolated from blood of healthy donors by the Ficoll/Histopaque density gradient method [41]. To study phagocytosis, we used a recently described phagocytosis assay[9], with some adaptations. Phagocytosis was performed in a round bottom 96-well plate. For opsonization, mAm-expressing Newman Δ*spa*/*sbi* (20 µL 3.75 × 107 cells/mL) were mixed with threefold dilutions of serum, heat inactivated serum, mAbs in RPMI-H or mAbs in 1% ΔIgG/IgM serum (20 µL volume) for 15 min at 37 °C on a shaker (750 rpm). Subsequently, neutrophils (10 µL 7.5 × 106 cells/mL) were added, giving a 10:1 bacteria-to-cell ratio and incubated for 15 min at 37 °C on a shaker (750 rpm) in a final volume of 50 µL. To block Fc gamma receptors, neutrophils were pre-incubated for 15 minutes with FLIPr-like (10 µg/mL). The recombinant protein FLIPr-like was expressed and purified as described before [15]. The reaction was stopped with 1% ice-cold para- formaldehyde. The binding/internalization of mAm-bacteria to the neutrophils was detected using flow cytometry (BD FACSVerse) and data were analyzed based on FSC/SSC gating of neutrophils using FlowJo software. Phagocytosis was defined by the percentage of cells with a positive fluorescent signal (% GFP-positive cells) of all neutrophils representing the overall phagocytosis efficacy.

IgG and complement binding to *S. aureus*.

For detection of mAb binding, mAm-expressing Newman Δ*spa*/*sbi* (20 µL 3.75 × 107 cells/mL) were mixed with threefold dilutions mAbs in RPMI-H (20 µL volume) for 15

min at 37 °C on a shaker (750 rpm). After washing, bacteria were incubated for 30 min at 4°C in 30 µL RPMI-H with goat anti-human kappa-AlexaFluor488 (1:1000, Southern Biotech). For detection of C3b deposition, bacteria were mixed with threefold dilutions of serum, heat inactivated serum or mAbs in 1% ΔIgG/IgM serum (20 µL volume) for 15 min at 37 °C on a shaker (750 rpm). Subsequently, mAbs were incubated for 30 min at 4°C in 30 µL RPMI-H with anti-C3b AF647 detection antibody (3 µg/ml). After incubation with detection antibodies, bacteria were washed and fixed in 1% paraformaldehyde (PFA) (Polysciences) in RPMI-H. Samples were measured by flow cytometry (BD FACSVerse), and data analyzed by FlowJo Software (Version 10). Only mAm-positive events were analyzed. Data are presented as geometric mean fluorescence intensity (GeoMFI ± SD).

Culture of hFcγR-CHO cell lines and CR HEK cell lines

CHO cells expressing human FcγRIIA (CD32A) R131 and H131 were generated at University of Erlangen-Nürnberg laboratory [22]. CHO cell lines stably transfected with human FcγRs were maintained in RPMI medium supplemented with 10% FCS, 2 mM glutamine, 1 mM sodium pyruvate, 0.1 mg/mL pen/strep, 0.1 mM non-essential amino acids and 0.05 mg/mL G418 (Gibco) at 37%, 5% CO2. Cells were collected by brief trypsinization, washed and resuspended into RPMI-H at a concentration of 7.5x106 cells/mL. Viability was >95% as assessed with trypan blue. For stabile expression of CR3, we cloned the CD18 (NM_000211.4) and CD11b (NM_001145808.1) cDNA in the bicistronic expression vectors pIRESpuro3 and pIREShyg3 vector (Clontech), respectively. First, the pIRESpuro3/CD18 construct was transfected into HEK293T cells using Lipofectamin 2000 (Life Technologies). One day after transfection, cells were put under selection pressure using 1 µg/ml puromycin in DMEM with 10%FCS. A few weeks later, puromycin resistant cells were subsequently transfected with the pIREShyg3/CD11b construct and selected for stabile CD11b expression using 250 µg/ml hygromycin. Stabile CR3 expression was verified by flow cytometry (BD FACSVerse) using anti-CD11b-APC (clone ICRF44) and anti-CD18-FITC (clone 6.7) antibodies (BD). For binding of bacteria bound IgG to CD32A and CR3 cell lines, mAm-bacteria were opsonized and incubated with cell lines as described above for phagocytosis. The binding of mAm-bacteria to the cell lines was detected using flow cytometry (BD FACSVerse) and data were analyzed based on FSC/SSC gating of cells using FlowJo software. Phagocytosis was defined by the percentage of cells with a positive fluorescent signal (% GFP-positive cells) of all cells representing the overall phagocytosis efficacy.

Opsonization of bacteria with purified complement components

The following 100 % serum equivalent concentrations were used. C1 complex: 174 nM, C1-inhibitor: 1714 nM, C2: 215 nM, C3: 6684 nM, C4: 200 nM. First, mAm-expressing

Newman Δ*spa*/*sbi* (20 µL 3.75 × 107 cells/mL) were mixed with a concentration range of mAb and C1 (13,34 µL volume) for 15 min at 4 °C on a shaker (750 rpm). Then, a mixture of C1-inhibitor, C2, C4 and C3 (6,67 µL volume) was added and incubated for 15 min at 37 °C on a shaker. The opsonized bacteria were analyzed for C3b deposition or used in hFcγR-CHO cell line binding experiments as described above.

Soluble CD23 binding

MAm-expressing Newman Δ*spa*/*sbi* (20 µL OD_{600} 0.1) were mixed with a concentration range of mAbs in buffer or in 1% ΔIgG/IgM serum for 20 min at 37°C on a shaker (750 rpm). After washing, bacteria were incubated with 25 µL HuCD32H167 His (R&D 1 µg/mL) for 30 min at 4°C. For detection, bacteria were washed and incubated with 25 µL mouse anti-HIS (Hytest anti His6-tag, 5H1, 1 µg/mL) for 30 min at 4°C, washed and further incubated with goat anti-mouse-Ig-APC (BD biosciences, 550826, 1/200) for 30 min at 4°C. After incubation with detection antibodies, bacteria were washed and fixed in 1% paraformaldehyde (PFA) (Polysciences) in RPMI-H. Samples were measured by flow cytometry (BD FACSVerse), and data analyzed by FlowJo Software (Version 10). Data are presented as geometric mean fluorescence intensity (GeoMFI ± SD).

Ethical statement

Human serum and blood were obtained from healthy donors after informed consent was obtained from all subjects, in accordance with the Declaration of Helsinki. Approval from the Medical Ethics Committee of the University Medical Center Utrecht was obtained (METC protocol 07-125/C, approved March 1, 2010).

Statistical analysis

Statistical analysis was performed with GraphPad Prism v.8.3 software, using different tests as indicated in the figure legends.

Acknowledgements

The authors greatly thank prof. Falk Nimmerjahn (University of Erlangen-Nürnberg) for providing FcγR expressing CHO cell lines and dr. Dani Heesterbeek for critically reading and revising the manuscript. This project was financially supported by a grant from Health~Holland (LSHM17026 to JAGS).

References

1. Nimmerjahn, F. & Ravetch, J. V. Fcγ receptors as regulators of immune responses. *Nat. Rev. Immunol.* **8**, 34–47 (2008).
2. Takai, T., Li, M., Sylvestre, D., Clynes, R. & Ravetch, J. V. FcR γ chain deletion results in pleiotrophic effector cell defects. *Cell* **76**, 519–529 (1994).
3. Ricklin, D., Hajishengallis, G., Yang, K. & Lambris, J. D. Complement: A key system for immune surveillance and homeostasis. *Nat. Immunol.* **11**, 785–797 (2010).
4. Diebolder, C. A. *et al.* Complement Is Activated by IgG Hexamers Assembled at the Cell Surface. *Science (80-.).* **343**, 1260–1263 (2014).
5. Bohlson, S. S., Garred, P., Kemper, C. & Tenner, A. J. Complement nomenclature-deconvoluted. *Front. Immunol.* **10**, 1–6 (2019).
6. Janssen, B. J. C., Christodoulidou, A., McCarthy, A., Lambris, J. D. & Gros, P. Structure of C3b reveals conformational changes that underlie complement activity. *Nature* **444**, (2006).
7. Dustin, M. L. Complement Receptors in Myeloid Cell Adhesion and Phagocytosis. *Microbiol. Spectr.* **4**, (2016).
8. Vandendriessche, S., Cambier, S., Proost, P. & Marques, P. E. Complement Receptors and Their Role in Leukocyte Recruitment and Phagocytosis. *Front. Cell Dev. Biol.* **9**, 1–25 (2021).
9. Boero, E. *et al.* Use of Flow Cytometry to Evaluate Phagocytosis of *Staphylococcus aureus* by Human Neutrophils. *Front. Immunol.* **12**, 1–15 (2021).
10. Zwarthoff, S. A. *et al.* C1q binding to surface-bound IgG is stabilized by C1r2s2 proteases. *Proc. Natl. Acad. Sci. U. S. A.* **118**, (2021).
11. Stemerding, A. M. *et al. Staphylococcus aureus* Formyl Peptide Receptor–like 1 Inhibitor (FLIPr) and Its Homologue FLIPr-like Are Potent FcγR Antagonists That Inhibit IgG-Mediated Effector Functions . *J. Immunol.* **191**, 353–362 (2013).
12. de Vor, L. *et al.* Human monoclonal antibodies against *Staphylococcus aureus* surface antigens recognize in vitro and in vivo biofilm. *Elife* **11**, 1–25 (2022).
13. Lowy, F. D. *Staphylococcus aureus* Infections. *N. Engl. J. Med.* **339**, 520–532 (1998).
14. Dryla, A. *et al.* Comparison of antibody repertoires against *Staphylococcus aureus* in healthy individuals and in acutely infected patients. *Clin. Diagn. Lab. Immunol.* **12**, 387–398 (2005).
15. Prat, C. *et al.* A Homolog of Formyl Peptide Receptor-Like 1 (FPRL1) Inhibitor from *Staphylococcus aureus* (FPRL1 Inhibitory Protein) That Inhibits FPRL1 and FPR . *J. Immunol.* **183**, 6569–6578 (2009).
16. Cruz, A. R. *et al.* Staphylococcal protein A inhibits complement activation by interfering with IgG hexamer formation. *Proc. Natl. Acad. Sci. U. S. A.* **118**, (2021).
17. Zhang, L., Jacobsson, K., Vasi, J., Lindberg, M. & Frykberg, L. A second IgG-binding protein in *Staphylococcus aureus*. *Microbiology* **144**, 985–991 (1998).
18. Fong, R. *et al.* Structural investigation of human *S. aureus*-targeting antibodies that bind wall teichoic acid. *MAbs* **10**, 979–991 (2018).
19. Hazenbos, W. L. W. *et al.* Novel Staphylococcal Glycosyltransferases SdgA and SdgB Mediate Immunogenicity and Protection of Virulence-Associated Cell Wall Proteins. *PLoS Pathog.* **9**, e1003653 (2013).

20. Zwarthoff, S. A., Magnoni, S., Aerts, P. C., van Kessel, K. P. M. & Rooijakkers, S. H. M. Method for Depletion of IgG and IgM from Human Serum as Naive Complement Source. in *Methods in molecular biology (Clifton, N.J.)* vol. 2227 21–32 (2021).
21. Vidarsson, G., Dekkers, G. & Rispens, T. IgG Subclasses and Allotypes: From Structure to Effector Functions. *Front. Immunol.* **5**, 520 (2014).
22. Anja Lux, N., Yu, X., Scanlan, C. N., Lux, A. & Nimmerjahn, F. Rs γ Glycosylation on IgG Binding to Human Fc Impact of Immune Complex Size and Impact of Immune Complex Size and Glycosylation on IgG Binding to Human FcgRs. *J Immunol Mater. Suppl. J. Immunol.* **190**, 4315–4323 (2018).
23. Wang, G. *et al.* Molecular Basis of Assembly and Activation of Complement Component C1 in Complex with Immunoglobulin G1 and Antigen. *Mol. Cell* **63**, 135–145 (2016).
24. de Jong, R. N. *et al.* A Novel Platform for the Potentiation of Therapeutic Antibodies Based on Antigen-Dependent Formation of IgG Hexamers at the Cell Surface. *PLOS Biol.* **14**, e1002344 (2016).
25. van Osch, T. L. J. *et al.* Fc Galactosylation Promotes Hexamerization of Human IgG1, Leading to Enhanced Classical Complement Activation. *J. Immunol.* **207**, 1545–1554 (2021).
26. Caaveiro, J. M. M., Kiyoshi, M. & Tsumoto, K. Structural analysis of Fc/FcγR complexes: A blueprint for antibody design. *Immunol. Rev.* **268**, 201–221 (2015).
27. Ugurlar, D. *et al.* Structures of C1-IgG1 provide insights into how danger pattern recognition activates complement. *Science (80-.).* **359**, 794–797 (2018).
28. Berends, E. T. M. *et al.* Molecular insights into the surface-specific arrangement of complement C5 convertase enzymes. *BMC Biol.* **13**, 93 (2015).
29. Saggu, G. *et al.* Cis interaction between sialylated FcγRIIA and the αI-domain of Mac-1 limits antibody-mediated neutrophil recruitment. *Nat. Commun.* **9**, 5058 (2018).
30. Strasser, J. *et al.* Unraveling the Macromolecular Pathways of IgG Oligomerization and Complement Activation on Antigenic Surfaces. *Nano Lett.* **19**, 4787–4796 (2019).
31. Makou, E. *et al.* Combining spr with atomic-force microscopy enables singlemolecule insights into activation and suppression of the complement cascade. *J. Biol. Chem.* **294**, 20148–20163 (2019).
32. Aderem, A. & Underhill, D. M. MECHANISMS OF PHAGOCYTOSIS IN MACROPHAGES. *Annu. Rev. Immunol.* **17**, 593–623 (1999).
33. Walbaum, S. *et al.* Complement receptor 3 mediates both sinking phagocytosis and phagocytic cup formation via distinct mechanisms. *J. Biol. Chem.* **296**, 100256 (2021).
34. Kumari, S., MG, S. & Mayor, S. Endocytosis unplugged: multiple ways to enter the cell. *Cell Res.* **20**, 256–275 (2010).
35. Mehlhop, E. *et al.* Complement Protein C1q Inhibits Antibody-Dependent Enhancement of Flavivirus Infection in an IgG Subclass-Specific Manner. *Cell Host Microbe* **2**, 417–426 (2007).
36. Wang, S. *et al.* Antibody-dependent enhancement (ADE) of SARS-CoV-2 pseudoviral infection requires FcγRIIB and virus-antibody complex with bivalent interaction. *Commun. Biol.* **5**, 262 (2022).
37. Garred, P., Mollnes, T. E., Lea, T. & Fischer, E. Characterization of a Monoclonal Antibody MoAb bH6 Reacting with a Neoepitope of Human C3 Expressed on C3b, iC3b, and C3c. *Scand. J. Immunol.* **27**, 319–327 (1988).
38. Sibbald, M. J. J. B. *et al.* Synthetic effects of secG and secY2 mutations on exoproteome biogenesis in *Staphylococcus aureus*. *J. Bacteriol.* **192**, (2010).

39. De Jong, N. W. M., Van Der Horst, T., Van Strijp, J. A. G. & Nijland, R. Fluorescent reporters for markerless genomic integration in *Staphylococcus aureus*. *Sci. Rep.* **7**, (2017).
40. Pang, Y. Y. *et al.* agr-Dependent Interactions of *Staphylococcus aureus* USA300 with Human Polymorphonuclear Neutrophils. *J. Innate Immun.* **2**, 546–559 (2010).
41. Surewaard, B. G. J. *et al.* Staphylococcal alpha-phenol soluble modulins contribute to neutrophil lysis after phagocytosis. *Cell. Microbiol.* **15**, (2013).
42. Gonzalez, M. L., Frank, M. B., Ramsland, P. A., Hanas, J. S. & Waxman, F. J. Structural analysis of IgG2A monoclonal antibodies in relation to complement deposition and renal immune complex deposition. *Mol. Immunol.* **40**, 307–317 (2003).
43. Lehar, S. M. *et al.* Novel antibody-antibiotic conjugate eliminates intracellular *S. aureus*. *Nature* **527**, 323–328 (2015).
44. Kabat, E. A., Wu, T. T., Perry, H. M., Gottesman, K. S. & Foeller, C. *Sequences of proteins of immunological interest*. *Analytical Biochemistry* vol. 138 (1984).

Supplementary information

Supplementary figures

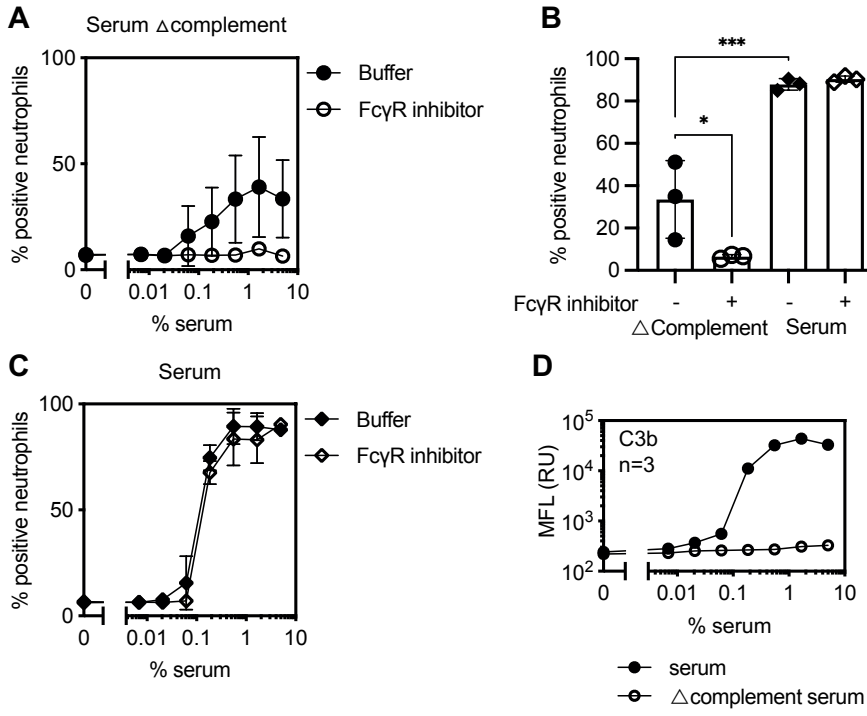

Figure S1 (A,B) Phagocytosis of Newman Δ/ by human neutrophils (MOI 10:1) in **(A)** absence (serum Δcomplement) or **(B)** presence of complement (serum). MAmetrine expressing bacteria were incubated with a concentration range of **(A)** heat-inactivated serum (serum Δ complement) or **(B)** normal human serum. Neutrophils were incubated with buffer or 10 µg/mL FLIPr-like (FcγR inhibitor). Phagocytosis was quantified by flow cytometry and plotted as percentage mAmetrine positive events of the neutrophil population. Data represent mean ± SD of three independent experiments. **(C)** Comparison of induced phagocytosis in absence and presence of 5% serum. One-way ANOVA was performed to test for the effect of complement heat inactivation on phagocytosis and displayed as *P ≤ 0.05, **P ≤ 0.01, ***P ≤ 0.001 and ****P ≤ 0.0001. **(D)** C3b deposition in serum and serum Δcomplement. MAmetrine expressing Newman Δspa/sbi were incubated in a concentration range of serum and serum Δcomplement. C3b deposition was detected by flow cytometry using an anti-neoC3b-AF647 antibody conjugate and plotted as AF647 GeoMFI of the mAmetrine positive bacterial population. Data represent mean ± SD of three independent experiments.

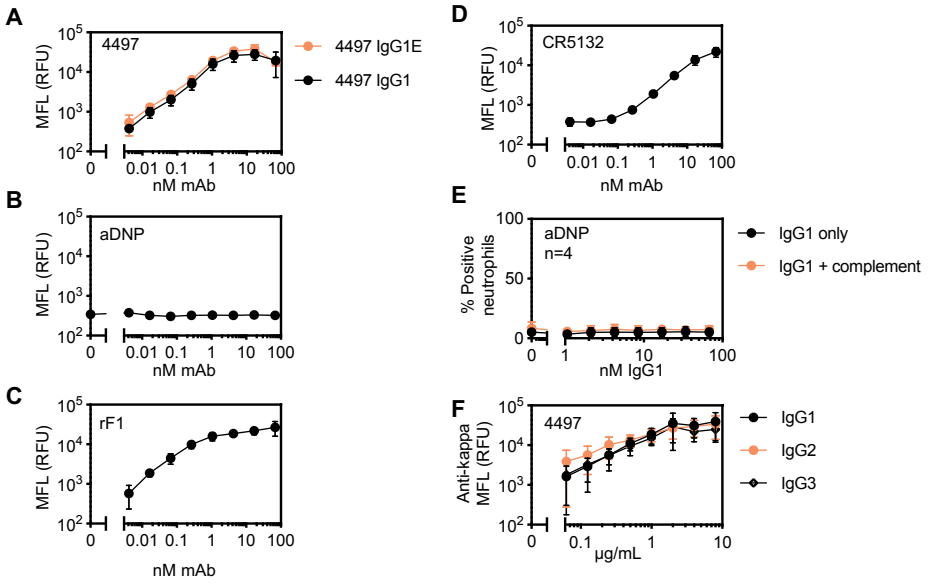

Figure S2. mAb binding to Newman Spa-Sbi. MAmetrine expressing Newman Δspa/sbi were incubated in a concentration range of **(A)** 4497-IgG1 and 4497-IgG1 E345K, **(B)** aDNP-IgG1, **(C)** rF1-IgG1, **(D)** CR5132-IgG1. mAb binding was detected by flow cytometry using an anti-kappa-AF647 antibody conjugate and plotted as AF647 GeoMFI of the mAmetrine positive bacterial population. Data represent mean ± SD of three independent experiments. **(E)** Phagocytosis of Newman Δspa/sbi by human neutrophils (MOI 10:1) in absence or presence of complement. MAmetrine expressing bacteria were incubated with a concentration range of aDNP-IgG1 (control antibody) in buffer (IgG1 only) or 1% IgG/IgM-depleted normal human serum (IgG1+complement). Phagocytosis was quantified by flow cytometry and plotted as percentage mAmetrine positive events of the neutrophil population. Data represent mean ± SD of n=4 independent experiments. **(F)** MAmetrine expressing Newman Δspa/sbi were incubated in a concentration range of 4497-IgG1, IgG2 and IgG3. MAb binding was detected by flow cytometry using an anti-kappa-AF647 antibody conjugate and plotted as AF647 GeoMFI of the mAmetrine positive bacterial population. Data represent mean ± SD of three independent experiments.

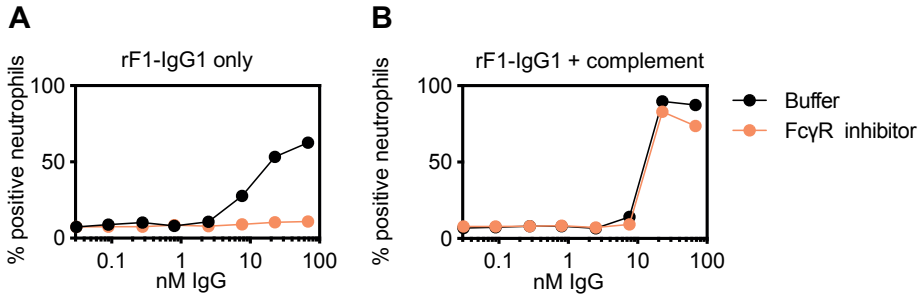

Figure S3. (A,B) Phagocytosis of ATCC14990 by human neutrophils (MOI 10:1) in absence or presence of complement. FITC labeled bacteria were incubated with a concentration range of rF1-IgG1 in buffer (**A,** IgG1 only) or 1% IgG/IgM-depleted normal human serum (**B,** IgG1+complement). Neutrophils were incubated with buffer or FLIPr-like (FcγR inhibitor). Phagocytosis was quantified by flow cytometry and plotted as percentage FITC positive events of the neutrophil population. Data represent one independent experiment.

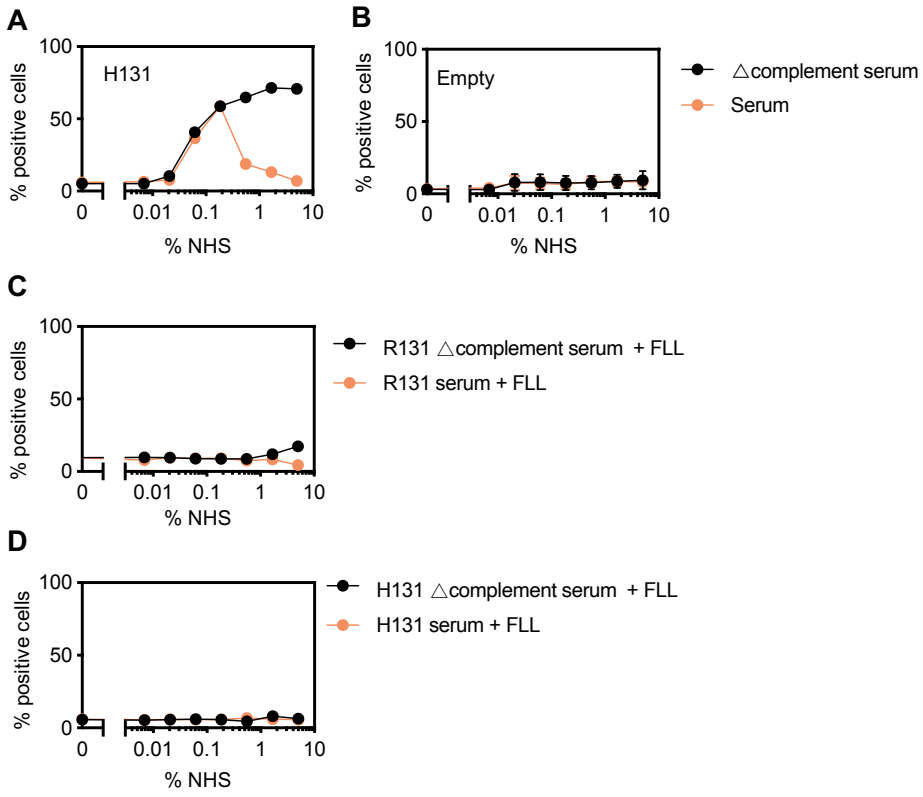

Figure S4. (A,B) Binding of Newman Δspa/sbi to CD32A H131 expressing CHO cells **(A)** and WT CHO cells **(B)** (MOI 10:1). MAmetrine expressing bacteria were incubated with a concentration range of serum or serum Δ complement. **(C,D)** binding to **(C)** R131 CD32A cells and **(D)** H131 CD32A cells in presence of FLIPr-like (FcγR inhibitor). Binding to cell lines was quantified by flow cytometry and plotted as percentage mAmetrine positive events of the cell line population. Data represent mean ± SD of n=1 (H131) and n=3 (WT CHO) independent experiments.

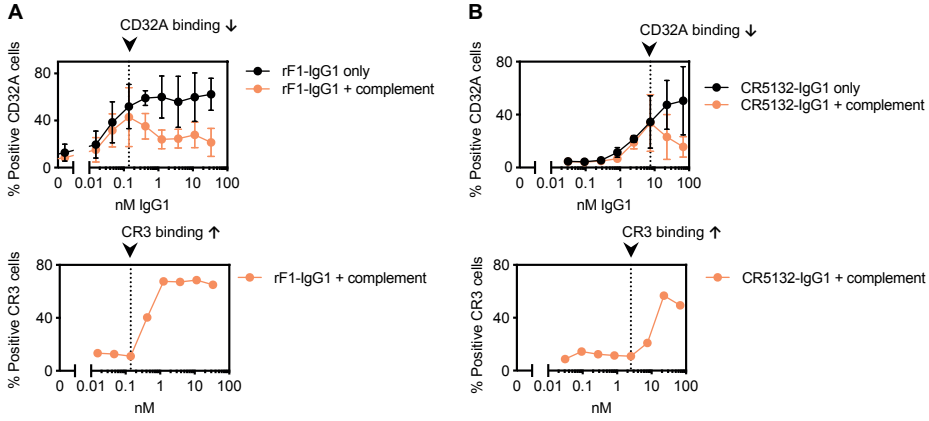

Figure S5. Binding of Newman Δspa/sbi to CD32A expressing CHO cells or CR3 expressing HEK cells (MOI 10:1) induced by **(A)** rF1-IgG1 or **(B)** CR5132-IgG1. MAmetrine expressing bacteria were incubated with a concentration range of IgG1 in buffer (IgG1 only) or 1% ΔIgG/IgM serum (IgG1+complement). Binding to cell lines was quantified by flow cytometry and plotted as percentage mAmetrine positive events of the cell line population. Data represent mean ± SD of n=4 (rF1-igG1) and n=3 (CR5132-IgG1) independent experiments.

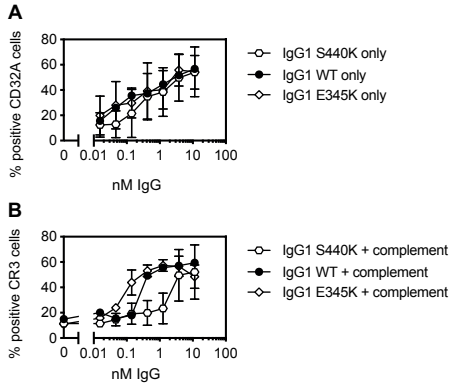

Figure S6. Binding of Newman Δspa/sbi to **(A)** CD32A expressing CHO cells or **(B)** CR3 expressing HEK cells (MOI 10:1) induced by 4497-IgG1 WT, E345K or S440K monoclonal antibodies. MAmetrine expressing bacteria were incubated with a concentration range mAb in buffer (**A,** IgG1 only) or 1% ΔIgG/IgM serum (**B,** IgG1+complement). Binding to cell lines was quantified by flow cytometry and plotted as percentage mAmetrine positive events of the cell line population.

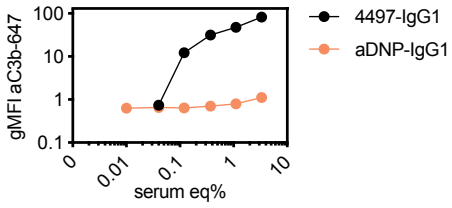

Figure S7. C3b deposition induced by 4497-IgG1 after addition of purified classical pathway components. MAmetrine expressing Newman Δspa/sbi were incubated in a concentration range of 4497-IgG1/aDNP IgG1 in a concentration range of serum equivalent purified C1, C1-INH, C2, C4 and C3. C3b deposition was detected by flow cytometry using an anti-neoC3b-AF647 antibody conjugate and plotted as AF647 GeoMFI of the mAmetrine positive bacterial population. Data represent data of n=1 independent experiments.

Supplementary tables

Table S1. Variable and constant heavy chain and light chain amino acid sequences used for antibody production.

Clone, *target*	Sequence	Reference
VH variable heavy chain		
G2a2, *Anti-DNP*	DVRLQESGPGLVKPSQSLSLTCSVTGYSITNSYYWNWIRQFP-GNKLEWMVYIGYDGSNNYNPSLKNRISITRDTSKNQFFLKLNS-VTTEDTATYYCARATYYGNYRGFAYWGQGTLVTVSA	[42]
4497, *Anti-WTA(β)*	EVQLVESGGGLVQPGGSLRLSCSASGFSFNSFWMHWVRQVP-GKGLVWISFTNNEGTTTAYADSVRGRFIISRDNAKNTLYLEMNN-LRGEDTAVYYCARGDGGLDDWGQGTLVTVSS.	WO/2014/193722 A1 [43 18]
CR5132	EVLESGGGLVQPGGSLRLSCSDSGFSFNNYWMTWVRQAPGK-GLEWVANINRDGSDKYHVDSVEGRFTISRDNSKNSLYLQMNN-LRADDAA VYFCARGGRTTSWYWRNWGQGTLVTVSS	US 2012/0141493 A1
rF1, *Anti-GlcNac pan-SDR*	EVQLVESGGGLVQPGGSLRLSCAASGFTLSRFAMSWVRQA-PGRGLEWVASINSGNNPYYARSVQYRFTVSRDVSQNTVS-LQMNNLRAEDSATYFCAKDHPSSGWPTFDSWGPGTLVTVSS	WO/2016/090040 Seq13 [19]
VL variable light chain		
G2a2, *Anti-DNP*	DIRMTQTTSSLSASLGDRVTISCRASQDISNYLNWYQQKPDGT-VKLLIYYTSRLHSGVPSRFSGSGSGTDYSLTISNLEQEDIATYF-CQQGNTLPWTFGGGTKLEIK	[42]
4497, *Anti-WTA(β)*	DIQLTQSPDSLAVSLGERATINCKSSQSIFRTSRNKNLLNWY-QQRPGQPPRLLIHWASTRKSGVPDRFSGSGFGTDFTLTIT-SLQAEDVAIYYCQQYFSPPYTFGQGTKLEIK	WO/2014/193722 A1 [43] [18]
CR5132	STDIQMTQSPSTLSASVGDRVTITCRASQSISSWLAWYQQKP-GKAPKLLIYKASSLESGVPSRFSGSGSGTEFTLTISSLQPDDFA-TYYC QQYNSYPLTFGGGTKLEIK	US 2012/0141493 A1
rF1, *Anti-GlcNac pan-SDR*	DIQLTQSPSALPASVGDRVSITCRASENVGDWLAWYRQKPG-KAPNLLIYKTSILESGVPSRFSGSGSGTEFTLTISSLQPDDFA-TYYCQHYMRFPYTFGQGTKVEIK	WO/2016/090040_ Seq14 [19]

Table S1. Variable and constant heavy chain and light chain amino acid sequences used for antibody production. ()

Clone, *target*	Sequence	Reference
HC constant regions		
IgG1	ASTKGPSVFPLAPSSKSTSGGTAALGCLVKDYFPEPVTVSWNS-GALTSGVHTFPAVLQSSGLYSLSSVVTVPSSSLGTQTYICNVNH-KPSNTKVDKKVEPKSCDKTHTCPPCPAPELLGGPSVFLFPPKP-KDTLMISRTPEVTCVVVDVSHEDPEVKFNWYVDGVEVHNAKT-KPREEQYNSTYRVVSVLTVLHQDWLNGKEYKCKVSNKALPA-PIEKTISKAKGQPREPQVYTLPPSREEMTKNQVSLTCLVKG-FYPSDIAVEWESNGQPENNYKTTPPVLDSDGSFFLYSKLTVDK-SRWQQGNVFSCSVMHEALHNHYTQKSLSLSPGK	[44]
IgG2	ASTKGPSVFPLAPCSRSTSESTAALGCLVKDYFPEPVTVSWNS-GALTSGVHTFPAVLQSSGLYSLSSVVTVPSSNFGTQTYTCNVD-HKPSNTKVDKTVERKCCVECPPCPAPPVAGPSVFLFPPKPK-DTLMISRTPEVTCVVVDVSHEDPEVQFNWYVDGVEVHNAKT-KPREEQFNSTFRVVSVLTVVHQDWLNGKEYKCKVSNKGLPA-PIEKTISKTKGQPREPQVYTLPPSREEMTKNQVSLTCLVKG-FYPSDIAVEWESNGQPENNYKTTPPMLDSDGSFFLYSKLTVDK-SRWQQGNVFSCSVMHEALHNHYTQKSLSLSPGK	
IgG3	ASTKGPSVFPLAPCSRSTSGGTAALGCLVKDYFPEPVT-VSWNSGALTSGVHTFPAVLQSSGLYSLSSVVTVPSSSLGTQ-TYTCNVNHKPSNTKVDKRVELKTPLGDTTHTCPRCPEPK-SCDTPPPCPRCPEPKSCDTPPPCPRCPEPKSCDTPPPCPRC-PAPELLGGPSVFLFPPKPKDTLMISRTPEVTCVVVDVSHED-PEVQFKWYVDGVEVHNAKTKPREEQYNSTFRVVSVLT-VLHQDWLNGKEYKCKVSNKALPAPIEKTISKTKGQPRE-PQVYTLPPSREEMTKNQVSLTCLVKGFYPSDIAVEWESS-GQPENNYNTTPPMLDSDGSFFLYSKLTVDKSRWQQGNIFSCS-VMHEALHNRFTQKSLSLSPGK	Derived from pFuse vector (Invivogen)
LC constant regions		
Kappa class	RTVAAPSVFIFPPSDEQLKSGTASVVCLLNNFYPREAK-VQWKVDNALQSGNSQESVTEQDSKDSTYSLSSTLTLSKADY-EKHKVYACEVTHQGLSSPVTKSFNRGEC	[44]

CHAPTER 6

General discussion

Staphylococcal infections
Can antibodies help?

Lisanne de Vor

Staphylococcal infections – can antibodies help?

Staphylococci are important human pathogens that cause life threatening infections. Due to the steep rise in antibiotic resistance and the ability of staphylococci to form biofilm, these infections are becoming a serious threat for public health. Therefore, there is an urgent need for alternative strategies to tackle staphylococcal infections. Scientific progress in the last decade has made it possible to produce human recombinant antibodies that can be administered as therapeutics in a safe and non-immunogenic way [1]. By genetic engineering, the effector function of these therapeutic antibodies can now be manipulated. At present, less than five therapeutic antibodies are approved for the treatment of bacterial infections [2]. These antibodies function by neutralization of bacterial virulence factors, such as toxins or adhesion molecules [3,4]. Besides neutralization, therapeutic antibodies could activate the human immune system to clear the pathogen via the Fc tail or serve as a vehicle to carry antibacterial agents to the site of infection. The research presented in this thesis focused on the engineering of monoclonal antibodies for the use against *Staphylococcus aureus (S. aureus)* and *Staphylococcus epidermidis (S. epidermidis)* in single cell and biofilm form. Here, I will elaborate on the value of the main results in this thesis for the development of successful antibody-based therapies to combat staphylococcal infections. Furthermore, we will discuss general considerations and challenges for the development of such therapies.

What are good immune enhancing antibodies?

The right antigen

The work in this thesis indicates that for the development of antibody-based therapies against staphylococci, the choice for the right antigen is of great importance. It was already known that antibodies should bind the bacterial surface in order to induce immune activation, but the question remained all surface binding antibodies can trigger immune activation. Here, we describe important antigen characteristics to consider for the development of immune enhancing antibody therapy.

Epitope density

Given the importance of complement opsonization for effective neutrophil responses against staphylococci, we envision that the ideal epitope for anti-staphylococcal mAbs allows for IgG clustering and thus efficient C1 binding and subsequent activation of the classical pathway. One characteristic of the Fab domain that can influence clustering of IgG molecules is the epitope density [5,6]. In **Chapter 4** and **Chapter 5** we for the first time compared mAbs recognizing different structures on the staphylococcal surface.

The mAb backbones were identical (IgG1) but they were produced with different Fab domains. We found that IgG1 molecules that showed binding at lower concentrations could induce phagocytosis more efficiently. In both chapters**,** the most potent antibodies were directed against highly abundant epitopes on the staphylococcal surface. These epitopes were GlcNAc groups on the SDR protein (clone rF1) for *S. epidermidis* **(Chapter 4)** and *S. aureus* **(Chapter 5)** and beta-GlcNAc groups on WTA (clone 4497) for *S. aureus* **(Chapter 5)**. Thus, our studies suggest that high density epitopes are ideal for complement enhancing mAb-based therapies and that finding the right antigen is crucial in the development of successful mAb-based therapies.

Expression of the antigen throughout the infection cycle including biofilm

Staphylococci can cause a wide range of infections because they can adapt to different host environments via complex gene regulation networks [7,8]. Particularly for *S. aureus*, adhesion factors that facilitate adhesion to host tissues are expressed in the beginning of infection, while the expression of secreted toxins and proteases is enabled later in infection to enable tissue invasion or dissemination from biofilm [9]. For example, in **Chapter 2** we found a mAb (clone T1-2 against ClfA) that recognized *S. aureus* only in the stationary phase but not in logarithmic phase. Thus, not all antigens are suitable for targeting staphylococci throughout the complete infection cycle, and surface structures that are present throughout the complete infection cycle, such as *S. aureus* WTA, are preferred. Because WTA is a dense antigen and WTA is expressed by all *S. aureus* strains, it seems to be an ideal antigen for anti-*S. aureus* therapies, although we think that future work is needed to draw such conclusions.

Expression by most clinical isolates

For the broad application of mAbs it is of importance that they react with conserved antigens that are expressed by most clinical isolates. In **Chapter 2**, almost all mAbs were shown to bind all isolates in a collection of clinical isolates derived from different biofilm associated infections (endocarditis, prosthetic joint, catheter). The mAb recognizing α-GlcNAc WTA (clone 4461) recognized only a fraction of the isolates, in line with literature describing 35.7% of clinical isolates being TarM positive [10]. The 4497-clone recognizing the β-GlcNAc modification would be of more interest to target *S. aureus*, because nearly all sequenced *S. aureus* strains are positive for TarS, the enzyme responsible for the β-GlcNAc modification [10]. This is also one of the reasons why we chose the 4497-clone for the development of Fab-enzyme fusion proteins in **Chapter 3**. *S. epidermidis* WTA differs from *S. aureus* WTA because the two species express different modification enzymes. Furthermore, *S. aureus* WTA has a ribotolphosphate backbone and *S. epidermidis* WTA has a glycerolphosphate backbone [11,12]. Therefore, in **Chapter 4** we searched mAbs that recognize *S. epidermidis* isolates. Here we identi-

fied two mAbs (CR5133, CR6453) that recognized all clinical isolates in the panel, but these mAbs were poor complement activators. Interestingly, the best performing wild type mAb regarding complement activation, clone rF1 directed against GlcNAc-SDR proteins, was only able to recognize 50% of the clinical isolates. Thus, the work in this thesis stresses the importance of performing broad screenings for antigen expression by the majority of clinical isolates.

Antigens in biofilm

Next to different gene expression in infection stages, gene and protein expression can differ greatly between the planktonic and biofilm modes of bacterial growth [13,14]. Apart from the identification of one antibody recognizing extracellular polymeric substance (EPS) component poly-N-acetyl glucosamine (PNAG)[15], not much work was published on antibodies recognizing staphylococcal biofilm [4,16]. When targeting biofilm related infections, antibodies that label bacteria in planktonic and biofilm state would be beneficial. This is important because in the biofilm life cycle planktonic cells can be released from a biofilm and disseminate to other locations in the body. In **Chapter 2** we show that mAbs recognizing common surface components of *S. aureus* can recognize these bacteria in planktonic state but also in biofilm state, regardless of the biofilm types (PNAG-dependent or PNAG-independent). The fact that mAbs against surface structures can be used to target biofilm bacteria is of great importance for biofilm research, because previously it was thought that the biofilm EPS could shield bacteria from immune recognition [17].

To target biofilm, future research can also focus on mAbs that recognize secreted proteins. While this sounds contradictory, recent proteomic and transcriptomic analyses showed that several evasion molecules (Eap, CHIPS, SAK, SSL10) and toxins (Hla, LukAB/GH, LukED, HlgAB, HlgCB, PSMs) are highly expressed in different *S. aureus* biofilm models compared to planktonic cultures of the same strain [18–20]. Most of these factors, especially Eap, were found to be incorporated into the EPS, while other factors are secreted into the environment as well [18,21]. Other factors including Sbi, Aur, SCIN, Ecb, Efb, FLIPr, FLIPrL, PVL and Nuc are also found in the EPS but were not highly expressed compared to planktonic *S. aureus* [18]. Recent publications propose that positively charged bacterial proteins interact with negatively charged extracellular DNA and cell wall molecules in the *S. aureus* biofilm in order to maintain the biofilm structure [20]. In **Chapter 2,** we also detect the incorporation of secreted SpA in the biofilm EPS and high binding of anti-SpA-IgG3 (clone 10919). The high local concentration of some of these molecules, especially the ones that are secreted and normally diffuse away from the bacterium, could be used to recognize biofilm infections compared to planktonic bacteria and be used as a diagnostic tool. Whether targeting of EPS structures leads to

efficient opsonization of biofilm bacteria remains an outstanding question, as discussed below in "*Evasion by staphylococci – Biofilm formation*".

Discovery of new mAb clones

In this thesis we limited ourselves to the use of only previously described human mAb clones. With the development of several novel techniques that will facilitate the discovery new mAb clones in the near future, such as single B cell cloning and B cell sequencing [22], we anticipate that many new mAb clones will be discovered in the near future. The epitope density, affinity of the mAb clone for the epitope and the antigen expression levels by clinical isolates in different stages of the pathogenic life cycle could all influence the therapeutic potential of an antibody. Therefore, it is important to screen newly discovered mAb clones for these characteristics.

The ideal Fc tail

Scientific progress in monoclonal antibody production now allows us to optimize the Fc tail of antibodies and thereby tailor the antibodies function to our wishes. The work in this thesis indicates that Fc engineering provides a unique opportunity to potentiate the capacity of against staphylococci.

Hexamer enhancing point mutations

For example, Fc mutations that modify the interaction of a mAb's Fc part with C1q to increase antibody mediated complement deposition are being explored. Recent studies showed already on gram-negative pathogen *Neisseria gonorrhea* and on tumor cells that single amino acid mutations such as E430G or E345K can potentiate the capacity of mAbs to induce complement mediated lysis via the formation of MAC pores in the cell membrane [5,23–25]. Moreover, we previously reported that the same mutations can be used to improve complement dependent phagocytosis of *S. aureus* [26] and *Streptococcus pneumoniae* [27]. In **Chapter 4** and **5** we further explored the application of the E345K single point mutation for the use in mAbs with different Fab domains recognizing surface structures on *S. epidermidis* (**Chapter 4**) or *S. aureus* (**Chapter 5**). This work revealed that E345K mutations can be applied to multiple different anti-staphylococcal mAbs to enhance phagocytosis via enhanced complement deposition. These were the first studies comparing mAbs with different Fab domains, and we found out that the mutation has a larger effect when the wild type mAb clone is not an efficient activator of the complement system. Moreover, we added *S. epidermidis* to the list of bacteria where this approach can be successfully used.

The effect of subclasses

In **Chapter 4** and **5,** we also compared the effect of converting IgG1 to other subclasses. The different IgG subclasses are highly conserved but differ in the constant region, which is involved in binding to both FcγRs and C1q. As a result, the different subclasses have different affinities for FcγRs (IgG3>IgG1>IgG4>IgG2) and C1q (IgG3>IgG1>IgG2) [28]. Overall, IgG3 was always performing slightly better than IgG1 in phagocytosis assays for both *S. epidermidis* (**Chapter 4**) and *S. aureus* (**Chapter 5**). However, our data in **Chapter 4** indicates that introducing the hexamer enhancing E345K mutation can enhance mAbs to a similar extent or more than switching to IgG3 subclass. Introducing the E345K mutation in the IgG3 backbone did not yield additional improvements. As IgG1 is established to be safe for antibody therapy in other fields than infectious diseases, such as oncology and autoimmune diseases [29], is easier to produce and to purify than IgG3 [30] and has a longer half-life [31], the first subclass of choice therefore would be IgG1. However, *S. aureus* expresses the evasion protein Staphylococcal protein A (SpA) [32], which sequesters IgG molecules via their Fc tail and thereby prevents complement activation [33] and binding to Fc receptors [34]. Because the Fc tail of most IgG3 (VH3- [35] is not recognized by SpA [36], IgG3 molecules can induce phagocytosis in the presence of SpA. Since SpA also appears to be sequestered in the biofilm EPS **(Chapter 2)**, we anticipate that monoclonal antibodies of the IgG3 subclass or IgG1 subclass with mutations to prevent SpA binding can be more successful than IgG1 for anti-*S. aureus* therapies.

CR or FcγR-mediated phagocytosis?

Another antibody property to consider when choosing the optimal Fc tail is the interaction with Fc receptors. Previous work has already pointed out that complement plays an important role in enhancing the uptake of bacteria [26,37–39]. However, the contribution of Fc receptors in the phagocytic process was still unclear. In **Chapter 5** we show that complement opsonized bacteria are engulfed only via the interaction with complement receptors (CRs). Our experimental set up resembles the situation in serum, where complement components are constantly present. However, the relative amount of complement components in the tissues outside of the blood vessels are not known and could be very different, therefore skewing towards FcγR dependency. Although we observed good killing of *S. epidermidis* via CR-mediated phagocytosis **(Chapter 4)**, a remaining question is whether FcγR-mediated phagocytosis and CR-mediated phagocytosis differ from each other. Should FcγR-mediated phagocytosis lead to better killing of staphylococci than CR-mediated phagocytosis, the future focus could be on the engineering of mAbs that strongly interact with FcγR but are unable to activate the complement reaction.

Evasion by staphylococci

Above, we described considerations in the design of optimal mAbs for anti-staphylococcal therapy. However, we should not forget that staphylococci are no innocent bystanders; they actively obstruct immune attack. Especially *S. aureus* has evolved many mechanisms to evade antibody binding, complement deposition, phagocytosis and intracellular killing via the secretion of several so-called immune evasion proteins [40]. In addition, both *S. aureus* and *S. epidermidis* are both known for their ability to form biofilms on implanted medical devices and host tissues. Below we describe these challenges and how we believe these challenges can be tackled.

Evasion of opsonization and phagocytosis

The first challenge is the ability of *S. aureus* to evade opsonization and phagocytosis. The bacterium expresses multiple proteases (staphylokinase [41] and GluV8 [42]) that cleave surface bound IgG and thereby reduce opsonophagocytosis. Furthermore, *S. aureus* expresses two proteins, Staphylococcal protein A (SpA)[32] and Staphylococcal binder of immunoglobulin (Sbi) [43], that bind the Fc regions of IgG molecules with high affinity and thereby block C1q binding [33] and Fc receptor mediated phagocytosis [34]. Additionally, FLIPr and FLIPr-like block multiple FcRs and consequently inhibit FcR-mediated phagocytosis [38]. *S. aureus* also secretes multiple proteins that interfere with the complement reaction. Collagen adhesin (Cna) binds C1q and inhibits activation of the classical pathway [44]. Aureolysin cleaves C3 in the surrounding of the bacterium, which is then degraded by host factors and not deposited on the bacterial surface [45]. Next to IgG binding, Sbi inhibits C3 cleavage into C3b by forming a complex with C3 and complement regulator Factor H [46,47]. Extracellular adherence protein (Eap) blocks formation of lectin and classical pathway C3 convertases [48] and Staphylococcal Complement INhibitor (SCIN) binds to C3 convertases of the classical, lectin and alternative pathway, thereby blocking C3b deposition and C5a production [37]. In addition to all evasion mechanism described above, *S. aureus* also produces toxins, another class of evasion proteins that kill immune cells including neutrophils directly by lysing the membrane [49,50].

Taken together, *S. aureus* has evolved several mechanisms that could impair standard IgG1-based mAb therapy, by directly cleaving mAbs, sequestering mAbs by SpA binding, blocking mAb induced complement deposition and killing neutrophils directly. To prevent that immune activating antibody therapy is impaired by *S. aureus* evasion molecules, we anticipate that they must be administered in combination with multiple neutralizing antibodies that target evasion molecules. When neutralizing antibodies are directed against surface molecules, another approach could be to optimize them for immune activation and create mAbs with a double function: facilitating phagocytosis

and neutralizing evasion molecules. Moreover, as discussed previously in '*The ideal Fc tail: The effect of subclasses',* antibodies that do not react with SpA (IgG3 subclass) may be useful. Some of the mentioned strategies could possibly be combined in the same antibody molecule. An example of such a mAb has been described by Janssen Research and Development. The mAb binds the SDR protein on the staphylococcal surface via one binding domain and neutralizes leucocidins via a second binding domain. In addition, the Fc tail has been engineered to resist SpA and Sbi binding and proteolysis by GluV8 [WO2015089073]. We think that this mAb could be further improved by adding the hexamer enhancing E345K or E430G mutations to improve complement opsonization and phagocytosis by neutrophils.

Intracellular survival

Another challenge is the ability of *S. aureus* to persist intracellularly within host cells. By doing so, the bacterium is protected from the host immune system and antibiotics [50–52]. Several approaches are being explored to target intracellular *S. aureus*. For example, Genentech has produced an antibody drug conjugate (ADC) that combines the opsonic 4497 mAb and the anti-staphylococcal antibiotic Rifampicin [53] [WO 2014194247 A1]. The ADC can target intracellular bacteria because the ADC is internalized together with the bacterium and the antibiotic is activated through proteolytic release mediated by proteases in the phagosome.

Biofilm formation

S. epidermidis and *S. aureus* are both notorious for their ability to form biofilm on implanted devices and host tissues. Especially for *S. epidermidis,* which lacks most virulence factors that *S. aureus* expresses, biofilm formation can be seen as one of the primary immune evasion mechanisms [54].

The first challenge in developing immune activating therapeutic antibodies for biofilm infections is to determine the best epitope for immune activation within a biofilm. Previous work suggests that when the complement system is highly activated on staphylococcal EPS components such as PNAG, it is not deposited close to the bacterial surface itself and therefore acts as a decoy for the actual target: the bacterium encased in the PNAG matrix. Besides a decoy for complement activation, PNAG could also act as a 'sink' for antibody opsonization. *In vitro* experiments revealed that IgG can penetrate biofilm, but antibodies against PNAG in rabbit serum rather bind to PNAG in the EPS than to PNAG on the bacterial surface [55]. Because of this, the biofilm was protected against antibody mediated opsonic killing by neutrophils. Also, adding isolated PNAG to planktonic bacteria protected against phagocytic killing, indicating that an excess of PNAG in the biofilm captures antibodies and prevents binding close to the bacterial surface

[55]. Instead of being directed to the EPS, antibody binding and complement deposition might need to be localized close to the bacterial surface to ensure a localized neutrophil response that is sufficient to eliminate staphylococci. In **Chapter 2** we showed that mAbs recognizing surface components can bind to PNAG-positive and PNAG-negative *S. aureus* biofilm, but the question remains whether these mAb molecules will be able to interact with complement components or whether they will be shielded by the biofilm EPS.

A second challenge is the ability of neutrophils to phagocytose bacteria from a biofilm. Neutrophils are able to engulf particles up to their own cell size (~10 μm) [56]. When exposed to polystyrene beads bigger than 11 μm, neutrophils exhibit frustrated phagocytosis. Thus, the ability of neutrophils to phagocytose bacterial aggregates (such as biofilm) bigger than 10 μm depends on the ability of the phagocyte to break intercellular interactions and fragment the biofilm in smaller pieces. This might be ensured by coupling therapeutic antibodies with biofilm degrading enzymes, like the fusion proteins we produced in **Chapter 3.** Furthermore, we know that phagocyte granules contain proteases (e.g. elastase, cathepsin G and proteinase 3), DNAses and enzymes such as lysozyme that can hydrolyze peptidoglycan linkages [56,57]. This theoretically means that neutrophils can break down certain types of biofilms, but this remains to be confirmed. Presence of PNAG has been shown to protect *S. epidermidis* from phagocytosis by neutrophils [58]. To our knowledge, neutrophils do not contain PNAG degrading enzymes, which might explain the increased resistance to neutrophil phagocytosis of *S. epidermidis* biofilms compared to *S. aureus* biofilms [59].

The natural immune response has more problems in clearing biofilm related infections than infections by planktonic bacteria. However, neutrophils seem to be able to recognize and phagocytose bacteria in a biofilm to a certain extent [59–62]. For example, we used confocal microscopy to visualize the interaction between fluorescently labeled neutrophils and GFP *S. aureus* biofilm. After opsonization with human serum, containing natural occurring antibodies and complement factors, we observed neutrophils were able to crawl over the biofilm and phagocytose clumps of bacteria over a time span of 30 minutes **(Figure 1)**. As intracellular killing following phagocytosis is the most effective way for neutrophils to eliminate staphylococci, stimulation of this process seems a promising approach to combat biofilm infections. This could for example be achieved via mAbs that activate the complement system and are conjugated to EPS degrading enzymes. Altogether, the continuous battle after infection seems a tight balance between the human immune responses and bacterial evasion strategies, including biofilm formation. Future research is necessary to determine whether immune activat-

ing mAbs can help to overcome these evasion mechanisms and shift the balance in the advantage of the human body.

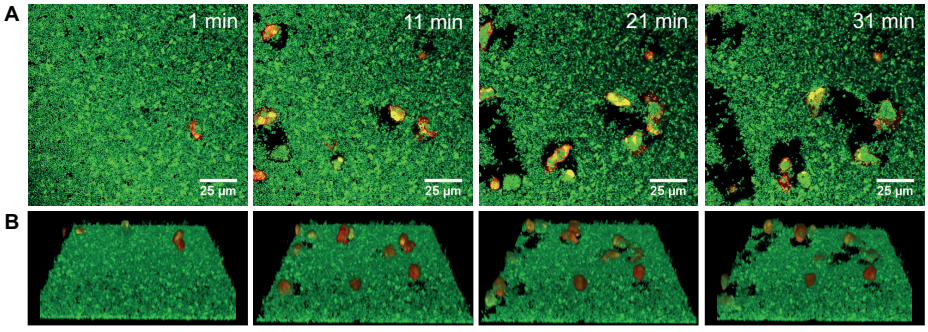

Figure 1. Phagocytosis of biofilm by human neutrophils. *S. aureus* (GFP, green) biofilm was grown for 24 hours in Cellview slides. Neutrophil membranes were labeled with DiD cell-labeling solution (red) and nuclei with Syto82 (yellow). Biofilm was incubated with 1% human serum before neutrophils were added. Z-stacks were aqcuired for 30 minutes at 37°C.

Acknowledgements

The authors greatly thank Remy Muts for critically reading the manuscript

References

1. Irani, V. *et al.* Molecular properties of human IgG subclasses and their implications for designing therapeutic monoclonal antibodies against infectious diseases. *Mol. Immunol.* **67**, 171–182 (2015).
2. Whaley, K. J. & Zeitlin, L. Emerging antibody-based products for infectious diseases: Planning for metric ton manufacturing. *Hum. Vaccin. Immunother.* **18**, (2022).
3. Sause, W. E., Buckley, P. T., Strohl, W. R., Lynch, A. S. & Torres, V. J. Antibody-Based Biologics and Their Promise to Combat *Staphylococcus aureus* Infections. *Trends Pharmacol. Sci.* **37**, 231–241 (2016).
4. Raafat, D., Otto, M., Reppschläger, K., Iqbal, J. & Holtfreter, S. Fighting *Staphylococcus aureus* Biofilms with Monoclonal Antibodies. *Trends Microbiol.* **27**, 303–322 (2019).
5. Diebolder, C. A. *et al.* Complement Is Activated by IgG Hexamers Assembled at the Cell Surface. *Science (80-.).* **343**, 1260–1263 (2014).
6. Wang, B. *et al.* Regulation of antibody-mediated complement-dependent cytotoxicity by modulating the intrinsic affinity and binding valency of IgG for target antigen. *MAbs* **12**, (2020).
7. Balasubramanian, D., Harper, L., Shopsin, B. & Torres, V. J. *Staphylococcus aureus* pathogenesis in diverse host environments. *Pathog. Dis.* **75**, 1–13 (2017).
8. Jenul, C. & Horswill, A. R. Regulation of *Staphylococcus aureus* Virulence . *Microbiol. Spectr.* **7**, 3–31 (2019).
9. Lister, J. L. & Horswill, A. R. *Staphylococcus aureus* biofilms: recent developments in biofilm dispersal. *Front. Cell. Infect. Microbiol.* **4**, (2014).
10. Winstel, V. *et al.* Wall Teichoic Acid Glycosylation Governs *Staphylococcus aureus* Nasal Colonization. *MBio* **6**, (2015).
11. Du, X. *et al. Staphylococcus epidermidis* clones express *Staphylococcus aureus*-type wall teichoic acid to shift from a commensal to pathogen lifestyle. *Nat. Microbiol.* **6**, 757–768 (2021).
12. Koprivnjak, T., Weidenmaier, C., Peschel, A. & Weiss, J. P. Wall Teichoic Acid Deficiency in *Staphylococcus aureus* Confers Selective Resistance to Mammalian Group IIA Phospholipase A 2 and Human β-Defensin 3. *Infect. Immun.* **76**, 2169–2176 (2008).
13. Brady, R. A., Leid, J. G., Camper, A. K., Costerton, J. W. & Shirtliff, M. E. Identification of *Staphylococcus aureus* proteins recognized by the antibody-mediated immune response to a biofilm infection. *Infect. Immun.* **74**, 3415–3426 (2006).
14. Resch, A., Rosenstein, R., Nerz, C. & Götz, F. Differential gene expression profiling of *Staphylococcus aureus* cultivated under biofilm and planktonic conditions. *Appl. Environ. Microbiol.* **71**, 2663–2676 (2005).
15. Kelly-Quintos, C., Cavacini, L. A., Posner, M. R., Goldmann, D. & Pier, G. B. Characterization of the opsonic and protective activity against *Staphylococcus aureus* of fully human monoclonal antibodies specific for the bacterial surface polysaccharide poly-N-acetylglucosamine. *Infect. Immun.* **74**, 2742–2750 (2006).
16. Soliman, C. *et al.* Structural basis for antibody targeting of the broadly expressed microbial polysaccharide poly-N-acetylglucosamine. *J. Biol. Chem.* **293**, 5079–5089 (2018).
17. Zapotoczna, M., McCarthy, H., Rudkin, J. K., O'Gara, J. P. & O'Neill, E. An Essential Role for Coagulase in *Staphylococcus aureus* Biofilm Development Reveals New Therapeutic Possibilities for Device-Related Infections. *J. Infect. Dis.* **212**, 1883–1893 (2015).

18. Formosa-Dague, C. *et al.* Sticky Matrix: Adhesion Mechanism of the Staphylococcal Polysaccharide Intercellular Adhesin. *ACS Nano* **10**, 3443–3452 (2016).
19. Vuong, C. *et al.* Polysaccharide intercellular adhesin (PIA) protects *Staphylococcus epidermidis* against major components of the human innate immune system. *Cell. Microbiol.* **6**, 269–275 (2004).
20. Dengler, V., Foulston, L., DeFrancesco, A. S. & Losick, R. An electrostatic net model for the role of extracellular DNA in biofilm formation by *Staphylococcus aureus*. *J. Bacteriol.* **197**, 3779–3787 (2015).
21. Vuong, C. *et al.* A crucial role for exopolysaccharide modification in bacterial biofilm formation, immune evasion, and virulence. *J. Biol. Chem.* **279**, 54881–54886 (2004).
22. Pedrioli, A. & Oxenius, A. Single B cell technologies for monoclonal antibody discovery. *Trends in Immunology* vol. 42 at https://doi.org/10.1016/j.it.2021.10.008 (2021).
23. Gulati, S. *et al.* Complement alone drives efficacy of a chimeric antigonococcal monoclonal antibody. *PLOS Biol.* **17**, e3000323 (2019).
24. de Jong, R. N. *et al.* A Novel Platform for the Potentiation of Therapeutic Antibodies Based on Antigen-Dependent Formation of IgG Hexamers at the Cell Surface. *PLOS Biol.* **14**, e1002344 (2016).
25. Wang, G. *et al.* Molecular Basis of Assembly and Activation of Complement Component C1 in Complex with Immunoglobulin G1 and Antigen. *Mol. Cell* **63**, 135–145 (2016).
26. Zwarthoff, S. A. *et al.* C1q binding to surface-bound IgG is stabilized by C1r2s2 proteases. *Proc. Natl. Acad. Sci. U. S. A.* **118**, (2021).
27. Aguinagalde, L. *et al.* Promoting Fc-Fc interactions between anti-capsular antibodies provides strong complement-dependent immune protection against Streptococcus pneumoniae *bioRxiv* 2022.01.21.477211 (2022) doi:10.1101/2022.01.21.477211.
28. Vidarsson, G., Dekkers, G. & Rispens, T. IgG Subclasses and Allotypes: From Structure to Effector Functions. *Front. Immunol.* **5**, 520 (2014).
29. Castelli, M. S., McGonigle, P. & Hornby, P. J. The pharmacology and therapeutic applications of monoclonal antibodies. *Pharmacol. Res. Perspect.* **7**, (2019).
30. Chu, T. H., Patz, E. F. & Ackerman, M. E. Coming together at the hinges: Therapeutic prospects of IgG3. *MAbs* **13**, (2021).
31. Morell, A., Terry, W. D. & Waldmann, T. A. Metabolic properties of IgG subclasses in man. *J. Clin. Invest.* **49**, 673–680 (1970).
32. Forsgren, A. & Sjöquist, J. 'Protein A' from *S. aureus*. I. Pseudo-immune reaction with human gamma-globulin. *J. Immunol.* **97**, 822–7 (1966).
33. Cruz, A. R. *et al.* Staphylococcal protein A inhibits complement activation by interfering with IgG hexamer formation. *Proc. Natl. Acad. Sci. U. S. A.* **118**, (2021).
34. Cruz, A. R. *et al.* Staphylococcal protein A inhibits IgG-mediated phagocytosis by blocking the interaction of IgGs with FcγRs and FcRn. *bioRxiv* 2022.01.21.477287 (2022) doi:10.1101/2022.01.21.477287.
35. Hillson, J. L., Karr, N. S., Oppliger, I. R., Mannik, M. & Sasso, E. H. The structural basis of germline-encoded VH3 immunoglobulin binding to staphylococcal protein A. *J. Exp. Med.* **178**, (1993).
36. LOGHEM, E., FRANGIONE, B., RECHT, B. & FRANKLIN, E. C. Staphylococcal Protein A and Human IgG Subclasses and Allotypes. *Scand. J. Immunol.* **15**, 275–278 (1982).
37. Rooijakkers, S. H. M. M. *et al.* Immune evasion by a staphylococcal complement inhibitor that acts on C3 convertases. *Nat. Immunol.* **6**, 920–927 (2005).

38. Stemerding, A. M. *et al. Staphylococcus aureus* Formyl Peptide Receptor–like 1 Inhibitor (FLIPr) and Its Homologue FLIPr-like Are Potent FcγR Antagonists That Inhibit IgG-Mediated Effector Functions . *J. Immunol.* **191**, 353–362 (2013).
39. Boero, E. *et al.* Use of Flow Cytometry to Evaluate Phagocytosis of *Staphylococcus aureus* by Human Neutrophils. *Front. Immunol.* **12**, 1–15 (2021).
40. de Jong, N. W. M., van Kessel, K. P. M. & van Strijp, J. A. G. Immune Evasion by *Staphylococcus aureus*. *Microbiol. Spectr.* **7**, 1–27 (2019).
41. Rooijakkers, S. H. M., van Wamel, W. J. B., Ruyken, M., van Kessel, K. P. M. & van Strijp, J. A. G. Anti-opsonic properties of staphylokinase. *Microbes Infect.* **7**, 476–484 (2005).
42. Drapeau, G. R., Boily, Y. & Houmard, J. Purification and Properties of an Extracellular Protease of *Staphylococcus aureus*. *J. Biol. Chem.* **247**, 6720–6726 (1972).
43. Zhang, L., Jacobsson, K., Vasi, J., Lindberg, M. & Frykberg, L. A second IgG-binding protein in *Staphylococcus aureus*. *Microbiology* **144**, 985–991 (1998).
44. Kang, M. *et al.* Collagen-binding microbial surface components recognizing adhesive matrix molecule (MSCRAMM) of gram-positive bacteria inhibit complement activation via the classical pathway. *J. Biol. Chem.* **288**, 20520–20531 (2013).
45. Laarman, A. J. *et al. Staphylococcus aureus* Metalloprotease Aureolysin Cleaves Complement C3 To Mediate Immune Evasion . *J. Immunol.* **186**, 6445–6453 (2011).
46. Burman, J. D. *et al.* Interaction of human complement with Sbi, a staphylococcal immunoglobulin-binding protein: Indications of a novel mechanism of complement evasion by *Staphylococcus aureus*. *J. Biol. Chem.* **283**, 17579–17593 (2008).
47. Haupt, K. *et al.* The *Staphylococcus aureus* protein Sbi acts as a complement inhibitor and forms a tripartite complex with host complement factor H and C3b. *PLoS Pathog.* **4**, e1000250 (2008).
48. Woehl, J. L. *et al.* The Extracellular Adherence Protein from *Staphylococcus aureus* Inhibits the Classical and Lectin Pathways of Complement by Blocking Formation of the C3 Proconvertase . *J. Immunol.* **193**, 6161–6171 (2014).
49. Spaan, A. N., Van Strijp, J. A. G. & Torres, V. J. Leukocidins: Staphylococcal bi-component pore-forming toxins find their receptors. *Nat. Rev. Microbiol.* **15**, 435–447 (2017).
50. Surewaard, B. G. J. J. *et al.* Inactivation of staphylococcal phenol soluble modulins by serum lipoprotein particles. *PLoS Pathog.* **8**, e1002606 (2012).
51. Spaan, A. N., Surewaard, B. G. J., Nijland, R. & van Strijp, J. A. G. Neutrophils Versus *Staphylococcus aureus* : A Biological Tug of War. *Annu. Rev. Microbiol.* **67**, 629–650 (2013).
52. Kobayashi, S. D. *et al.* Rapid neutrophil destruction following phagocytosis of *Staphylococcus aureus*. *J. Innate Immun.* **2**, 560–575 (2010).
53. Lehar, S. M. *et al.* Novel antibody-antibiotic conjugate eliminates intracellular *S. aureus*. *Nature* **527**, 323–328 (2015).
54. Le, K. Y., Park, M. D. & Otto, M. Immune evasion mechanisms of *Staphylococcus epidermidis* biofilm infection. *Front. Microbiol.* **9**, 1–8 (2018).
55. Cerca, N., Jefferson, K. K., Oliveira, R., Pier, G. B. & Azeredo, J. Comparative antibody-mediated phagocytosis of *Staphylococcus epidermidis* cells grown in a biofilm or in the planktonic state. *Infect. Immun.* **74**, 4849–4855 (2006).
56. Herant, M., Heinrich, V. & Dembo, M. Mechanics of neurophil phagocytosis: Experiments and quantitative models. *J. Cell Sci.* **119**, 1903–1913 (2006).

57. Rosenberg-Arska, M., Van Strijp, J. A. G., Hoekstra, W. P. M. & Verhoef, J. Effect of human polymorphonuclear and mononuclear leukocytes on chromosomal and plasmid DNA of Escherichia coli. Role of acid DNase. *J. Clin. Invest.* **73**, 1254–1262 (1984).
58. Kristian, S. A. *et al.* Biofilm Formation Induces C3a Release and Protects *Staphylococcus epidermidis* from IgG and Complement Deposition and from Neutrophil-Dependent Killing . *J. Infect. Dis.* **197**, 1028–1035 (2008).
59. Günther, F. *et al.* Host defence against *Staphylococcus aureus* biofilms infection: Phagocytosis of biofilms by polymorphonuclear neutrophils (PMN). *Mol. Immunol.* **46**, 1805–1813 (2009).
60. Meyle, E. *et al.* Destruction of bacterial biofilms by polymorphonuclear neutrophils: Relative contribution of phagocytosis, DNA release, and degranulation. *Int. J. Artif. Organs* **33**, 608–620 (2010).
61. Stroh, P. *et al.* Host defence against *Staphylococcus aureus* biofilms by polymorphonuclear neutrophils: Oxygen radical production but not phagocytosis depends on opsonisation with immunoglobulin G. *Immunobiology* **216**, 351–357 (2011).
62. Leid, J. G., Shirtliff, M. E., Costerton, J. W. & Stoodley, P. Human leukocytes adhere to, penetrate, and respond to *Staphylococcus aureus* biofilms. *Infect. Immun.* **70**, 6339–6345 (2002).

Closing pages

In het kort

Stafylokokken zijn bacteriën die op de huid leven en verschillende ziektes kunnen veroorzaken, zoals bloedvergiftiging, huid-, hart-, en implantaatinfecties. Door het ontstaan van antibioticaresistentie, wordt behandeling van deze infecties steeds moeilijker. Voor implantaatinfecties geldt, naast antibioticarestentie, dat de behandeling bemoeilijkt wordt door biofilmvorming op het implantaat. In een biofilm beschermen bacteriën zich tegen antibiotica en immuuncellen door een zelfgeproduceerde beschermlaag van suikers, eiwitten en DNA. Omdat huidige therapieën (antibiotica) slecht werken, is het dus noodzakelijk om alternatieve therapieën te ontwikkelen voor de behandeling van stafylokokken. In dit proefschrift is onderzocht of toediening van antistoffen gebruikt kan worden als therapie. Antistoffen kunnen lichaamsvreemde structuren (zoals bacteriën) binden en markeren als indringer voor het immuunsysteem. In dit proefschrift hebben we onder andere laten zien dat sommige antistoffen ook stafylokokken in een biofilm kunnen binden, ondanks de beschermlaag. Dit betekent dat antistoffen wellicht gebruikt kunnen worden om therapie voor implantaatinfecties te ontwikkelen. Vervolgens hebben we antistoffen gekoppeld aan enzymen die dit beschermlaagje kunnen wegknippen, omdat bacteriën na het vrijkomen uit biofilm weer gevoelig worden voor antibiotica en herkenning door immuuncellen. Ook hebben we laten zien dat een aanpassing in antistoffen, die initieel ontwikkeld is om de immuunreactie te versterken, ook op stafylokokken kan worden toegepast. Met deze aanpassing kunnen antistoffen zelfs het onderontwikkelde immuunsysteem van te vroeg geboren baby's activeren om de bacterie te elimineren. De bevindingen beschreven in dit proefschrift, kunnen bijdragen aan de ontwikkeling van antistoftherapie voor infecties met stafylokokken.

Nederlandse samenvatting

Introductie

Infecties met stafylokokken zijn moeilijk te behandelen.

Op onze huid leven miljarden bacteriën, waaronder bacteriën van het soort stafylokokken. Wanneer stafylokokken, met name *Staphylococcus aureus,* onze eerste verdedigingslinie (de huid) doorbreken, kunnen ze verschillende ziektes veroorzaken, zoals huidinfecties, longontsteking, ontsteking van het hart, botinfectie en bloedvergiftiging. Normaal gesproken worden dit soort infecties behandeld met antibiotica, maar door het ontstaan van antibioticaresistente stafylokokken zoals de MRSA-bacterie (ook wel bekend als 'ziekenhuisbacterie'), wordt behandeling met antibiotica steeds moeilijker. Er zijn nog maar een paar antibioticasoorten beschikbaar als laatste redmiddel om infecties met resistente bacteriën te behandelen.

Naast antibioticaresistentie zijn stafylokokken (*Staphylococcus aureus* en *Staphylococcus epidermidis*) berucht vanwege hun vermogen om biofilm te vormen op weefsel zoals in longen en chronische wonden, en op medische implantaten, zoals orthopedische implantaten en hartkleppen **(figuur 1)**. In een biofilm worden de stafylokokken omgeven door een zelfgeproduceerd netwerk van suikers, eiwitten en DNA. Dit netwerk zorgt ervoor dat de bacteriën tolerant zijn voor behandeling met antibiotica en slechter door het lichaamseigen immuunsysteem kunnen worden opgeruimd. Wanneer een bacterie loskomt uit de biofilm kan dit resulteren in verspreiding van de infectie. Door het toenemende gebruik van medische implantaten is biofilm-vorming een groeiend probleem. Op dit moment is 25% van de infecties die worden opgelopen in het ziekenhuis gerelateerd aan medische implantaten.

Omdat infecties met stafylokokken extreem slecht te behandelen zijn met de huidige therapieën, is het nodig om alternatieve behandelmethoden te ontwikkelen. In dit proefschrift hebben we meer inzicht proberen te krijgen in het gebruik van antistoftherapie tegen infecties met stafylokokken.

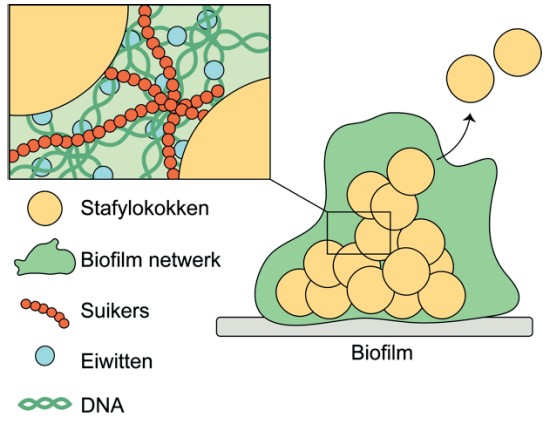

Figuur 1. Schematische weergave van een biofilm. stafylokokken zijn berucht vanwege hun vermogen om biofilm te vormen op medische implantaten. In een biofilm worden bacteriën omgeven door een zelfgeproduceerd netwerk van suikers, eiwitten en DNA. Dit netwerk zorgt ervoor dat de bacteriën tolerant zijn voor behandeling met antibiotica en slechter door het lichaamseigen immuunsysteem kunnen worden opgeruimd. Wanneer een bacterie loskomt uit de biofilm kan dit resulteren in verspreiding van de infectie.

Antistoffen spelen een centrale rol in de immuunreactie tegen stafylokokken

Antistoffen zijn eiwitten die in ons lichaam geproduceerd worden door een type immuuncellen, de B cellen, als reactie op lichaamsvreemde deeltjes zoals bacteriën. Elke B cel produceert een uniek antistof (een monoklonaal antistof), gericht tegen een uniek lichaamsvreemd deeltje. Antistoffen zijn in grote hoeveelheden aanwezig in ons bloed en kunnen zeer specifiek bacteriën herkennen. Antistoffen **(figuur 2)** zijn Y-vormige eiwitten met twee armen (Fab-armen) die een lichaamsvreemde structuur kunnen binden De staart van de Y-vorm wordt het Fc-domein genoemd en kan met het immuunsysteem reageren. Na binding aan het bacteriële celoppervlak via de Fab-armen zetten antistoffen een reactie in gang **(figuur 3)**. De reactie wordt gevormd door complementeiwitten (C-eiwitten), een groep eiwitten in het bloed die elkaar als een kettingreactie kan activeren. Een belangrijk resultaat is de productie van C3b eiwitten. Deze eiwitten hechten zich massaal aan het oppervlak van de bacterie en markeren de bacterie als indringer. Immuun cellen kunnen antistoffen en C3b eiwitten op de bacterie herkennen met Fc-receptoren en complement receptoren en worden zo gestimuleerd om de bacterie aan te vallen.

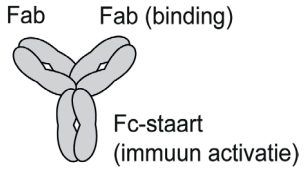

Figuur 2. Schematische weergave van de structuur van een antistof. Antistoffen zijn Y-vormige eiwitten met twee armen (Fab-armen) die een lichaamsvreemde structuur kunnen binden. De staart van de Y-vorm wordt het Fc-domein genoemd en kan met het immuunsysteem reageren.

De belangrijkste immuun cel die stafylokokken kan elimineren is de neutrofiel. Dit is de meest voorkomende witte bloedcel, die bacteriën onschadelijk kan maken door ze op te nemen. Na opname wordt de bacterie gedood in cel compartimenten die gevuld zijn met enzymen, antimicrobiële eiwitten en reactieve zuurstofverbindingen. Dit proces heet fagocytose, van het Griekse *phagein*: eten/verslinden. Het markeren van bacteriën door antistoffen en complement eiwitten heet opsonisatie. Deze term komt van het Griekse "*opson*" dat specerij betekent. Op eenzelfde manier als specerijen maken antistoffen en complement het opeten van bacteriën makkelijker voor neutrofielen.

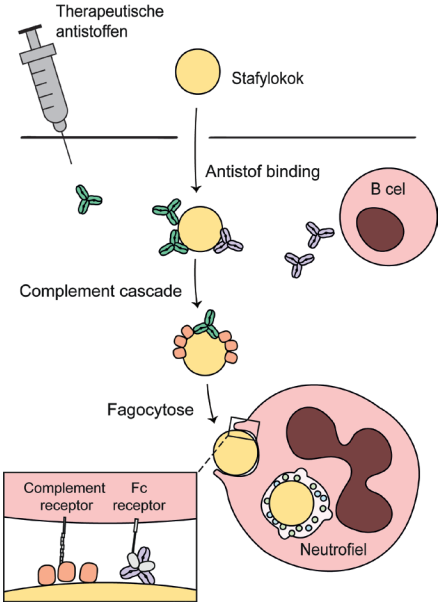

Figuur 3. Immuunrespons tegen stafylokokken. Wanneer een bacterie ons lichaam binnendringt, stimuleert het afweersysteem B cellen om natuurlijke antistoffen tegen de bacterie aan te maken. Deze antistoffen kunnen het bacteriële celoppervlak herkennen en binden. Vervolgens zetten de gebonden antistoffen de een kettingreactie de complement cascade in gang. Deze kettingreactie leidt tot de productie van C3b eiwitten die zich massaal aan het bacteriële oppervlak hechten. Immuun cellen genaamd neutrofielen kunnen de bacterie herkennen met Fc receptoren (die antistoffen herkennen) en complement receptoren (die C3b eiwitten herkennen). Dit stimuleert neutrofielen om de bacterie op te nemen (fagocytose). Na fagocytose wordt de bacterie gedood in cel compartimenten die gevuld zijn met antimicrobiële stoffen. Wanneer ons afweersysteem er niet goed in slaagt om een bacteriële infectie te elimineren, kunnen therapeutische antistoffen wellicht worden in gezet om fagocytose te stimuleren.

Ontwikkeling van antistoftherapie

In de afgelopen jaren is het mogelijk geworden om monoklonale antistoffen te identificeren uit B cellen. Vervolgens kunnen deze antistoffen in grote hoeveelheden in het lab geproduceerd worden, en veilig toegediend worden aan patiënten. Ook is het mogelijk om monoklonale antistoffen in het lab te modificeren om zo de functie te versterken. Hierdoor is de interesse in antistoftherapie de laatste jaren toegenomen. De meeste antistoftherapieën worden gebruikt voor de behandeling van kanker of autoimmuunziekten, maar over het gebruik van antistoftherapie voor infectieziekten is nog weinig bekend. Omdat antistoffen een centrale rol spelen in de immuunrespons tegen stafylokokken, zou antistoftherapie bijvoorbeeld ook toegediend kunnen worden wanneer het immuunsysteem er niet in slaagt deze bacteriën te vernietigen. Voor bacteriën die biofilm hebben gevormd, is het nog niet duidelijk hoe de immuunrespons precies verloopt. Waarschijnlijk is hier een andere aanpak nodig, en moeten bacteriën eerst losgemaakt worden uit het beschermlaagje van de biofilm. Antistoffen zouden in het geval van biofilmvorming bijvoorbeeld gekoppeld kunnen worden aan enzymen die het beschermlaagje wegknippen en de bacteriën zo beschikbaar maken voor fagocytose. De functie van antistoffen is dan om de enzymen specifiek naar de plek van de infectie te brengen.

Bevindingen

Allereerst probeerden we monoklonale antistoffen te identificeren die stafylokokken kunnen herkennen wanneer ze in een biofilm groeien. Biofilm is een erg complexe structuur en het biofilm netwerk kan bestaan uit verschillende componenten (suikers, eiwitten en DNA) in verschillende verhoudingen. Aan het begin van deze studie was er maar één monoklonaal antistof geïdentificeerd dat biofilm van stafylokokken kon herkennen, en dus gebruikt kon worden voor antistoftherapie tegen staphylococcus biofilm. Echter, dit antistof herkent een suiker dat maar door 30% van de klinische stammen wordt gebruikt. Omdat de gedeelde factor in alle staphylococcus biofilm infecties de bacterie zelf is, hebben we in **hoofdstuk 2** onderzocht of antistoffen die structuren op het oppervlak van de bacterie herkennen dit ook nog kunnen wanneer de bacterie bedekt is met biofilm componenten. In totaal vonden we vier monoklonale antistoffen die stafylokokken in biofilm konden binden. Ook bonden deze stoffen de biofilm gevormd alle klinische stammen die we getest hebben. Vervolgens hebben we één monoklonaal antistof gekozen en in een muismodel aangetoond dat dit antistof na injectie in de bloedbaan kan lokaliseren naar een implantaat met biofilm. Deze antistoffen kunnen dus wellicht worden gebruikt om antistoftherapie tegen biofilm infecties te ontwikkelen.

Wanneer een stafylokok loskomt uit een biofilm, wordt ze weer gevoelig voor antibiotica en immuun cellen. Daarom wordt er veel onderzoek gedaan naar het gebruik van enzymen die het netwerk van DNA, eiwitten of suikers kapot kunnen knippen. Dit soort enzymen (DNase; knipt DNA, en DispersinB; knipt suikers), zijn veelbelovend tegen biofilmvorming op makkelijk bereikbare plekken zoals chronsiche wonden of de longen. Echter, het gebruik voor infecties op minder bereikbare plekken is gecompliceerd, omdat de enzymen niet op de plek van infectie terecht komen. In de behandeling van kanker worden antilichaam-drug-conjugaten ingezet om toxische stoffen af te leveren in de tumor. In **hoofdstuk 3** beschrijven we een manier om monoklonale antistoffen aan DNase of Dispersin te koppelen. De resulterende fusie-eiwitten behouden hun specificiteit voor de stafylokok en zijn enzymatisch actief in het losmaken van stafylokokken uit biofilm. Dit soort antistof-enzym conjugaten kunnen veelbelovend zijn in het gebruik tegen biofilm gerelateerde staphylococcus infecties.

In **hoofdstuk 4** vergelijken we het gebruik van monoklonale antistoffen als alternatief voor Intraveneus Immunoglobulin (IVIG), de standaardtherapie bij infectie met *S. epidermidis* bij vroeggeboren baby's (neonaten). Neonaten hebben een verhoogd risico op deze infectie door hun onderontwikkelde immuunsysteem. IVIG een mix is van antistoffen geïsoleerd uit het bloed van gezonde donoren, die gericht zijn tegen verschillende lichaamsvreemde structuren, waaronder *S. epidermidis*. In tegenstelling tot IVIG herkennen monoklonale antistoffen éénzelfde lichaamsvreemde structuur en ze zijn daarom veel specifieker. In dit onderzoek observeerden we dat activatie van het complementsysteem essentieel was voor het fagocyteren en elimineren van *S. epidermidis.* Vervolgens hebben we de Fc-staart van de monoklonale antistoffen gemuteerd (een wijziging in de bouwstenen van het antistof) met een mutatiestrategie die ervoor zorgt dat de complementcascade beter in gang kan worden gezet. Hiermee kon de eliminatie van *S. epidermidis* nog verder worden verhoogd. Ook toonden we aan dat deze 'verbeterde' monoklonale antistoffen ook met het neonatale complement systeem reageren en zo fagocytose kunnen stimuleren.

In **hoofdstuk 5** beschrijven we een dubbele rol van het complement systeem in het sturen van fagocytose via Fc-receptoren en complementreceptoren. Op een geopsoniseerde bacterie zijn antistoffen en C3b aanwezig, die respectievelijk herkend kunnen worden door Fc-receptoren en complement receptoren. In hoofdstuk 5 observeren we dat na de depositie van complement eiwitten, de herkenning van antistoffen door Fc-receptoren geblokkeerd wordt. De manier waarop een bacterie wordt opgenomen (via Fc-receptoren of complement receptoren) kan invloed hebben op het elimineren van de bacterie. Deze nieuwe inzichten in de dubbele rol van complement na activatie door antistoffen kan belangrijk zijn in het ontwikkelen van nieuwe antistof therapieën.

Als laatste zijn in **hoofdstuk 6** alle bevindingen van dit proefschrift samengevat en in de context van het onderzoeksveld geplaatst. We bespreken wat we hebben geleerd en hoe onze bevindingen kunnen bijdragen aan de ontwikkeling van therapeutische antistoffen tegen infecties met stafylokokken.

Ter conclusie

Door het onderzoek in dit proefschrift begrijpen we beter hoe antistoffen via het complementsysteem fagocytose van stafylokokken kunnen stimuleren Ook hebben we meer inzicht gekregen in het gebruik van monoklonale antistoffen tegen biofilm infecties. De bevindingen beschreven in dit proefschrift, kunnen bijdragen aan de ontwikkeling van antistoftherapie tegen stafylokokken infecties.

Dankwoord (acknowledgements)

Can anybody help?

Zoals antistoffen neutrofielen kunnen helpen om stafylokokken te elimineren (zie de Nederlandse Samenvatting als je voorgaande zin niet begrijpt, hopelijk geeft dat duidelijkheid), zijn er heel wat mensen die het uitvoeren van dit promotieonderzoek voor mij behapbaar hebben gemaakt. Zij hebben ervoor gezorgd dat ik aan de afgelopen 4,5 jaar terugdenk als de tijd van mijn leven. Dit was nooit zo geweest zonder de goede begeleiding, samenwerkingen, collega's, vrienden en familie waarvan ik heb kunnen genieten. Daarom wil ik hieronder alle personen bedanken die ik niet had kunnen missen tijdens het maken van dit proefschrift.

Allereerst: bedankt **Suzan**, voor al het vertrouwen wat je me hebt gegeven. Al vanaf dag één stelde je me voor als de 'biofilm expert' van jouw onderzoeksgroep – al was ik hier zelf niet direct van overtuigd. Bedankt dat ik altijd bij je terecht kon, zeker wanneer ik toch even iets minder stoer was dan verwacht. Jouw helikopterview is meermaals goed van pas gekomen als ik het overzicht kwijt was. En dan te bedenken dat je dit niet alleen voor mijn project doet, maar voor de hele onderzoeksgroep! Ik ben ontzettend blij dat we nog langer kunnen samenwerken.

Kok, pas vanaf jaar 3 werd jij als copromotor bij mijn project betrokken. Natuurlijk was je de eerste twee jaar al mijn vraagbaak in het lab, maar vanaf toen kon ik helemaal fijn met je sparren over nieuwe proeven en data-analyse. Bedankt voor al je antwoorden en vooral voor de tijd de je altijd vrij kon maken.

Daarnaast waren ook **Harrie** en **Jos** betrokken bij de begeleiding. **Harrie,** bedankt voor de ruimte die je me gaf om binnen onze samenwerking mijn eigen projecten op te zetten. **Jos**, zonder jou geen levendige discussies tijdens de groepsbesprekingen. Met een, op het eerste gezicht, simpele vraag kun jij mensen op een goede manier aan het denken zetten. Fijn dat ook bij jou de deur altijd open stond voor een praatje.

Zonder leescommissie geen promotie, dus ook wil ik ook **prof. dr. Koenderman**, **prof. dr. Horswill**, **prof. dr. Kluijtmans**, **prof. dr. van Els** en **prof. dr. Nijs** bedanken het kritisch doorlezen (en goedkeuren!) van mijn proefschrift.

Verder was dit proefschrift er ook nooit gekomen zonder alle samenwerkingen. Ten eerste wil ik **Bruce van Dijk, Bart van der Wal, dr. Vogely** en alle andere betrokkenen van **de afdeling Orthopedie** bedanken voor de samenwerking, welke heeft geleid tot een mooie publicatie in eLife. Op naar meer! **Bart van der Wal**, ik vertel nog vaak over

de knieoperatie die ik mocht bijwonen, en dat ik toch wel eventjes moest gaan zitten toen je ‘knabbeltje’ erbij pakte. Het heeft veel indruk gemaakt! Daarnaast bedank ik **Michiel** en **Coco**, geweldig dat onze twee projecten zo mooi samen kwamen en het zo vlot kon worden opgeschreven. Also, a huge thanks to the people in the lab of **Alex Horswill** at UC Denver for making me feel at home from the first day of my visit. **Alex,** thanks for giving me the opportunity to learn from your team. Especially thank you **Kuba** and **Jeff** for all the help with troubleshooting the biofilm work. En, zeker niet te vergeten, alle studenten die mij geholpen hebben. **Anne, Miriam** en **Linda**, zonder jullie bijdrage in de vorm van scriptie/stage was dit boekje een stuk dunner geweest.

Dan nu een hele grote shout-out naar mijn paranimfen. **Dennis**, wát hebben wij elkaar gevonden de afgelopen jaren. Niet alleen onze outfits bleken een match te zijn. Je blijft me verbazen met (woord)grappen die nog slechter dan slecht zijn, en soms nog grover dan grof. Als niemand het hoort, kun je alles zeggen. Maar, dit is niet jouw enige spacealisme. Het is geweldig hoe onvermoeibaar enthousiast jij kunt zijn over nieuwe ontdekkingen, groot of klein, en het is heerlijk om te zien hoe je je aan het ontpoppen bent in Amsterdam. Helaas zijn we al eventjes geen collega’s meer, maar gelukkig wel vrienden. En dan **Remy**, eigenlijk was jij er als bachelor student ook al vanaf het begin bij. Nu, ontelbaar niet-toonbare selfies (en prachtige profielfoto’s) later, ben ik blij dat jij mijn par(ty)nimf bent. Mevrouw Potvis wil jou enorm bedanken voor alle keren dat je zei: “Dit kan jij, Lies” bij instortingsgevaar; “Gaat ie lekker, Lies?” als mijn grapjes net iets te ver gingen; en voor het fanatiek terug-klagen als office buddy afgelopen jaar. Die PhD ga jij rocken, daar heb ik geen twijfels over bij iemand die zo eerlijk, sterk en georganiseerd is als jij.

Er zijn nog een heleboel collega’s zonder wie dit proefschrift er niet was geweest. **Carla** en **Piet,** zonder jullie had dit boekje precies 0 wetenschappelijke hoofdstukken geteld. Ik wil niet weten hoeveel kilo antistof jullie de afgelopen jaren hebben geproduceerd. En **Lisette**, als er iemand een aanpakker is, ben jij het wel. Ook dankzij jou kon hoofdstuk 4 in sneltreinvaart de deur uit. **Maartje**, ik weet niet hoe het lab (en vooral het leukste laantje in 406, ook mede mogelijk gemaakt door **Adinda** en **Anneroos**) eruit had gezien zonder jou. Je hebt mij ontelbare keren geholpen met protocollen, locaties, concentraties en wat niet. Dankzij jou en **Erik** is het lab een heerlijke georganiseerde chaos om in te werken. **Yvonne**, duizendmaal dank voor alle keren dat jij de eindeloze UMC-administratie uit handen hebt genomen.

Er is natuurlijk niets fijner dan zin hebben om naar je werk te gaan vanwege je leuke collega’s. **Dani**, be-ya, van deze kleine mede-dwerg ben je voorlopig nog niet af. Nu ik zelf bijna klaar ben met dit proefschrift, heb ik nog meer respect voor de manier

waarop jij het zo koelbloedig hebt afgerond. Misschien ben jij wel de grootste hulk van ons twee (maar zeker niet lullek). Dank je voor de leuke tijd, en proost op nog meer leuke MMB jaren samen! **Eva**, het is fijn om je weer te zien shinen op de afdeling. Ik heb jouw eerlijkheid, persoonlijke interesse en kritische vragen gemist de afgelopen maanden. **Hendrik,** herr Boebelmeister, your dreams are not boring, so keep dreaming. **Bart,** van feestende post-doc naar co-promotor van menig PhD student. Wat hebben we gelachen tijdens carnaval en wintersport, maar wat heb je me ook vaak aan het denken gezet met je kritische blik tijdens discussies. **Sjors**, goeiemorgen!! Altijd leuk om het licht aan te mogen doen als jij 's ochtends nog in het donker zit te werken. **Leire**, your energy is priceless. Happy that you're back in Utrecht. And **Julia**, thanks for donating some of your enthusiasm. I could mention many, many other people that made the MMB a great place to live, ehhh… work, but I will do it in a few sentences because we need to finish this book, finally. Thanks to all (former-) members of the **Rooijakkers/ Strijp group**, for creating a safe environment to work in, and for all your valuable input during work discussions. BIG THANK YOU to all the other **MMB oreos and fun peepz** that worked at the MMB in the past years, *I liked it… a lot*. Thanks for the skiing trips, non-memorable bock beer festivals and so much more. **Nightshift crew** (iykyk), thanks for the best upside down VrijMiBo ever. And always remember; there are multiple ways to Berlin, but from Paris is best (famous Danish saying).

Promotieonderzoek is niet iets waarbij je aan het eind van de dag je laptop dichtklapt en er dan pas de volgende ochtend weer aan denkt. Daarom wil ik ook een aantal mensen bedanken die minstens net zo belangrijk zijn geweest voor mijn gemoedstoestand de afgelopen jaren. **Romy,** with all my heart… thank you voor alle thuiswerksessies, weekendjes weg, sport-uurtjes en de uiterst inspirerende woorden: "type gewoon". **Inkie** en **Floor:** hoe jullie brein werkt snap ik soms niet, maar de output is geniaal, ik kan er geen genoeg van krijgen. **Noortje**, wat was het heerlijk om als derdewiel bij jou en **Pauline** op de bank te ploffen met een bordje eten en een film. En **Lotte**, dank je voor alle aandacht ondanks het moeilijke jaar wat je zelf achter de rug hebt <3.

Twee zielen, geen gedachte. Of misschien toch wel veel gedachten, die ik gelukkig altijd bij je kwijt kan. Al moet je ze soms lospeuteren. **Jennie**, wat heb ik veel aan je gehad de afgelopen maanden. Er valt nog zo veel te ontdekken, ik heb enorm veel zin in ons volgende avontuur.

Lieve **papa, mama, Mars, Jori, Mees** en **Saar.** Misschien was ik de afgelopen jaren wat onbereikbaar, maar ik wist dat er altijd een thuisbasis was om op terug te vallen. Bedankt dat jullie altijd voor mij klaar staan, wat er ook gebeurt, welke keuze ik ook maak.

About the author

Lisanne de Vor was born on March 30th 1993 and raised in Houten, the Netherlands. She graduated her pre-university education (Atheneum) in 2010 at College the Heemlanden in Houten. She was then trained as a scientist, graduating in Biomedical Sciences (Bachelor's degree, 2011-2014, Utrecht University), with a focus on infectious diseases and immunity (Master's degree Infection and Immunity, 2015-2017, Utrecht University). Lisanne has worked in several research fields at different institutes. In 2015, she performed a research internship in the Laboratory of Translational Immunology in the UMC Utrecht under the supervision of dr. Marianne Boes and dr. Stefan Nierkens, studying the effect of tumor secreted factors on dendritic cells. She then went abroad to study staphylococcal host-pathogen interactions on the skin under the supervision of dr. Keira Melican and prof. dr. Agneta Richter-Dahlfors at the Karolinska Institute in Stockholm, Sweden. Lisanne's work during the master's programme contributed to several publications in peer-reviewed journals. After graduating, Lisanne returned to the UMC Utrecht to start her doctoral education at the department of Medical Microbiology in the group of prof. dr. Suzan Rooijakkers, studying the use of monoclonal antibodies for the treatment of staphylococcal infections, financed by Health~Holland, Top Sector Life Sciences & Health. The main findings of this work have been described in this thesis, have been presented at multiple international scientific conferences, and have been published in peer-reviewed journals.

List of publications

Related to this thesis

de Vor L, Rooijakkers SHM, van Strijp JAG. Staphylococci evade the innate immune response by disarming neutrophils and forming biofilms. FEBS Lett. 2020 Aug;594(16):2556-2569.

de Vor L, van Dijk B, van Kessel K, Kavanaugh JS, de Haas C, Aerts PC, Viveen MC, Boel EC, Fluit AC, Kwiecinski JM, Krijger GC, Ramakers RM, Beekman FJ, Dadachova E, Lam MG, Vogely HC, van der Wal BC, van Strijp JA, Horswill AR, Weinans H, Rooijakkers SH. Human monoclonal antibodies against *Staphylococcus aureus* surface antigens recognize in vitro and in vivo biofilm. Elife. 2022 Jan 6;11:e67301.

de Vor L, Beudeker CR, Flier A, Scheepmaker LM, Aerts PC, Vijlbrief DC, Bekker MN, Beurskens FJ, van Kessel KPM, de Haas CJC, Rooijakkers SHM, van der Flier M. Monoclonal antibodies effectively potentiate complement activation and phagocytosis of *Staphylococcus epidermidis* in neonatal human plasma.
Front Immunol. 2022 Jul 29;13:933251.

Other publications

Schulz A, Jiang L, **de Vor L**, Ehrström M, Wermeling F, Eidsmo L, Melican K.
Neutrophil Recruitment to Noninvasive MRSA at the Stratum Corneum of Human Skin Mediates Transient Colonization. Cell Rep. 2019 Oct 29;29(5):1074-1081.e5.

de Graaf JF, **de Vor L**, Fouchier RAM, van den Hoogen BG. Armed oncolytic viruses: A kick-start for anti-tumor immunity. Cytokine Growth Factor Rev. 2018 Jun;41:28-39.

PhD Training Certificate - Graduate School of Life Sciences

Discipline-specific educational activities	# ECTS
PhD Spring meeting 2018, 2019	1.5
PhD Retreat 2018, 2019, 2020, 2021	2.55
Introduction in Techniques and Facilities	0.3
Van Kinsbergen Infection & Immunity Advanced+ course	1.5
General educational activities	
PhD day 2019, 2021, 2022	0.7
Toetsing I – toetsvragen ontwikkelen	0.6
Supervision research of MSc students at GSLS	1.2
Onderwijs in kleine groepen	0.6
Start to teach	0.6
Research planning and time management	0.4
Infographics and iconography	0.3
Scientific art work with Adobe Photoshop	0.6
Mindfulness and stress reduction	3.0
Introduction to Python (CSND)	1.5
Biobusiness Summer School 2021	1.5
Symposia/conferences (oral/poster presenter) and other activities	
EBJIS 2019	0.6
KNVM/NVMM Spring meeting 2019, 2021	1.2
Science for life 2019	0.6
Young Microbiologists Symposium 2020	0.6
Staph symposium 2021	0.3
CORVOS Complement & beyond symposium 2021	0.3
Lab visit prof. A. Horswill UC Denver	6.0
TOTAL NUMBER OF ECTS	26.15